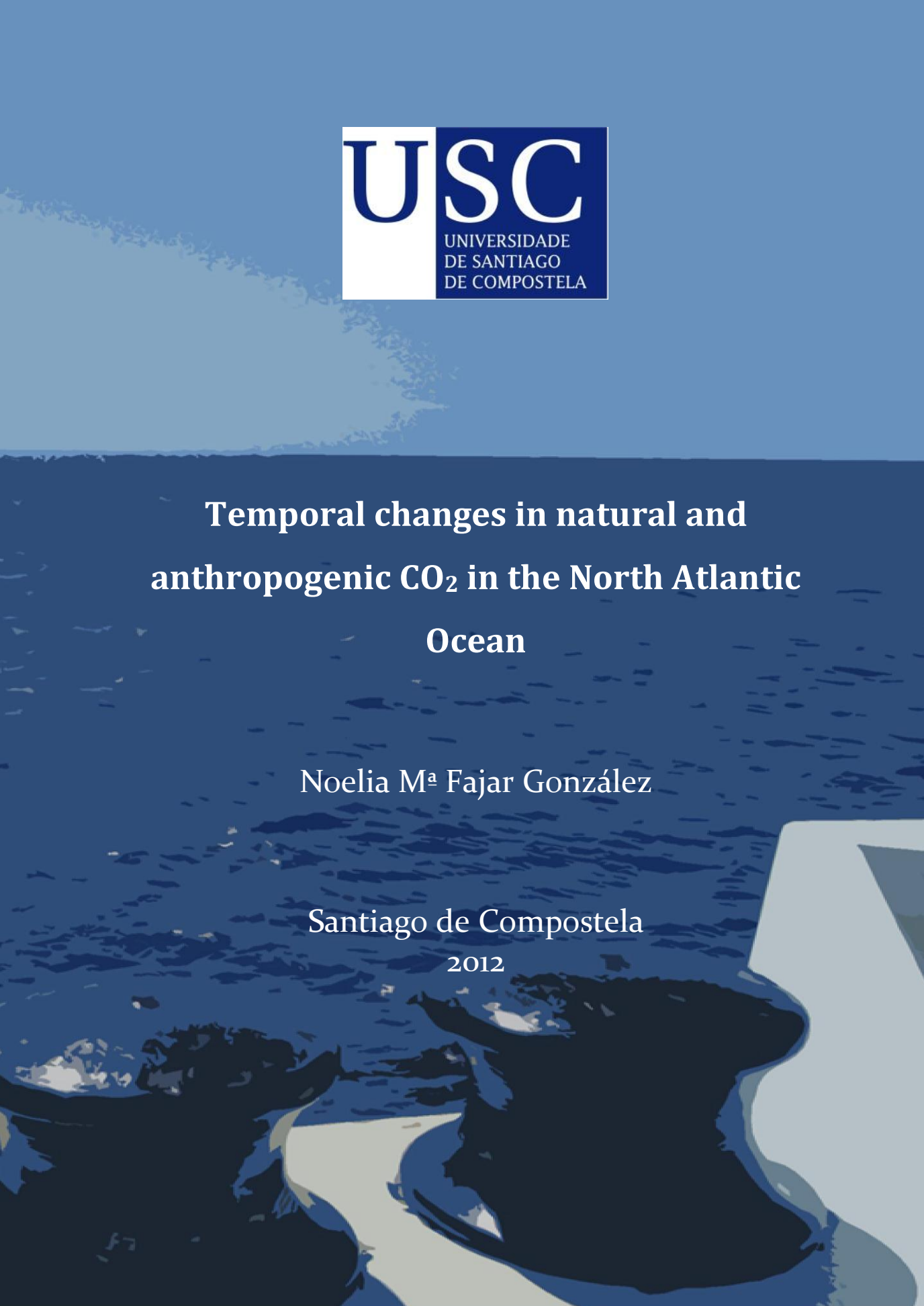

# Temporal changes in natural and anthropogenic $CO_2$ in the North Atlantic Ocean

Noelia Mª Fajar González

Santiago de Compostela
2012


# Temporal changes in natural and anthropogenic $CO_2$ in the North Atlantic Ocean

Noelia Mª Fajar González

Santiago de Compostela

2012

Los Profesores de Investigación del Departamento de Oceanología del Instituto de Investigaciones Marinas (IIM) perteneciente al Consejo Superior de Investigaciones Científicas (CSIC), **Dr. Fiz Fernández Pérez** y **Dra. Aida Fernández Ríos**, en calidad de directores de tesis,

Hacen constar:

> Que la presente memoria titulada "**Cambios temporales en el $CO_2$ natural y antropogénico en el Océano Atlántico Norte** / *Temporal changes in natural and anthropogenic $CO_2$ in the North Atlantic Ocean*" presentada por la licenciada **Noelia Mª Fajar González** para optar al grado de Doctora en Química con *Mención Internacional* por la Universidad de Santiago de Compostela, fue realizada bajo nuestra dirección y cumple con las condiciones exigidas para su presentación, la cual autorizamos.

Y para que así conste y surta los efectos oportunos, firmamos la presente en Vigo, 5 de Diciembre de 2012.

Dr. Fiz Fernández Pérez  Dra. Aida Fernández Ríos

La Profesora Titular del Departamento de Química Analítica, Nutrición y Bromatología de la Universidad de Santiago de Compostela, **Dra. Rosa Antonia Lorenzo Ferreira**, en calidad de codirectora,

Autoriza:

> A la licenciada **Noelia Mª Fajar González** a la presentación de la memoria titulada "**Cambios temporales en el $CO_2$ natural y antropogénico en el Océano Atlántico Norte** / *Temporal changes in natural and anthropogenic $CO_2$ in the North Atlantic Ocean*" para optar al grado de Doctora en Química con *Mención Internacional* por esta universidad.

Y para que así conste y surta los efectos oportunos, firma la presente en Santiago de Compostela, 5 de Diciembre de 2012.

Dra. Rosa Antonia Lorenzo Ferreira

Esta Tesis de Doctorado se realizó dentro del Grupo de $CO_2$ del Departamento de Oceanología del Instituto de Investigaciones Marinas (IIM) perteneciente al Consejo Superior de Investigaciones Científicas (CSIC). El CSIC junto con el Fondo Social Europeo (FSE) ha financiado a Noelia Mª Fajar González con una beca predoctoral de su programa Junta para la Ampliación de Estudios (JAE) durante el periodo 2008-2012.

Memoria presentada por Noelia Mª Fajar González para optar al grado de Doctora en Química con Mención Internacional por la Universidad de Santiago de Compostela

Santiago de Compostela, 2012

A mi “buela”

*Latitud: 41.4ºN*
*Longitud: 13.9ºO*
*Tª: 2.5ºC*
*Salinidad: 34.9psu*
*Profundidad: 5439m*

# Agradecimientos

Posiblemente no es “científicamente correcto” decir qué parte de un trabajo es más importante. Todo el trabajo es importante, y en todas las partes aprendes algo nuevo, sobre todo cuando te equivocas...que en mi caso son muchas y variadas veces. Pero tengo muy claro que sin toda la gente que directa o indirectamente me ha ayudado, apoyado y animado durante estos últimos años, esta tesis no hubiera sido posible. Por ello, este *capítulo* es muy importante para mí, y por eso, es por y para vosotros. ☺

Fiz y Aida. Además de jefes habéis hecho de mamá y papá muchas veces, y de amigos otras tantas, pero durante estos últimos cuatro años habéis sido los perfectos capitanes de mi expedición por el océano y el sistema del carbonato. Quiero agradeceros la paciencia que habéis tenido y que tenéis conmigo, resolviendo siempre todas mis dudas, una y otra vez hasta que lo entiendo. Me habéis dado libertad para “jugar” en el laboratorio, para tomar mis propias decisiones (y equivocarme) e incluso protestar, pero siempre con la seguridad de tener vuestro respaldo y apoyo. Claramente, sin todo lo que he aprendido a vuestro lado, esto no sería posible. ☆

Toñi, desde que me fui de Santiago siempre me has animado a seguir adelante, escogiendo las palabras de apoyo adecuado y alegrándote con mis logros. Además, este último mes has sido la guía perfecta en todos los papeleos. ★

Jose y Sandra, porque sin darse cuenta me impulsaron hasta aquí. Justo cuando más necesitaba una guía, me motivaron para continuar mis pasos en ciencia y querer ser doctora. 📖

A todos mis compañeros de Oceanología del IIM, Rosa, Trini, Isabel, Bea, Clara, Mar, Nico, Kiko, Paco, Pepe, María José, Susana, Fernando, Diana, Carmen, Des, Belén y María, y en especial a mis compis del grupo de $CO_2$, Dr. Fraga, Toni, Merche, Marcos, Pau, Mónica, Antón, Lidia, Miguel, Maribel y Alba, porque desde el minuto uno de mi llegada al instituto me he sentido un miembro más del equipo, compartiendo cafés, esas delicias del congelador, risas y también penas.👍

Mis niñas, Bea, Lidia, Clara, Alba y Maribel. ¿Cómo llegamos a este punto? Fuimos entrando poco a poco, conociéndonos a ratos y compartiendo cada día un minuto más. ¡No sé como expresar en palabras lo mucho que significáis para mí! Primero fue Bea, siempre dispuesta a echar una mano, desde las preguntas más fáciles, ¿que es una isopicna? Hasta las de nota ¿Qué voy a hacer con mi vida? Lidia, el descubrimiento de mi primera campaña oceanográfica, aunque nuestros caracteres hacen que no siempre estemos de acuerdo, sabemos encontrar el punto medio. Clara, desde los primeros días que aquella manzana

“viajaba” hasta ser tus “polluelas” ¡Cuantísimos charlas, buenos ratos y discusiones! Alba, a pesar de no tener el placer de tratarte desde tu llegada, te has ido haciendo un huequito en mi día a día, compartiendo momentos inolvidables como “¡¡¡Nooooeeeeee!!! ¡¡¡Tierra!!!” Y Maribel, eres la última adquisición, la pequeña, pero llegaste pisando fuerte! Debe ser tu pez de los tres deseos...Sin vosotras mis comidas habrían sido más aburridas, y mi corazoncito estaría más vacío. 🏆

Pau, ¿que hubiera sido de mí si no compartiéramos camarote en Caibox? ¡No quiero ni pensar lo triste y aburrido que hubiera sido el despacho sin ti! Has sido muy buena guía en mi viaje en las masas de agua, OMP, interpolaciones... pero también en la vida en general. Hemos compartido un montón de penas y alegrías, y me has enseñado a ver claro que no todo es “porque me quieres”. He definido todavía más mi carácter compartiendo contigo el día a día, dándole importancia a lo que la tiene y restándosela a lo que no. ¡Eres mi gran apoyo! ✳

Mónica, “mi jefa chunga”, te debo todas las técnicas que aprendí desde que llegué al IIM. Toda la paciencia que desarrollamos poniendo a punto el SOMMA, las interminables hora de laboratorio de ¡No entiendo nada! Has tenido la paciencia suficiente para resolver todas mis “duditas” y enseñarme donde está todo y como debe ir colocado... ¡aunque a veces fuera a miles de kilómetros y por teléfono! Por todo eso, pero, sobre todo, por demostrarme tu amistad y apoyo, soy tu incondicional. 🌻

Antón, más que "por extensión", por toda la paciencia que tienes conmigo, por todas las veces que "casi la lío", pierdo mis datos o tiro el ordenador por la ventana (que no han sido pocas) ...Por todas las charlas que hemos tenido, y no sólo de ciencia. Porque siempre tienes un minutito y una sonrisa. 💻

A todos mis compañeros de las campañas CAIBOX, MOC²Ecuatorial y CATARINA. Porque las vivencias del barco son muy intensas. En especial al grupito de CAIBOX, Miguel, Marcos, Merche, Pau, Vane, Nico y Kiko, por aquellas geniales vacaciones post-campaña. De MOC, a Elisa y Pilar, ¡mis niñatas! , que junto con Fran hicimos de las "mazmorras" del Hespérides, nuestro cuartel general ¡Gracias por seguir formando parte de esto! Y de CATARINA, no puedo hacer distinciones, porque en el peor momento, supisteis sacarme a flote. ☸

My colleagues and friends from Norwich. When I was thinking about going to visit the LGMAC, I never thought that my visit would be so productive. Thanks for making me feel one of you. I would especially like to thank Ollie, without you, my stay probably would have been a mess. Thanks for your support and those quintessential English things. 🚲

Mis amigos de La Guardia, ¿cuantos años hace que lleváis aguantando mis alegrías, penas, locuras, enfados...? Marcos, Miguel, Ángela, Tecla, Ío, *Emma*, Rebe, Pablo, Silvia, Liber, Xabi, Lucía A., Yoli, Diego, Lucía G., Nelson, Mari, Isma, Eva, Sara, Chedi, Tamara, Sonia, Leti, Laura G., Judith, Blanca, Javi R.,

Laura B., Berto, Álvaro, Sonia, Andrea, Rosa, Miguel, Kon, Lucía R., Javi, *Sheila*, Patri G., Oscar, Patri A., Noemí y Oti. Porque como digo siempre "sin amor no hay nada" y sospecho que es eso lo que nos mantiene unidos. Desde los que empezamos desde pequeñitos hasta las más recientes incorporaciones, los que siguen aquí y también los que se han marchado, siempre sabéis arrancarme una sonrisa, animarme cuando estoy triste, escucharme cuando sólo necesito hablar y aconsejarme cuando lo pido. Discutir también ayuda ¡¿eh?! Porque a pesar de ser una "chancarella" me hacéis sorpresas, videos, fotos, regalos, me despedís y recibís siempre con una sonrisa, me seguís cuando no estoy e incluso presumís de mí ¡Jolín! ¡Hasta tengo un Óscar por Kunfu Panda! ¡Sois los mejores! ♫

Mi familia pisina, Belén, Carol, Ángela, Rebe y Andrea, aunque no os vemos tan a menudo como quisiera, siempre tenemos una buena ocasión para darnos cuenta que el tiempo no pasa por nosotras ¡sois geniales! Nuestras "alineaciones planetarias" me dan siempre el impulso que necesito para seguir. 🛸

Mi familia, vosotros si que os lo merecéis ¡Siempre ahí! Por eso os quiero dejar para el final, porque da igual que se llame baile, pintura, guitarra, inglés, COU, licenciatura, master, doctorado... si no fuera por vuestro apoyo incondicional, no habría conseguido llegar nunca hasta aquí. Mamá y papá, sois el eje de mi vida, a pesar de que muchas veces no os cuento lo suficiente o lo necesario para que entendáis del todo lo que hago,

siempre me apoyáis y me animáis a seguir adelante, sois pacientes y comprensivos… sois el engranaje que hace que "nuestro barco" funcione, nos mantiene a todos unidos y que me aporta la tranquilidad suficiente para poder afrontar otras "tempestades". Pepín y Rosi, gracias por hacerme pensar en otras cosas y distraerme de mis "estreses" y darme otro punto de vista, aunque no siempre lo comparta. Goya, ¡la niña de mis ojos! Me envías cartas, correos y dibujos, has ido decorando mi vida, desde la habitación de casa hasta la de Norwich, pasando el despacho de Vigo, haciéndome saber siempre cuanto me quieres. Y Marcos…, en los últimos años has aguantado días de sol, lunas brillantes y flores hermosas, y estás ahí! Pero lo mejor, es que a pesar de haber pasado también por días de lluvia, tormentas y huracanes, sigues estando ahí. ¡Os quiero! ❤


La Guardia, 2 de Diciembre 2012

# Índice/*Index*

Temporal changes in natural and anthropogenic $CO_2$ in the North Atlantic Ocean

Cambios temporales en el $CO_2$ natural y antropogénico en el Océano Atlántico Norte

# Resumen

El ciclo del carbono en el océano se ve afectado por los cambios en el clima y, a su vez, la alteración del mismo provoca cambios en otros ciclos. Las grandes cantidades de $CO_2$ emitidas a la atmósfera entran en el océano mediante procesos físicos y biológicos, donde este $CO_2$ que penetra en el agua genera, en primera instancia, ácido carbónico ($H_2CO_3$) el cual rápidamente se trasforma en carbonato ($CO_3^{2-}$) y bicarbonato ($HCO_3^-$). Dentro de las variables medibles del sistema del carbonato o del $CO_2$ se encuentran la fugacidad de $CO_2$ ($fCO_2$), carbono inorgánico total disuelto ($C_T$), alcalinidad total ($A_T$), y pH. Actualmente se puede considerar una quinta variable, el $CO_3^{2-}$, que desde el 2008 se puede medir directamente. La particularidad del sistema del $CO_2$ es que conociendo al menos dos de estas variables se pueden determinar las otras dos usando una serie de ecuaciones termodinámicas. En primer lugar en esta tesis se evalúa la consistencia interna del sistema del $CO_2$ de modo que los errores en los cálculos termodinámicos sean mínimos. Para ello, se dispone de medidas de pH, $A_T$, $C_T$ y, por primera vez, de $[CO_3^{2-}]$ en el Atlántico Norte. Esto, junto con las más recientes mejoras de las ecuaciones termodinámicas y una selección de cuatro pares de constantes de disociación, permite reducir la diferencia no sólo entre las medidas y los valores calculados de $C_T$, sino también de $[CO_3^{2-}]$ y confirmar que las constantes de disociación propuestas para aguas naturales, resultan más apropiadas que las de aguas sintéticas. La buena correlación entre $[CO_3^{2-}]$ calculado y medido permite completar los perfiles de $[CO_3^{2-}]_{in\ situ}$ para las diferentes campañas del Atlántico Norte y relacionarlas con las masas de agua presentes en cada región.

Una vez conocido en detalle el sistema del $CO_2$, el siguiente paso es hacer el control de calidad de esos datos. Para ello se cuenta con los procesos utilizados durante la elaboración de las bases de datos globales GLODAP y CARINA. Las campañas con datos del sistema del $CO_2$, poco fiables o dudosos, que se habían descartado en GLODAP, no se reconsideraron en CARINA, a pesar de que se incluyó también el pH. Por ello, campañas como las WOCE A06 y A07 de 1993 no están disponibles en ninguna de ellas. Sin embargo, es posible descargar todos los datos de pH, $A_T$ y $C_T$ de estas campañas de la web CCHDO. El uso combinado de estos datos y de las bases de datos GLODAP, CARINA y MOC$^2$Ecuatorial, hace posible señalar que los datos de pH eran válidos, aunque tenían un sesgo, que se corrige satisfactoriamente en esta tesis. Asimismo, la herramienta recientemente desarrollada, 3DwMLR permite evaluar los datos de $A_T$ y calcular nuevos datos cuando es necesario. Debido a la disponibilidad de los nuevos recuperados de pH y $A_T$ se pueden recuperar también los datos de $C_T$, de modo que se obtiene una base de datos de carbono evaluada y recuperada para las campañas A06 y A07.

Durante los últimos cuatro años, el Grupo de $CO_2$ del Instituto de Investigaciones Marinas de Vigo ha participado en varias campañas en el Océano Atlántico, de las cuales, cuatro cubren un área importante del Océano Atlántico Norte. Estas expediciones son CAIBOX 2009, MOC$^2$Equatorial 2010, OVIDE 2010 y A24ºN 2011, que junto con la enorme cantidad de datos biogeoquímicos disponibles en las bases de datos globales, es posible abordar cuestiones que despiertan el interés de la comunidad científica,

como son el aumento del $C_{ant}$, la acidificación y la desoxigenación del océano. Para estudiar estos cambios se plantean dos zonas de estudio diferenciadas, el Océano Atlántico Ecuatorial y la Cuenca Ibérica.

En el Océano Atlántico Ecuatorial se plantea un estudio sobre acidificación, desoxigenación y $C_{ant}$ considerando los datos de las campañas A06 1993 y MOC$^2$Ecuatorial 2010, que siguieron exactamente la misma ruta con una diferencia de diecisiete años. Una forma sencilla para evaluar estos cambios es la división de la sección 7.5ºN en cuatro regiones, dos a cada lado de la dorsal Atlántica, y seis capas de densidad determinadas por las masas de agua características de la zona. De este modo, en cada una de estas zonas se puede dar el valor de cambio pH, $O_2$ y $C_{ant}$, calculando la diferencia entre los valores de 2010 y los de 1993. Además, estos cambios se relacionan con las masas de agua presentes en la zona, de modo que los resultados ponen de manifiesto, por ejemplo, el aumento hacia el oeste de la lengua de *Antarctic Intermediate Water* con valores de pH más bajos en 2010 que en 1993. Además, la acidificación que se muestra en la *upper North Atlantic Deep Water* está fuertemente ligada a la desoxigenación y los mayores incrementos de [$C_{ant}$] son más importantes en general en la *South Atlantic Central Water*.

Por otro lado, y aprovechando que la región de la Cuenca Ibérica ha sido objeto de muestreos repetidos en diferentes años, se ha planteado la estima de las [$C_{ant}$] con sus correspondientes tasas de almacenamiento en un período de casi dos décadas. Para ello se

emplean las medidas de $A_T$, $C_T$, pH y nutrientes disponibles de la campaña CAIBOX 2009, junto con los de OACES 1993, CHAOS1998 y OACES 2003. Para las estimaciones de $C_{ant}$ se utilizan las técnicas de *back-calculation* $\varphi C_T^o$ y TrOCA. Al igual que en la región Atlántica Ecuatorial, se divide la columna de agua en seis capas de densidad atendiendo a la distribución termohalina de la Cuenca Ibérica. Los almacenamientos de $C_{ant}$ obtenidos para la columna de agua se comparan con otros trabajos cuyas zonas de estudio son próximas a la Cuenca Ibérica. Por otro lado, se estiman también la tasa de almacenamiento de $C_{ant}$ desde 1993 a 2009, que comparando estos resultados con los de Ríos et al., (2001), se observa un incremento de la captación de $C_{ant}$ en los primeros 2000m de profundidad.

# I. Introducción / *Introduction*

# 1. Introducción

El dióxido de carbono ($CO_2$) es un gas incoloro, denso y poco reactivo cuyas moléculas están compuestas por dos átomos de oxígeno y uno de carbono (Figura 1). Después del vapor de agua, es el segundo gas más importante de los gases del efecto invernadero (Greenhouse Gas, GHG) aunque no es un gas contaminante en sí mismo. Estos GHG gases han estado presentes en la atmósfera en cantidades muy reducidas durante la mayor parte de la historia de la Tierra, siendo los que desarrollan el llamado efecto invernadero, proceso por el cual ciertos gases de la atmósfera retienen gran parte de la radiación infrarroja emitida por la Tierra y la remiten de nuevo a la superficie terrestre calentando la misma. Sin esta irradiación, la Tierra alcanzaría temperaturas de -18ºC (33ºC menos que actualmente) lo que haría la vida en la Tierra inviable. El $CO_2$ y el vapor de agua están presentes en la atmósfera de manera natural, aunque su concentración puede verse modificada por la actividad humana. Con el comienzo de la Revolución industrial en el siglo XVIII, la humanidad ha emitido grandes cantidades de $CO_2$ a la atmósfera, principalmente como resultado de la quema de combustibles fósiles o el cambio en el uso de la tierra (Le Quéré et al., 2009; Sabine et al., 2004). Debido a ello la concentración de $CO_2$ en la atmósfera, que inicialmente era de 280 ppm, ha ido aumentando progresivamente hasta la actualidad. En 1958, el Dr. Charles

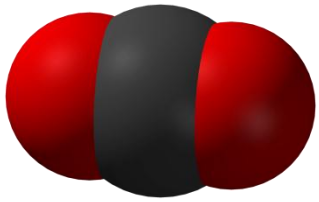

Figura 1. Molécula de $CO_2$

Keeling empezó a hacer medidas directas de $CO_2$ atmosférico en el observatorio Mauna Loa (Hawaii), siendo estas mediciones la primera evidencia significativa del rápido aumento de $CO_2$ en la atmósfera (Keeling, 1960). Estos datos se han ido recogiendo en la *Curva de Keeling* donde se muestra el continuo crecimiento de $CO_2$ (ppm) en la atmósfera desde 1958 (Figura 2). Los datos más recientes del Observatorio de Mauna Loa (Hawaii) indican una concentración de $CO_2$ atmosférico de 391 ppm en octubre de 2012 (Trans and Keeling, 2012).

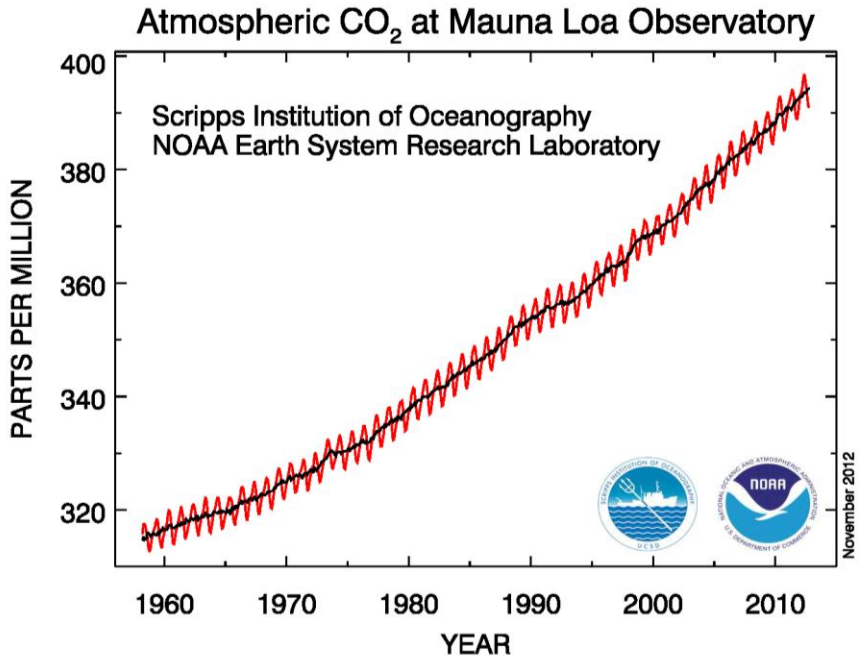


**Figura 2 Curva de Keeling. Media mensual de la concentración atmosférica de $CO_2$ desde 1958. La línea roja representa medias mensuales de medidas de las concentraciones de $CO_2$, mientras que la línea negra representa las mismas mediciones pero restándole el efecto del ciclo estacional.**

Durante el siglo XX la energía producida por la quema de combustibles fósiles supuso un 80% de las emisiones de $CO_2$. Destacan los resultados de un estudio reciente en el que se ha observado que dichas emisiones han aumentado un 29% entre 2000 y 2008 y un 41% respecto a las emisiones de 1990, emitiéndose a la atmósfera 7.7 GtC/año. El cambio del uso de la tierra es la segunda mayor fuente de emisiones de $CO_2$ debido principalmente a la deforestación y las industrias madereras y supone aproximadamente una emisión de 1.1 GtC/año (Le Quéré et al., 2009). Hasta hace poco se pensaba que, en varios siglos, el océano era capaz de retirar entre el 70 y el 80 % del $CO_2$ antropogénico ($C_{ant}$) de la atmósfera (Sabine and Tanhua, 2010). Sin embargo, estudios recientes han demostrado que sólo aproximadamente el 55% del $CO_2$ emitido es transferido de la atmósfera al océano y a la tierra (Ballantyne et al., 2012; Le Quéré et al., 2009). Como promedio, desde 1959 hasta 2008, sólo el 43% de las emisiones han permanecido en la atmósfera, y el restante 57 % se reparte casi a partes iguales entre el océano y la tierra, almacenando 2.3 y 2.4 GtC/año, respectivamente. En la figura 3 se pueden ver todas estas aportaciones al cómputo global de $CO_2$ (Canadell and Shobhakar, 2001).

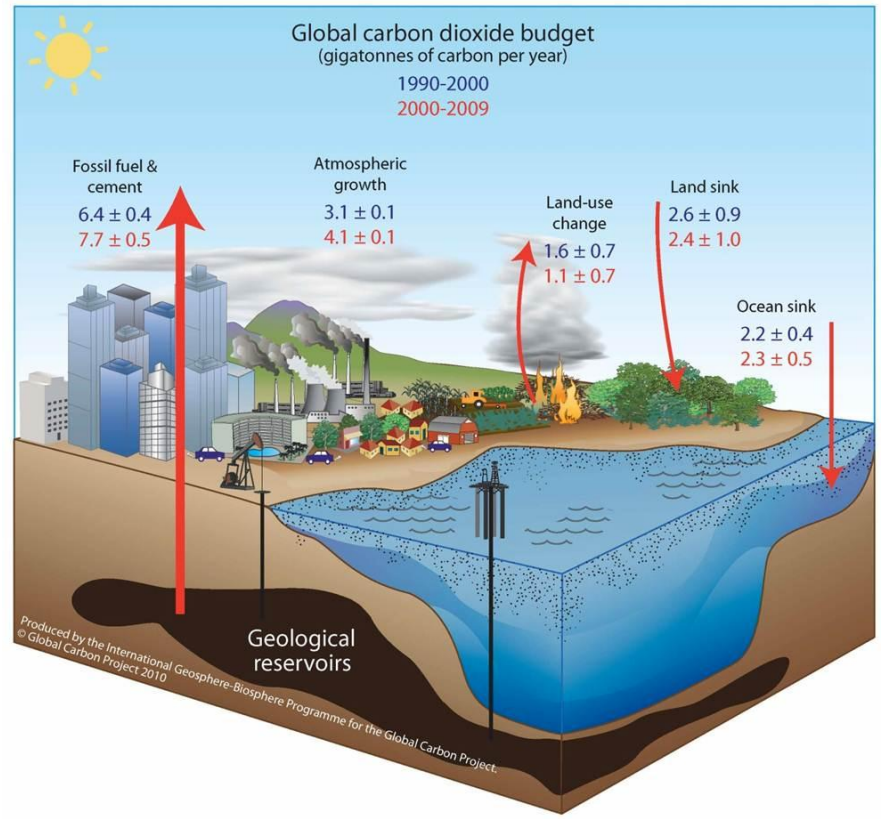


**Figura 3 Cómputo general de $CO_2$ emitido a la atmósfera y captado tanto por la tierra como por el océano (1 GtC = $10^{15}$ g C, 1 Kg C = 3.67 Kg $CO_2$).**

El océano juega un papel muy importante en la captura de $C_{ant}$ emitido a la atmósfera, dado que durante los últimos 200 años ha sido un sumidero neto de $CO_2$ (Gruber et al., 2009). Esta disolución de $C_{ant}$ trae graves consecuencias para el océano debido a que el agua de mar se acidifica, o se hace menos básica (disminución del pH). Este proceso es el llamado *Acidificación Oceánica* (Feely et al., 2009). Como se puede ver en la figura 4, a medida que el $CO_2$ atmosférico aumenta, el contenido de $CO_2$ disuelto en aguas superficiales indicado a través de su presión parcial ($pCO_2$),

aumenta proporcionalmente, pero el pH del agua de mar disminuye de forma rápida y similar.

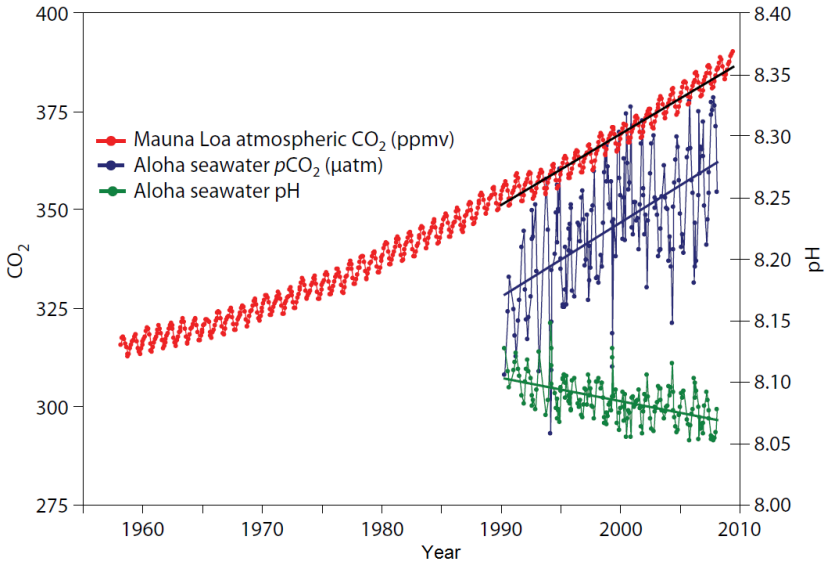


**Figura 4 Relación proporcional entre el aumento de $CO_2$ atmosférico (línea roja) el $CO_2$ disuelto en la superficie oceánica ($pCO_2$) y con la disminución del pH del agua de mar.**

De hecho, de acuerdo con modelos de reconstrucción de las condiciones pasadas, el pH de la superficie oceánica ha disminuido alrededor de 0.1 unidades desde la era preindustrial, bajando de ~8.2 hasta el presente ~8.1 (Orr et al., 2005). Algunos estudios recientes demuestran que la captación actual de $CO_2$ por parte del océano superficial y su consiguiente acidificación ocurren unas 100 veces más rápido que durante el final de la última glaciación (hace 20000 años) (Laffoley and Baxter, 2010).

Además de la acidificación, el aumento del $CO_2$ atmosférico trae consigo otro problema al océano, la desoxigenación. (Gruber,

2011). La desoxigenación es el proceso por el cual el oxígeno disuelto ($O_2$) del agua de mar reduce su concentración hasta un punto donde se vuelve perjudicial para los organismos acuáticos que viven en el sistema, debido a que el $O_2$ afecta a procesos biogeoquímicos marinos (Keeling et al., 2010). Tanto la desoxigenación como la acidificación se producen en el océano global, aunque con marcadas diferencias regionales. Por ejemplo, los impactos de la acidificación de los océanos tienden a ser más fuertes en las latitudes altas, mientras que las regiones de latitudes intermedias o bajas son más vulnerables a la desoxigenación del océano.

## 1.1 Ciclo del carbono en el océano.

El ciclo del carbono (C) en el océano está regulado por procesos físicos y biológicos. La bomba de solubilidad o bomba física es la que controla la distribución del carbono inorgánico disuelto ($C_T$) en el océano y la captación de $CO_2$. De los procesos biológicos como la fotosíntesis, la respiración y/o la remineralización de la materia orgánica se encarga la bomba biológica o la bomba de tejidos blandos, y de la disolución y formación de partículas de carbonato, la bomba de carbonato ($CaCO_3$) (Gruber et al., 1996).

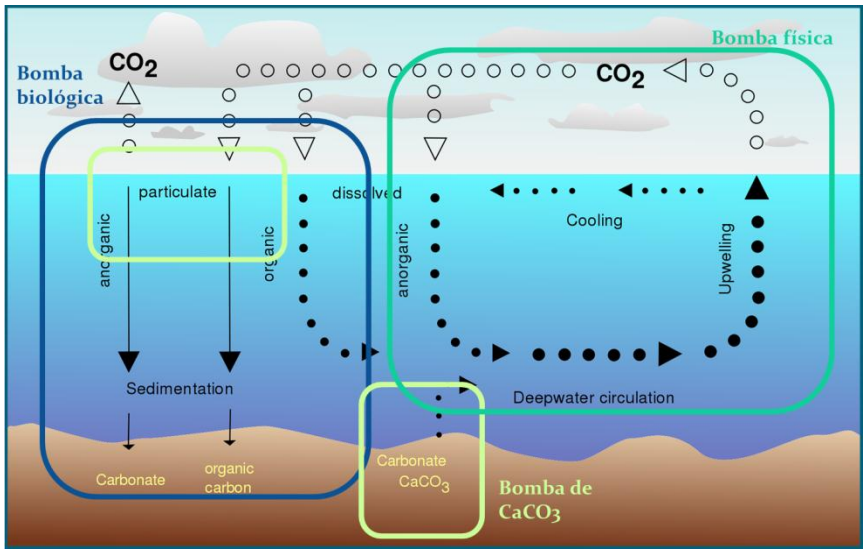


**Figura 5 La bomba física, la bomba biológica y la bomba de $CaCO_3$. Procesos implicados en el ciclo del carbono.**

- La **bomba física** es la responsable del intercambio de $CO_2$ en la interfase atmósfera-océano debido a la solubilidad del $CO_2$, y regula también el proceso inducido por la circulación termohalina que transporta dicho $CO_2$ al océano profundo. La circulación termohalina oceánica conecta todos los océanos como si fuese una gran cinta transportadora (Figura 6). Aguas saladas y cálidas alcanzan altas latitudes en el Atlántico Norte que, en invierno, se enfrían y se hunden, por pérdida de flotabilidad, a grandes profundidades en el proceso conocido como formación de aguas profundas. En el momento de la formación de las aguas profundas, éstas

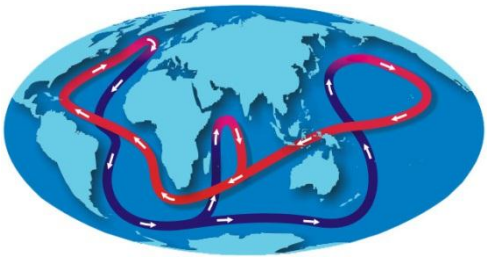

**Figura 6 Esquema de la Circulación termohalina**

captan $CO_2$ por el efecto de la solubilidad y comienzan su recorrido hacia el sur donde se unirán a las aguas frías profundas recién formadas en la Antártica. Entonces, este flujo de agua profunda accede a los océanos Índico y Pacífico dirigiéndose hacia el norte en cada uno de ellos. Una vez en superficie las aguas del Índico y Pacífico norte retornan al Atlántico por el Cabo de Buena Esperanza, alcanzando de nuevo el Atlántico Norte donde se enfriará, hundirá y comenzará de nuevo el ciclo de la cinta. Cada ciclo completo de la cinta transportadora lleva unos 1000 años.

- La **bomba biológica** consiste en la transformación del carbono inorgánico disuelto de la superficie del océano en material orgánico en sedimentación, creando un flujo de carbono orgánico hacia el mar profundo. En ella están involucrados los procesos de fotosíntesis, alimentación, respiración y descomposición de los organismos vivos de la capa fótica. El fitoplancton absorbe el $CO_2$ disuelto para sintetizar materia orgánica, alimento básico para la cadena trófica, que pone en marcha el ciclo de la vida. Los restos de los organismos muertos, materia orgánica, son transportados hacia las capas más profundas de los océanos por sedimentación, donde se oxidan y se descomponen. Una parte de esta materia orgánica alcanza el lecho marino incorporándose a los sedimentos.

- La **bomba de $CaCO_3$**, por el contrario, en las capas superficiales, libera $CO_2$ a través de algunos organismos como los cocolitofóridos o foraminíferos, que necesitan sintetizar $CaCO_3$ para sus esqueletos y conchas consumiendo iones de carbonato. Este $CaCO_3$ se encuentra principalmente en forma de calcita y aragonito. El $CaCO_3$ se precipita durante la fotosíntesis y se hunde hacia el fondo junto con el carbono orgánico exportado. Durante el proceso de calcificación disminuye la alcalinidad total ($A_T$) porque se están consumiendo iones bicarbonato, mientras que en la disolución de $CaCO_3$ aumenta $A_T$.

No podemos entender el ciclo del carbono sin tener en cuenta el ciclo del oxígeno ($O_2$) en el océano. El $O_2$ se disuelve en el océano de modo que entra directamente en los procesos de fotosíntesis, respiración y oxidación de la bomba biológica. Los cambios en la [$O_2$] son diagnósticos de cambios en la eficiencia de la bomba biológica, que puede influir, por ejemplo, en la velocidad a la que los océanos absorben $C_{ant}$ (Keeling and Garcia, 2002). En latitudes medias y altas durante la primavera y el verano, cuando la capa superior del océano se calienta por contacto con la atmósfera, los océanos son una fuente de $O_2$ a la atmósfera, mientras que en otoño e invierno, cuando la capa superior del océano se enfría, los océanos son un sumidero de $O_2$ desde la atmósfera. Estos intercambios estacionales aire-mar de $O_2$ se ven impulsados, en parte por los intercambios biológicos vinculados a la estratificación estacional, el suministro de nutrientes y la irradiación, y en parte, por los efectos de la solubilidad del $O_2$ (Keeling et al., 2010).

Además, los ciclos de C y $O_2$ están íntimamente relacionados con los ciclos del nitrógeno (N) y del fósforo (P) debido a que las variaciones de $O_2$, $CO_2$ y nutrientes ocurren durante la fotosíntesis y la mineralización de materia orgánica particulada. En 1934, Redfield señaló que las proporciones de C, N y P permanecían constantes en el fitoplancton siguiendo la relación C:N:P = 106:16:1. En 1963 calculó el $O_2$ producido o consumido durante la síntesis o mineralización de la materia orgánica, obteniendo la relación $-\Delta O_2{:}\Delta C{:}\Delta N{:}\Delta P$ = 138:106:16:1. Estas relaciones salen del balance fotosíntesis – mineralización:

$$C_{106}H_{171}O_{42}N_{16}P + 149O_2 + 124OH^- \rightarrow 106CO_3H^- + 16NO_3^- + PO_4H^{2-} + 94H_2O$$

La estequiometria que se muestra en la reacción anterior corresponde a las mejoras de estas relaciones empíricas propuestas por Fraga et al., (1998): $-\Delta O_2{:}\Delta C{:}\Delta N{:}\Delta P$ = 149:106:16:1.

## 1.2 El sistema del $CO_2$ en agua de mar.

Debido a la alta solubilidad del $CO_2$, éste se disuelve en el agua de mar produciendo ácido carbónico ($H_2CO_3$), que por inmediata disociación da lugar a iones bicarbonato ($HCO_3^-$) y carbonato ($CO_3^{2-}$). Las reacciones implicadas en el sistema del carbonato son:

$$CO_2(g) \overset{K_o}{\leftrightarrow} CO_2(aq)$$

$$CO_2(aq) + H_2O \leftrightarrow H_2CO_3$$

$$H_2CO_3 \overset{K_1^*}{\leftrightarrow} H^+ + HCO_3^-$$

$$HCO_3^- \overset{K_2^*}{\leftrightarrow} H^+ + CO_3^{2-}$$

$$Ca^{2+} + CO_3^{2-} \overset{K_{sp}}{\leftrightarrow} CaCO_3$$

Donde $K_0$ es la constante de solubilidad y $K_1^*$ y $K_2^*$ son la primera y segunda constantes del equilibrio de disociación del ácido carbónico, respectivamente, y $K_{sp}$ es la constante de solubilidad del carbonato cálcico.

Típicamente, el sistema del carbonato en el agua de mar o sistema de $CO_2$ se ha caracterizado por cuatro variables medibles analíticamente: fugacidad de $CO_2$ ($fCO_2$), carbono inorgánico total disuelto ($C_T$), alcalinidad total ($A_T$), y pH. Gracias al reciente método para medir $CO_3^{2-}$ (Byrne and Yao, 2008) se puede considerar una quinta variable del sistema del carbonato. Es importante destacar que conociendo dos variables del sistema del $CO_2$ es posible conocer las otras usando las ecuaciones termodinámicas del sistema.

La presión parcial del dióxido de carbono (***p*CO₂**) en el agua de mar viene dada por la ley de Henry:

$$pCO_2 = K_0[CO_2]_{aq}$$

Dado el comportamiento no ideal del $CO_2$, se debe usar la fugacidad del $CO_2$ en lugar de la presión parcial ($fCO_2 = f \cdot pCO_2$). Sin

embargo $f$ = 0.997 a 25 ºC, por lo que se suele asumir que el $CO_2$ se comporta como un gas ideal, y por tanto $fCO_2 \approx pCO_2$.

El $\mathbf{C_T}$ se define como la suma de las formas disueltas de $CO_2$:

$$C_T = [CO_2] + [HCO_3^-] + [CO_3^{2-}]$$

La contribución relativa de cada una de las especies es 90:9:1 para $[HCO_3^-]$, $[CO_3^{2-}]$ y $[CO_2]$ respectivamente. Por esto, el $CO_2$ que se ve envuelto en el intercambio agua – atmósfera es una parte minoritaria del $C_T$ total.

La alcalinidad es la variable del sistema del carbonato más difícil de definir. De una forma sencilla, **alcalinidad** es la capacidad del agua para neutralizar ácidos o aceptar protones. Ésta representa la suma de las bases que pueden ser valoradas en una muestra de agua. Dado que la alcalinidad de aguas superficiales está determinada generalmente por el contenido de carbonatos, bicarbonatos e hidróxidos, ésta se toma como un indicador de dichas especies iónicas. No obstante, la presencia de algunas sales de ácidos débiles como boratos, silicatos, nitratos y fosfatos puede también contribuir a la alcalinidad. Estos iones negativos en solución están comúnmente asociados o pareados con iones positivos de calcio, magnesio, potasio, sodio y otros cationes. El bicarbonato constituye la forma química de mayor contribución a la alcalinidad. Según Dickson et. al. (2007b), una rigurosa definición de alcalinidad sería: el número de moles de iones $H^+$ equivalente al exceso de protones aceptores (bases de ácidos débiles con $K < 10^{-4.5}$ a 25ºC y fuerza

iónica 0) sobre protones dadores (ácidos con $K > 10^{-4.5}$) en 1 kg de muestra. La expresión de la alcalinidad total ($\mathbf{A_T}$) siguiendo sus recomendaciones sería:

$$A_T = [HCO_3^-] + 2[CO_3^{2-}] + [B(OH)_4^-] + [OH^-] + [HPO_4^{2-}] + 2[PO_4^{3-}] + [SiO(OH)_3] + [NH_3] + [HS^-] + [H^+]_F - [HSO_4^-] - [HF] - [H_3PO_4]$$

Donde la alcalinidad debida al carbonato ($A_C$) es $A_C = [HCO_3^-] + 2[CO_3^{2-}]$. Tanto $C_T$ como $A_T$ se expresan en $\mu mol \cdot kg^{-1}$.

El sistema del carbonato es el tampón natural para el pH. En la actualidad existen cuatro escalas de pH en agua de mar que difieren en la naturaleza de las disoluciones reguladoras usadas para la calibración (principalmente en sulfato y fluoruro):

- La escala NBS (National Bureau Scale) que está definida por una serie de disoluciones tampón estándar con valores de pH cercanos a los pH reales de agua de mar ($pH_{NBS} \approx pH_a$): $pH_a = -\log a_{H+}$ donde *a* es la actividad de los iones hidrógeno.

- Escala "Free":$pH_F = -\log[H^+]_F$

- La escala "Total Ion Hidrógeno": $pH_T = -\log([H^+]_F + [HSO_4^-]) = -\log [H^+]_T$

- Escala "Agua de Mar" (SWS): $pH_{sws} = -\log([H^+)_F + [HSO_4^-] + [HF]) = -\log[H^+]_{sws}$

Las disoluciones usadas en la escala "NBS" tienen una fuerza iónica más baja que la del agua de mar, y por ello, no se recomienda su

uso en la caracterización del pH de agua de mar (Zeebe and Wolf-Gladrow, 2001). Sin embargo, en la medida de $pH_T$ se resuelve el problema de las diferencias de fuerza iónica entre muestras y tampón, por ello es la escala de pH más usada en la actualidad (Dickson et al., 2007b).

En el gráfico de Bjerrum [figura 7 (Barker and Ridgwell, 2012)] se muestran las proporciones relativas de $[HCO_3^-]$, $[CO_3^{2-}]$ y $[CO_2]$ en agua de mar respecto a valores determinados de salinidad, temperatura y presión (líneas gruesas, S = 35 psu, T = 25 ºC, P = 0 bares, líneas finas S = 35 psu, T = 0 ºC, P = 0 bares y líneas discontinuas S = 35 psu, T = 0 ºC, P = 300 bar). La región sombreada muestra el rango de pH del océano actual.

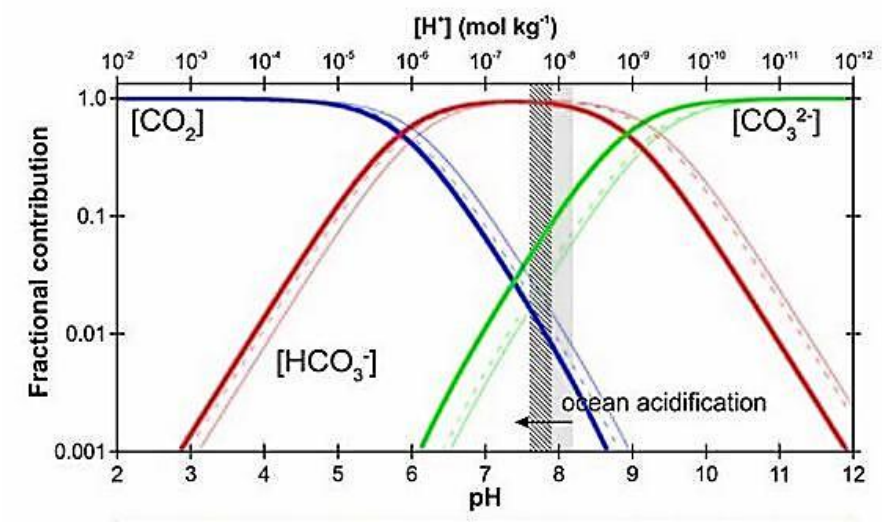


**Figura 7 Gráfico de Bjerrum donde se muestra el sistema del carbonato en función del pH.**

En este gráfico, el pH de los puntos de corte entre las diferentes especies viene dado por $pK_1^*$ y $pK_2^*$, por lo tanto, es importante tener bien definidas las constantes de disociación, $K_1^*$ y $K_2^*$.

Desde principios del siglo XX, diferentes autores han medido estas constantes de disociación (Buch et al., 1932; Dickson yMillero, 1987; Goyet y Poisson, 1989; Hansson, 1973; Lueker et al., 2000; Lyman, 1956; Mehrbach et al., 1973; Millero, 2010; Millero et al., 2006; Roy et al., 1993). Durante este período, las constantes de Mehrbach et al., (1973), calculadas en agua de mar natural, fueron las más mencionadas y sirvieron de base para futuros trabajos. De hecho, el reajuste de Dickson y Millero (1987) se convirtió en el más recomendado para su uso durante los noventa en la *Global* $CO_2$ *Survey* (Lee et al., 2000). Las constantes de disociación estimadas en agua de mar sintética por Goyet y Poisson (1989) son consistentes con las de Roy et al., (1993), dado que se obtienen resultados similares cuando ambos pares de constantes se utilizan para determinar la coherencia interna del sistema de carbonato (Lee y Millero, 1995; Lee et al, 1996, 1997; Millero et al, 1993). A principios del siglo XXI, Lueker et al., (2000) reformularon las constantes de Mehrbach et al., (1973) para tratar de mejorarlas y para calcular $pK_1^*$ y $pK_2^*$ en agua natural y escala total de iones de hidrógeno. Más tarde, Millero et al., (2002) determinaron nuevas $pK_1^*$ y $pK_2^*$ a partir de medidas en los océanos Atlántico, Índico, Antártico y Pacífico, que concordaban con las de Mehrbach et al., (1973). También evaluaron sus nuevas constantes con las obtenidas por Lueker et al., (2000) a $fCO_2$ bajas. En el mismo año, Mojica Prieto y Millero (2002) propusieron otro conjunto de constantes de

agua de mar natural, y demostraron que la diferencia entre $pK_1^*$ y $pK_2^*$ en agua de mar artificial y real está principalmente relacionada con la interacción de pares iónicos de bicarbonato y boro. Estos logros fueron considerados por Millero et al., (2006), quienes desarrollaron un conjunto de ecuaciones válidas para valores de salinidad de 0 a 50 y temperatura de 0 a 50 ºC para las aguas estuáricas y marinas. El conjunto más reciente de constantes está descrito en Millero (2010), pero sólo se ajusta a estuarios. En esta tesis se han seleccionado cuatro pares de constantes de disociación: Mehrbach et al., (1973) reajustadas por Dickson y Millero (1987), Goyet y Poisson (1989), Lueker et al., (2000) y Millero et al., (2006), cuyos valores a 25ºC de temperatura y salinidad 35 se dan en la tabla 1.

Tabla 1 Constantes de disociación

| Autor | $pK_1^*$ | $pK_2^*$ |
|---|---|---|
| Dickson y Millero (1987) | 5.8457 | 8.9454 |
| Goyet y Poisson (1989) | 5.8487 | 8.9189 |
| Lueker et al., (2000) | 5.8471 | 8.9659 |
| Millero et al., (2006) | 5.8401 | 8.9636 |

Además, en las ecuaciones termodinámicas del sistema del carbono inorgánico se necesitan otras constantes, la constante de hidrólisis de Millero (1995), la constante de disociación del ácido bórico (Dickson, 1990b) y del ión bisulfato ($HSO_4^-$) (Dickson, 1990a). La constante de formación del ión fluoruro ($F^-$) se toma de Dickson y Riley (1979) y el cociente universal B/Cl de Lee et al. (2010).

## 1.3 Bases de datos globales

En la actualidad, debido a la captura de $C_{ant}$ por el océano, la acidificación de los océanos es más rápida que en cualquier otro momento de los últimos siglos (Pelejero et al, 2010), afectando también al estado de saturación de aragonito y calcita (Doney et al, 2009, Riebesell et al., 2010). Con el fin de evaluar los cambios recientes en el sistema del carbonato a través de observaciones, sería ventajosa la inclusión de todas las variables medibles del sistema del carbonato ($A_T$, $C_T$, pH, *f*CO2), junto con las últimas mejoras termodinámicas (las nuevas constantes de disociación) y los cambios recientes en el cociente boro- cloro (B / Cl) (Lee et al., 2010) para la modernización de las bases de datos globales.

Durante la década de 1990, se han llevado a cabo los programas internacionales de investigación oceánica, *World Ocean Circulation Experiment* (WOCE), *Joint Global Ocean Flux Study* (JGOFS) y *Ocean-Atmosphere Carbon Exchange Study* (OACES), en los que conjuntamente se realizaron estudios exhaustivos del sistema de carbono. Gracias a los esfuerzos de colaboración entre científicos de diferentes países, todos los datos de las campañas desarrolladas en estos proyectos se fusionaron en una base de datos global y completamente calibrada: GLODAP (*Global Ocean Project Data Analysis*), donde fueron divididos por océanos (Key et al, 2004). Esta base de datos es pública y está disponible en la web GLODAP

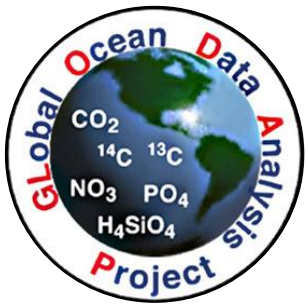

Figura 8 Logo de GLODAP

dentro del *Carbon Dioxide Information Analisis Center* (CDIAC). Entre los objetivos generales de GLODAP cabe destacar la obtención de las distribuciones de algunas variables del sistema de carbono ($A_T$, $C_T$, $pCO_2$), que posibilitan la estimación de los cambios de carbono natural y antropogénico, además de evaluar su inventario (Key et al., 2004).

Años después, CARINA (*Carbon Dioxide in the Atlantic Ocean*) (Key et al., 2010) amplió la cobertura de GLODAP considerando la gran cantidad de campañas oceanográficas, tanto históricas como recientes, realizadas en el Océano Atlántico y los océanos Ártico y Antártico. A pesar de que muchos de los procedimientos que se utilizan durante CARINA fueron adoptados de GLODAP, CARINA ha incluido mejoras importantes en sus productos, tales como la recopilación de datos de pH. Los productos CARINA además de gran cantidad de información de apoyo están disponibles en el sitio web CARINA, también dentro del CDIAC.

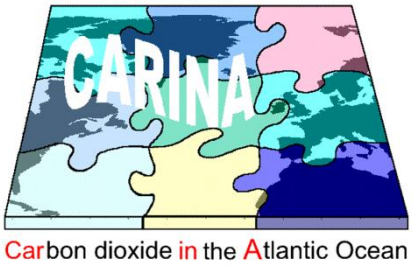

Figura 9 Logo de CARINA

Uno de los puntos clave de ambas bases de datos fue la extensa calibración y los procedimientos de control de calidad que fueron diseñados para corregir los sesgos de medición y para eliminar los datos erróneos. El sesgo asumido por ambas bases de datos GLODAP y CARINA para estos parámetros de carbono fueron ± 0.005 unidades de pH, ± 6 µmol·kg$^{-1}$ de $C_T$ y ± 4 µmol·kg$^{-1}$ de $A_T$ (Key et al., 2004 y Key et al., 2010).

Actualmente se ha creado GLODAPv2 (Informe IOCCP Número 24, 2011), un esfuerzo de colaboración en el que se fusionarán tres bases de datos globales, GLODAP, CARINA y PACIFICA (Pacific Carbon, Ishii et al., 2011), además de las campañas más recientes del programa CLIVAR (*Climate variability and predictability*) detalladas en la web GO-SHIP. De este modo habrá muchos más datos del sistema de carbonato que estarán disponibles, e incluso se podrán reconsiderar o recuperar datos que no se incluyeron en las anteriores versiones.

## 1.4 El Océano Atlántico

El Océano Atlántico se extiende desde el Océano Glacial Ártico, en el norte, hasta el Océano Antártico, en el sur y está dividido por la dorsal Atlántica. Es el segundo océano más extenso de la Tierra después del Océano Pacífico y ocupa el 20% de la superficie del planeta, y el 26% del total de tierras sumergidas. Es además el océano más joven del planeta. El Océano Atlántico juega un papel de importancia global en lo referente al clima, ya que de sus corrientes depende en buena medida el clima de los continentes ribereños.

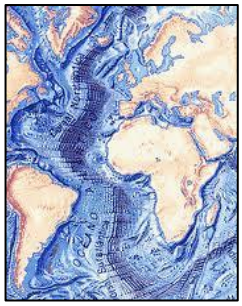

Figura 10. Fondo oceánico del Atlántico

Particularmente, la importancia del Atlántico Norte radica en que es una región de formación de masas de agua profundas, encargadas de impulsar en gran parte la Circulación Meridional Oceánica

(MOC en inglés) o circulación termohalina (Rosón et al., 2003). Concretamente, en altas latitudes del Atlántico Norte, la *North Atlantic Deep Water* (NADW) se forma en una amplia zona situada entre el Mar de Labrador y el Mar de Groenlandia. En realidad es el resultado de la mezcla de tres masas de agua, una formada por hundimiento en el Mar de Labrador (*Labrador Sea Water*, LSW) y las otras dos resultado de flujos de desbordamiento desde los mares Árticos a través de los estrechos batimétricos de Islandia y Dinamarca (*Iceland-Scotland Overflow Water* (ISOW) y *Denmark Straight Overflow Water*). Una vez formada, esta masa se extiende desde las cercanías del sur de Groenlandia alcanzando unas profundidades de entre 2000 y 4000 metros, surca el Atlántico hacia el sureste y alcanza Brasil, donde vuelve a girar hacia el este para desembocar en las costas de África Meridional y unirse a las corrientes de agua circumpolares Antárticas. Otra masa de agua característica del Atlántico Norte es la *Mediterranean Water* (MW). La MW se forma a partir de un conjunto de masas de agua que se forman, tanto en el Mar Mediterráneo oriental como en el Golfo de León, por el enfriamiento de las aguas intensamente salinas y densas. La MW sale del Mar Mediterráneo por rebosamiento por el Estrecho de Gibraltar, produciéndose una intensa mezcla con las Aguas Centrales del Atlántico Norte que la lleva a situarse a unos 1200m en la columna de agua. En la figura 11 se muestra un esquema muy general de la formación de estas masas de agua y su situación en la columna de agua. Las aguas cálidas están representadas por las flechas rojas, mientras que las aguas intermedias profundas vienen indicadas por las flechas azules. En

esta figura, además de la NADW y la MW, se puede ver también como las masas de agua intermedias y frías, *Antarctic Intermediate Water* (AAIW) y *Antartic Bottom Water* (AABW) respectivamente, circulan hacia el norte con menor y mayor densidad que la NADW, respectivamente.

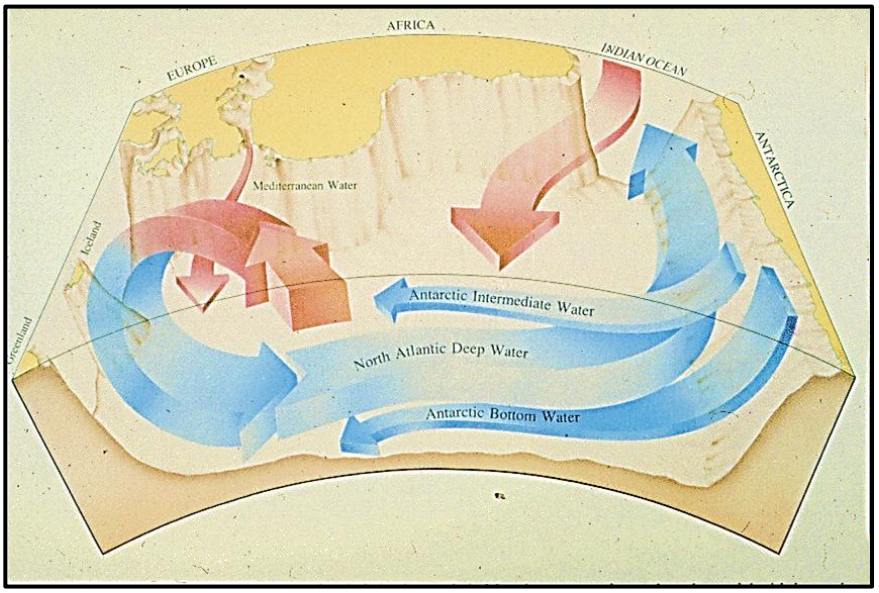


**Figura 11 Esquema de la rama de la Meridional Overturning Circulation (MOC) en el Atlántico Norte.**

La MOC lleva aguas superficiales cálidas y salinas hasta altas latitudes del océano norte y las devuelve hacia el sur a través del ecuador como aguas frías y profundas (Bryden et al., 2005). Asociado al movimiento de estas masas de agua, hay un transporte, también hacia el sur, de $CO_2$ natural, $O_2$ y nutrientes asociado a la rama del Atlántico Norte de la MOC (Álvarez et al., 2003). Además hay que sumar el hecho de que el Océano Atlántico subtropical es la zona en la que se produce el mayor transporte de calor hacia el norte

(Bryden et al., 1996) por lo que hace una contribución sustancial al clima cálido y moderado de Europa.

Considerando que el $CO_2$ captado a través de la superficie del océano, penetra en el océano interior y se acumula en la columna de agua, cabe destacar que en el Océano Atlántico se obtienen altos flujos de captación y cantidades relativamente grandes de acumulación. En concreto, en términos de almacenamiento de $C_{ant}$ destaca el hecho de que, a pesar de que el Océano Atlántico cubre solamente el 15% del área global del océano, almacena el 23% del $C_{ant}$ oceánico total (Sabine et al., 2004).

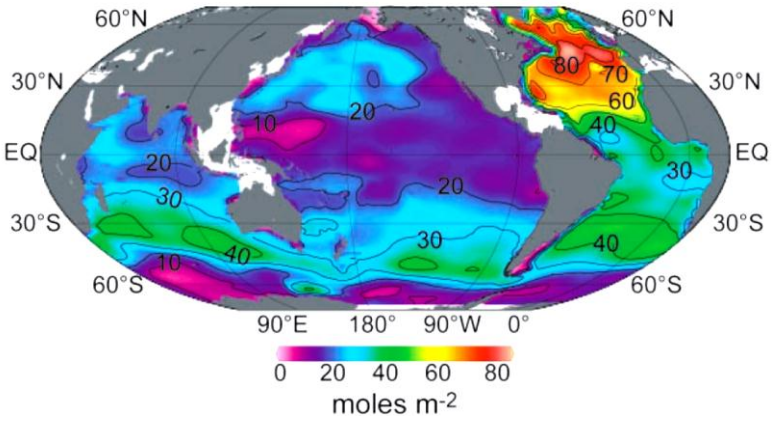


Figura 12 Inventario de $C_{ant}$ en columna de agua en mol/$m^2$

En cuanto a la desoxigenación, tanto datos históricos como modelos climáticos muestran que ésta ha sido intensa en el Atlántico tropical (Stramma et al., 2008) y que, en concreto, la región del Océano Atlántico ecuatorial occidental es una de las áreas con alta vulnerabilidad respecto a la desoxigenación (Gruber, 2011).

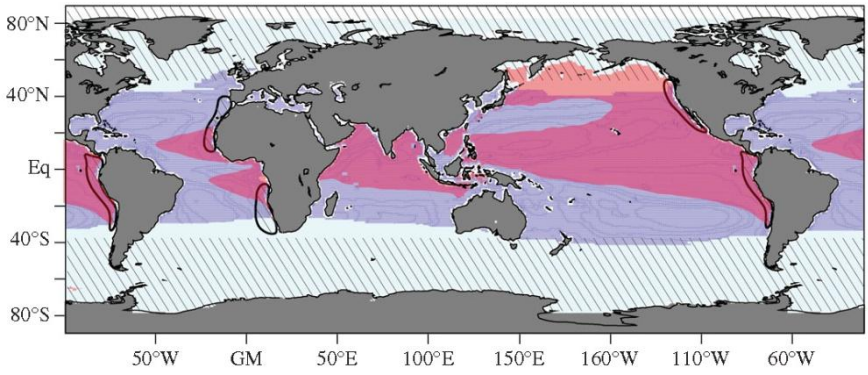


**Figura 13. Zonas oceánicas con vulnerabilidad para la desoxigenación (zonas sombreadas en rosa)**

Por todo ello, se ha intensificado el número de expediciones en el Atlántico Norte y así intentar estudiar en más detalle, no sólo todo lo relacionado con los ciclos biogeoquímicos y la posible alteración de los mismos, sino también para evaluar procesos físicos, como las corrientes, transportes y tasas de formación de las masas de agua. El planteamiento de repetir determinadas secciones a través de los años tiene la intención de poder estudiar los patrones y/o cambios de la circulación y transporte, no sólo de las masas de agua del Atlántico Norte, sino también de las variables biogeoquímicas más relevantes. Poder establecer esta variación temporal permitirá un mayor conocimiento de las relaciones océano–atmósfera en el Atlántico Norte y el descubrimiento de alteraciones en los ciclos biogeoquímicos y sus consecuencias futuras. Como ejemplo de la cantidad de campañas oceanográficas que se han venido desarrollando, en la figura 14 se muestra el mapa del Océano Atlántico Norte con las campañas que están recogidas actualmente en CARINA.

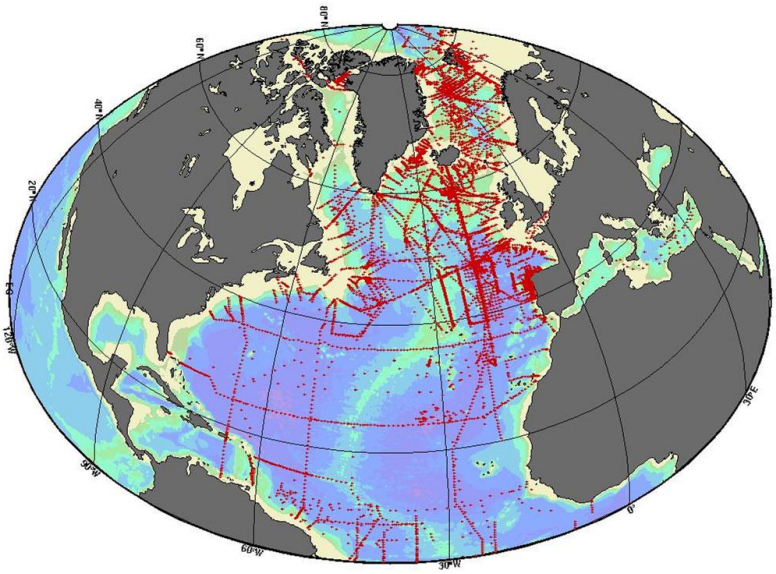

**Figura 14 Mapa del Océano Atlántico Norte con las campañas oceanográficas recogidas en CARINA database.**

Pero, realmente, estas no son todas las campañas disponibles. Cada grupo de investigación tiene un tiempo determinado para hacer públicos los datos de una campaña. De hecho, durante los últimos cuatro años, el Grupo de $CO_2$ del Instituto de Investigaciones Marinas de Vigo ha participado en varios proyectos, tanto nacionales como internacionales, que cubren un área importante del Océano Atlántico Norte y de los cuales se han obtenido los datos que se presentan en esta tesis. Estas expediciones son CAIBOX 2009, MOC$^2$Equatorial 2010, OVIDE 2010 y A24ºN 2011. Como breve resumen de estas secciones se dirá que CAIBOX 2009 se llevó a cabo a en la Cuenca Ibérica en verano de 2009 a bordo del B/O Sarmiento de Gamboa. El transecto total de ésta campaña está formado por una sección latitudinal frente a la costa de Vigo, seguido de una sección longitudinal a lo largo de los 20ºW y,

finalmente, una sección transversal que atravesó el estrecho entre Fuerteventura y Lanzarote, llegando hasta la costa africana. MOC$^2$Ecuatorial 2010 se llevó a cabo durante la primavera del 2010 bordo del BIO Hespérides cruzando el Océano Atlántico Ecuatorial desde Fortaleza (Brasil) hasta Mindelo (Cabo Verde). En su planteamiento se diseñó como una repetición de la campaña CITHER I en 1993 dentro del programa WOCE A06. OVIDE 2010 se llevó a cabo en verano de 2010 a bordo del N/O Thalassa. Su trayecto atravesó la cuenca europea desde Figueira da Foz (Portugal) a Groenlandia y cruzó la cordillera del Reykjanes. La sección OVIDE lleva repitiéndose desde 2002 cada dos años. El crucero A24N 2011 se llevó a cabo a lo largo de 24.5 º N en invierno del 2011 a bordo del B /O Sarmiento de Gamboa. Esta campaña se lleva realizando en el Océano Atlántico Subtropical cada seis años desde 1992 con medidas del sistema del carbonato. Esta campaña fue la octava etapa del programa de circunnavegación MALASPINA 2010 que pretendía repetir los pasos de Alessandro Malaspina (1754 - 1810), quien dirigió la primera expedición científica española de circunnavegación.

Considerando todo este abanico de campañas disponibles, los estudios descritos en esta tesis se han desarrollado en dos regiones del Océano Atlántico Norte, la cuenca ibérica y el Océano Atlántico Ecuatorial (Figura 15).

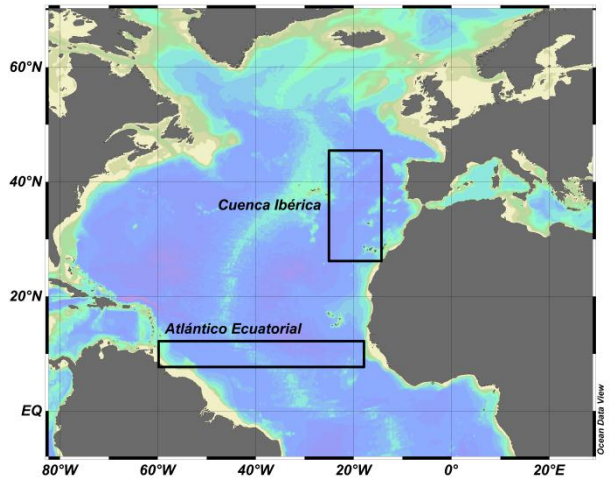


Figura 15 Regiones de estudio: Cuenca Ibérica y Océano Atlántico Ecuatorial.

### 1.4.1 La Cuenca ibérica

La región estudiada se localiza frente a la Península Ibérica y encierra el área desde 45ºN de latitud hasta las Islas Canarias (25ºN) y entre 20ºW y 8ºW de longitud. Esta zona se encuentra dentro del giro del Atlántico Norte, se conoce como "zona de inter-giro" (Pollard et al., 1996) y está encerrada entre la corriente del Atlántico Norte (45-53ºN) y la Corriente de Azores (34-35ºN, Péliz et al., 2005). La estructura termohalina vertical de esta región está claramente dominada en la capa superior por el *Madeira Mode Water* (MMW) (Álvarez et al., 2005), el *Eastern North Atlantic Central Water* (ENACW) con dos ramas diferenciadas, de origen subpolar ($ENACW_P$) y de origen subtropical ($ENACW_T$) (Ríos et al., 1992, Castro et al., 1998, Álvarez et al., 2005) y un pequeño porcentaje de agua Antártica (AA) (Ríos et al., 1992, Álvarez et al.,

2005). Entre las masas de agua intermedia y profunda es importante tener en cuenta la presencia de la MW (Fraga et al., 1982), que es el agua proveniente del Mar Mediterráneo y la más salina de la columna de agua. Las capas más profundas de la columna de agua están dominadas por la LSW (Castro et al., 1998), la *Northeast Atlantic Deep Water* (NEADW), que está dividida en dos componentes, uno superior ($NEADW_u$) y otro inferior ($NEADW_l$), y la ISOW, que se extiende por las capas inferiores (Álvarez et al., 2005).

### 1.4.2 El Océano Atlántico Ecuatorial

La región de estudio se extiende desde la Guayana Francesa hasta la costa de África, cruzando el Océano Atlántico Ecuatorial a través del paralelo 7.5 ºN. Esta sección está situada en un área cercana a la *InterTropical Convergence Zone* (ITCG) y junto a las corrientes zonales *North Equatorial Current* (NEC) y *South Equatorial Current* (SEC) (Stramma y Schott, 1999). Concretamente, en la Cuenca oeste, la sección está de dos a tres grados al norte de la *North Equatorial Under Current* (NEUC) (Arhan et al., 1998) mientras que en la cuenca oeste está dentro de la circulación ciclónica del Domo de Guinea (Brandt et al., 2010). La estructura termohalina vertical de esta región está claramente dominada por la *South Atlantic Central Water* (SACW) (Stramma y England, 1999; Stramma y Schott, 1999) y la *Subantartic Mode Water* (SAMW) en las capas superiores del océano. Las aguas intermedias están claramente dominadas por la presencia de la AAIW (Stramma y

England, 1999; Stramma y Schott, 1999). La NADW (Steinfeldt et al., 2007) hace notar su presencia por medio de dos ramas diferenciadas, la superior (uNADW) y la inferior (lNADW). El agua de mayor densidad es la AABW (Johnson, 2008), que se encuentra justo por debajo de la NADW (Rhein et al., 1998).

## 2. Planteamiento y Objetivos de la tesis

Como se ha visto, el ciclo del carbono en el océano se ve afectado por los cambios en el clima y, a su vez, la alteración del mismo provoca cambios en otros ciclos y/o variables biogeoquímicas, trayendo, todo ello, consecuencias nefastas para los ecosistemas oceánicos. En el sistema del carbonato intervienen diferentes variables ($fCO_2$, $C_T$, $A_T$ y pH), pero conociendo al menos dos de ellas se pueden determinar las otras dos. De las metodologías analíticas de medida de cada una de ellas se describe detalladamente en la subsección *2. Métodos de análisis de las variables del sistema del carbonato (pH, $A_T$, $C_T$ y $CO_3^{2-}$) y $O_2$* (dentro de II. Datos y métodos), pero cabe destacar aquí la importancia de que estas medidas sean precisas y exactas individualmente, para no arrastrar más que el error analítico de las medidas a los cálculos. De esta manera se consigue un sistema del carbono internamente consistente independientemente de que las variables del carbonato sean medidas o calculadas. Para ello, teniendo en cuenta los diferentes pares de constantes de disociación establecidos durante los últimos cuarenta años, se han seleccionado cuatro de ellos [Mehrbach et al., (1973) reajustadas por Dickson y Millero (1987), Goyet y Poisson (1989), Lueker et al., (2000) y Millero et al., (2006)] para evaluar la consistencia interna del sistema del carbonato. En la sección III. Resultados y Discusión, el ***Capítulo 1. Medidas del sistema del carbonato y consistencia interna en el Atlántico Norte*** se estudiará ampliamente la consistencia interna del

sistema del carbonato así como la inclusión de nuevos avances metodológicos que permitan mejorar las medidas de partida.

Una vez conocido en detalle el sistema del carbonato, el siguiente paso es hacer el control de calidad de esos datos. Para ello se cuenta con la experiencia demostrada durante la elaboración de las bases de datos globales GLODAP y CARINA. Durante la elaboración de CARINA, los cruceros con datos poco fiables o dudosos del sistema del carbonato que se habían descartado en GLODAP, no se reconsideraron, a pesar de que en CARINA se incluyó también el pH. Por ello, campañas como las WOCE A06 y A07 de 1993 no están disponibles ni en GLODAP ni en CARINA. Sin embargo, es posible descargar todos los datos del sistema del carbonato de la web de *CLIVAR and Carbon Hydrographic Data Office* (CCHDO). En la sección III. Resultados y Discusión, el ***Capítulo 2. Datos de carbono de las campañas WOCE A06 y A07***, trata sobre el uso combinado de las bases de datos GLODAP, CARINA y MOC$^2$Ecuatorial para evaluar y corregir el sesgo existente en los datos de pH tanto de la campaña A06 como de la A07. Además, al evaluarse de nuevo los datos de $A_T$ y $C_T$, se obtuvieron las mismas conclusiones que durante el control de calidad previo. Habiendo recuperado los datos de pH y considerando nuevas herramientas de cálculo, se ha fijado el objetivo de recuperar también los datos de $C_T$ y $A_T$ de A06 y A07, de modo que se obtenga una buena base de datos de 1993 para poder comparar con la sección repetida del 2010 (MOC$^2$Ecuatorial).

Teniendo en cuenta la enorme cantidad de datos biogeoquímicos que se han recopilado a lo largo de los años, es posible abordar diferentes cuestiones que despiertan el interés de la comunidad científica, como son el aumento del $C_{ant}$, la acidificación y la desoxigenación. Para estudiar los dos últimos procesos, no se necesitan más herramientas que unas buenas medidas de pH y $O_2$ pero en el caso del $C_{ant}$, hay que tener en cuenta una serie de estimaciones.

Los cambios en la química del carbonato están inducidos por la absorción de $CO_2$ por el océano. En este punto, la atención de la comunidad científica marina se centra en las estimaciones del componente antropogénico ($C_{ant}$) del carbono inorgánico total ($C_T$), porque, a pesar de las nuevas técnicas y avances tecnológicos, es imposible diferenciar entre las moléculas de $CO_2$ naturales y antropogénicas. Por ello, desde el final del siglo XX, se han desarrollado diferentes técnicas para estimar la concentración y consiguiente acumulación de $C_{ant}$ en los océanos (Brewer, 1978). Estas técnicas de *back-calculation*, que nacieron con el objetivo de estimar indirectamente el $C_{ant}$, se basan en restarle al $C_T$ los efectos de remineralización de la materia orgánica, la disolución del $CaCO_3$ (Chen y Millero, 1979) y el desequilibrio $CO_2$ aire-mar (Gruber et al., 1996). Varios tipos de estos métodos han sido aplicados a los diferentes océanos o a regiones parciales del mismo: $\Delta C^*$ (Gruber et al., 1996), LM05 (Lo Monaco et al., 2005), TrOCA (Körtzinger et al., 1998; Touratier et al., 2007) y $\varphi C_T^o$ (Pérez et al., 2008; Vázquez-Rodríguez et al., 2009a). Además, existen otros métodos basados en trazadores transitorios que permiten estimar la edad de

las masas de agua como "shortcut method" de Thomas e Ittekkot (2001) o el método *Transient Time Distribution* (TTD) de Waugh et al., (2006).

Sabiendo esto y habiendo recuperado los datos de la campaña A06, se puede plantear un estudio sobre acidificación, desoxigenación y $C_{ant}$ en el Océano Atlántico Ecuatorial (Figura 15). Con una diferencia de diecisiete años entre ellas, las campañas A06 1993 y MOC$^2$Ecuatorial 2010 siguieron exactamente la misma ruta. Por ello, se ha pensado en una forma sencilla para evaluar los cambios ocurridos en pH, $O_2$ y $C_{ant}$. En la sección III. Resultados y Discusión, ***Capítulo 3. Changes in the Equatorial Atlantic Ocean in terms of Oxygen and Carbonate System variables,*** se detalla la evaluación del cambio en pH, $O_2$ y $C_{ant}$ en cada una de las regiones definidas en la región del Océano Atlántico Ecuatorial. Estas regiones se han diferenciado en función de la distinta circulación profunda que se da a cada lado de la dorsal Atlántica, lo que nos lleva a dividir la sección de estudio en cuatro regiones, dos al este de la dorsal y dos al oeste. Además, en función de la distribución termohalina de dicha región, se ha dividido la columna de agua de cada una de las cuatro regiones en seis capas de densidad que vendrán determinadas por las masas de agua características de la zona.

Aprovechando que la región de la Cuenca Ibérica (Figura 15) ha sido objeto de muestreos repetidos en diferentes años, se ha planteado el objetivo de estimar las concentraciones de $C_{ant}$ y las correspondientes tasas de almacenamiento en un período de casi dos

décadas. Para ello se han usado las medidas de $A_T$, $C_T$, pH y nutrientes disponibles de la ya mencionada campaña CAIBOX 2009, junto con las de: OACES 1993, CHAOS1998 y OACES 2003. Para las estimaciones de $C_{ant}$ se han usado las técnicas de *back-calculation* $\varphi C_T^o$ y TrOCA y, al igual que en la región Atlántica Ecuatorial, se ha dividido la columna de agua en seis capas de densidad atendiendo a la distribución termohalina de la Cuenca Ibérica. Por ello, en la sección III. Resultados y Discusión, ***Capítulo 4. Tendencias de $CO_2$ antropogénico a lo largo del 20ºW en la cuenca Ibérica***, se detallarán todos estos aspectos, proporcionando una tasa de almacenamiento de $C_{ant}$ en la Cuenca Ibérica para los últimos veinte años.

## 2.1 Objetivos

El presente trabajo se centra en cuatro puntos principales, que se pueden definir como los objetivos de la tesis:

1. Evaluación de las primeras mediciones directas de $CO_3^{2-}$ y de la consistencia interna del sistema del carbonato, usando una selección de pares de constantes y en base a las mediciones de laboratorio de $C_T$, $A_T$ y pH realizadas durante las campañas que surcaron el Atlántico Norte.

2. Recuperación de los datos de pH y revaluación y cálculo de los datos de $C_T$ y $A_T$ de las campañas A06 y A07 en base al uso combinado de las bases de datos GLODAP, CARINA y MOC$^2$Ecuatorial, junto a las técnicas de control de calidad y

nuevas metodologías de cálculo utilizadas por la comunidad científica.

3. Estudio de la desoxigenación, acidificación y cambio en la concentración de $C_{ant}$ en el Océano Atlántico ecuatorial, en base a los datos de $O_2$, pH, $C_T$ y $A_T$ de las campañas A06 1993 y MOC$^2$Ecuatorial 2010.

4. Estimación de las tasas de almacenamiento de $C_{ant}$ en función del tiempo transcurrido para una sección meridional repetida en el 20ºW (campañas OACES 1993, CHAOS1998 y OACES 2003 y CAIBOX 2009), frente a la península Iberica. Esto conlleva la estimación de las concentraciones de $C_{ant}$ para cada una de las campañas mediante el uso de dos métodos de *back–calculation* y además permite la evaluación de los almacenamientos de $C_{ant}$.

## 3. Approach and objectives

The carbon cycle in the ocean is affected by changes in climate and, at the same time, its alteration causes changes in other cycles or / and biogeochemical variables, bringing all this, adverse consequences for ocean ecosystems. The $CO_2$ system in seawater has been characterized by four measurable carbonate system variables (total dissolved inorganic carbon ($C_T$), total alkalinity ($A_T$), fugacity of $CO_2$ ($fCO_2$) and pH) and by the thermodynamic relations, which involve the dissociation constants of carbonic acid. Thanks to the recent spectrophotometric method for measuring $CO_3^{2-}$, a fifth carbonate variable can be considered. Knowing two of the five observables carbonate system variables, the remaining ones are computed using the thermodynamics constants. The analytical methodologies for each variable are detailed in subsection *2. Analytical methodologies to measure carbonate variables (pH, $A_T$, $C_T$ y $CO_3^{2-}$) and $O_2$* (inside II. Data and methodology), but, in order to get an internally consistent system, it is worth saying here the importance of precision and accuracy of these measurements.

Taking into account the improvements made in terms of pairs of dissociation constants during the last forty years, four of them were selected [Mehrbach et al., (1973) refitted by Dickson and Millero (1987), Goyet and Poisson (1989) , Lueker et al., (2000) and Millero et al., (2006)] to evaluate the internal consistency of the $CO_2$ system. Inside section III. Results and Discussion, in ***Chapter 1. Carbonate system measurements and internal consistency in***

***the North Atlantic Ocean*** will be extensively studied the internal consistency of the carbonate system and new methodological advances to improve the baseline measurements.

Once the $CO_2$ system is well-known, the next step is to make the data quality control. In order to do that, the proven experience of GLODAP and CARINA datasets in quality control will be helpful. CARINA, cruises with unreliable or questionable data carbonate system that have been discarded in GLODAP, were not considered neither in CARINA, although it also included pH in the new dataset. Therefore, campaigns such as A06 and A07 WOCE 1993 are not available in GLODAP neither CARINA. However, the carbonate system data of A06 and A07 cruises are still available at CLIVAR and Carbon Hydrographic Data Office (CCHDO) website. Section III. Results and Discussion, ***Chapter 2. Carbon data from WOCE A06 and A07 cruises***, deals with the combined use of the databases GLODAP, CARINA and MOC$^2$Ecuatorial to assess and correct the existing pH bias of both A07 and A06. The re-evaluation of $A_T$ and $C_T$ data gave us the same conclusions as for prior quality control, but having recovered pH data and considering new calculation tools, both set of data will be recovered for A06 and A07 cruises.

Taking into account the huge amount of biogeochemical data that has been collected over the years, different issues of scientific interest, for instance, the increase of $C_{ant}$, ocean acidification or deoxygenation could be studied. The two last studies only need good pH and $O_2$ measurements, but $C_{ant}$ must be estimated.

Despite all new techniques discerning between natural $CO_2$ and $C_{ant}$ is quite complex Owing to that, at the end of XX century, Brewer (1978) and Chen and Millero (1979) used different calculations based on $A_T$, $C_T$ and dissolved oxygen [$O_2$] measurements to estimate [$C_{ant}$]. Since that, several authors have been tried to improve these so called back-calculation methods [ΔC*(Gruber et al., 1996), LM05 (Lo Monaco et al., 2005), TrOCA (Touratier et al., 2007) or $\varphi C_T^0$ (Vázquez-Rodríguez et al., 2009a)], even using tracers as chlorofluorocarbons (CFCs) to estimate the water mass ages (Thomas and Ittekkot, 2001; Waugh et al., 2006). In the present work, TrOCA (Touratier et al., 2007) and $\varphi C_T^0$ (Vázquez-Rodríguez et al., 2009a) have been selected to obtain $C_{ant}$ estimations. These methods are detailed in subsection *3. Methodology to estimate anthropogenic $CO_2$ (TrOCA y $\Phi C_T^0$)* (inside II. Data and methodology).

Taking into account that A06 cruise and MOC$^2$Ecuatorial data were spanned along 7.5ºN within a difference of seventeen years, an acidification, deoxygenation and $C_{ant}$ study is planned in the Equatorial Atlantic Ocean. In order to do that, a simple way to evaluate the changes in pH, $O_2$ and $C_{ant}$ was thought. These sections are divided into four differentiated regions, two at each side of the Mid- Atlantic Ridge, and, in turn, the water column is divided into six density layer related with the main waters masses of the studied region. Inside Section III. Results and Discussion, ***Chapter 3. Changes in the Equatorial Atlantic Ocean in terms of Oxygen and Carbonate System variables***, shows the differences between 1993 and 2010 mean variables.

A more specific $C_{ant}$ study is proposed in the Iberian Basin. Taking into account the combination of repeated cruises in this area (i.e., the recent CAIBOX 2009, together with OACES 1993, CHAOS1998 and OACES 2003), the distribution and temporal variability of [$C_{ant}$] are studied along the Iberian Basin. Two back-calculation techniques, $\varphi C_T^o$ and TrOCA are used to estimate [$C_{ant}$]. Inside section III. Results and Discussion, ***Chapter 4. Trends of the anthropogenic $CO_2$ along 20ºW in the Iberian basin***, shows how the water column is divided into six density layers according with the termohaline distribution of water masses and the $C_{ant}$ storage in each of them. In addition, the $C_{ant}$ storage rates were also calculated in each layer. Both the $C_{ant}$ storage and the $C_{ant}$ storage rates are compared with other works in the same area.

## 3.1 Objectives

This thesis is focussed on four main goals:

1. To evaluate the first $CO_3^{2-}$ open ocean measurements and the internal consistence of the carbonate system using a selection of four pairs of dissociation constants and $C_T$, $A_T$ and pH ocean and lab measurements.

2. Recovery of pH and revaluation and calculation of $C_T$ and $A_T$ of A06 and A07 WOCE cruises, using the combined of GLODAP, CARINA and MOC$^2$Ecuatorial databases, together with the quality control techniques and new calculation tools used by the scientific community.

3. Evaluation of deoxygenation, ocean acidification and [$C_{ant}$] change in equatorial Atlantic Ocean, based on the $O_2$, pH, $C_T$ and $A_T$ data of MOC$^2$Ecuatorial (2010) and A06 (1993) cruises.

4. Estimation of the $C_{ant}$ storage and the $C_{ant}$ storage rates in the Iberian Basin during a period of almost two decades based on the biogeochemical data of OACES 1993, CHAOS1998 y OACES 2003 y CAIBOX 2009 cruises.

# II. Datos y métodos / *Data and methodology*

# 1. Data

All data used in the present manuscript belong to nine oceanographic cruises spanned along the North Atlantic Ocean, which, chronologically ordered, are WOCE A07 1993, WOCE A06 1993, OACES 1993, CHAOS 1998, OACES 2003, CAIBOX 2009, MOC$^2$Equatorial 2010, OVIDE 2010 and A24N 2011. The geographical distribution is shown in figure 1.1.

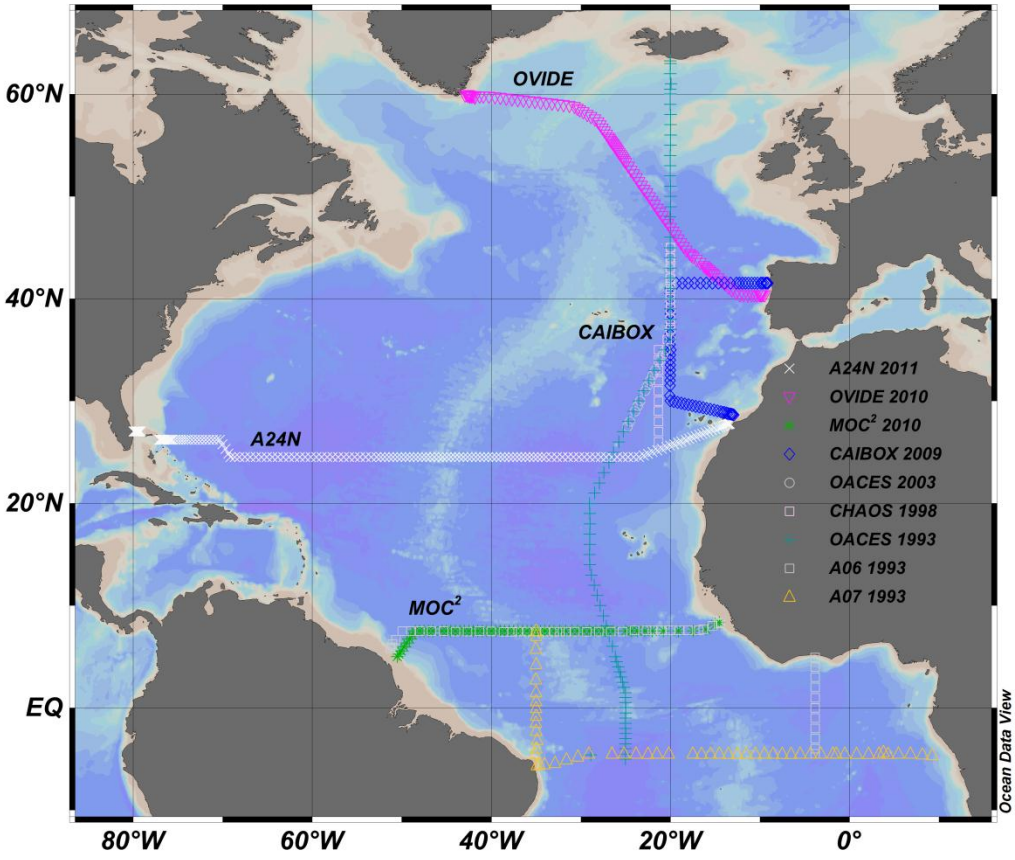


Figure 1.1. Cruises spanned along the Atlantic Ocean used in this thesis.

The hydrographic and carbon information of WOCE A07 1993, WOCE A06 1993, OACES 1993, CHAOS 1998, OACES 2003 are available in the websites of the Ocean Data Analysis Project (GLODAP) (Sabine et al., 2005) and the Carbon in the Atlantic Ocean (CARINA) (Key et al., 2010) datasets. Both webs are hosted on the Carbon Dioxide Information Analysis Center (CDIAC) where recent and historical cruises can be found. Information related to these cruises is detailed in the section below, A06 and A07 in chapter 2 and both OACES and CHAOS in chapter 4.

In the present section a brief description of the "home-made" cruises are given. In the latest four years, the $CO_2$ group of IIM-CSIC in Vigo (Spain) ($CO_2$group) has been involved in several national and international programs (GOSHIP) that covered an important area of the North Atlantic Ocean. These expeditions were CAIBOX 2009 (hereafter CAIBOX), MOC$^2$Equatorial 2010 (hereafter MOC$^2$), OVIDE 2010 (hereafter OVIDE) and A24ºN 2011 (hereafter A24N).

CAIBOX was carried out along the Iberian Basin from 25$^{th}$ July to 14$^{th}$ August in 2009 on board the R/V Sarmiento de Gamboa. This cruise was integrated in the CAIBEX project ("Shelf-ocean Exchanges in the Canary – Iberian Large Marine Ecosystem", CAIBEX). CAIBOX is formed by one latitudinal section in front of the coast of Vigo (41.5ºN), one transversal section near the Canary Islands (from 20ºW 30ºN to 13ºW 28.6ºN), and one longitudinal section along 20ºW. The study drawn up in chapter 4 uses data from the latter longitudinal section. A General Oceanic CTD with a 24

Niskin bottles (12 L) rosette was thrown in twenty four stations along the 20ºW section. Temperature, salinity, $O_2$ and pH were measured in each depth, whereas nutrients and $A_T$ and $C_T$ were taken at specific depths according to the thermohaline distribution. In addition, sea water samples of $CO_3^{2-}$were analysed in fourteen stations and throughout the whole water column along 20ºW CAIBOX.

$MOC^2$ cruise was spanned along the zonal section 4ºS - Equator - 4ºN in the Brazilian coast and the transoceanic 7.5ºN on board the Spanish R/V Hespérides. $MOC^2$ was carried out from 5th April to 16th May 2010 crossing the Equatorial Atlantic Ocean from Fortaleza (Brazil) to Mindelo (Cape Verde Islands). This cruise was part of the Spanish project $MOC^2$ (Memoria oceánica del clima: mecanismos y rutas de formación de aguas superficiales en el Atlántico ecuatorial, $MOC^2$Ec) and it is a repetition of the CITHER I cruise in 1993, which was inside the WOCE program (A06 WOCE cruise). Along the $MOC^2$, samples of $A_T$, pH and $O_2$ were analysed on the Hespérides chemistry lab, while collected $C_T$ samples were measured after in the $CO_2$ lab of IIM. During $MOC^2$ was the second time when $CO_3^{2-}$ samples were measured.

OVIDE was carried out on the French R/V Thalassa from 8th June and 8th July 2010. This cruise covered the West European Basin from Lisbon (Portugal) to Greenland crossing the Reykjanes Ridge. The OVIDE 2010 was the fifth repetition of the OVIDE hydrological section as part of the CLIVAR programme (OVIDE). During OVIDE, apart from hydrographic measurements, pH and $A_T$

measurements were sampled from bottle depths at selected stations and analysed on board. Also, individual samples of $C_T$ were taken in selected stations to be analysed at IIM laboratory.

The A24N cruise was carried out along 24.5ºN from 27$^{th}$ January to 15$^{th}$ March 2011 on board the Spanish R/V Sarmiento de Gamboa. This cruise was the 8$^{th}$ leg of the circumnavigation program MALASPINA 2010 (http://www.expedicionmalaspina.es/). A General Oceanic CTD with a twenty four Niskin bottles rosette was thrown in one hundred sixty seven stations along the 24.5ºN. Temperature, salinity, nutrients, $O_2$ and pH were measured in each depth and station, whereas $A_T$ was taken each two stations and $C_T$ only in selected stations.

# 2. Analytical methodologies to measure carbonate variables *(pH, $A_T$, $C_T$ y $CO_3^{2-}$)* and $O_2$

pH, $C_T$, and $A_T$ were measured during the CAIBOX, MOC$^2$, OVIDE and A24N cruises. In addition, during the CAIBOX and MOC$^2$ cruises, $CO_3^{2-}$ concentration ($[CO_3^{2-}]$) was also measured using a new methodology (Byrne and Yao, 2008). The analytical methodologies used are widely described in the subsections detailed below (*2.1 – 2.5*). Moreover, $O_2$ samples were taken at almost all the stations to be measured by Winkler method (*subsection 2.5*).

The accuracy of $A_T$, $C_T$ and pH measurements was checked with sample analysis of certified reference material (CRM) of $CO_2$ supplied by Andrew Dickson (Scripps Institution of Oceanography, University of California) from different batches. Unfortunately, absorbance of $CO_3^{2-}$ cannot be measured in CRMs because the absorbance of the ion $Hg^{2+}$, added to CRMs as a preservative, is so high that the $CO_3^{2-}$signal is attenuated (Martz et al., 2009). Due to that, five lab experiments varying pH were planned as a control test to validate the internal consistency of carbonic system variables when the studied variable is $[CO_3^{2-}]$ (*subsection 2.6*).

## 2.1 pH

Seawater pH samples were taken at twenty four depths at all stations along CAIBOX, MOC$^2$, and A24N and thirty two depths in OVIDE. The pH measurements were made using the spectrophotometric method described in Clayton and Byrne (1993). This method consists of adding a volume of an indicator dye to the seawater sample and measuring the absorbance of the sample (Byrne and Breland, 1989; Byrne et al., 1988; Clayton and Byrne, 1993). The indicator used was m-cresol purple (mCP) because sulphonephthalein indicators are the most appropriate for surface-to-deep pH profiles in the open ocean. The reaction of interest at seawater pH is the second dissociation $HI^-_{(aq)} = H^+_{(aq)} + I^{2-}_{(aq)}$ in which I is the indicator. Then, the total hydrogen ion concentration can be determined by $pH = pK_2 + \log_{10} [I^{2-}]/[HI^-]$. $[I^{2-}]/[HI^-]$ ratio is calculated following Dickson (Dickson, 1993) and Dickson et al. (2007a) taking into account the different absorption spectra and their maximum absorption wavelength ($\lambda_{HI}$ = 434 nm and $\lambda_I$ = 578 nm). To human eye, mCP as $H_2I$ appears pink, as $HI^-$ yellow and as $I^{2-}$ purple (Clayton and Byrne, 1993). Due to being a colourimetric method, it is possible to sense the sample pH only watching it after analysis. In figure 2.1 the pH scale varies from 7.2 (yellow) to 8.1 (purple).

**Figure 2.1 Increasing pH scale. From left to right: 7.2, 7.4, 7.7, 7.9, 8.1 and natural water before analysis.**

**Figure 2.2 Taking pH samples directly from the Niskin bottle.**

pH samples were taken directly from the Niskin bottles into special optical glass spectrophotometric Hellma cells of 28 mL of volume and 100 mm of path length. These cells were carefully stored in a thermostatic bath with controlled temperature at 25.0ºC for around one hour before the analysis. Absorbance measurements were performed with a Shimadzu UV 2401 PC spectrophotometer (CAIBOX, MOC$^2$ and OVIDE) and a Perkin Elmer Lambda 800 UV-VIS spectrophotometer (A24N) at three wavelengths, the two mentioned above ($\lambda$ = 434 and 578 nm) and a non-absorbing wavelength ($\lambda$ = 730 nm). The absorbance values were measured

before and after the addition of 75 µL of mCP (~ 0.2 mM) to the seawater sample.

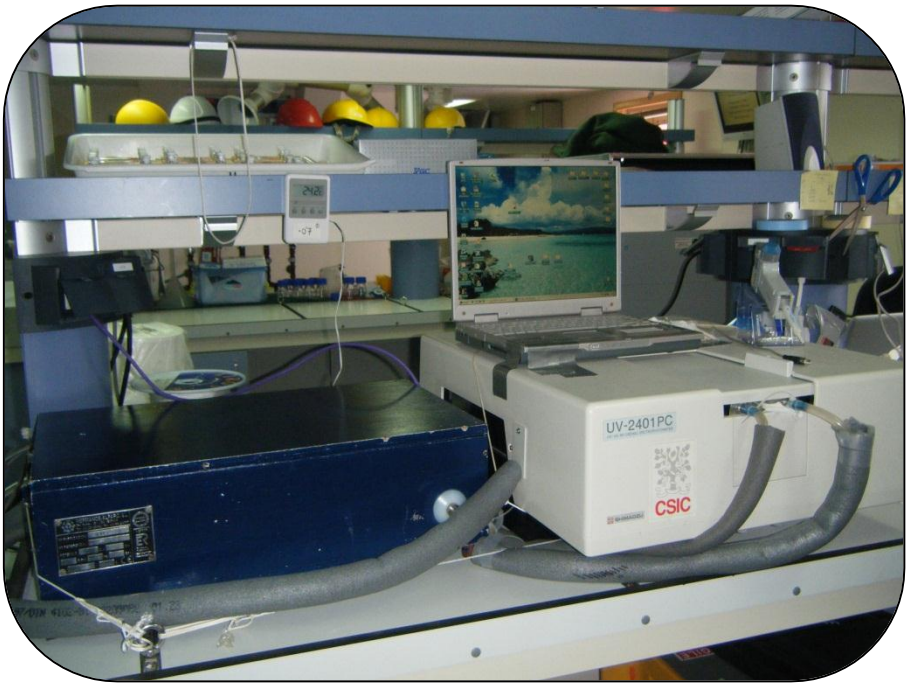


**Figure 2.3 pH measurement equipment on board R/V Sarmiento de Gamboa laboratory. Tray with cells (top on the felt), thermostatic bath (blue box on the bottom), mCP pipette and spectrophotometer.**

The pH values were obtained following the equations described in Dickson et al. (2007a), who include the correction due to the difference between seawater and the indicator acidity (ΔR). In order to check the precision of pH measurements corrected by ΔR ($pH_{\Delta R}$), six pH samples of open ocean surface water were considered and the standard deviation obtained was of ± 0.0006 and ± 0.0004 pH units for Shimadzu and Perkin Elmer Lambda, respectively, both

values meaning better precision than the 0.001 pH units reported in Dickson et al. (2007a).

The mCP used in this study was provided by Sigma-Aldrich. The study of Yao et al. (2007) stated that impurities in the indicator dye of different manufacturers cause uncertainty in the measured pH values, one of these manufacturers being Sigma-Aldrich. Thus, the equation provided by Yao et al. (2007) was also applied to the spectrophotometric pH measurements ($pH_{meas}$). Taking into account all the corrections, the spectrophotometric pH is defined here as:

Equation 1

$$pH = pH_{\Delta R} - [0.0010 + 0.0008 \cdot (pH_{meas} - 7.2) + 0.0042 \cdot (pH_{meas} - 7.2)^2]$$

DelValls et al. (1998) proposed to correct the pH values obtained with mCP by adding 0.0047 pH units to the pH value. This correction has been accepted by some authors (Byrne et al., 1999; Lamb et al., 2001; Lee et al., 2000) but also omitted by others (Lueker et al., 2000; Millero et al., 2006; Mojica Prieto and Millero, 2002) and even rejected (Millero et al., 2002). In Chapter 1 this correction will be evaluated.

## 2.2 $A_T$

Samples of $A_T$ were taken during CAIBOX, MOC$^2$, OVIDE and A24N in at least half of the total stations. In order to analyse these $A_T$ samples on board, the water was transferred directly from the Niskin bottle to 600 mL borosilicate glass bottles and stored for

Figure 2.4 Seawater $A_T$ sample recently collected to be stored and later analysed.

twenty-four hours before the analyses. Following Chanson and Millero (2007), the $A_T$ samples were not filtered. Measurements of $A_T$ were done by an automatic potentiometric titrator (Titrando 801 Metrohm) with a combined glass electrode (Perez and Fraga, 1987). A gravimetrically calibrated Knudsen pipette (~195 mL) was used to transfer the samples into an open Erlenmeyer flask in which the potentiometric titration was carried out with HCl (0.1 M). The final volume of titration was determined by means of two pH endpoints very close to one another, i.e., 4.45 and 4.42 (Mintrop et al., 2000).

In order to estimate the accuracy of the $A_T$ method, alkalinity measurements of CRM of $CO_2$ were also analysed following the same procedure. The measured CRM batches were batch 84 for CAIBOX, batch 99 for MOC$^2$ and OVIDE and batch 100 for A24N. In addition, an extra calibration (substandard) was made by using a closed container of 50 L filled with open ocean surface water from the first station of each cruise. This water was measured at the beginning and at the end of each $A_T$-analysis session to show the drift of $A_T$ concentration with time respect to the reference water. The observed drifts between stations and along the cruise are included in the calculations of $A_T$. Two replicates of each $A_T$ sample, CRM and drift were analysed obtaining a standard

deviation not greater than ± 0.5 µmol·kg$^{-1}$ between replicates. As mentioned in Dickson et al. (2007a), the bias of this potentiometric method is less than ± 2 µmol·kg$^{-1}$.

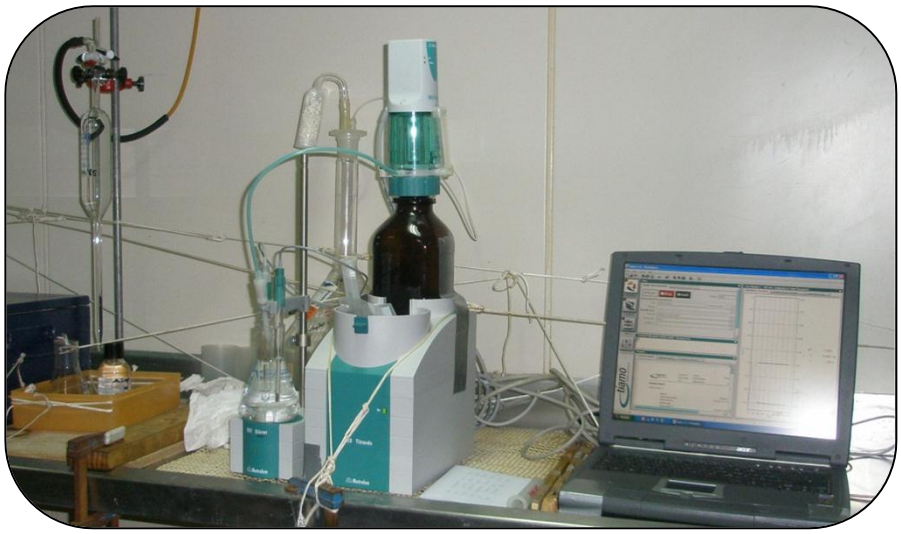

**Figure 2.5 $A_T$ measuring equipment. Knudsen pipette, Erlenmeyer flask, Titrando with coupled HCl flask and laptop.**

## 2.3 $C_T$

Along CAIBOX, MOC$^2$, OVIDE and A24N, discrete samples (n = 53, 50, 31 and 43, respectively) of $C_T$ were taken in the water column to be measured at the $CO_2$ lab of the IIM using a SOMMA (Single-Operator Multiparameter Metabolic Analyzer) system connected to a model CM101_093 coulometer (UIC.INC, Joliet, ILLINOIS, USA).

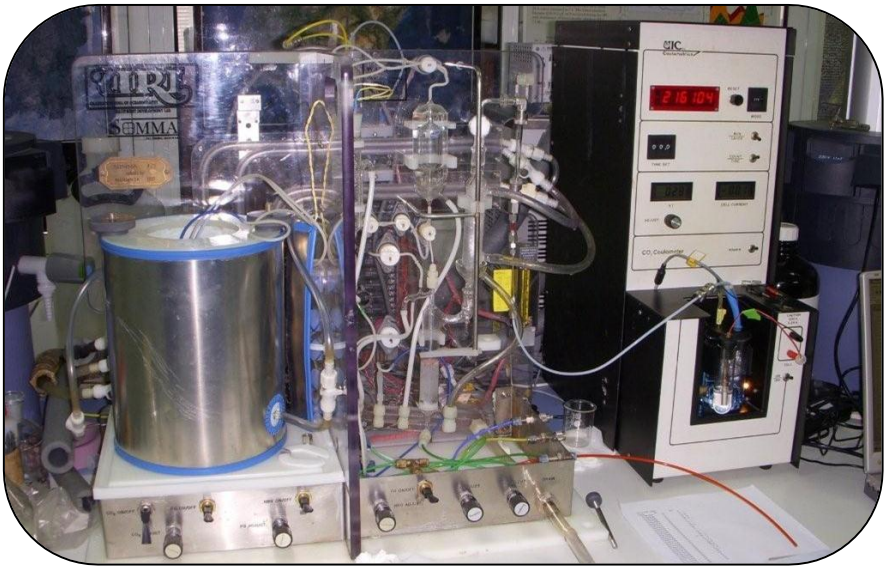


Figure 2.6 SOMMA system during a session of analysis in the $CO_2$ lab of IIM.

The procedures of sampling the water in 600 mL borosilicate glass bottles are described in Dickson et al. (2007a). These $C_T$ samples were measured by the coulometric method based on Johnson et al. (1993, 1998): a sample aliquot of 20 mL is acidified with $H_3PO_4$ in a glass stripping chamber and the resulting $CO_2$ gas is carried by a $CO_2$-free $N_2$ gas into a coulometric cell, in which the coulometric titration is performed.

In every $C_T$-analysis session, calibrations were performed with CRM of $CO_2$ to check the accuracy of the measurements. The measured CRM batches were batch 74 for CAIBOX and batch 100 for MOC$^2$, OVIDE and A24N. In addition, in order to control the SOMMA system drift, an extra calibration was made by using one closed container of 50 L filled with surface water from the "Ría de Vigo" (Northwest of Spain). This water was measured at the

beginning, middle and end of each daily $C_T$-analysis session, observing no changes along the day or between days. Two replicates of each $C_T$ sample, including CRM and drift, were analysed obtaining a difference between them no greater than ± 1 µmol·kg$^{-1}$. The analytical accuracy of this coulometric method is ± 2 µmol·kg$^{-1}$ (Millero, 2007).

## 2.4 $CO_3^{2-}$

Natural seawater samples of $CO_3^{2-}$ were collected from along fourteen and thirty stations in CAIBOX and MOC$^2$, respectively, at twenty four depths of the water column. These $CO_3^{2-}$ samples were analysed on board following the spectrophotometric method described in Byrne and Yao (2008), who designed a very quick and easy method of similar performance as the spectrophotometric pH method of Clayton and Byrne (1993). This method consists on the addition of a known quantity of Pb(II) solution to the seawater sample in order for this $Pb^{+2}$ to react with the dissolved $CO_3^{2-}$ of the sample obtaining the complex $PbCO_3$. The $[CO_3^{2-}]$ is calculated in terms of UV absorbance ratios using the equation 2 (eq. 5 of (Byrne and Yao, 2008).

Equation 2

$$-\log[CO_3^{2-}]_T = \log_{CO3}\beta_1 + \log\left(\frac{R - e_1}{e_2 - R \cdot e_3}\right)$$

The $\log_{CO3}\beta_1$ and the coefficients $e_1$, $e_2$ and $e_3$ were determined as a function of salinity (S) through equations 3-6 (eq. 11 and 17-19 of Byrne and Yao, 2008).

**Equations 3, 4, 5 and 6**

$$\log_{CO3}\beta_1 = 6.574 - 0.1235 \cdot S + 0.001514 \cdot S^2$$

$$e_1 = 0.3447 - 0.006662 \cdot S + 0.0001463 \cdot S^2$$

$$e_2 = 0.7749 - 0.01122 \cdot S + 0.000331 \cdot S^2$$

$$e_3 = 2.114 - 0.06600 \cdot S + 0.0009036 \cdot S^2$$

In equation 2, $R = \left(\frac{\lambda_2 - \lambda_3}{\lambda_1 - \lambda_3}\right)$, in which $\lambda_1$ (234 nm) is the UV absorbance wavelengths at the isobestic point of $PbCO_3$, $\lambda_2$ (250 nm) is the mean value of the wavelengths presenting high absorbance variation and $\lambda_3$ (350 nm) is a non-absorbing wavelength to correct the sample manipulation. Byrne and Yao recommended a recombination of equations 2-6 as the most appropriate. However, equations 2-6 are going to be used in the present work because an important difference of 8.6 ± 4.0 µmol·kg$^{-1}$ in $[CO_3^{2-}]$ can be obtained depending on the set of equations used. Taking in consideration all $CO_3^{2-}$ samples measured during CAIBOX and MOC[2] cruises, different tests were made in order to improve these $[CO_3^{2-}]$ and to decrease as much as possible the differences when $[CO_3^{2-}]$ is calculated with the thermodynamic equations of the carbonate system (see *subsection 2.4.1 and 2.4.2*).

The technique to collect the $CO_3^{2-}$ seawater samples is the same than for pH, with the difference that $CO_3^{2-}$ cells are made of quartz instead of optical glass. Seawater was transferred directly from Niskin bottles into cylindrical quartz Perkin Elmer cells of 28 mL of volume and 100 mm of path length. These cells were carefully stored in a thermostatic bath at 25ºC for at least one hour before the analysis. Absorbance measurements of $\lambda_1$, $\lambda_2$ and $\lambda_3$ were performed with a Perkin Elmer Lambda 800 UV-VIS spectrophotometer on board the R/V Sarmiento de Gamboa (CAIBOX cruise) and a Shimadzu UV 2401 PC spectrophotometer on board the R/V Hespérides ($MOC^2$ cruise). Thus, once the sample was directly measured as a reference solution, 225 µL of stock solution of $PbCl_2$ (1.1 mM) were added and the absorbance measurements were read again. In order to prove the precision of each spectrophotometer, six $CO_3^{2-}$ samples of open ocean surface water were measured and the standard deviations of ± 1.9 µmol·kg$^{-1}$ (precision 0.9%) for Perkin Elmer when $[CO_3^{2-}]$ = 210 µmol·kg$^{-1}$and ± 2.9 µmol·kg$^{-1}$for Shimadzu when $[CO_3^{2-}]$ = 230 µmol·kg$^{-1}$ (precision 1.3%) were obtained.

### 2.4.1 Influence of temperature

In order to know exactly whether temperature affects the measurements of $[CO_3^{2-}]$, a single experiment at different temperatures was done. Groups of six samples of open ocean water were stored in a thermostatic bath, which was stabilized at three different temperatures: 20, 25 and 30ºC. Immediately after

measuring $[CO_3^{2-}]$, the temperature was measured using a thermometer TFX410-1 (ebro Electronic GmbH&CO.KG). The mean temperature ranges obtained were 22.4 ± 0.1, 25.6 ± 0.4 and 28.6 ± 0.2ºC. $[CO_3^{2-}]$ was calculated at 25ºC following equations 2-6 and used as reference. In figure 2.7 the influence of temperature on $[CO_3^{2-}]$ is clearly shown.

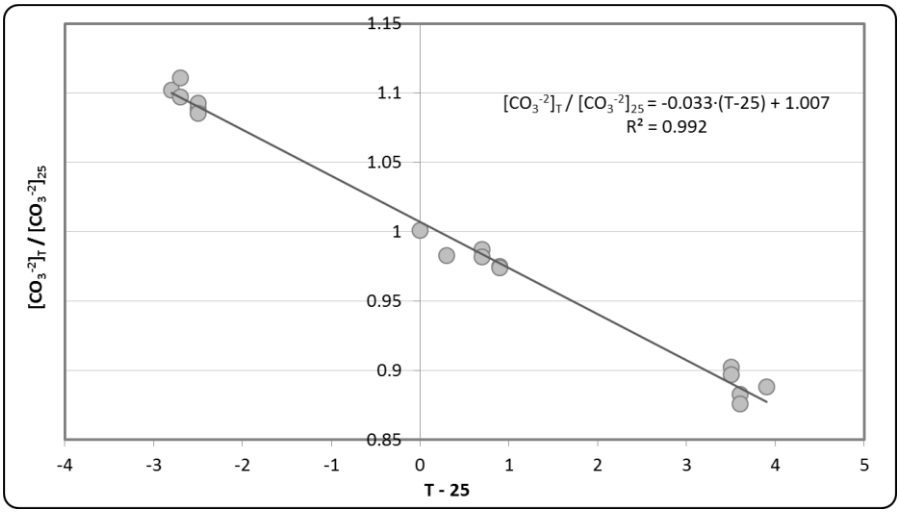


**Figure 2.7 Influence of the temperature in the $[CO_3^{2-}]$ measured by the spectrophotometric method of Byrne and Yao. The "y-axis" represents the $[CO_3^{2-}]_T/[CO_3^{2-}]_{25}$ ratio and the "x-axis" shows the difference between the measured temperature and the reference temperature (T-25).**

The determination coefficient ($R^2$ = 0.992) reveals a good correlation of the linear adjustment: $[CO_3^{2-}]_T/[CO_3^{2-}]_{25}$ = -(0.033 ± 0.001)·(T-25) + (1.007 ± 0.002). Even though $PbCO_3$ formation constant is not variable over a range of 15 and 35ºC (Soli et al., 2008), temperature does influence in $[CO_3^{2-}]$ measurements. Thus, equation 2 is transformed into a new one in which the variability with temperature is considered.

Equation 7

$$[CO_3^{2-}]_T = \frac{10^{\left(6-\left[\log_{CO3}\beta_1+\log\left(\frac{R-e_1}{e_2-R\cdot e_3}\right)\right]\right)}}{1-0.033\cdot(T-25)}$$

Consequently, in order to estimate $[CO_3^{2-}]$ more accurately, the temperature of each $CO_3^{2-}$ sample should be taken after each measurement.

### 2.4.2 Influence of $PbCl_2$ in the measurements of $[CO_3^{2-}]$.

Another important aspect when measuring $[CO_3^{2-}]$ is to take into account the slight acidification of the sample produced by the addition of $PbCl_2$. In a set of six laboratory experiments the pH of the sample was analysed with and without addition of $PbCl_2$. Results show that the $PbCO_3^0$ formation reaction in seawater ($Pb^{2+} + CO_3^{2-} \leftrightarrow PbCO_3^0$) produces a decrease in pH of 0.01 units in each individual sample. Moreover, when the $PbCl_2$ solution was added to the sample cell, dilution of $CO_3^{2-}$ ions present in the sample also occurred, resulting in a measured $[CO_3^{2-}]$ lower than the real one. Taking into account the concentration of $Pb^{2+}$ in the cell, the measured $[CO_3^{2-}]$ and the $PbCO_3^0$ equilibrium constant at salinity 35 [$K_{CO3\,\beta1}$, Table 1 of Byrne and Yao (2008)], the dilution of $CO_3^{2-}$ ion in terms of concentration of $PbCO_3^0$ can be estimated as:

Equation 8

$$[PbCO_3^0] = \frac{[Pb^{2+}][CO_3^{2-}]K_{CO_3\,\beta_1}}{1+[CO_3^{2-}]K_{CO_3\,\beta_1}}$$

In addition, each $CO_3^{2-}$ ion, which reacts with $Pb^{2+}$ in the $PbCO_3^0$ formation, is subtracting $A_T$ (2 mol for each mol of $PbCO_3^0$). In order to demonstrate both of these $PbCl_2$ influences, a numerical $[CO_3^{2-}]$ experiment was done. Nine seawater samples with $A_T$ and $C_T$ concentrations twice as large as natural values were supposed. The salinity was considered 35 and $C_T$ = 3470 µmol·kg$^{-1}$ while $A_T$ varied from 4000 to 3200 µmol·kg$^{-1}$ in steps of 100 µmol·kg$^{-1}$. $[CO_3^{2-}]$ and pH were calculated from $A_T$ and $C_T$ using the $CO_2$sys with MDM87 constants. Taking into account equation 8, the influence of the dilution of $CO_3^{2-}$ ion in $A_T$ ($A_{T\ PbCO3}$) and $C_T$ ($C_{T\ PbCO3}$) was estimated. $pH_{PbCO3}$ was also calculated from $A_{T\ PbCO3}$ and $C_{T\ PbCO3}$ using the $CO_2$sys with MDM87 constants, and hence, $[CO_3^{2-}]_{PbCO3}$. The difference $[CO_3^{2-}]$ - $[CO_3^{2-}]_{PbCO3}$ was plotted with pH - 8 obtaining the very good polynomial adjustment shown in figure 2.8 ($R^2$ = 0.999), covering the range of pH from 8.2 to 7.

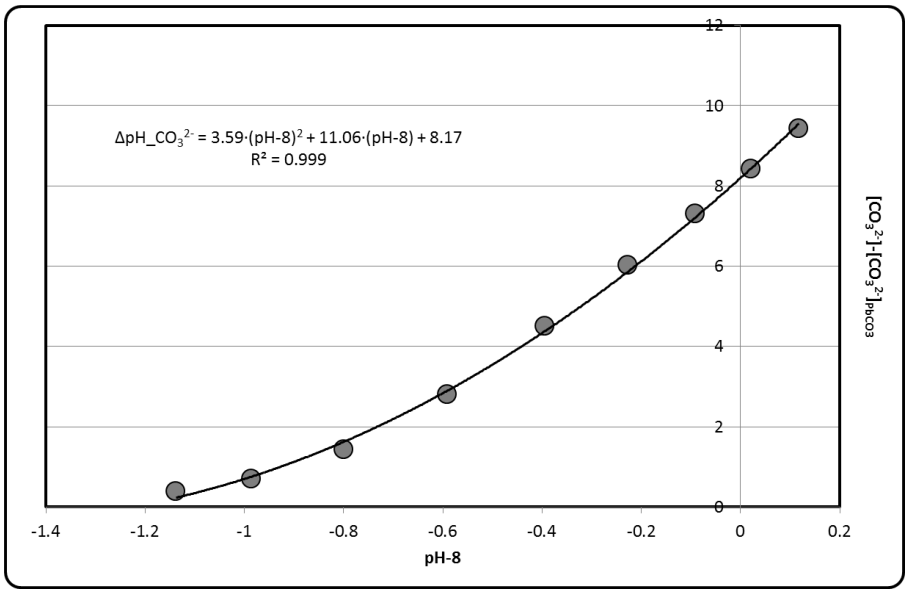


**Figure 2.8 Influence of the $PbCl_2$ in $[CO_3^{2-}]$. The difference $[CO_3^{2-}]$ - $[CO_3^{2-}]PbCO_3$ was plotted with pH-8 obtaining the adjustment $\Delta pH\_CO_3^{2-}$= (3.59 ± 0.35)·(pH - 8)$^2$ + (11.06 ± 0.37)·(pH - 8) + (8.17 ± 0.08) in µmol·kg-1 with the high determination coefficient of $R^2$ = 0.999.**

This chemical adjustment in µmol·kg$^{-1}$ was named $\Delta pH\_CO_3^{2-}$ {$\Delta pH\_CO_3^{2-}$= (3.59 ± 0.35)·(pH - 8)$^2$ + (11.06 ± 0.37)·(pH - 8) + (8.17 ± 0.08)} similarly to ΔR calculations proposed by Clayton and Byrne (1993). $\Delta pH\_CO_3^{2-}$ produces an increment of 5.6 ± 1.4 µmol·kg$^{-1}$ in the values of $[CO_3^{2-}]$ (eq. 7).

Taking into account all the innovations pointed out in the present study, a new equation to estimate accurately $[CO_3^{2-}]$ is finally presented.

**Equation 9**

$$[CO_3^{2-}]_T = \frac{10^{\left(6-\left[\log_{CO3}\beta_1+\log\left(\frac{R-e_1}{e_2-R\cdot e_3}\right)\right]\right)}}{1-0.033\cdot(T-25)} + \Delta pH\_CO_3^{2-}$$

Despite the mean value of $[CO_3^{2-}]$ described here (eq. 9) and $[CO_3^{2-}]$ recommended by Byrne and Yao (2008) (eqs. 20-23) only differ in 1 µmol·kg$^{-1}$, the precision of the method has been improved in the whole $[CO_3^{2-}]$ range, in both field and laboratory measurements. The obtained precisions were of 1.3% for field measurements and 1.2% for laboratory measurements.

## 2.5 Winkler Oxygen ($O_2$)

With the main purpose of calibrating the $O_2$ sensor of CTD, samples of $O_2$ were taken in all the stations at twenty four depths in CAIBOX, OVIDE and A24N, and in all stations in 7.5ºN section of MOC[2]. The $O_2$ samples were analysed following the widely applied Winkler method (1888).

The $O_2$ samples are always the first in being taken from the Niskin bottles of the rosette. Samples were collected in calibrated flasks (~ 113 mL) with a silicone pipe avoiding the formation of bubbles. Sample fixation (precipitation) were done by adding 0.6 mL of manganous salt ($MnCl_2$ .$4H_2O$) and 0.6 mL of alkali-iodide solution (NaOH + NaI).

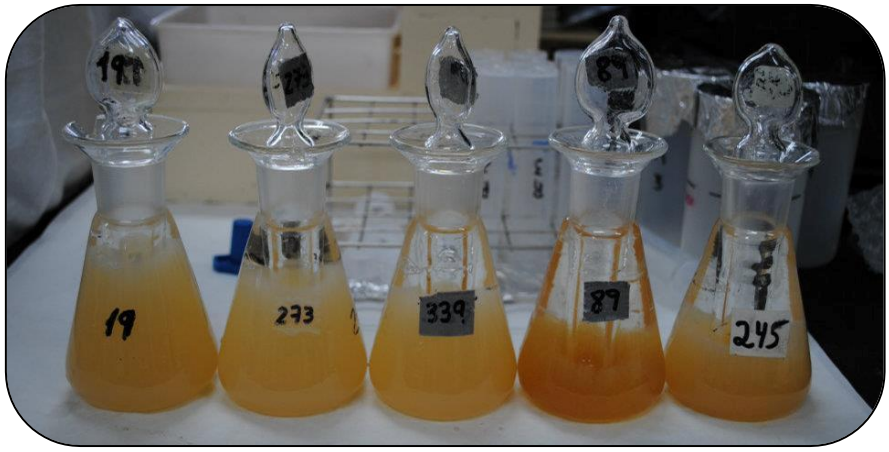


**Figure 2.9 Set of $O_2$ samples recently fixed. It is easy distinguish the precipitate at the bottom of flask 89, while in 19 is still suspended.**

These samples were stored at darkness at least 24 hours before being measured. Then, 0.8 ml of sulphuric acid was added to dissolve the precipitate and to titrate the $O_2$ sample with thiosulfate using an automatic 5ml burette "Titrando Metrohm". Concentration of thiosulfate solution was periodically controlled by standardization with potassium iodate 0.02N for each session. Blanks were also measured periodically during the cruise. The $O_2$ concentration was obtained in µmol $kg^{-1}$ by recording sampling temperature and thus having the mass of pickled sea water.


**Figure 2.10 Detail of the $O_2$ measurement process. At this moment the precipitate was dissolve and the titration is going to start.**

## 2.6 Laboratory experiments

Five natural surface seawater samples were taken in open ocean in the Iberian Basin in front of the Galician Coast (43ºN and 13ºW, approximately), poured into containers of 25 L and shipped from sea to the lab. Once in the lab, in order to know the pH of the test water, an aliquot was analysed, obtaining a pH value of 7.9. In order to obtain a better characterization of this test water and to know the organic matter concentration, several kinds of aliquots were also taken for nutrient measurements ($NO_3^-$, $NO_2^-$, $NH_4^+$, $PO_4^{2-}$ and $SiO_4^{2-}$), total organic carbon (TOC) and dissolved organic nitrogen (TDN), obtaining $NO_3^-$ = 0.50 µM, $NO_2^-$ = 0.05 µM, $NH_4^+$ = 0.4 µM,

$PO_4^{2-}$ = 0.02 µM, $SiO_4^{2-}$ = 1.39 µM, TOC = 91.8 mmol·m-3 and TDN = 9.7mol·m-3. Then, a plan was established in the lab to sample and measure pH, $A_T$, $C_T$ and $CO_3^{2-}$ together with salinity samples. First, the pH of each container was modified by addition of HCl (0.1 N) and $Na_2CO_3$ (0.05 M) in order to have five containers with different pH, i.e., 8.1, 7.9, 7.7, 7.4 and 7.2 units, approximately. Secondly, the water was transferred from each container to the specific recipients for each sample through a 20 µm Nylon filter coupled to a pipe. Finally, pH, $A_T$, $C_T$ and $CO_3^{2-}$ samples were analysed following the methodologies detailed above (*subsections 2.1 - 2.4*). In order to provide the accuracy of $A_T$ and $C_T$, batch 100 of CRM was also measured. Salinity was measured with Portasal Guildline 8410 A calibrated with standards (Ocean Scientific International Ltd Batch 150). The mean values of pH, $A_T$, $C_T$ and $CO_3^{2-}$ with their associated standard deviations and the number of repetitions of each variable are shown in table 2.1. The respective values of measured salinity are also shown.

**Table 2.1 Laboratory experiments. Mean values of $pH_{\Delta R}$, $A_T$, $C_T$ and $[CO_3^{2-}]$ with their associated standard deviation for each fixed pH (i.e., 7.2, 7.4, 7.7, 7.9 and 8.1) and the number of repetitions (n) of each variable are shown. The measured salinity of each experiment is also shown.**

| Lab Exp | Salinity | $pH_{\Delta R}$ | $A_T$ ($\mu mol \cdot kg^{-1}$) | $C_T$ ($\mu mol \cdot kg^{-1}$) | $CO_3^{2-}$ ($\mu mol \cdot kg^{-1}$) |
|---|---|---|---|---|---|
| 7.2 | 35.974 | 7.1921±0.0054 (n=8) | 2039.9±1.0 (n=3) | 2078.0±0.5 (n=4) | 35.5±0.3 (n=4) |
| 7.4 | 36.010 | 7.4288±0.0016 (n=8) | 2116.1±0.6 (n=7) | 2076.8±0.8 (n=16) | 60.8±0.6 (n=7) |
| 7.7 | 36.053 | 7.6899±0.0005 (n=4) | 2213.0±0.4 (n=4) | 2081.9±1.4 (n=8) | 106.3±0.8 (n=3) |
| 7.9 | 36.111 | 7.9657±0.0018 (n=8) | 2374.1±0.5 (n=7) | 2103.2±0.6 (n=16) | 184.5±1.0 (n=8) |
| 8.1 | 36.183 | 8.1005±0.0010 (n=5) | 2558.1±0.8 (n=3) | 2187.9±0.5 (n=8) | 254.7±2.2 (n=4) |

# 3. Methodology to estimate anthropogenic $CO_2$ (TrOCA y $\Phi C_T^0$)

Since the beginning of the revolution era, humankind has emitted large quantities of $CO_2$ into the atmosphere (Le Quéré et al., 2009) rising the global average atmospheric $CO_2$ from 280 ppm at the start of industrial revolution to 391 ppm in October 2012 (Trans and Keeling, 2012).The oceans play a crucial role in mitigating the effects of the carbon dioxide ($CO_2$) emitted to the atmosphere (Khatiwala et al., 2009). During the last 200 years, the ocean have been a net $CO_2$ sink (Gruber et al., 2009), uptaking, together with the land sink, ~ 55% of anthropogenic $CO_2$ ($C_{ant}$) from the atmosphere (Ballantyne et al., 2012; Le Quéré et al., 2009). Nowadays, the attention of the marine scientific community is focussed on estimating the anthropogenic component ($C_{ant}$) of the total inorganic carbon ($C_T$). The difficulty of estimating [$C_{ant}$] stems from the fact that it cannot be directly measured and besides, it results a quite difficult task to differentiate between the anthropogenic signal (less than 4%,) and the natural one (~10%) from the large background variability of $C_T$ in the ocean.

In the latest seventies, Brewer (1978) and Chen and Millero (1979) used different calculations based on $A_T$, $C_T$ and dissolved oxygen [$O_2$] measurements to estimate [$C_{ant}$]. Since that, several authors have been trying to improve these so called back-calculation methods [ΔC*(Gruber et al., 1996), eMLR (Friis et al., 2005), LM05 (Lo Monaco et al., 2005), TrOCA (Touratier et al., 2007) or

$\varphi C_T^0$ (Vázquez-Rodríguez et al., 2009a)], even using tracers as chlorofluorocarbons (CFCs) to estimate the water mass ages (Thomas and Ittekkot, 2001; Waugh et al., 2006). However, due to all of them having advantages and disadvantages (Sabine and Tanhua, 2010) there is no clear consensus about the more adequate method to estimate $C_{ant}$. Despite some authors have shown $C_{ant}$ concentrations using the estimations derived from one of these methods: $\Delta C^*$ (Macdonald et al., 2003; Rosón et al., 2003) TTD (Tanhua et al., 2008) or $\varphi C_T^0$ (Pérez et al., 2010b; Rios et al., 2012) another authors have opted by running jointly two or more methods, $\Delta C^*$ and eMLR (Brown et al., 2010), TrOCA and $\varphi C_T^0$ (Castaño-Carrera et al., 2012; Fajar et al., 2012; Pérez et al., 2010a), $\Delta C^*$, TrOCA and $\varphi C_T^0$ (Flecha et al., 2012) or $\Delta C^*$, LM05, TrOCA and $\varphi C_T^0$ (Vázquez-Rodríguez et al., 2009b). In the present work, among all back-calculation techniques, two recent ones, TrOCA (Touratier et al., 2007) and $\varphi C_T^0$ (Vázquez-Rodríguez et al., 2009a) have been selected in order to obtain $C_{ant}$ estimations. The methodology for estimating $C_{ant}$ in both of them is based on removing from $C_T$ the carbon contributions after the time of water mass formation due to the oxidation/reduction processes of the organic matter and the processes of dissolution of $CaCO_3$ as well as the concentration of $C_T$ at the moment of the water mass formation. In order to help to understand the main back-calculation principles, firstly, a brief description of $\Delta C^*$ is given, followed by a more detailed description of TrOCA and $\varphi C_T^0$.

## 3.1 The ΔC* method

The classical ΔC* (Gruber et al., 1996) was based on the $C_{ant}$ estimations of Brewer (1978) and Chen and Millero (1979). These first approaches estimated $C_{ant}$ as the $C_T$ concentration difference between current and preindustrial conditions:

Equation 10

$$C_{ant} = C_T - C^0_{T\,eq} - \Delta C_{bio}$$

where $C^0_{T\,eq}$ stands for the equilibrium $C_T$ concentration for a preindustrial atmosphere (280 ppm) and $\Delta C_{bio}$ represents the changes in $C_T$ due to the remineralization of the organic matter and the dissolution of $CaCO_3$:

Equation 11

$$\Delta C_{bio} = R_{C/O} \cdot AOU - \frac{1}{2}\left(A_T - A^0_T + R_{N/O} \cdot AOU\right)$$

Where $r_{C/O}$ and $r_{N/O}$ are the stoichiometric ratios for carbon and nitrogen, respectively (Anderson and Sarmiento, 1994; Broecker, 1974; Fraga et al., 1998). AOU is the apparent oxygen utilization, which is defined as the difference between the saturation $O_2$ concentration ($O^0_{2\,sat}$) and the observed $O_2$ concentration [(AOU = $O^0_{2\,sat} - O_2$) (Ito et al., 2004)]). $O^0_{2\,sat}$, which depends on potential temperature (Θ) and salinity, is the saturation concentration of $O_2$ in the determined water mass at the time of water mass formation. $A^0_T$ is the preformed alkalinity or the alkalinity the water mass had when it was last in contact with the atmosphere.

Gruber et al. (1996) added a new term to the equation 10 to account for the air-sea $CO_2$ disequilibrium of a water parcel ($\Delta C_{dis}$), which is established at the moment the water mass lost contact with the atmosphere:

Equation 12

$$C_{ant} = C_T - C^0_{T\,eq} - \Delta C_{bio} - \Delta C_{dis}$$

Where

Equation 13

$$\Delta C^* = C_T - C^0_{T\,eq} - \Delta C_{bio}$$

The ΔC* method has to make some implicit assumptions, i.e., the stoichiometric ratios ($r_{C/O}$ and $r_{N/O}$) are considered constant, the $O_2$ preformed concentration is given by $O^0_{2\,sat}$, the $A^0_T$ is invariant over time and that the ocean has been operating in a steady state since preindustrial times (effective $\Delta C_{dis}$ has not changed over the time) is also assumed. For instance, the ΔC* technique eliminates the nonlinear effects due to the water mixing and takes into account the preindustrial $C_T$ of each considered water mass (Gruber et al., 1996) but it is also subjected to known biases due to the various assumptions and approximations made (Matsumoto and Gruber, 2005)

$\Delta C_{dis}$ ($\Delta C_{dis} = \Delta C^* - C_{ant}$ ) can be estimated quite directly for deep potential surfaces in the interior of the ocean which are not entirely affected by $C_{ant}$. For the shallower potential density surfaces, the information of the water age from the measurements of titrium and

helium isotopes together with the history of the increase of atmospheric $CO_2$ over the last 200 years is used to reconstruct the $\Delta C_{dis}$. Gruber et al. (1996) considered the errors associated to the analytical determinations of the tracers and the stoichiometric ratios to be independent and uncorrelated. Thus the error of $\Delta C^*$ was estimated of around 9 $\mu mol \cdot kg^{-1}$ by propagation of errors. Further information about the method is detailed in Gruber et al., (1996).

## 3.2 The TrOCA method

The TrOCA method is an easy-to-apply technique because it only needs measurements of potential temperature ($\Theta$), $O_2$, $C_T$ and $A_T$ to define its quasi-conservative TrOCA tracer (Tracer combinig Oxygen, inorganic Carbon and total Alkalinity) based on Redfield ratios. $C_{ant}$ is estimated from the difference between the measured TrOCA and the conservative tracer $TrOCA^0$ which is defined from "natural" concentrations of $O_2$, $C_T$ and $A_T$. Originally, $TrOCA^0$ was computed only as function of $\Theta$ (Touratier and Goyet, 2004), but it was in 2007 when Touratier and Goyet proposed an improved equation based on $\Delta^{14}C$ and CFC-11 tracers (Touratier et al., 2007). The equation to obtain $C_{ant}^{TrOCA}$ is unique for the whole ocean and the resultant $C_{ant}^{TrOCA}$ estimations are better correlated with CFC tracers than even $\Delta C^*$ (Touratier et al., 2007), but the theoretical fundaments of TrOCA have also some implicit assumptions: $A_T$ is not affected by the increase of atmospheric $CO_2$ as well as the distribution of $O_2$ in the ocean at a large scale and $[O_2]$ at the water

surface is saturated. The biases derived from these assumptions are detailed in Yool et al. (2010).

The TrOCA approach estimates the anthropogenic $CO_2$ using the following equation:

Equation 14

$$C_{ant}^{TrOCA} = \frac{TrOCA - TROCA^0}{a}$$

where the tracer TrOCA is defined as:

Equation 15

$$TrOCA = O_2 + a\left(C_T - \frac{1}{2}A_T\right)$$

and $TrOCA^0$ is a conservative tracer which was deduced from $\Delta^{14}C$ and CFC-11 tracers and defined as:

Equation 16

$$TrOCA^0 = e^{\left(b + c\cdot\theta + \frac{d}{A_T^2}\right)}$$

The dimensionless coefficients a, b, c and d used in the previous equations are:

Equations 17, 18, 19 and 20

$$a = 1.279 \pm 7.3 \cdot 10^{-3}$$

$$b = 7.511 \pm 5.2 \cdot 10^{-3}$$

$$c = -1.087 \cdot 10^{-2} \pm 2.5 \cdot 10^{-5}$$

$$d = - 7.81 \cdot 10^{5} \pm 2.9 \cdot 10^{4}$$

The estimated error for $C_{ant}^{TrOCA}$ estimations is of ± 6.25 µmol·kg$^{-1}$ and it was calculated by propagation of randomly perturbed errors.

## 3.3 The $\varphi C_T^0$ method

Finally, the $\varphi C_T^0$ method is an approach oriented to biogeochemical processes based on the ΔC* principles, but including some improvements. In the $\varphi C_T^0$ method, the subsurface layer (100-200m) is used since it accurately represents the wintertime water masses formation conditions and avoids the short-term variability of the uppermost layers (Vázquez-Rodríguez et al., 2012). This layer is used to compute the $A_T^0$ and $\Delta C_{dis}$ terms. The $\varphi C_T^0$ $C_{ant}$ concentrations are directly estimated in waters above the 5ºC isotherm while in cold deep waters (< 5ºC) they are estimated by using an extended Optimum MultiParameter (eOMP) analysis. This procedure especially improves the $C_{ant}$ estimations in cold deep waters involved in complex mixing processes between Arctic and Antarctic water masses. In addition, due to the imprecise assumption of invariable $\Delta C_{dis}$ (Matsumoto and Gruber, 2005), the $\varphi C_T^0$ method proposes an approximation to the spatial and temporal variability of $\Delta C_{dis}$ ($\Delta\Delta C_{dis}$) (Vázquez-Rodríguez et al., 2009a).

The equation that describes $C_{ant}$ calculated from $\varphi C_T^0$ is the following:

Equation 21

$$C_{ant} = \frac{\Delta C^{*} - \Delta C^{t}_{dis}}{1 + \varphi \frac{|\Delta C^{t}_{dis}|}{C^{sat}_{ant}}}$$

where $\Delta C^{t}_{dis}$ is the present-day $\Delta C_{dis}$, $C^{sat}_{ant}$ is the theoretical saturation concentration of $C_{ant}$ of the sample, depending mostly on the atmospheric *p*CO2 at the moment of the water mass formation, $\varphi$ = 0.55±0.10 is a proportionality factor assumed to be constant elsewhere from the equator where it is positive, and $\Delta C^{*}$ is described in equation 13 $\Delta C^{t}_{dis}$ can be estimated following Gruber et al. (1996), as the difference between the $C_T$ in the mixed layer at the time of water mass formation and the theoretical $C_T$ in equilibrium with the corresponding atmospheric $pCO_2$ (thermodynamic equations). But since the values of $\Delta C^{t}_{dis}$ depend on conservative tracers [Θ, S, NO and PO (Broecker, 1974)], this term can be also estimated using a multilinear regression model which for the $\varphi C^{o}_{T}$ method results in:

Equation 22

$$\Delta C^{t}_{dis} = a + b(\Theta - 10) + c(S - 35) + d(NO - 300) + e(PO - 300)$$

with the specific parametric coefficients a, b, c, d and e varied with different temperature and latitudinal intervals (Vázquez-Rodríguez et al., 2009a). These coefficients for the North Atlantic Ocean are given in table 3.1.

Table 3.1 Parametric coefficients to calculate $\Delta C^t_{dis}$ for the North Atlantic Ocean

| Region | Latitude Band | Θ Interval (ºC) | a | b | c | d | e |
|---|---|---|---|---|---|---|---|
| **Atlantic** | 70ºN- 70ºS | $5 \leq \Theta < 8$ | −7.1 | 1.29 | 11.1 | - | - |
| **N. Atl.** | 20ºN -70ºN | $8 \leq \Theta < 18$ | −13.4 | 1.18 | - | - | 0.17 |
| **N. Atl.** | 20ºN -70ºN | $18 \leq \Theta \leq 25$ | −38.6 | 1.67 | 16.3 | −0.32 | 0.52 |

Recent studies revealed the increasing air-sea $pCO_2$ gradient from preindustrial times which makes rather imprecise the assumption of $\Delta C^t_{dis}$ constant in time (Hall et al., 2004; Matsumoto and Gruber, 2005)(Hall et al., 2004; Matsumoto and Gruber, 2005) and its variability ($\Delta\Delta C_{dis}$) should be considered and is defined as:

Equation 23

$$\Delta\Delta C_{dis} = \Delta C^t_{dis} - \Delta C^{\pi}_{dis} = -\varphi \left(\frac{C_{ant}}{C^{sat}_{ant}}\right) |\Delta C^t_{dis}|$$

Detailed description of the $\varphi C_T^0$ method can be found in Vázquez - Rodríguez et al., (2009a), included the propagation of the randomly perturbed errors process in order to obtain an uncertainty of ±5.2 $\mu mol \cdot kg^{-1}$ for the $\varphi C_T^0$ method. The MATLAB script to run $\varphi C_T^0$ method is available at the $CO_2$ Group webpage.

# III. Resultados y discusión / *Results and discussion*

# Chapter 1 / *Capítulo 1*

## Carbonate system measurements and internal consistency in the North Atlantic Ocean

## *Medidas del sistema del carbonato y consistencia interna en el Atlántico Norte*

# 1. Carbonate system measurements and internal consistency in the North Atlantic Ocean.

## Resumen

La absorción de $CO_2$ por el océano y su consecuente acidificación están aumentando la preocupación de la comunidad científica. Se han realizado muchos esfuerzos para determinar el papel y / o la importancia de los diferentes componentes del ciclo del carbono. Uno de los aspectos cruciales en el estudio del ciclo del carbono es contar con un sistema de carbonato consistente internamente. Desde el principio del siglo XX, diferentes autores se han interesado en la precisa medida de las constantes de disociación del ácido carbónico en aguas naturales y sintéticas. Algunas de estas constantes se evalúan aquí junto con los recientes cambios en la cociente boro / cloro, con el fin de hallar la combinación más apropiada para estimar la consistencia interna a diferentes rangos de pH en función del carbono inorgánico total ($C_T$) y la $[CO_3^{2-}]$. Las constantes de disociación propuestas para aguas naturales, resultan más apropiadas que las de aguas sintéticas, en particular, las constantes de Millero et al. (2006) dan los valores que mejor encajan con los medidos (por ejemplo, $C_{Tcalc}$-$C_{Tmeas}$ = - 0.3 ± 4.0 µmol·kg$^{-1}$). Las medidas de $[CO_3^{2-}]$ en el Atlántico Norte se han utilizado por primera vez para evaluar la consistencia interna. En este trabajo se propone una nueva ecuación para mejorar el método espectrofotométrico de $CO_3^{2-}$, considerando los efectos de la temperatura y de la adición de $PbCl_2$. Estas mejoras resultan en una

reducción del error relativo en la medida de $[CO_3^{2-}]$ a 1,2%. La buena correlación entre $[CO_3^{2-}]$ calculado y medido permite completar los perfiles de $[CO_3^{2-}]_{in\ situ}$ para las diferentes campañas del Atlántico Norte que se estudian aquí. Estas distribuciones de $[CO_3^{2-}]_{in\ situ}$ están relacionadas con las masas de agua características de cada región. En las campañas ecuatoriales, cabe destacar el mínimo de $[CO_3^{2-}]_{in\ situ}$ coincidente con la expansión de la Agua Intermedia Antártica.

## Abstract

The oceanic anthropogenic $CO_2$ uptake and the consequent ocean acidification are increasing concerns for the scientific community. Many efforts have been undertaken to determine the relative role and/or importance of the different carbon cycle components. One of the most crucial aspects of studying the carbon cycle is to have an internally consistent carbonate system. Since the beginning of the 20$^{th}$ century, different authors have been interested in the accurate measurement of the dissociation constants of the carbonic acid in natural and synthetic waters. Here, some of these constants are evaluated together with the recent changes in the boron to chlorinity ratio, to find the most appropriate combination to estimate the internal consistency at different pH ranges in terms of total inorganic carbon ($C_T$) and $[CO_3^{2-}]$. The dissociation constants proposed for natural waters, are more appropriated than those for synthetic waters. The constants of Millero et al. (2006) give values that best fit the measurements (e.g. $C_{Tcalc}$-$C_{Tmeas}$ = - 0.3 ± 4.0 µmol·kg$^{-1}$). North Atlantic $CO_3^{2-}$ measurements have been used for the first time to assess the internal consistency. A new equation is here proposed to improve the spectrophotometric $CO_3^{2-}$ method, taking into account the effects of temperature and the addition of $PbCl_2$. These improvements result on a reduction of the relative error in the $[CO_3^{2-}]$ measurements to 1.2%. Due to the good fit between calculated and measured $[CO_3^{2-}]$, $[CO_3^{2-}]_{in\ situ}$ profiles for North Atlantic cruises studied here can be completed. The distributions of $[CO_3^{2-}]_{in\ situ}$ in each cruise are related to the

characteristics of water masses present in each region. A $[CO_3^{2-}]_{in\ situ}$ minimum in the equatorial cruises coincides with the expansion of the Antarctic Intermediate Water.

## 1.1 Introduction

Since the beginning of the industrial period in the 18th century, large quantities of anthropogenic $CO_2$ have been emitted into the atmosphere (Le Quéré et al., 2009). Less than a half of these emissions remain in the atmosphere and so, the remainder has been taken up by the ocean or by the land biosphere (Sabine et al., 2004). Typically, the $CO_2$ system in seawater has been characterized by four measurable carbonate system variables (total dissolved inorganic carbon ($C_T$), total alkalinity ($A_T$), fugacity of $CO_2$ ($fCO_2$) and pH) and by the thermodynamic relations, which involve the dissociation constants of carbonic acid ($K_1^*$ and $K_2^*$, respectively for the first and second dissociation equilibrium). Thanks to the recent spectrophotometric method for measuring $CO_3^{2-}$, a fifth carbonate variable can be considered. This new methodology developed by Byrne and Yao (2008) allows the measurements of $CO_3^{2-}$ with a precision of 2.3%. Knowing two of the five observables carbonate system variables, the remaining ones are computed using the thermodynamics constants. The accuracy of these computations (internal consistency) depends on the reliability of the dissociation constants and the accuracy of the observations.

Since the beginning of the 20th century to the present day, the increasing interest in the accurate measurement of these dissociation constants has been reported by different authors (Buch et al., 1932; Dickson and Millero, 1987; Goyet and Poisson, 1989; Hansson, 1973; Lueker et al., 2000; Lyman, 1956; Mehrbach et al., 1973; Millero, 2010; Millero et al., 2006; Roy et al., 1993). During this

period, the constants of Mehrbach et al. (1973) calculated in natural seawater were the most mentioned and provided the basis for further work. In fact, their refit by Dickson and Millero (1987) became the most recommended for use during the 1990s global $CO_2$ survey (Lee et al., 2000). The dissociation constants estimated in synthetic seawater by Goyet and Poisson (1989) are in good agreement with the dissociation constants of Roy et al. (1993), obtaining similar results when they both are used to determine the internal consistency of the carbonate system (Lee and Millero, 1995; Lee et al., 1996, 1997; Millero et al., 1993). At the beginning of the 21$^{st}$ century, Lueker et al. (2000) reformulated Mehrbach et al. (1973) constants to try to improve them and to calculate $pK_1^*$ and $pK_2^*$ in natural water at total hydrogen ion scale. Later, Millero et al. (2002) determined new $pK_1^*$ and $pK_2^*$ from measurements of Atlantic, Indian, Southern and Pacific oceans, which agree with those from Mehrbach et al. (1973). They also evaluated their new constants with those from Lueker et al. (2000) at low $fCO_2$. In the same year, Mojica Prieto and Millero (2002) proposed another natural seawater set of constants, and they demonstrated that the difference between $pK_1^*$ and $pK_2^*$ in artificial and real seawater was mainly related to the ion-pair interaction of boric and bicarbonate ions. These recent achievements were taken into consideration by Millero et al. (2006), who developed a set of equations valid for values of salinity from 0 to 50 and temperature from 0 to 50ºC for estuarine and marine waters. The most recent pair of constants is described in Millero (2010), but they are only adjusted to estuarine environments. Taking into account the different pairs of

dissociation constants established during the latest forty years, four of them (Mehrbach et al. (1973), their refit by Dickson and Millero (1987), Lueker et al. (2000) and Millero et al. (2006)) are selected to evaluate the internal consistency of the carbonate system.

At the present time, the acidification of the oceans is faster than at any time in recent centuries (Pelejero et al., 2010), affecting also the saturation estate of aragonite and calcite (Doney et al., 2009; Riebesell et al., 2010). In order to assess the recent changes in the carbonate system through observations, the inclusion of all measurable carbonate variables, together with the latest thermodynamic improvements and the recent changes in the boron to chlorinity (B/Cl) ratio (Lee et al., 2010) would be advantageous in modernizing the global database (e.g., GLODAPv2, *IOCCP Report Number 24*, 2011). The present work is based on lab and North Atlantic measurements and reports the first $CO_3^{2-}$ observations along transoceanic sections in the characteristic water masses. Field $CO_3^{2-}$ measurements are used for the first time, together with the conventional pH, $C_T$, and $A_T$ measurements, to assess the internal consistency of the carbonic system at different pH ranges. Due to the lack of $fCO_2$ discrete samples, the internal consistency in terms of $fCO_2$ cannot be assessed here. Combining the latest advances in analytical techniques with the knowledge of the carbonate system, a significant improvement in the internal consistency was revealed. In addition, improvements to the recent spectrophotometric $CO_3^{2-}$ method (Byrne and Yao, 2008) are also proposed.

## 1.2 Data and Methodology

The $CO_2$ group of IIM-CSIC in Vigo (Spain) ($CO_2$group) has been involved in several national and international programs (GOSHIP) that cover an important area of the North Atlantic Ocean. In these expeditions, the group has measured three of the four established carbonic variables, i.e., $A_T$, $C_T$ and pH. These expeditions were $MOC^2$Equatorial 2010 (hereafter $MOC^2$), OVIDE 2010 (hereafter OVIDE), A24ºN 2011 (hereafter A24N) and CAIBOX 2009 (hereafter CAIBOX). The geographical distribution of these four cruises covering the North Atlantic Ocean is shown in figure 1.1.

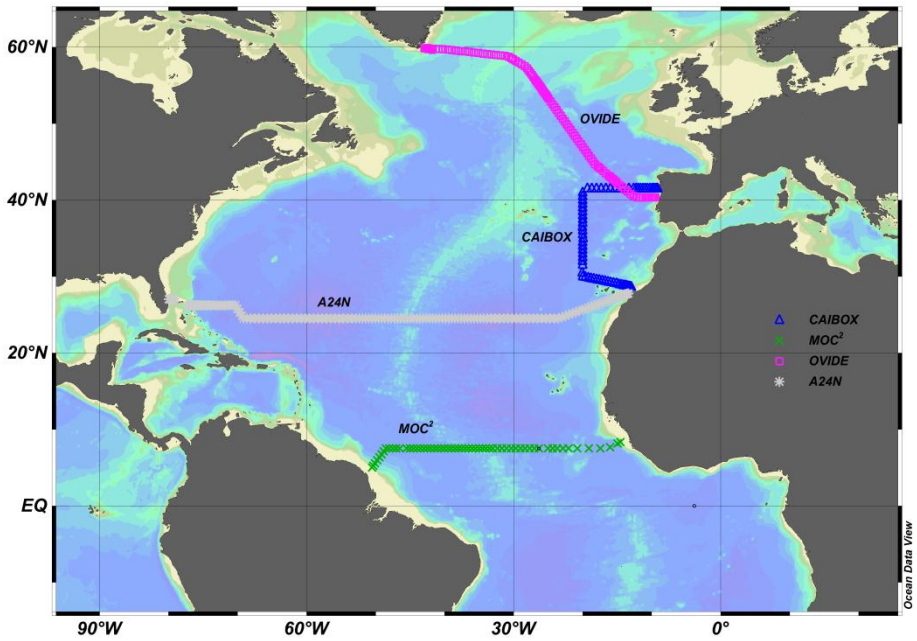


**Figure 1.1 Geographical distribution of studied cruises in the North Atlantic Ocean. CAIBOX cruise are denoted by grey triangles, white crosses represent $MOC^2$ cruise, black squares are the selected marks to OVIDE cruise and the light grey asterisks represent the A24N cruise.**

The MOC$^2$ cruise was carried out along 7.5ºN on board the Spanish R/V Hespérides from April to May 2010 crossing the Equatorial Atlantic Ocean from Fortaleza (Brazil) to Cape Verde Islands. The OVIDE cruise was carried out on the French R/V Thalassa from June to July 2010, covering the West European Basin from Lisbon (Portugal) to Greenland crossing the Reykjanes Ridge. The A24N cruise was carried out along 24.5ºN from January to March 2011 on board the Spanish R/V Sarmiento de Gamboa. The CAIBOX cruise was carried out along the Iberian Basin from July to August 2009 on board the R/V Sarmiento de Gamboa.

pH, $C_T$, and $A_T$ were measured during the CAIBOX, MOC$^2$, OVIDE and A24N cruises. In addition, during the CAIBOX and MOC$^2$ cruises, $[CO_3^{2-}]$ was also measured using a new methodology (Byrne and Yao, 2008). Together with the carbonate system variables, the salinity data provided by the conductivity sensor of the CTD were also reported in this work. The analytical methodologies used are widely described in section 2. *Analytical methodologies to measure carbonate variables and $O_2$* (inside II. Data and methodology) together with their accuracies. The vertical distributions of salinity, pH, $A_T$ and measured $[CO_3^{2-}]$ of CAIBOX and MOC$^2$ cruises are shown in figure 1.2.

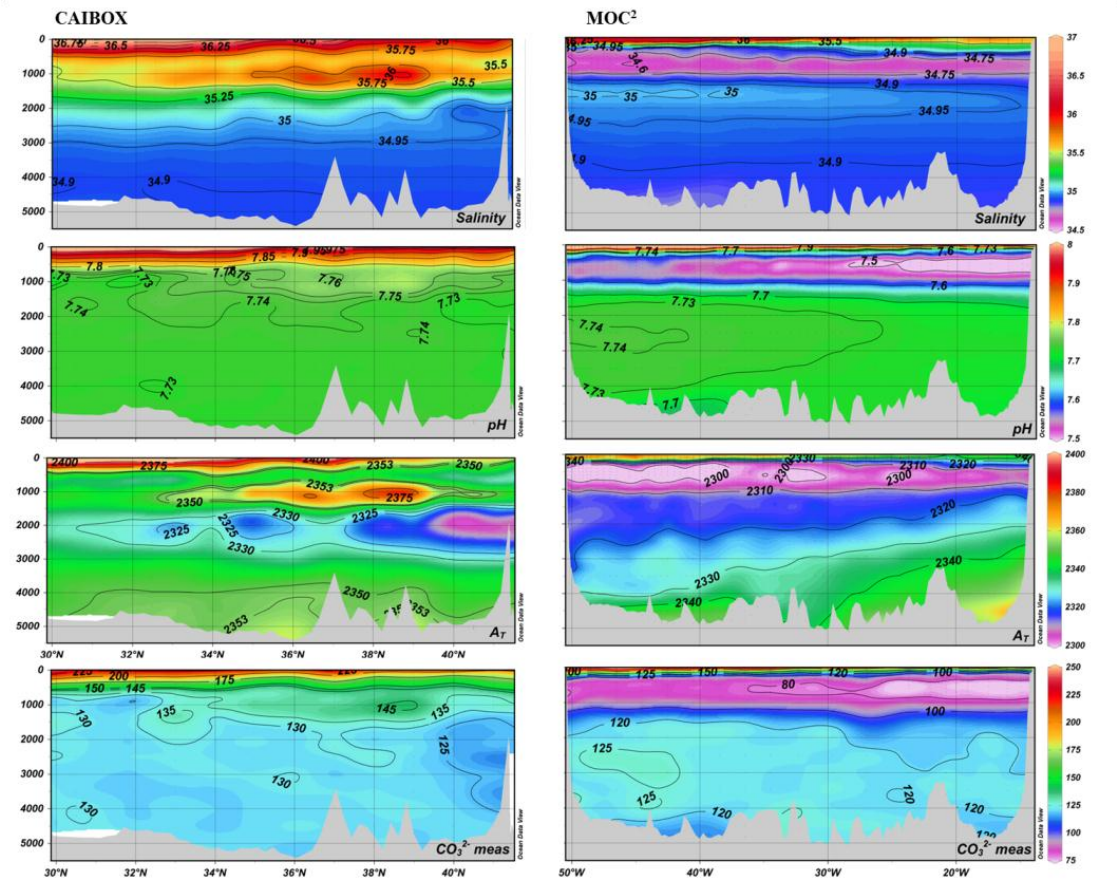


Figure 1.2 Vertical distribution of salinity, pH, $A_T$ and measured [$CO_3^{2-}$] of CAIBOX (left panels) and MOC² (right panels) cruises.

### 1.2.1 Constants of carbonate system

Knowing two of the five measurable carbonate variables (pH, $A_T$, $C_T$, $fCO_2$ and $CO_3^{2-}$), the other three can be calculated using the inorganic carbon system thermodynamic equations. Inside these thermodynamic equations, there are several constants to take into account. Four pairs of carbonic acid dissociation constants ($K_1$* and $K_2$*) were compared in the present work. Three pairs of dissociation

constants calculated in natural seawater: Millero et al. (2006) (hereafter M06), Mehrbach et al. (1973) refitted by Dickson and Millero (1987) (hereafter MDM87) and Lueker et al. (2000) (hereafter LDK00), and one pair calculated in synthetic waters by Goyet and Poisson (1989) (hereafter GP89). The hydrolysis constant of water was taken from Millero (1995). Dissociation constants for boric acid and ion $HSO_4^-$ (bisulphate) were taken from Dickson (1990b) and Dickson (1990a), respectively. The fluoride formation constant was taken from Dickson and Riley (1979). The universal B/Cl ratio for the North Atlantic Ocean was taken from Lee et al. (2010).

## 1.3 Results and Discussion

### 1.3.1 Comparison between measured and calculated $C_T$.

The measurements of pH, $A_T$ and $C_T$ from CAIBOX, MOC$^2$, OVIDE and A24N cruises, and in the described lab experiments, were used to examine the internal consistency of the carbonic system using the above cited dissociation constants for carbonic acid, i.e., M06, GP89, MDM87 and LDK00. Further considerations must be detailed before the examination is done. For instance, the B/Cl ratio taken was 0.2414 ± 0.0009 $mg \cdot kg^{-1} \cdot ‰^{-1}$, which was obtained from North Atlantic Ocean measurements among others (Lee et al., 2010) instead of the generally accepted ratio of 0.232 ± 0.005 $mg \cdot kg^{-1} \cdot ‰^{-1}$ by Uppström (1974). This new B/Cl ratio resulted to be more internally consistent with MDM87 constants

than the Uppström (1974) ratio, when the measured $A_T$ is compared with calculated $A_T$ from $C_T$ and pH (Lee et al., 2010). The improvements achieved in terms of internal consistency by the use of Lee (Lee et al., 2010) ratio were tested in the present work. The effect of B/Cl ratio is implicit in all the carbonic system but the most important influence can be discerned when $C_T$ is calculated, in which this ratio produces a decrease of approximately 2 $\mu mol \cdot kg^{-1}$ lower that the one obtained with the Uppström ratio. Moreover, another important innovation was applied in this work: the correction of the spectrophotometric pH (eq. 1) by Yao el at (2007), who asserted that the mCP impurities can contribute to pH offsets as large as 0.01 pH units. Because of being a parabolic correction, it does not linearly affect all ranges of pH as the DelValls (DelValls and Dickson, 1998) correction does, and surface water samples require a more significant offset than the deep ocean waters (Liu et al., 2011; Yao et al., 2007).

Taking into account these two new effects [the new B/Cl ratio and pH corrected by Yao (eq. 1)], the carbonate internal consistency was done by examining the difference between calculated and measured $C_T$ ($\delta C_T = C_{Tcalc} - C_{Tmeas}$), using pH and $A_T$ as input measurements. The $\delta C_{T\ CAIBOX}$, $\delta C_{T\ MOC2}$, $\delta C_{T\ OVIDE}$, $\delta C_{T\ A24N}$ were individually studied and also altogether ($\delta C_{T\ cruises}$) with the aim of giving the general differences. These data were divided into four different pH groups according to the distribution of $\delta C_T$ in terms of pH: $7.49 < pH \leq 7.60$, $7.60 < pH \leq 7.85$, $7.85 < pH \leq 8.02$ and $8.02 < pH \leq 8.14$. Similarly, $\delta C_T$ from laboratory experiments ($\delta C_{T\ lab}$) were divided into the pH of each experiment. In figure 1.3 all these

$\delta C_T$ are plotted in terms of carbonic acid dissociation constants, in figures 1.3a and 1.3b the obtained results from $\delta C_{T\ cruises}$ and $\delta C_{T\ lab}$, respectively, are shown. The $\delta C_{T\ CAIBOX}$, $\delta C_{T\ MOC2}$, $\delta C_{T\ OVIDE}$ and $\delta C_{T\ A24N}$ values are also represented in figures 1.3c, 1.3d, 1.3e and 1.3f, respectively. These $\delta C_T$ with their associated standard deviations can be also seen in table 1.1.

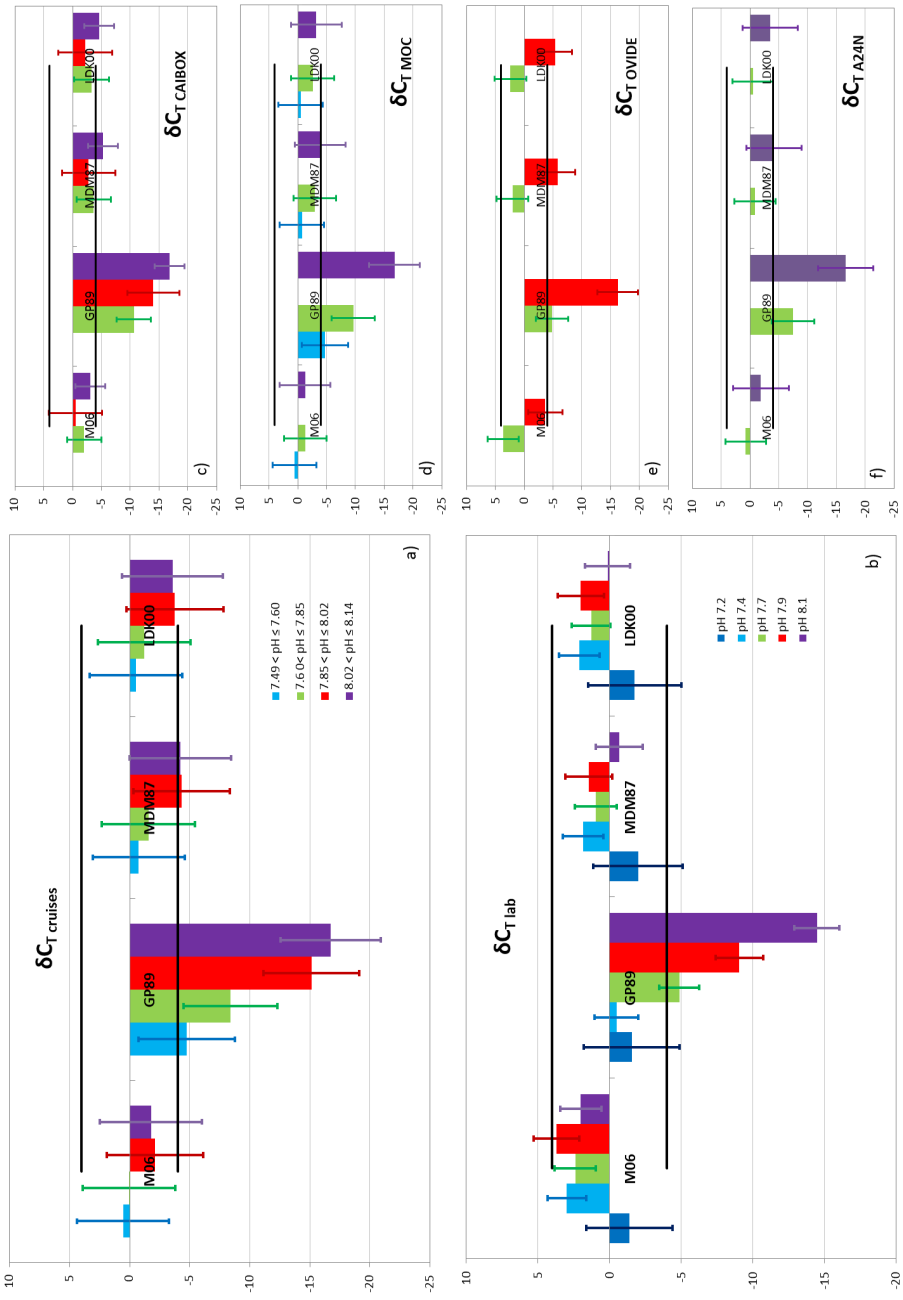


Figure 1.3 These bar charts plot in the "x-axis" the carbonic acid dissociation constants used (i.e., M06, GP89, MDM87 and LDK00) and in the "y-axis", $\delta C_T$ ($C_{Tcalc}$ - $C_{Tmeas}$) value with their confidence interval (μmol·kg$^{-1}$). The horizontal black lines show the maximum error allowed in the calculated $C_T$ using the pH and $A_T$ as measured inputs. The $\delta C_{T\ cruises}$ (a), $\delta C_{T\ CAIBOX}$ (c), $\delta C_{T\ MOC2}$ (d), $\delta C_{T\ OVIDE}$ (e)and $\delta C_{T\ A24N}$ (f) are grouped in terms of pH: 7.49 < pH ≤ 7.60 (blue bars), 7.60 < pH ≤ 7.85 (green bars), 7.85 < pH ≤ 8.02 (red bars) and 8.02 < pH ≤ 8.14 (purple bars). Similarly, the $\delta C_{T\ lab}$ (3) are divided into the pH value of each experiment, i.e., 7.2 (dark blue bar), 7.4 (light blue bar), 7.7 (green bar), 7.9 (red bar) and 8.1(purple bar).

**Table 1.1 Mean value of $\delta C_T$ ($C_{Tcalc}$ - $C_{Tmeas}$) in µmol·kg$^{-1}$ with their associated standard deviation for each pair of carbonic acid dissociation constants: M06, GP89, MDM87 and LDK00. The $\delta C_{T\ cruises}$, $\delta C_{T\ CAIBOX}$, $\delta C_{T\ MOC2}$, $\delta C_{T\ OVIDE}$ and $\delta C_{T\ A24N}$ are grouped in terms of pH: 7.49 < pH ≤ 7.60, 7.60 < pH ≤ 7.85, 7.85 < pH ≤ 8.02 and 8.02 < pH ≤ 8.14. Similarly, the $\delta C_{T\ lab}$ are divided into the pH value of each experiment, i.e., 7.2, 7.4, 7.7, 7.9 and 8.1.**

| | $\delta C_T$ (µmol·kg$^{-1}$) | | | |
|---|---|---|---|---|
| **pH range** | **M** | **GP89** | **MDM87** | **LDK00** |
| | | **$\delta C_{T\ cruises}$** | | |
| 7.49<pH≤7.60 | 0.5±3.8 | -4.8±4.0 | -0.8±3.8 | -0.5±3.8 |
| 7.60<pH≤7.85 | 0.1±3.8 | -8.4±3.9 | -1.6±3.8 | -1.3±3.8 |
| 7.85<pH≤8.02 | -2.1±4.0 | -15.1±4.0 | -4.3±4.0 | -3.7±4.0 |
| 8.02<pH≤8.14 | -1.8±4.3 | -16.7±4.2 | -4.2±4.2 | -3.6±4.2 |
| | | **$\delta C_{T\ CAIBOX}$** | | |
| 7.60<pH≤7.85 | -2.0±3.0 | -10.7±3.0 | -3.7±3.0 | -3.3±3.0 |
| 7.85<pH<8.02 | -0.5±4.6 | -14.0±4.5 | -2.8±4.6 | -2.2±4.6 |
| 8.02<pH≤8.14 | -3.1±2.6 | -16.8±2.6 | -5.3±2.6 | -4.6±2.5 |
| | | **$\delta C_{T\ MOC}$** | | |
| 7.49<pH≤7.60 | 0.5±3.8 | -4.8±4.0 | -0.8±3.8 | -0.5±3.8 |
| 7.60<pH≤7.85 | -1.3±3.7 | -9.7±3.8 | -3.0±3.7 | -2.6±3.7 |
| 7.85<pH≤8.02 | - | - | - | - |
| 8.02<pH≤8.14 | -1.3±4.4 | -16.8±4.4 | -3.9±4.4 | -3.2±4.4 |
| | | **$\delta C_{T\ OVIDE}$** | | |
| 7.60<pH≤7.85 | 3.7±2.7 | -4.8±2.7 | 2.0±2.7 | 2.4±2.7 |
| 7.85<pH<8.02 | -3.7±2.9 | -16.3±3.5 | -5.8±3.0 | -5.3±3.0 |
| | | **$\delta C_{T\ A24N}$** | | |
| 7.60<pH≤7.85 | 0.8±3.5 | -7.5±3.7 | -0.9±3.5 | -0.5±3.5 |
| 8.02<pH≤8.14 | -1.9±4.8 | -16.6±4.8 | -4.2±4.8 | -3.5±4.8 |
| | | **$\delta C_{T\ lab}$** | | |
| pH 7.2 | -1.4±3.0 | -1.5±3.3 | -2.0±3.1 | -1.8±3.2 |
| pH 7.4 | 3.0±1.4 | -0.5±1.5 | 1.8±1.4 | 2.1±1.4 |
| pH 7.7 | 2.4±1.4 | -4.9±1.4 | 1.0±1.5 | 1.3±1.4 |
| pH 7.9 | 3.7±1.6 | -9.1±1.7 | 1.5±1.6 | 2.0±1.6 |
| pH 8.1 | 2.0±1.4 | -14.5±1.6 | -0.7±1.6 | 0.1±1.6 |

In general terms, the best agreement between $C_{Tcalc}$ and $C_{Tmeas}$ is obtained when the dissociation acid constants are calculated in

natural water, i.e. M06, MDM87 and LDK00, in which case $\delta C_{T\ cruises}$ (Fig. 1.3a) are inside the allowed limits of error. $\delta C_{T\ cruises}$ using the M06 constant vary from -2.1 ± 4.0 µmol·kg$^{-1}$ to 0.5 ± 3.8 µmol·kg$^{-1}$. These values are smaller than those involving MDM87 and LDK00 constants which vary from -0.8 ± 3.8 µmol·kg$^{-1}$ to -4.3 ± 4.0 µmol·kg$^{-1}$ and from -0.5 ± 3.8 µmol·kg$^{-1}$ to -3.7 ± 4.0 µmol·kg$^{-1}$, respectively. Contrarily, the dissociation acid constants calculated in synthetic water (GP89) produce much more significant $\delta C_T$ values (Fig. 1.3a) than those calculated in natural waters, $\delta C_{T\ cruises}$ vary from -4.8 ± 4.0 µmol·kg$^{-1}$ to -16.7 ± 4.2 µmol·kg$^{-1}$. The difference between constants calculated in natural or synthetic waters is also shown in the laboratory experiments (Fig. 1.3b), in which it is difficult to distinguish which of the natural constants produces the best $\delta C_{T\ lab}$ data (M06 varies from -1.4 ± 3.0 µmol·kg$^{-1}$ to 3.7 ± 1.6 µmol·kg$^{-1}$, MDM87 varies from -2.0 ± 3.1 µmol·kg$^{-1}$to 1.8 ± 1.4 µmol·kg$^{-1}$ and LDK00 varies from -1.8 ± 3.2 µmol·kg$^{-1}$to 2.1±1.4 µmol·kg$^{-1}$). It is possible to point out that GP89 constants, in general, do not produce a good agreement between $C_{Tcalc}$ and $C_{Tmeas}$, their $\delta C_{T\ lab}$ varying from -14.5 ± 1.6 µmol·kg$^{-1}$ to -0.5 ± 1.5 µmol·kg$^{-1}$.

In the particular case of GP89 constants, $\delta C_{T\ lab}$ and $\delta C_{T\ cruises}$ values seem to decrease with pH (Fig. 1.3), suggesting that these constants are more reliable at lower pH because the differences between natural and synthetic waters are higher in $K_2^*$ than $K_1^*$. This is also clearly shown in $\delta C_T$ of individual cruises (Fig. 1.3c, 1.3d, 1.3e and 1.3f, respectively). The $\delta C_{T\ MOC2}$ at $7.49 < pH \leq 7.60$ (blue bar) show a high value close to the error of -4.8 ± 4.0 µmol·kg$^{-1}$. At 7.60

< pH ≤ 7.85 (green bar) the values vary from $\delta C_{T\ OVIDE}$ = -4.8 ± 2.7 µmol·kg$^{-1}$ to $\delta C_{T\ CAIBOX}$ = -10.7 ± 3.0 µmol·kg$^{-1}$ while at 7.85 < pH ≤ 8.02 (red bar) the values of $\delta C_{T\ CAIBOX}$ and $\delta C_{T\ OVIDE}$ are both -15 µmol·kg$^{-1}$, approximately. This value is very similar to those of $\delta C_{T\ CAIBOX}$, $\delta C_{T\ MOC2}$ and $\delta C_{T\ A24N}$ (~ -17 µmol·kg$^{-1}$) at 8.02 < pH ≤ 8.14 (purple bar). Due to the general increasing trend of the absolute $\delta C_T$ values with pH, some bias could be applied when these GP89 constants are used in other non-direct applications, for instance, in the calculation of $C_{eq}$ involved in the ΔC* back-calculation method (Gruber et al., 1996) to estimate the anthropogenic $CO_2$.

The aim of the present work is also to discern which of M06, MDM87 and LDK00 constants are the most internally consistent. Independently of the pH range and of $C_{Tmeas}$ origin (field or lab), $\delta C_T$ obtained by MDM87 and LDK00 only differ in 0.5 µmol·kg$^{-1}$, $\delta C_T$ from LDK00 being always lower. Thus, MDM87 and LDK00 constants can be considered as the same pair of constants, in order to compare them with M06 constants. At pH ranges lower than 7.85 (7.49 < pH ≤ 7.60 and 7.60 < pH ≤ 7.85) (Fig. 1.3a), choosing between pairs of dissociation constants is very complicated because there are not significant differences in $\delta C_{T\ cruises}$ (only a slight difference of 1.5 µmol·kg$^{-1}$ between M06 and MDM87). Nevertheless, at pH > 7.85 (7.85 < pH ≤ 8.02 and 8.02 < pH ≤ 8.14), $\delta C_{T\ cruises}$ of M06 and MDM87 differ in ~2.2 µmol·kg$^{-1}$. At 8.02 < pH ≤ 8.14 (purple bar), $\delta C_{T\ cruises}$ value of M06 (-1.8 ± 4.3 µmol·kg$^{-1}$) is lower than those from MDM87 (-4.2 ± 4.2 µmol·kg$^{-1}$). This favours the selection of M06 constants as the more appropriate ones, i.e., the most internally consistent. Confirming that, $\delta C_T$

$_{CAIBOX}$, $\delta C_{T\ MOC2}$, and $\delta C_{T\ A24N}$ (Fig. 1.3c, d and f) show the lowest absolute values in all pH ranges. On the contrary, this choice could not be made based on $\delta C_{T\ lab}$ due to the small mean difference between M06 and MDM87 (~1.6 $\mu mol \cdot kg^{-1}$), which can be produced by a different organic matter concentration in both sampled waters (Bradshaw and Brewer, 1988a, 1988b).

In order to evaluate how the addition of 0.0047 units of pH, correction proposed by DelValls et at. (1998), affects the internal consistency, $C_{Tcalc}$ was calculated from "spectrophotometric pH + 0.0047" and measured $A_T$ and compared with $C_{Tcalc}$ estimated from "spectrophotometric pH" (Table 1.2).

Table 1.2 Determination coefficient ($R^2$) and slope of the obtained linear fit and normalized between $C_{Tcalc}$ and $C_{Tmeas}$ for the all cruises group (n = 177) and each pair of carbonic acid dissociation constants (M06, GP89, MDM87 and LDK00) when the $C_{Tcalc}$ were calculated from "spectrophotometric pH" and from "spectrophotometric pH + 0.0047". The mean values of $\delta C_{T\ cruises}$ ($\delta C_T = C_{Tcalc} - C_{Tmeas}$) with their standard deviation are also shown in µmol·kg$^{-1}$ for each pair of constants.

| | Spectrophotometric pH | | | | | Spectrophotometric pH + 0.0047 | | | | |
|---|---|---|---|---|---|---|---|---|---|---|
| $K_1^*$ & $K_2^*$ | $R^2$ | α ± STD | $\delta C_{T\ cruises}$ ± STD | $_NR^2$ | $_N\alpha$ ± STD | $R^2$ | α ± STD | $\delta C_{T\ cruises}$ ± STD | $_NR^2$ | $_N\alpha$ ± STD |
| **M06** | 0.996 | 1.008±0.005 | -0.3±4.0 | 0.998 | 1.006±0.003 | 0.996 | 1.014±0.005 | -2.5±4.1 | 0.998 | 1.010±0.003 |
| **GP89** | 0.996 | 1.050±0.005 | -9.9±5.4 | 0.998 | 1.034±0.003 | 0.996 | 1.056±0.005 | -12.2±5.7 | 0.998 | 1.038±0.003 |
| **MDM87** | 0.996 | 1.013±0.005 | -2.1±4.0 | 0.998 | 1.010±0.003 | 0.996 | 1.019±0.005 | -4.3±4.2 | 0.998 | 1.014±0.003 |
| **LDK00** | 0.996 | 1.011±0.005 | -1.7±4.0 | 0.998 | 1.008±0.003 | 0.996 | 1.018±0.005 | -3.9±4.1 | 0.998 | 1.013±0.003 |

The determination coefficient ($R^2$) and the slope of the obtained linear fit between $C_{Tcalc}$ and $C_{Tmeas}$ for all cruises (n = 177) and each pair of carbonic acid dissociation constants (M06, GP89, MDM87 and LDK00) are shown in table 1.2. The normalized $C_T$ values were also calculated taking into account the relation "$_NC_T = C_T \cdot 35$ / salinity" and their corresponding normalized linear fit ($_NC_{Tcalc}$ versus $_NC_{Tmeas}$), which is also shown in table 1.2. Considering $C_{Tcalc}$ from "spectrophotometric pH", a good correlation was found between $C_{Tcalc}$ and $C_{Tmeas}$ ($R^2$ = 0.996 and $_NR^2$ = 0.998) independently of the dissociation constants used. In terms of slope, the linear fit achieved by M06 constants is clearly closer to one, corroborated also by the minimum $\delta C_{T\ cruises}$ = -0.3 µmol·kg$^{-1}$. When results from "spectrophotometric pH + 0.0047" were considered, the correlation between $C_{Tcalc}$ and $C_{Tmeas}$ is almost the same and M06 are the most appropriate constants too (Table 1.2). But the addition of 0.0047 units produces an increase in $C_{Tcalc}$ of approximately 2 µmol·kg$^{-1}$, and consequently, the increase of $\delta C_{Tcruises}$.

The carbonic dissociation constants determined in natural waters (M06, MDM87 and LDK00) produce the lowest absolute values of $\delta C_T$ (in field and in laboratory, fig. 1.3), compared with the constants determined in synthetic waters (GP89). The minimum $\delta C_{T\ cruises}$ and the most robust linear fit between $C_{Tcalc}$ and $C_{Tmeas}$ are obtained with M06 constants. Thus, the most recent pH correction (Yao et al., 2007) and constants (Lee et al., 2010; Millero et al., 2006) are strongly recommended in field measurements in order to achieve the most consistent $C_{Tcalc}$.

The appropriate choice of dissociation constants is also a key point in terms of acidification. Due to the fact that in many historical cruises or even in the GLODAP database there are not pH measurements, thermodynamic equations can be used to calculate pH data from measured $C_T$ and $A_T$. Taking into account the measured $C_T$ and $A_T$ of the North Atlantic Ocean (CAIBOX, MOC$^2$, OVIDE and A24N) studied in this work, pH data were calculated using different sets of dissociation constants. The use of the most appropriate dissociation constants M06 and the B/Cl ratio of Lee (Lee et al., 2010), result in pH values 0.0003 ± 0.0007 lower than the measured ones, while the use of LDK00 or MDM87 constants produces pH values lower by 0.0033 ± 0.0007 or 0.0041 ± 0.0007, respectively, than the measured pH data. However, these results are exceeded by GP89constants (calculated in synthetic seawater), reaching pH values 0.0201± 0.0007 lower than the measured ones.

### 1.3.2 Internal consistency of $[CO_3^{2-}]$

The $[CO_3^{2-}]$ of CAIBOX and MOC$^2$ cruises was determined following the equation (eq. 9, see *data and methodology* section). In order to evaluate the internal consistency of the $CO_2$ system in terms of $[CO_3^{2-}]$, the $[CO_3^{2-}]$ was calculated ($[CO_3^{2-}]_{calc}$) by using pH and $A_T$ as input measurements and M06, GP89, MDM87 and LDK00 dissociation acid constants. According to the evaluation of $C_T$ consistency, the B/Cl ratio was taken from Lee et al. (2010) and the spectrophotometric pH was corrected by Yao et al. (2007).

The internal consistency was evaluated by means of $\delta CO_3^{2-}$ in µmol·kg$^{-1}$, i.e., the differences between calculated and measured $[CO_3^{2-}]$ ($\delta CO_3^{2-} = [CO_3^{2-}]_{calc} - [CO_3^{2-}]_{meas}$). In figure 1.4, $\delta CO_3^{2-}{}_{cruises}$ (Fig. 1.4a), $\delta CO_3^{2-}{}_{CAIBOX}$ (Fig. 1.4c) and $\delta CO_3^{2-}{}_{MOC2}$ (Fig. 1.4c) were studied in four different pH groups (coloured bars in fig. 1.4) for each pair of constants, M06, GP89, MDM87 and LDK00. $\delta CO_3^{2-}{}_{lab}$ is also shown in figure 1.4b, in which the pH values are those fixed by the experiment.

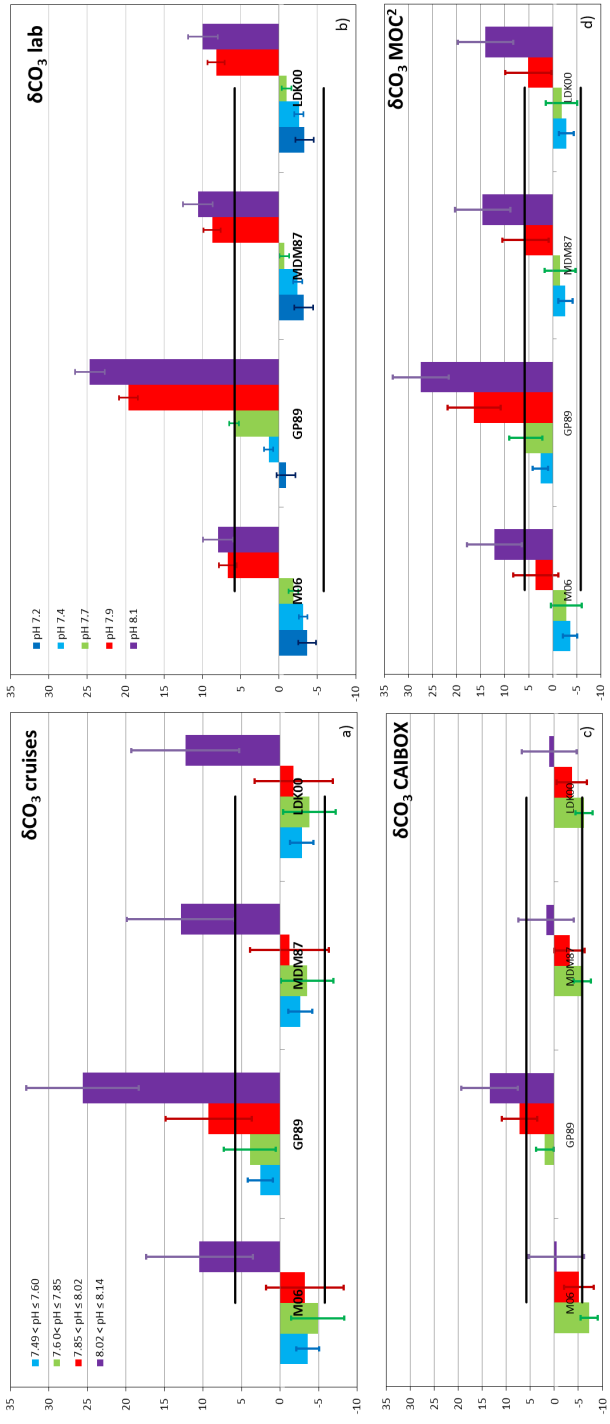


Figure 1.4 $\delta CO_3^{2-}$ ($CO_3^{2-}$ calc - $CO_3^{2-}$ meas) ("y-axis") in µmol·kg$^{-1}$ are plotted with the carbonic acid dissociation constants: M06, GP89, MDM87 and LDK00 ("x-axis"). The $\delta CO_3^{2-}$ cruises, $\delta CO_3^{2-}$ CAIBOX and $\delta CO_3^{2-}$ MOC2 (Fig. 6a, 6c and 6d, respectively) are grouped in terms of pH: 7.49 < pH ≤ 7.60 ($\delta CO_3^{2-}$ blue bars), 7.60 < pH ≤ 7.85 ($\delta CO_3^{2-}$ green bars), 7.85< pH ≤ 8.02 ($\delta CO_3^{2-}$ red bars) and 8.02 < pH ≤ 8.14 ($\delta CO_3^{2-}$ purple bars). Similarly, the $\delta CO_3^{2-}$ lab shown in figure 6b are divided into the pH value of each experiment, i.e., 7.2 ($\delta CO_3^{2-}$ dark blue bar), 7.4 ($\delta CO_3^{2-}$ light blue bar), 7.7 ($\delta CO_3^{2-}$ green bar), 7.9 ($\delta CO_3^{2-}$ red bar) and 8.1($\delta CO_3^{2-}$ purple bar). The horizontal black lines correspond to the relative errors of 2.3% in calculated carbonate (± 5.8 µmol·kg$^{-1}$ when $[CO_3^{2-}]$ = 250 µmol·kg$^{-1}$) estimated by pH and $A_T$ as measured inputs (Byrne and Yao, 2008).

The mean $\delta CO_3^{2-}$ values with their associated standard deviation in $\mu mol \cdot kg^{-1}$ are shown for each cruise in table 1.3.

**Table 1.3 Mean value of $\delta CO_3^{2-}$ ($CO_3^{2-}{}_{calc}$ - $CO_3^{2-}{}_{meas}$) in $\mu mol \cdot kg^{-1}$ with their associated standard deviation for each pair of carbonic acid dissociation constants: M06, GP89, MDM87 and LDK00. The $\delta CO_3^{2-}{}_{cruises}$, $\delta CO_3^{2-}{}_{CAIBOX}$, $\delta CO_3^{2-}{}_{MOC2}$, $\delta CO_3^{2-}{}_{OVIDE}$ and $\delta CO_3^{2-}{}_{A24N}$ are grouped in terms of pH: 7.49 < pH ≤ 7.60, 7.60 < pH ≤ 7.85, 7.85 < pH ≤ 8.02 and 8.02 < pH ≤ 8.14. Similarly, the $\delta CO_3^{2-}{}_{lab}$ are divided into the pH value of each experiment, i.e., 7.2, 7.4, 7.7, 7.9 and 8.1.**

| | $\delta CO_3^{2-}$ ($\mu mol \cdot kg^{-1}$) | | | |
|---|---|---|---|---|
| **pH range** | **M** | **GP89** | **MDM87** | **LDK00** |
| | | $\delta CO_3^{2-}{}_{cruises}$ | | |
| 7.49<pH≤7.60 | -3.6±1.5 | 2.6±1.6 | -2.6±1.5 | -2.8±1.5 |
| 7.60<pH≤7.85 | -4.9±3.4 | 3.9±3.4 | -3.5±3.4 | -3.8±3.4 |
| 7.85<pH≤8.02 | -3.2±5.0 | 9.3±5.6 | -1.2±5.1 | -1.8±5.1 |
| 8.02<pH≤8.14 | 10.5±6.9 | 25.6±7.3 | 12.9±7.0 | 12.3±7.0 |
| | | $\delta CO_3^{2-}{}_{CAIBOX}$ | | |
| 7.60<pH≤7.85 | -7.3±1.8 | 2.0±1.8 | -5.8±1.8 | -6.2±1.8 |
| 7.85<pH<8.02 | -5.1±3.1 | 7.3±3.7 | -3.2±3.2 | -3.7±3.1 |
| 8.02<pH≤8.14 | -0.5±2.8 | 13.5±2.8 | 1.7±2.8 | 1.0±2.8 |
| | | $\delta CO_3^{2-}{}_{MOC}$ | | |
| 7.49<pH≤7.60 | -3.6±1.5 | 2.6±1.6 | -2.6±1.5 | -2.8±1.5 |
| 7.60<pH≤7.85 | -2.9±3.2 | 5.6±3.5 | -1.5±3.2 | -1.8±3.2 |
| 7.85<pH≤8.02 | 3.6±4.7 | 16.4±5.5 | 5.6±4.8 | 5.1±4.8 |
| 8.02<pH≤8.14 | 12.1±5.7 | 27.5±5.8 | 14.6±5.7 | 14.0±5.7 |
| | | $\delta CO_3^{2-}{}_{OVIDE}$ | | |
| 7.60<pH≤7.85 | - | - | - | - |
| 7.85<pH<8.02 | - | - | - | - |
| | | $\delta CO_3^{2-}{}_{A24N}$ | | |
| 7.60<pH≤7.85 | - | - | - | - |
| 8.02<pH≤8.14 | - | - | - | - |
| | | $\delta CO_3^{2-}{}_{lab}$ | | |
| pH 7.2 | -3.7±1.2 | -0.9±1.2 | -3.2±1.2 | -3.3±1.2 |
| pH 7.4 | -3.1±0.6 | 1.4±0.6 | -2.4±0.6 | -2.6±0.6 |
| pH 7.7 | -1.9±0.6 | 5.8±0.6 | -0.7±0.6 | -1.0±0.6 |
| pH 7.9 | 6.7±1.1 | 19.6±1.2 | 8.7±1.1 | 8.2±1.1 |
| pH 8.1 | 8.0±2.0 | 24.7±1.9 | 10.6±1.9 | 9.9±1.9 |

The lowest $\delta CO_3^{2-}{}_{cruises}$ values shown in figure 1.4a are obtained with M06, MDM87 and LDK00 constants. At pH < 8.02, the $\delta CO_3^{2-}{}_{cruises}$ using M06 constants vary from -3.2 ± 5.0 µmol·kg$^{-1}$ to -4.9 ± 3.4 µmol·kg$^{-1}$. MDM87 and LDK00 produce very close $\delta CO_3^{2-}{}_{cruises}$ values, varying from -1.2 ± 5.1 µmol·kg$^{-1}$ to -3.5 ± 3.4 µmol·kg$^{-1}$ and from -1.8 ± 5.1 µmol·kg$^{-1}$ to -3.8 ± 3.4 µmol·kg$^{-1}$, respectively. However, at pH > 8.02 the $CO_3^{2-}{}_{calc}$ obtained with these M06, MDM87 and LDK00 constants are approximately 11 µmol·kg$^{-1}$ higher than the $[CO_3^{2-}]_{meas}$. As Byrne and Yao said [see Fig. 8 of Byrne and Yao (2008)], when $[CO_3^{2-}]$ are greater than 150 µmol·kg$^{-1}$, there is a scattering in the relation $\delta CO_3^{2-}$ and $[CO_3^{2-}]_{calc}$. In this study, the scatter is towards positive $\delta CO_3^{2-}$ values while in Byrne and Yao (2008) is towards negative, but the difference between $[CO_3^{2-}]_{meas}$ and $[CO_3^{2-}]_{calc}$ is of a very similar magnitude. This different behaviour mainly depends on the ionic media and the dissolved organic matter because, at the same pH range (8.02 < pH ≤ 8.14), $\delta CO_3^{2-}{}_{CAIBOX}$ (Fig. 1.4c) are only 1 µmol·kg$^{-1}$ while $\delta CO_3^{2-}{}_{MOC2}$ (Fig. 1.4d) are around 13 µmol·kg$^{-1}$. In the laboratory experiments (Fig. 1.4b, Table 1.3), the lowest $\delta CO_3^{2-}{}_{lab}$ are also obtained with pH < 7.7 and M06, MDM87 and LDK00 constants. These $\delta CO_3^{2-}{}_{lab}$ vary from -0.7 ± 0.6 µmol·kg$^{-1}$ at pH = 7.7 with MDM87 constants to -3.7 ± 1.2 µmol·kg$^{-1}$ at pH = 7.2 with M06 constants. The greatest positive values of $\delta CO_3^{2-}{}_{lab}$ at pH 7.9 (blue bars) and 8.1 (green bars) ~9 µmol·kg$^{-1}$ and ~10 µmol·kg$^{-1}$, respectively (Fig. 1.4b). In both these lab experiments, some minuscule crystals were observed inside the $CO_3^{2-}$ cell before measurements, which can indicate $CO_3^{2-}$ precipitation before the

addition of $PbCl_2$. This means that, at those elevated pH, the measured $[CO_3^{2-}]$ could therefore be less than the real one.

Taking into account GP89 constants, the $\delta CO_3^{2-}{}_{cruises}$ (Fig. 1.4a, Table 1.3) vary from 2.6 ± 1.6 µmol·kg$^{-1}$ to 25.6 ± 7.3 µmol·kg$^{-1}$ and the $\delta CO_3^{2-}{}_{lab}$ (Fig. 1.4b, Table 1.3) range is from -0.9 ± 1.2 µmol·kg$^{-1}$ to 24.7 ± 1.9 µmol·kg$^{-1}$. The increase of $\delta CO_3^{2-}{}_{cruises}$ and $\delta CO_3^{2-}{}_{lab}$ with pH is clearly observed in figures 1.4a and b, suggesting, similarly to $C_T$ comparison, that these constants produce better agreement between $[CO_3^{2-}]_{calc}$ and $[CO_3^{2-}]_{meas}$ at pH lower than 7.7. Once more, these synthetic constants produce higher deviations than the constants estimated in natural water.

In order to discern what constants are more internally consistent with $[CO_3^{2-}]$ among M06, MDM87 and LDK00, $\delta CO_3^{2-}$ were evaluated altogether ($\delta CO_3^{2-}{}_{cruises}$ at whole pH range). This $\delta CO_3^{2-}$ using M06 constants was -3 ± 5 µmol·kg$^{-1}$ while for both MDM87 and LDK00 pairs of constants $\delta CO_3^{2-}$ were -2 ± 6 µmol·kg$^{-1}$. Despite the low mean values of MDM87 and LDK00, M06 constants are proposed to be used in the calculations of $[CO_3^{2-}]$ since they produce less standard deviation. $[CO_3^{2-}]_{calc}$ estimated using M06 constants fit very well ($R^2$ = 0.987) with $[CO_3^{2-}]_{meas}$ through the linear adjustment: $[CO_3^{2-}]_{calc}$= (1.059 ± 0.005)·$[CO_3^{2-}]_{meas}$ - (11.2 ± 0.6).

### 1.3.3 Variability of $CO_3^{2-}$ i.s. and $\Omega_{arag}$ in the North Atlantic Ocean.

Due to the good fit between $[CO_3^{2-}]_{meas}$ and $[CO_3^{2-}]_{calc}$, it is possible to display the complete $CO_3^{2-}$ profile of the four cruises studied in this work. The $[CO_3^{2-}]_{in\ situ}$ was calculated from measured $A_T$ and pH (spectrophotometric pH, eq. 1) using the $CO_2$sys with M06 constants together with the B/Cl ratio from Lee et al. (2010). The resultant profiles are plotted in figure 1.5, from the north part of the Atlantic Ocean (OVIDE cruise, Fig. 1.5a) towards the most equatorial part of the Atlantic Ocean (MOC$^2$ cruise, Fig. 1.5d).

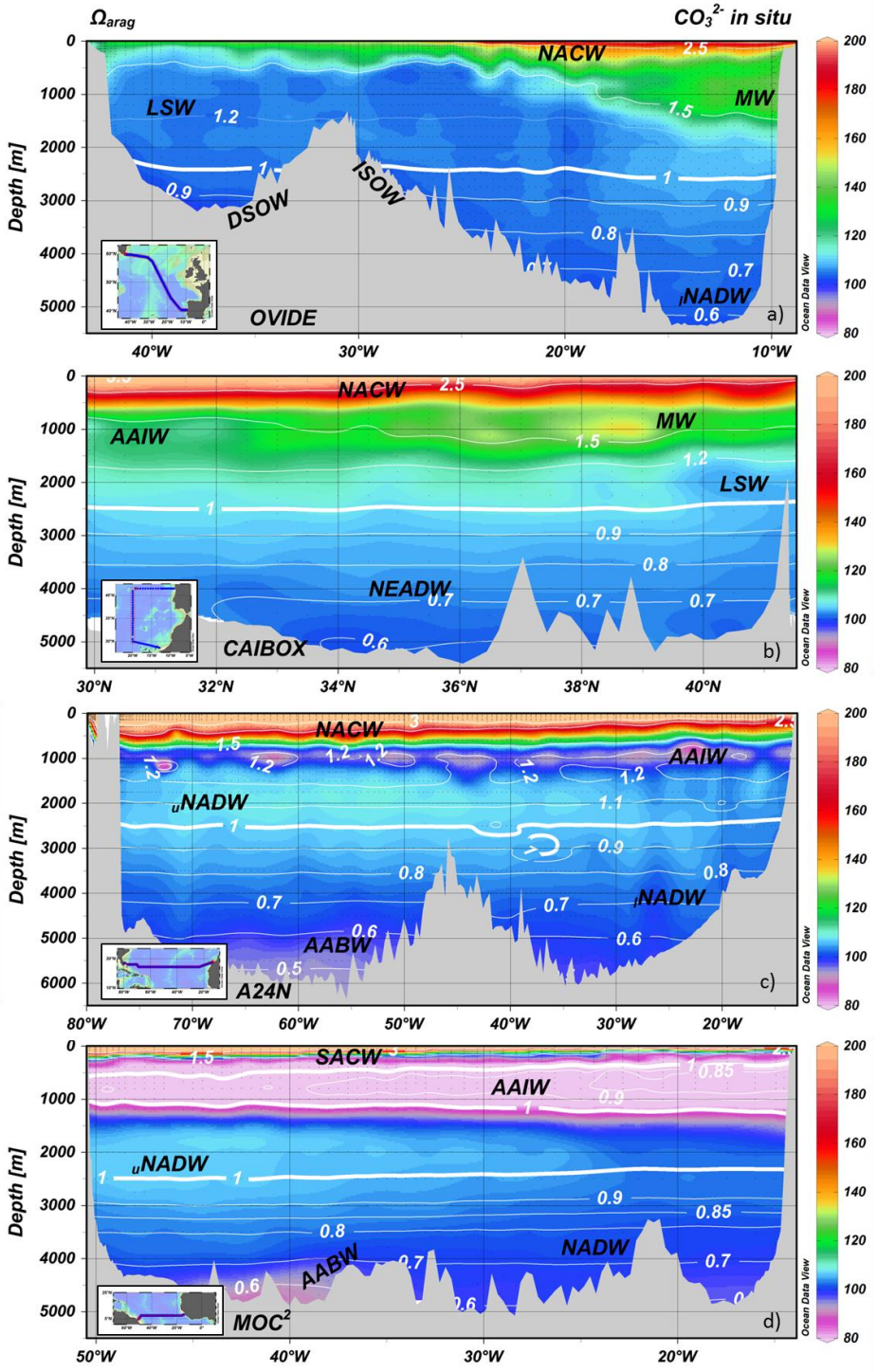
Ωarag
CO3 2- in situ
Depth [m]
NACW
MW
LSW
ISOW
DSOW
OVIDE
a)
AAIW
NEADW
CAIBOX
b)
uNADW
lNADW
AABW
A24N
c)
SACW
MOC2
d)
Ocean Data View

**Figure 1.5. $[CO_3^{2-}]_{in\ situ}$ of OVIDE, CAIBOX, A24N and MOC$^2$ cruises. These $CO_3^{2-}{}_{in\ situ}$ were calculated from measurements inputs of $A_T$ and spectrophotometric pH. The coloured profiles show $[CO_3^{2-}]_{in\ situ}$ while $\Omega_{arag}$ are shown as solid white contours. The water masses present in each basin are also shown: Antartic Bottom Water (AABW), Antartic Intermediate Water (AAIW), Denmark Straight Overflow Water (DSOW), Iceland Scotland Overflow Water (ISOW), Labrador Sea Water (LSW), Mediterranean Water (MW), North Atlantic Central Water (NACW), North Atlantic Deep Water, upper and lower (uNADW and lNADW), North East Atlantic Deep Water (NEADW) and South Atlantic Central Water (SACW).**

In order to link the $[CO_3^{2-}]_{in\ situ}$ with the different water masses of the North Atlantic Ocean (Broecker, 2003), the vertical thermohaline structure of this region is described by means of the following water masses (Millero, 2006; Schmitz Jr, 1996). The upper layers are clearly dominated by North Atlantic Central Water (NACW) (Pollard et al., 1996) in OVIDE, CAIBOX and A24N and by South Atlantic Central Water (SACW) (Brea et al., 2004; Mémery et al., 2000) in MOC$^2$. A small percentage of Antarctic Intermediate Water (AAIW) (Ríos et al., 1992) is shown in the southern part of CAIBOX, but clearly appears in A24N and MOC$^2$ around 1000m of depth. Mediterranean Water (MW) (Fraga et al., 1982), which is the outflow from the Mediterranean Sea and the most saline water of the water column, located on the eastward margin of OVIDE and central part of the Iberian Basin in CAIBOX, and it appears between intermediate and deep water masses. Deeper layers of the water column are dominated by Labrador Sea Water (LSW) (Yashayaev et al., 2008) in OVIDE and CAIBOX, while North East Atlantic Deep Water (NEADW) (Castro et al., 1998) and Iceland Scotland and Denmark Straight Overflow Waters (ISOW and DSOW) (Álvarez et al., 2004) span in the bottom layers of CAIBOX and OVIDE, respectively. On the westward zone of OVIDE, North Atlantic Deep Water (NADW) (Stramma and

England, 1999) appears and it is also differentiated in its upper (uNADW) and lower (lNADW) branches in A24N and MOC$^2$. Antartic Bottom Water (AABW) (Johnson, 2008; Rhein et al., 1998) slightly appears at the westward margin of A24N, while it appears clearly at bottom layers in MOC$^2$.

The surface waters, NACW and SACW, are characterized by the highest $[CO_3^{2-}]_{in\ situ}$, which varies from ~140 - 150 to ~250 µmol·kg$^{-1}$ reaching their highest values near the sea surface (~200 - 220 µmol·kg$^{-1}$ values in NACW in OVIDE and CAIBOX, fig. 7a, b; ~250 µmol·kg$^{-1}$ in SACW in A24N and MOC$^2$, Fig. 1.5c, d). The MW shows $[CO_3^{2-}]_{in\ situ}$ around 120 - 130 µmol·kg$^{-1}$ associated to the characteristic maximum salinity of these waters (Fig. 1.5a, b). At a similar depth but southward, it is worth highlighting the minimum $[CO_3^{2-}]_{in\ situ}$ of AAIW ($[CO_3^{2-}]_{in\ situ} \approx 80$ µmol·kg$^{-1}$). This minimum $[CO_3^{2-}]_{in\ situ}$ is scattered in A24N (Fig. 1.5c) but it is clearly shown in MOC$^2$ (Fig. 1.5d). $[CO_3^{2-}]_{in\ situ}$ in LSW (Fig. 1.5a, b) is around 100 µmol·kg$^{-1}$ and in NADWs (differentiated in uNADW, lNADW and NEADW, Fig. 1.5a-d) it varies from 100 to 110 µmol·kg$^{-1}$. Finally the AABW carries $[CO_3^{2-}]_{in\ situ}$ of ~80 - 90 µmol·kg$^{-1}$ which can be seen at the bottom of figures 1.5c, d.

In terms of $\Omega_{arag}$, $\Omega_{arag} = 1$ at approximately 2500m of depth, can be seen in all the profiles as a highlighted white line (Fig. 1.5). It represents 100% of saturation and shows the limit between supersaturated waters (< 2500 m) and undersaturated ones (> 2500 m). The values of $\Omega_{arag}$ in the northernmost supersaturated waters, i.e., NACW at OVIDE and CAIBOX cruises (Fig. 1.5a, b) were

around 2.5 - 3 while the most equatorial ones (NACW at A24N, Fig. 1.5c, and SACW at MOC$^2$, Fig. 1.5d) reached values of $\Omega_{arag}$ close to 4. This slight difference of supersaturated waters must be associated to the cold water at high northern latitudes, driving low pH values favoured by high ventilation and $CO_2$ solubility. In the most equatorial cruises, A24N and MOC$^2$, corresponding to the $[CO_3^{2-}]_{in\ situ}$ minima of AAIW, $\Omega_{arag}$ = 1 is also achieved linked to the low pH produced by the accumulation of mineralization of organic matter. It is observed in A24N at ~ 1000m of depth (Fig. 1.5c), but in MOC$^2$, the area of undersaturated water is clearly enclosed between two $\Omega_{arag}$ = 1 (Fig. 1.5d). Taking into account deep (NADW) and bottom (AABW) waters, there are no significant differences in $\Omega_{arag}$, obtaining values of $\Omega_{arag} \approx 0.5$, regardless of latitude.

## 1.4 Conclusions

This study points out the fact that the carbonic acid dissociation constants estimated in natural waters (M06, MDM87, LDK00) seem to be much more reliable for field and laboratory carbonate measurements than those estimated in synthetic waters (GP89). In fact, M06 constants have been identified as the most internally consistent in terms of $C_T$ and $CO_3^{2-}$ minima, when they are combined with the new B/Cl ratio (Lee et al., 2010). Furthermore, the influence of the temperature and the addition of $PbCl_2$ on the spectrophotometric estimations of $CO_3^{2-}$ has been demonstrated and

a new formula has been proposed for $[CO_3^{2-}]$ determination, reducing the relative errors in 1.2%. Taking into account the good agreement between calculated and measured $[CO_3^{2-}]$, the complete $[CO_3^{2-}]_{\text{in situ}}$ distributions for each cruise were studied, in which the minimum $[CO_3^{2-}]$ (AAIW) enclosed between $\Omega_{arag} = 1$ is noticeable.

# *Chapter 2 / Capítulo 2*

## Carbon data of A06 and A07 WOCE cruises

## *Datos de carbono de las campañas WOCE A06 y A07*

# 2. Carbon data of A06 and A07 WOCE cruises

## Resumen

Las campañas oceanográficas WOCE realizadas durante la década de 1990 se incluyeron en la base de datos GLODAP, que es una base de datos global, bien evaluada y disponible. Los datos de carbono incluidos en GLODAP fueron sometidos a rigurosos controles de calidad y ajustes se realizan asumiendo sesgos no mayores de ± 0,005 unidades de pH, ± 6 µmol·kg$^{-1}$ para $A_T$ y ± 4 µmol·kg$^{-1}$ para el $C_T$. Los datos de $A_T$ y $C_T$ datos de las campañas WOCE A06 y A07 se consideraron no aptos para el análisis y por lo tanto no se incluyen en la base de datos GLODAP. Sin embargo, estos datos, junto con los datos de pH están todavía disponibles en la web de *CLIVAR and Carbon Hydrographic Data Office*. En este estudio también se confirmó la escasa calidad de estos datos de $A_T$ y $C_T$, mientras que se demostró la fiabilidad de los datos de pH. Se estimó el sesgo existente en los datos de $pH_{SWS25}$ de A06 y A07, y considerando los valores de $A_T$ obtenidos del método 3DwMLR, se calcularon los datos de $C_T$ de las campañas WOCE A06 y A07.

## Abstract

The WOCE cruises carried out during the 1990s were included in GLODAP database, which is an available and fully calibrated global database. Carbon data were subjected to rigorous quality control and some adjustments were done assuming biases not greater than ±0.005 units for pH, ±6 $\mu mol \cdot kg^{-1}$ for $A_T$ and ±4 $\mu mol \cdot kg^{-1}$ for $C_T$. The $A_T$ and $C_T$ data from the A06 and A07 WOCE cruises were considered unsuitable for analysis and thus not included in GLODAP database. However, these data together with pH data are still available in CLIVAR and Carbon Hydrographic Data Office web site. In this study the unreliable quality of the $A_T$ and $C_T$ data were also confirmed while contrarily the confidence in the pH data was demonstrated. The existent bias in the $pH_{SWS25}$ data of A06 and A07 were estimated and taking into account the $A_T$ values estimated using a 3D Moving Window MLR method, the $C_T$ data of A06 and A07 WOCE cruises can be calculated.

## 2.1 Introduction

The World Ocean Circulation Experiment (WOCE) together with the Joint Global Ocean Flux Study (JGOFS), and the Ocean-Atmosphere Carbon Exchange Study (OACES) were carried out during the 1990s. The three programs covered different ocean regions, improving the combined global coverage. The collaborative efforts between scientists concluded in the Global Ocean Data Analysis Project (GLODAP) (Sabine et al., 2005) as an easily usable and fully calibrated global database. Between the general goals of GLODAP, it is worth highlighting the distribution of the variables of the carbon system in order to estimate their changes and to evaluate the inventory of natural and anthropogenic carbon (Key et al., 2004). Thus, the data were merged into a common format database divided by oceans, which is available in the GLODAP website hosted by the Carbon Dioxide Information Analysis Center (CDIAC) (GLODAP).

For the Atlantic Ocean, there are not only several cruises merged in GLODAP (Key et al., 2004) database but also in CARbon IN the Atlantic Ocean (CARINA) (Key et al., 2010). CARINA database was generated in order to create a merged calibrated database from open ocean measurements of biogeochemical investigations, in particular, studies involving the carbon system. The wide set of historical and recent hydrographic cruises include the entire Atlantic, the Artic and Southern Ocean giving one CARINA data product for each region. The CARINA products and a significant volume of supporting information are available in the CARINA

web site also hosted by CDIAC (CARINA). Despite many of the procedures used during CARINA were adopted from GLODAP, CARINA allowed important improvements, such as including also the pH data in their final product. Thus, in order to obtain a complete database of carbon system variables, historical and recent cruises were taken from both GLODAP and CARINA databases in this work.

One key point in both GLODAP and CARINA databases were the extensive calibration and quality control procedures designed to correct measurement bias and to remove bad data in the carbon system measurements. The bias assumed by both GLODAP and CARINA databases for these carbon parameters were not greater than ±0.005 pH units, ±6 µmol·kg$^{-1}$ and ±4 µmol·kg$^{-1}$ for pH, $A_T$ and $C_T$, respectively (Key et al., 2004 and Key et al., 2010). The carbon system in sea water describes the equilibrium between dissolved $CO_2$ and carbonate and it is defined by four parameters, i.e. total inorganic carbon ($C_T$), total alkalinity ($A_T$), pH and fugacity of $CO_2$ ($fCO_2$). Knowing at least two of these parameters allows calculating the unknowns. In the present work, pH, $A_T$ and $C_T$ data were studied in the Equatorial Atlantic Ocean.

Carbon data of the recent cruise MOC$^2$Equatorial (Meridional Overturning Circulation - Memoria Oceánica del Clima, MOC$^2$Ecuatorial) – hereafter MOC$^2$ – was combined with GLODAP+CARINA database. The MOC$^2$ cruise was spanned along 7.5ºN during April-May in 2010 on board of R/VHespérides.

Variables of the carbon system, $C_T$, $A_T$ and pH, were analysed in the whole water column.

The A06 (Oudot, 1993b) and A07 WOCE (Oudot, 1993a) cruises were carried out on board of R/V L'Atalante as part of the French CITHER project. The A07 took place in January 1993 along 4.5°S while A06 took place in February– March 1993 along 7.5°N. Despite the $A_T$ and $C_T$ data of both cruises were considered unsuitable for analysis and thus dismissed from GLODAP database (Wanninkhof et al., 2003), these data together with the pH measurements are still available in CLIVAR and Carbon Hydrographic Data Office (CCHDO).

In this study, with the aim of making usable the A06 and A07 cruises in subsequent comparisons or calculations of carbon transport, the original carbon data of the A06 and A07 cruises were revised. Using the combined GLODAP + CARINA + $MOC^2$ database and the technique of crossover analysis, a quality control was carried out to estimate the bias in the original pH data. The $A_T$ was estimated using a recent 3D Moving Window MLR estimation method and the $C_T$ was calculated from this $A_T$ and pH.

## 2.2 Data

GLODAP and CARINA databases were widely revised and involved in different quality control processes in order to assure the highest veracity and consistency of their included measurements.

Carbon data from cruises through the Atlantic Ocean merged in both databases were downloaded from their respective web sites (GLODAP and CARINA). Table 2.1 shows all the cruises downloaded for this work together with A06 and A07 WOCE cruises, specifying cruise number, expocode, alias, database to which each cruise belongs, year and, in the last column, the proximity of each cruise to A06, A07 or both of them.

**Table 2.1 Information about the cruises selected from combined GLODAP and CARINA database including A06 and A07 cruises. The cruise number is the number assigned by GLODAP or CARINA databases, Expocode is the international name for the cruise, Alias is a little name for each cruise, Year is the year when the cruise were carried out, Database is the open access database to which each cruise belongs, and, in the last column, Crossovers means if the defined cruise was selected to use in crossover analysis of A06, A07 or both of them.**

| Cruise number | Expocode | Alias | Year | Database | Crossovers |
|---|---|---|---|---|---|
| **19** | 35A3CITHER3_2 | A13 | 1995 | GLODAP | A07 |
| **20** | 35A3CITHER3_1 | A14 | 1995 | GLODAP | A07 |
| **21** | 316N142_3 | A15 | 1994 | GLODAP | A06 & A07 |
| **22** | OACES91_1-2 | A16Sa | 1991 | GLODAP | A07 |
| **23** | OACES93 | A16Na | 1993 | GLODAP | A06 & A07 |
| **24** | 3230CITHER2_1-2 | A17 | 1994 | GLODAP | A06 & A07 |
| **35** | 316N83_a,c | A12/A13 | 1983 | GLODAP | A06 & A07 |
| **43** | GEOSECS_1-9 | GEOSECS | 1972 | GLODAP | A06 & A07 |
| **46** | TTOTAS_1-3 | TTO-TAS | 1982 | GLODAP | A06 & A07 |
| **48** | 318MSAVE_1-5_HYDROS4 | SAVE | 1987 | GLODAP | A06 & A07 |
| **61** | 29HE20010305 | (FICARAM II; HE073; WOCE A17 repeat) | 2001 | CARINA | A06 & A07 |
| **62** | 29HE20020304 | (FICARAM IV; HE081; WOCE A17 repeat) | 2002 | CARINA | A06 & A07 |
| **84** | 33LK19960415 | (33LKETAMBOT2_1; WOCE AR04h/AR15) | 1996 | CARINA | A06 & A07 |
| **86** | 33RO20030604 | (CLIVAR A16N_2003) | 2003 | CARINA | A06 & A07 |
| **87** | 33RO20050111 | (CLIVAR A16S_2005) | 2005 | CARINA | A07 |
| **95** | 35LU19950909 | (35LLETAMBOT1_1; WOCE AR04g) | 1995 | CARINA | A06 & A07 |
| **106** | 35TH19990712 | (35TH9907; Equalant99) | 1999 | CARINA | A06 & A07 |
| **10** | 35A3CITHER1_2 | A06 | 1993 | - | |
| **11** | 35A3CITHER1_1 | A07 | 1993 | - | |

The geographical distribution of these cruises is shown in figure 2.1, where the entire Atlantic Ocean basin is represented.

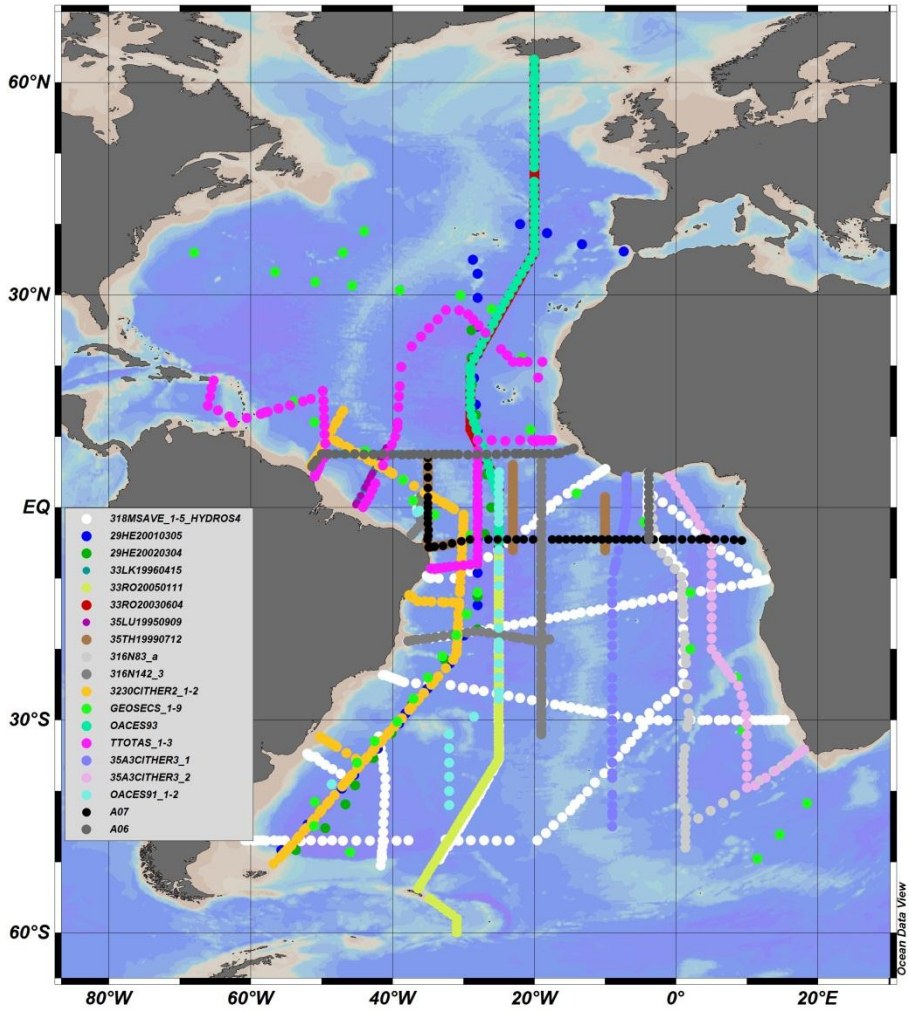


**Figure 2.1 Geographical distribution of selected cruises from the combined GLODAP and CARINA database carried out near A06 and A07 cruises. A06 and A07 cruises are also shown. Since MOC$^2$ cruise is a repetition of A06 stations it is not shown.**

Databases of A06 and A07 cruises are available in CCHDO web site (CCHDO). A06 and A07 cruises were carried out in the winter season 1993 along 7.5ºN and 4.5ºS, respectively, analysing pH and

$C_T$. Measurements of $C_T$ were made by gas chromatography according to the modified method as described in Oudot et al., (1995). pH measurements were based on the total hydrogen ion concentration scale ($pH_{SWS}$) using a Ross combination electrode calibrated in Tris buffer. The $A_T$ data of A06 and A07 cruises were determined from $C_T$ and pH measurements using the equation describing the terms of alkalinity contributions defined by UNESCO (Oudot et al., 1995). Contrarily to $A_T$ and $C_T$ data, the measured pH data from these both A06 and A07 cruises are quality data, although their temperature and calibration data are unknown. Due to that, new pH data at in situ temperature from $A_T$ and $C_T$ data were estimated and compared with the original pH data available in the databases. The good correlation ($pH_{is} = 1.041 \cdot pH_{orig} - 0.316$; $R^2=0.992$) showed that original pH data was reported at in situ temperature. Thus, in the present work the pH data were rescaled to $pH_{SWS25}$ combining $A_T$ and $C_T$ within the Excel $CO_2$sys program (Pierrot et al., 2006) and the acid constants from Mehrbach et al., (1973) refitted by Dickson & Millero (1987) together with the boron to chlorinity ratio from Lee et al., (2010).

MOC$^2$ cruise was carried out at spring season along 7.5ºN in 2010 on board the R/VHespérides. This 2010 cruise is a repetition of the leg spanned along 7.5ºN by the cruise A06 in 1993 (see geographical location of A06 in figure 1). $A_T$ and pH samples were analysed along the cruise, and some $C_T$ samples were also taken for coulometric analysis in the laboratory of IIM-CSIC (Vigo). Samples of $A_T$ were analyzed by an automatic potentiometric titrator with a combined glass electrode (Mintrop et al., 2000), whose

potentiometric titration was carried out using the two pH endpoints method according to Pérez and Fraga (1987). Seawater pH measurements were made using the spectrophotometric method described in Clayton and Byrne (1993) adding m-cresol purple as indicator and controlling the temperature at 25ºC by a thermostatic bath. The pH scale fixed in $MOC^2$ was the total scale ($pH_T$), but, with the aim of normalized pH data, $MOC^2$ $pH_T$ were rescaled to $pH_{SWS25}$ using the $CO_2$sys program and the constants applied before. Since $C_T$ data were not measured in the whole levels of the water column, $C_T$ data were calculated from $A_T$ and pH using the $CO_2$sys program. The coulometric $C_T$ measured (Johnson et al., 1993, 1998) were used to check the internal consistence between the calculated $C_T$ and measured $C_T$, observing a good agreement between them. To check the accuracy of the $A_T$ and $C_T$ methods, calibrations were performed with certified reference material (CRM) of $CO_2$ provided by Dr. Andrew Dickson.

## 2.3 Methodology

The phases to correct and re-estimate the A06 and A07 data were:

(1) Due to the low $A_T$ variability, a 3D moving window Multiple Linear Regression method (3DwMLR) developed by Velo et al., (2012) was applied to estimate the $A_T$ data of these cruises, defining successfully new $A_T$ data ($A_{T\ 3DwMLR}$). The widely secondary quality control ($2^{nd}$ QC) applied in CARINA, i.e., the crossovers analysis method (Tanhua, 2010; Tanhua et al., 2010a, 2010b; Velo

et al., 2010a) was used to check the confidence of these $A_{T\ 3DwMLR}$ data.

(2) Taking into account these $A_{T\ 3DwMLR,}$ the $pH_{SWS25}$ and the factor obtained by crossover analyses, new $C_T$ data ($C_{T\ new}$) were recalculated using the Excel version of $CO_2$sys program and the acid constants from Mehrbach et al., (1973) refitted by Dickson and Millero (1987) together with the boron to chlorinity ratio from Lee et al., (2010). The crossovers analysis was applied again to check the confidence of these $C_{T\ new}$ data. These first two steps are schematically depicted in figure 2.2.

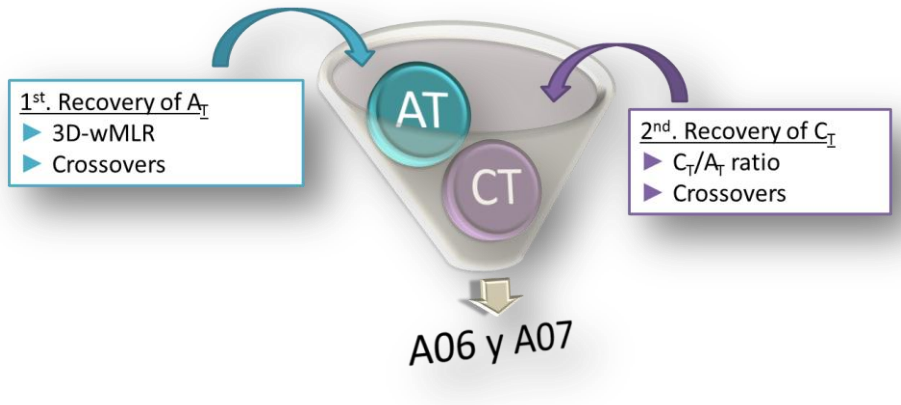


**Figure 2.2 Scheme with the main steps to recover carbon data of A06 and A07: 1st recovery of $A_T$ and 2nd recovery of $C_T$.**

(3) Once these $A_{T\ 3DwMLR}$ and $C_{T\ new}$ data were estimated, the $pH_{SWS25new}$data were calculated using the $CO_2$sys program and the constants previously detailed. The bias, which is necessary to correct $pH_{SWS25}$, is obtained by subtraction between $pH_{SWS25new}$and $pH_{SWS25}$.

### 2.3.1 The 3D Moving Window MLR method (3DwMLR)

$A_T$ is the parameter from the carbon system variables ($A_T$, $C_T$, pH and $fCO_2$) that can be computed most accurately with less uncertainty due to its low variability in the ocean. $A_T$ can be well correlated with salinity, silicate, and even temperature, as it is demonstrated, for instance, in Millero et al., (1998) and Lee et al., (2006) where $A_T$ has been estimated in surface waters by the linear relationship between SST and SSS. A 3DwMLR method developed by Velo et al. (2012) was applied to the available data of GLODAP and CARINA datasets to obtain a new dataset of estimated $A_T$ ($A_{T\ 3DwMLR}$) for A06 and A07 cruises.

The objective of the 3DwMLR method (Velo et al., 2012) is to improve the results of a typical MLR by using a 3D moving window around the node where $A_T$ is going to be calculated. Each bottle sample of A06/A07 cruises constitute the node in the algorithm designed to select a pool of data from the CARINA/GLODAP databases inside a box of varying size (latitude, and depth range) depending of the data availability (Velo et al., 2010b). The node and, accordingly, its box are moved along the A06 and A07 positions in order to make the MLR calculations. The algorithm combines pressure, potential temperature, salinity, nitrate, silicate, phosphate and oxygen as independent variables trying to incorporate the natural variability in order to get better predictions of $A_T$. Inside this algorithm, a robust regression algorithm which combines an ordinary regression algorithm with outlier detection was used given the most consistent inferred $A_T$. These $A_{T\ 3DwMLR}$

obtained by this 3DwMLR technique were tested in the Atlantic Ocean with $A_T$ obtained using a neural network analysis and with $A_T$ measured data. Both methods of estimating $A_T$ in the ocean produce acceptable results with an average error in the prediction lower than 5 $\mu mol \cdot kg^{-1}$.

### 2.3.2 2nd QC: Crossovers analysis

Crossovers analysis is an objective comparison of deep water data from one cruise with data from other cruises in the same area, available as a MATLAB tool-box in CDIAC web site (2nd_QC_Tool) (Tanhua, 2010). The result of a crossover analysis is an *offset* ± *standard deviation*, which is defined as the difference between two cruises, A (analysed cruise) and B (reference cruise), derived from the analysis. This tool interpolates vertical profiles of stations from A and B cruises in the nearest area and calculates the "difference profile". This procedure is repeated in each pair of stations and the result is a crossover offset media for each crossover pair. For $C_T$, $A_T$ and salinity, these offsets are quantified as an additive adjustment, while, in case of $O_2$ and nutrient data are quantified as a linear correction factor.

In this work, the crossovers analysis has three main goals, (1) to confirm that the previously estimated $A_{T\ 3DwMLR}$ data agree with GLODAP/CARINA quality criteria, i.e., biases are not greater than ±6 $\mu mol \cdot kg^{-1}$, (2) to calculate a factor which helps to recalculate the $C_{T\ new}$ data and (3) to confirm these $C_{T\ new}$ are inside the

GLODAP/CARINA quality criteria, i.e., biases are not greater than ±4 µmol·kg$^{-1}$.

### 2.3.3 Calculation of $C_T$ data

New $C_T$ data were calculated using the $CO_2$sys with the detailed constants involving the rescaled $pH_{SWS25}$ data and the estimated $A_{T\ 3DwMLR}$ data. Nonetheless, a bias in pH $pH_{SWS25}$ profile was slightly appreciated in figure 2.3, where the homogeneous profiles of A06 and A07 profiles related to MOC$^2$ $pH_{SWS25}$ profile are observed.

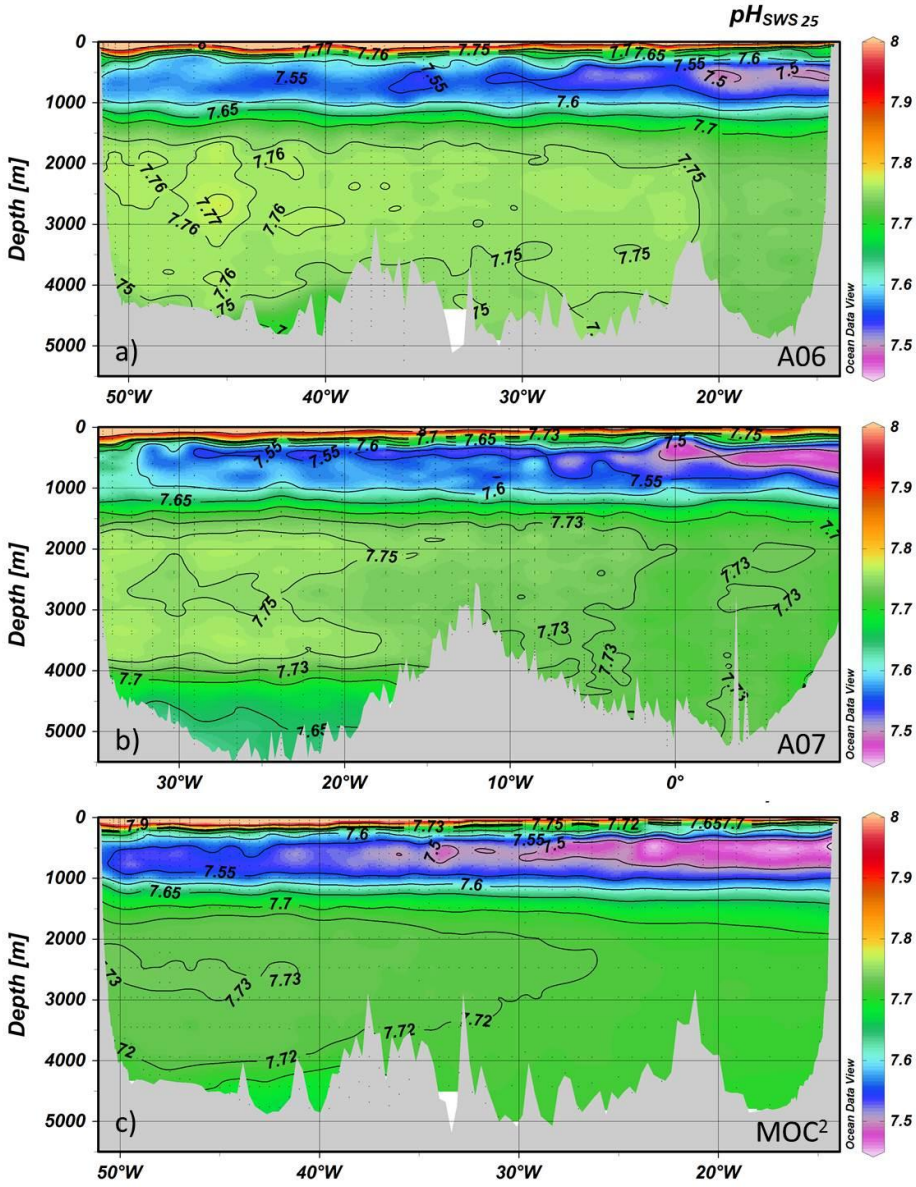


Figure 2.3 $pH_{SWS25}$ profiles of (a) A06, (b) A07 and (c) $MOC^2$ cruises. $pH_{SWS25}$ values from A06 and A07 cruises were rescaled at sea water scale at 25ºC using the $CO_2$sys, and the original pH data from $MOC^2$ cruise were also rescaled from $pH_T$.

This bias is clearly shown in the mean pH profiles of $MOC^2$ and A06 (Fig. 2.4a). The mean profile is the mean value of the defined

layers of depth. The layers from surface to 1000m are calculated each 200m, while from 1000m to bottom (~5000m) layers are defined each 500m. Due to the biased $pH_{SWS25}$, the new $C_T$ data have also a deviation (Fig. 2.4b).

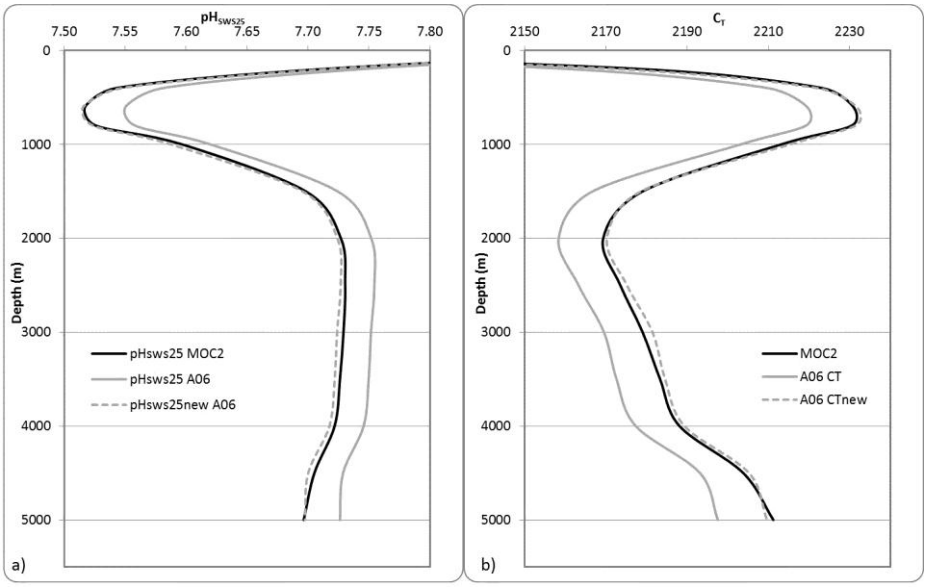


**Figure 2.4 Mean profiles of a) pHSWS25 and b) CT for A06 (grey lines) and MOC2 (black lines). The A06 continuous line displays the original data, while the dashed lines represent the recalculated data.**

In order to correct this deviation the crossover analysis method was applied to the cruises listed in table 2.1, estimating a factor for each A06 and A07 cruises. These factors were calculated as a function of the mean offset value of the crossover analysis and taking into account 2100 µmol $kg^{-1}$ as the mean $C_T$ value for deep water in the Atlantic Ocean. Then, the $C_{T\ new}$ data were recalculated by directly multiplication of $C_T$ and the factors, obtaining the $C_{T\ new}$ dataset for

both A06 and A07 cruises. In order to check the $C_{T\ new}$ dataset, the crossover analysis method was again applied providing confidence in these data according to CARINA and GLODAP quality control requirements.

## 2.4 Results and Discussion

### 2.4.1 $A_T$ data

In order to estimate the $A_T$ data of A06 and A07 cruises along the Equatorial Atlantic Ocean, the 3DwMLR method was applied to GLODAP and CARINA databases. The evident improvements reached by using this method are observed in figure 2.5, where the $A_T$ original (Fig. 2.5a and 2.5b) and $A_{T\ 3DwMLR}$ profiles (2.5c and 2.5d) of A06 and A07 cruises are shown. The figures 2.5a and 2.5b show the $A_T$ original data, while the $A_{T\ 3DwMLR}$ profiles (Fig. 2.5c and 2.5d) show more consistent profiles for both 7.5ºN and 4.5ºS legs, respectively. Even though the $A_{T\ orig}$ profiles show a columnar distribution there are common patterns in both $A_{T\ orig}$ and $A_{T\ 3DwMLR}$ profiles. For instance, the distribution of the upper waters is roughly similar reaching in both profiles the highest $A_T$ values and both showing the influence of the bottom waters. Moreover, the intermediate waters are also correlated with the water masses present in the Equatorial Atlantic Ocean. However, more homogeneous and clearer profiles are shown by $A_{T\ 3DwMLR}$ profiles for A06 and A07 cruises (Fig. 2.5c and 2.5d), accordingly with the

horizontal and vertical distribution of the water masses in this area. Importantly, the minimum of $A_T$ associated to the Antarctic Intermediate Waters is clearly shown in $A_{T\ 3DwMLR}$ in both A06 and A07 profiles (Fig. 2.5c and 2.5d).

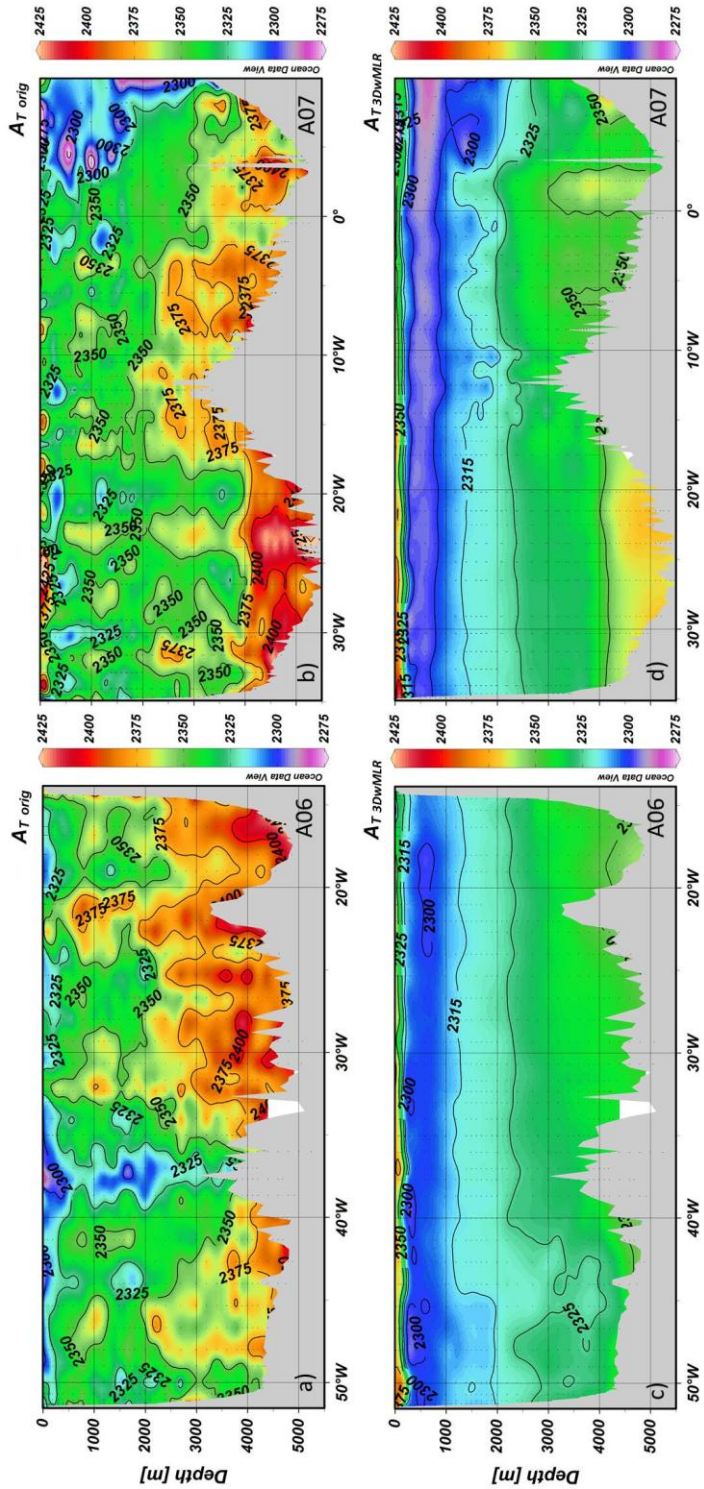


Figure 2.5 $A_T$ data. The upper panels show the unreliable $A_{T\,orig}$ profiles of A06 and A07 cruises (a and b, respectively) while the lower panels, (c) and (d) show the calculated $A_{T\,3DwMLR}$ profiles for A06 and A07, respectively.

In order to confirm the good quality of $A_{T\ 3DwMLR}$ data, the cruises listed in table 2.1 were used to run the crossover analysis of A06 and A07. The $A_{T\ 3DwMLR}$ offsets are summed up in the table 2.2 together with the standard deviation and the mean offset value.

**Table 2.2 Results from the crossover analysis applied to $A_{T\ 3DwMLR}$ and $C_T$ of A06 and A07 cruises. Cruise number is the number assigned by GLODAP or CARINA databases. Cruise Crossover ID is the identity given to each cruise in the crossover analysis. Offset and Uncertainty are the offset ± standard deviation obtained from crossover analysis, while the mean offset is the mean value of all offsets including in each $A_T$ or $C_T$ analysis.**

| | $A_{T\ 3DwMLR}$ | | | | | $C_T$ | | | |
|---|---|---|---|---|---|---|---|---|---|
| | Cruise number | Cruise Crossover ID | Offset | Uncertainty | Mean offset AT | Cruise Crossover ID | Offset | Uncertainty | Mean offset CT |
| A06 | 84 | 1 | -0.7 | 4.6 | -2.1 | 1 | -8.2 | 5.6 | -11.5 |
| | 86 | 2 | 0.2 | 1.8 | | 2 | -12.6 | 1.9 | |
| | 95 | 3 | -3.2 | 2.6 | | 3 | -9.8 | 3.3 | |
| | 106 | 4 | -8.7 | 3.3 | | - | - | - | |
| | 23 | 5 | -0.4 | 2.2 | | 4 | -13.2 | 2.0 | |
| | 24 | 6 | -5.7 | 2.0 | | 5 | -11.9 | 2.5 | |
| | 46 | 7 | -1.1 | 4.4 | | 6 | -13.1 | 4.3 | |
| | 48 | 8 | 3.1 | 7.6 | | - | - | - | |
| A07 | 84 | 1 | -0.7 | 8.1 | -1.0 | 1 | -8.2 | 6.7 | -9.2 |
| | 86 | 2 | -1.4 | 1.6 | | 2 | -5.2 | 2.8 | |
| | 87 | 3 | 0.4 | 2.5 | | 3 | -8.9 | 3.7 | |
| | 106 | 4 | 0.4 | 7.0 | | 4 | -9.2 | 9.1 | |
| | 19 | - | - | - | | 5 | -20.7 | 4.9 | |
| | 20 | 5 | -7.3 | 3.2 | | 6 | -8.0 | 3.4 | |
| | 21 | 6 | 3.1 | 3.3 | | 7 | -7.2 | 2.6 | |
| | 22 | 7 | 2.5 | 3.3 | | 8 | -12.2 | 1.5 | |
| | 23 | - | - | - | | 9 | -4.7 | 1.8 | |
| | 24 | 8 | -5.1 | 2.0 | | 10 | -7.7 | 1.9 | |
| | 48 | - | - | - | | 11 | -9.8 | 10.9 | |

The graphical representation of $A_{T\ 3DwMLR}$ crossovers (for both A06 and A07 cruises) is shown in upper panels of figure 2.6 (Fig. 2.6a and 2.6b). Each black dot in these graphs is the offset ± standard deviation value of cruise A (cruise crossover ID listed in table 2.2) taking cruise B as reference, i.e., A06 or A07 (Fig. 5a and 5b). In

general terms, all these offsets were not greater than ±6 µmol·kg$^{-1}$, which is the value of $A_T$ data bias accepted by CARINA and GLODAP databases. The mean crossovers offset values (black bold line in figure 2.6a and 2.6b and the last column of $A_T$ in table 2) obtained for $A_{T\ 3DwMLR}$ of A06 and A07 were -2.1±3.7 µmol·kg$^{-1}$ and -1.0 ±3.6 µmol·kg$^{-1}$, respectively. These mean offset values are also in the quality control of GLODAP and CARINA databases. Thus, biases were not necessary to be applied to $A_{T\ 3DwMLR}$ data.

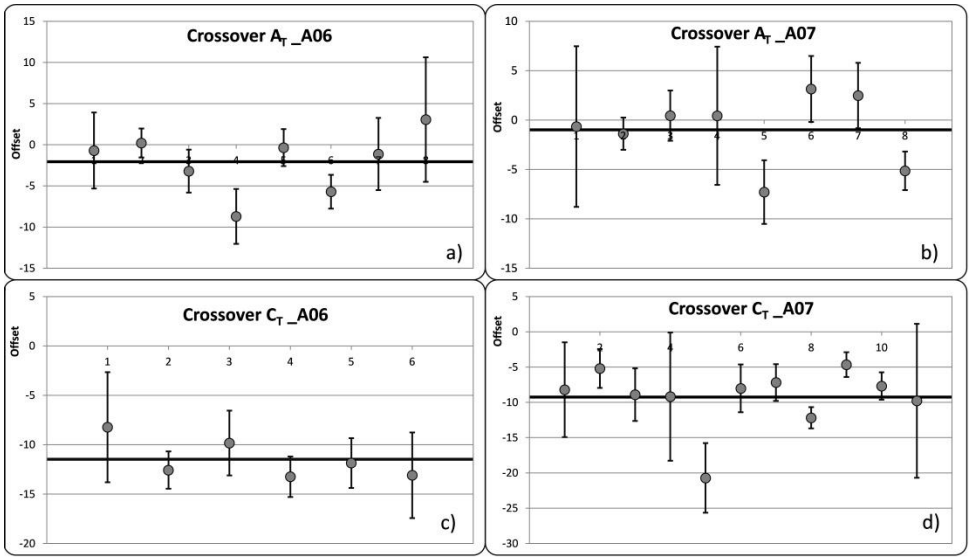


**Figure 2.6 Offsets obtained from the crossover analysis method applied to $A_{T\ 3DwMLR}$ (a and b for A06 and A07, respectively) and $C_T$ data (c and d for A06 and A07, respectively). In each individual graph, the "y axis" represents the offset value in µmol kg$^{-1}$ and the "x axis" the crossover ID given to each cruise. Each point is the obtained offset with their associated uncertainty.**

### 2.4.2 $C_T$ data

The original $C_T$ measurements of A06 and A07 cruises were dismissed from GLODAP because these data were out of the quality controls established. The inconsistence of these data is shown in the figures 2.7a and 2.7b, where the distribution of $C_T$ clearly lacks of continuity, even though the known patterns in surface, intermediate and bottom waters are lightly distinguished.

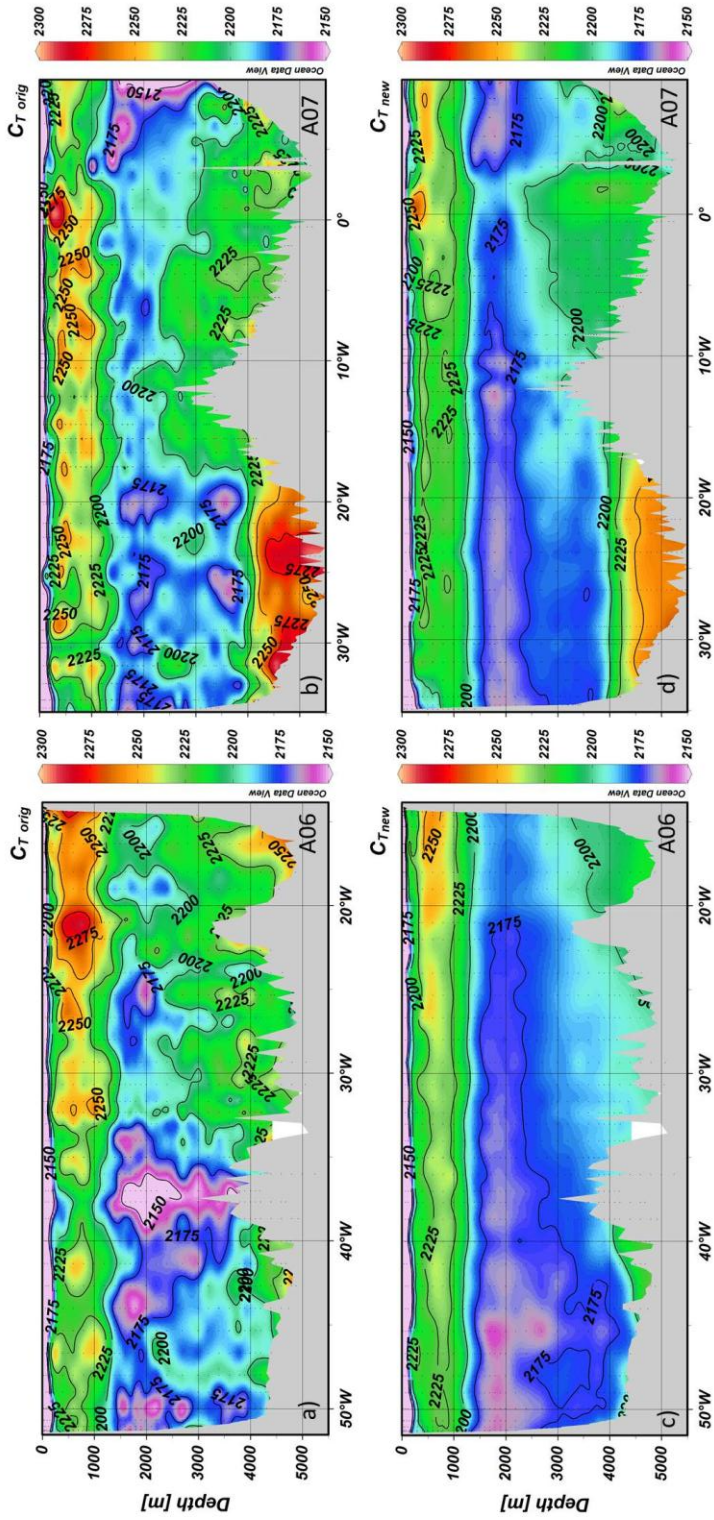


Figure 2.7 $C_T$ data. The (a) and (b) panels show the unsuitable $C_{T\,orig}$ profiles of A06 and A07 cruises, respectively, while the (c) and (d) panels show the recalculated $C_{T\,new}$ profiles of A06 and A07, respectively.

Taking into account the $pH_{SWS25}$ and the newest $A_{T\ 3DwMLR}$, the new $C_T$ data were calculated using the $CO_2$sys program and the acid constants from Mehrbach et al., (1973) fitted by Dickson & Millero (1987) together with the boron to chlorinity ratio from Lee et al., (2010). However, as expected in view of the mean pH profiles (Fig. 2.4a), the deviation shown in $pH_{SWS25}$ related to $MOC^2$ cruise is also transferred to these $C_T$ data (Fig. 2.4b). In this figure 2.4, the $MOC^2$ mean pH and $C_T$ profiles are shown as black continuous line, while the grey continuous line refers to A06 cruise. In order to correct this deviation, the crossover analysis for the $C_T$ data of A06 and A07 cruises was applied. The crossover analysis included the cruises listed in table 2.1 as reference data. The obtained $C_T$ offsets with their corresponding standard deviation for each cruises involved in the analysis were summed up in the table 2.2, and their graphical representation is shown in the figures 2.6c and 2.6d for A06 and A07 cruises, respectively. The offset values obtained for $C_T$ of A06 and A07 cruises were out of the quality control limits assumed by GLODAP and CARINA (±4 $\mu mol \cdot kg^{-1}$). The $C_T$ offset values for A06 crossover analysis varied from -8 to -14 $\mu mol \cdot kg^{-1}$ , giving a mean offset of -11.5±2.0 $\mu mol \cdot kg^{-1}$ , while, in the case of the A07 crossover analysis, the offset values varied from -4 to -20 $\mu mol \cdot kg^{-1}$ and their corresponding mean value was -9.2±4.3 $\mu mol \cdot kg^{-1}$ . Taking into account the mean offset value obtained for the A06 and A07 crossover analysis, two factors were calculated assuming that the mean $C_T$ value in the Atlantic Ocean is 2100 $\mu mol \cdot kg^{-1}$. These factors were 1.0055 and 1.0045 for $C_T$ data of A06 and A07, respectively.

Taking into account these factors, the $pH_{SWS25}$ and $A_{T\ 3DwMLR}$, a new $C_T$ dataset ($C_{T\ new}$) were calculated for A06 and A07 cruises. These $C_{T\ new}$ data are shown in lower panels of figure 2.7 (Fig. 2.7c and 2.7d), where homogeneous profiles of $C_{T\ new}$ can be observed. The distribution of the waters from surface to deep layers is now much more homogenous than the original $C_T$ ($C_{T\ orig}$). For example in A07 profile (Fig. 2.7d), the highest values of $C_T$ influenced by the Antarctic bottom waters are more outlined in $C_{T\ new}$ than in $C_{T\ orig}$, as well as the minimum values of intermediate water around 2000m of depth in A06 profile (Fig. 2.7c). This coherence is also shown when the mean $C_T$ profiles are plotted. In figure 2.4b the grey dashed line represents the $C_{T\ new}$ data of A06 which is in good agreement with $C_T$ data of MOC$^2$. In addition, a more formal test was also done to check if these $C_{T\ new}$ data were really consistent by running a crossover analysis of these corrected $C_{T\ new}$ values. In this case, the mean offset values of A06 and A07 cruises were near to cero, being both A06 and A07 datasets inside the limits allowed by GLODAP/CARINA quality criteria.

### 2.4.3 pH data

As mentioned above, the original pH data of A06 and A07 were rescaled at SWS and 25ºC ($pH_{SWS25}$) because of the unknown temperature and calibration data. The reliability of the $pH_{SWS25}$ profiles of A06 and A07 cruises was evident when these profiles were compared with their mate cruise in location, MOC$^2$ (Fig. 2.3). An extra test was done to check if these $pH_{SWS25}$ data from A06 and

A07 were in agreement with those from MOC$^2$, by calculating the mean pH profiles of these cruises (Fig. 2.4a). The deviation of these A06 mean $pH_{SWS25}$ profile (grey continuous lines) related to the MOC$^2$ mean pH profile (black continuous line) is clearly shown in Fig. 2.4a. To correct this deviation, the crossover analysis method was applied to the $pH_{SWS25}$ data of A06 and A07 cruises. However, there were not enough cruises (only four for A06 and five for A07) to obtain a truthful mean offset. In addition, the standard deviations were much higher than the offset value itself. Thus, the alternative method of estimating $A_{T\ 3DwMLR}$ and recalculating $C_{T\ new}$ was successfully developed and applied.

The estimated $A_{T\ 3DwMLR}$ and $C_{T\ new}$ of A06 and A07 cruises were used to calculate the $pH_{SWS25new}$ using the Excel $CO_2$sys program and the acid constants from Mehrbach et al., (1973) fitted by Dickson & Millero (1987) together with the boron to chlorinity ratio from Lee et al., (2010). The concordance between mean $pH_{SWS25new}$ profile of A06 (grey dashed line) and MOC$^2$ (bold continuous line) is shown in fig. 2.4a. Owing to that agreement, the A06 and A07 cruises have a new dataset of pH, these $pH_{SWS25new}$ data. Taking into account the subtraction between $pH_{SWS25new}$ and $pH_{SWS25}$ datasets, the necessary biases to correct $pH_{SWS25}$ of A06 and A07 were 0.028±0.004 and 0.024±0.003 units of pH, respectively.

## 2.5 Conclusions

The application of a 3DwMLR method to GLODAP and CARINA databases allowed to estimate the $A_{T\ 3DwMLR}$ datasets for A06 and A07 WOCE cruises with an average error lower than 5 $\mu mol \cdot kg^{-1}$. The pH bias of 0.028 and 0.024 for A06 and A07 respectively, was applied to $pH_{SWS25}$ obtaining the new $pH_{SWS25new}$ dataset of A06 and A07 cruise. Taking into account these $pH_{SWS25new}$ and the estimated $A_{T\ 3DwMLR}$ datasets, the $C_T$ data of A06 and A07 cruises were also calculated.

The existence of $A_T$, $C_T$ and pH data of A06 and A07 cruises suggests new branches of study about the carbon distribution in the Equatorial Atlantic Ocean. Taking into account the transport and the exchanges of mass, the carbon transport in that area could be estimated together with the storage of anthropogenic $CO_2$ in 1990s. A regional estimate of the accumulative oceanic sink for anthropogenic $CO_2$ could also be provided. Moreover, bearing in mind the $MOC^2$ cruise, the possibility of study the changes in anthropogenic carbon storage, calcite/aragonite horizon and pH from 1990s to present times are planned as a future work.

The innovative 3DwMLR method applied in this work can be considered a useful tool to estimate gaps of $A_T$ and other carbon variables in the Equatorial Atlantic Ocean, and obviously, in other areas of the Global Ocean. Moreover, the widely applied crossovers analysis is an easily and usable tool to check the quality of data. Thus, combining both 3DwMLR and crossovers analysis methods

could be used as a good methodology to improve, estimate and complete databases from a particular cruise or a group of cruises.

# *Chapter 3 /* Capítulo 3

## Changes in the Equatorial Atlantic Ocean in terms of $O_2$ and carbonate system variables

## *Cambios de $O_2$ y variables del sistema del carbonato en el Océano Atlántico Ecuatorial*

# 3. Changes in the Equatorial Atlantic Ocean in terms of Oxygen and carbonate system variables.

## Resumen

El océano desempeña un papel importante en los ciclos biogeoquímicos globales de compuestos de carbono, nitrógeno y otros muchos elementos biológicamente activos y compuestos químicos (Doney, 2010). Particularmente, el oxígeno disuelto ($O_2$) está involucrado en la mayoría de los procesos biogeoquímicos marinos (Keeling et al., 2010). La disminución global de $O_2$ en el océano, también llamada "desoxigenación oceánica", se ha asociado con el calentamiento global, impulsado, a su vez, por el aumento del $CO_2$ atmosférico. Debido a esto, existe también una asociación significativa entre la desoxigenación y acidificación oceánicas (Gruber, 2011). Aunque, en el Océano Atlántico, la extensión de las regiones con niveles de extremadamente baja [$O_2$] o hipóxicas ([$O_2$] $\leq 60$ $\mu mol \cdot kg^{-1}$) es pequeña en comparación con las de los océanos Pacífico e Índico, los datos históricos y los modelos climáticos muestran que la desoxigenación ha sido intensa en el Atlántico tropical y algunos autores señalan al Atlántico frente al resto de los océanos como aquél en el que es más probable que se den los mayores incrementos de área de las regiones hipóxicas (Stramma et al., 2008).

El presente trabajo estudia la desoxigenación en la zona ecuatorial del océano Atlántico utilizando bases de datos obtenidas a partir de dos campañas diferentes realizadas a lo largo del paralelo 7.5ºN: la sección WOCE A06 realizada en febrero-marzo de 1993 (Oudot, 1993) y la sección MOC$^2$Equatorial que se realizó en abril-mayo de 2010. En ambas se midieron la [O2] así como las variables del sistema del carbonato [pH, carbono inorgánico total ($C_T$) y alcalinidad total ($A_T$)]. Esto ha permitido estimar el $CO_2$ antropogénico ($C_{ant}$) utilizando dos técnicas de *back-calculation*, $\varphi C_T^o$ y TrOCA. En este trabajo se muestran los perfiles de pH, $O_2$ disuelto y $C_{ant}$. Para ver cambios puntuales en el pH, $O_2$ y $C_{ant}$ a lo largo de la sección 7.5 ºN y entre la A06 (1993) y la MOC$^2$Equatorial (2010), se dividió dicha sección en cuatro regiones zonales y seis capas de densidad relacionadas con las masas de agua principales del Océano Atlántico Ecuatorial. Los resultados ponen de manifiesto el aumento hacia el oeste de la lengua de *Antarctic Intermediate Water*, con valores de pH más bajos en 2010 que en 1993. Además, la acidificación que se muestra en la *upper North Atlantic Deep Water* está fuertemente ligada a la desoxigenación que presenta. Aquí, la media de la disminución de pH fue de ~0.014 unidades de pH (en valor absoluto) y se corresponde con una pérdida media de $O_2$ de ~ 10 μmol·kg$^{-1}$. En términos de $C_{ant}$, el aumento de la [$C_{ant}$] es notable en general en las capas superiores de la columna de agua, en donde el incremento medio fue de ~ 14 μmol·kg$^{-1}$.

## Abstract

The ocean plays an important role in the global biogeochemical cycles of carbon, nitrogen and many other biologically active elements and chemical compounds (Doney, 2010). Particularly, dissolved oxygen ($O_2$) affects most of the marine biogeochemical processes (Keeling et al., 2010). The global decrease of $O_2$ in the ocean also termed "Ocean deoxygenation", has been associated with global warming which is fundamentally driven by the increase in atmospheric $CO_2$. Because of this, it also exists a significant association between deoxygenation and acidification of the ocean (Gruber, 2011). Even though, in the Atlantic ocean, the extent of extremely low $O_2$ content ($[O_2]$) or hypoxic regions ($[O_2] \leq 60$ $\mu mol \cdot kg^{-1}$) are small compared with those of the Pacific and Indian oceans, historical data and climate models show that deoxygenation has been intense in the tropical Atlantic and some authors point out the Atlantic respect to the other oceans as the one with the potential for largest increases in the area of hypoxic regions (Stramma et al., 2008).

The present work studies the deoxygenation in the Equatorial Atlantic Ocean using databases obtained from two different cruises along the parallel 7.5°N: the A06 WOCE section which was carried out in February-March 1993 (Oudot, 1993b) and the MOC$^2$Equatorial cruise which was carried out in April-May 2010 . $[O_2]$ together with the variables of the carbonic system [i.e., pH, total inorganic carbon ($C_T$) and total alkalinity ($A_T$)] were measured in both cruises. Due to that it was possible to estimate

anthropogenic $CO_2$ ($C_{ant}$) using two back-calculation techniques, $\varphi C_T^o$ and TrOCA. The profiles of dissolved pH, $O_2$ and $C_{ant}$ are shown in this work. In order to see more punctual changes in pH, $O_2$, and $C_{ant}$ along the 7.5ºN section and between A06 (1993) and MOC$^2$Equatorial (2010) cruises, the further section was divided in four zonal regions and six density layers related to the main water masses of the Equatorial Atlantic Ocean. The results reveal the westward increase of the Antarctic Intermediate Water tongue with lower pH values in 2010 than in 1993. In addition, the acidification shown in the upper North Atlantic Deep Water is strongly linked to the deoxygenation it presents, where the mean pH decreasing of 0.014 (absolute value) pH units corresponds with a mean $O_2$ loss of ~10 µmol·kg$^{-1}$. In terms of $C_{ant}$, the increasing [$C_{ant}$] is remarkable overall in the upper waters of the water column, where the mean increase was ~ 14 µmol·kg$^{-1}$.

## 3.1 Introduction

Anthropogenic carbon dioxide ($C_{ant}$) emissions alter our oceans in numerous ways, some of which have reached considerable attention, like ocean acidification and sea level rise (Stramma et al., 2012). Ocean acidification is also a direct consequence of the ocean absorbing large amounts of the $C_{ant}$ emitted into the atmosphere as a result of human activities (Gruber, 2011). Ocean acidification refers to a reduction in the pH of the ocean over an extended period, typically decades or longer, caused primarily by the uptake of $CO_2$ from the atmosphere (Gattuso and Hansson, 2011). Recently, concern has emerged that $CO_2$-driven climate change causes decreasing dissolved oxygen ($O_2$) concentrations in the ocean with potentially large impacts on marine habitats and ecosystems (Keeling and Garcia, 2002).

The eastern equatorial Atlantic Ocean is one of the areas framed in the low-oxygen region with high vulnerability for deoxygenation (Gruber, 2011). Some authors have pointed out the Atlantic as the ocean with the potential for largest increases in the area of hypoxic regions (Stramma et al., 2008). This was confirmed by historical data combined with climate models, which show that deoxygenation has been intense in the tropical Atlantic, even though the hypoxic regions are small in this ocean compared with those of the Pacific and Indian oceans (Stramma et al., 2008). There are not enough $O_2$ measurements available to describe past variability and to detail a trend in the ocean (Stramma et al., 2012) and more with more quality $O_2$ sampling is required in order to document the

evolution of $O_2$ in the North Atlantic and to further improve the spatial and temporal coverage of the observations (Stendardo and Gruber, 2012).

Ocean warming, ocean acidification and ocean deoxygenation are acting simultaneously because they are fundamentally driven by the same underlying processes, i.e., the increase in atmospheric $C_{ant}$ and its resulting uptake by the oceans. Ocean warming and deoxygenation are also driven by the emission of other greenhouse gases, such as methane ($CH_4$), nitrous oxide ($N_2O$) and chlorofluorocarbon (CFC). But the contribution of $CO_2$ is by far the most important one (Gruber, 2011).

Mitigating the effects of the $CO_2$ emitted to the atmosphere (Khatiwala et al., 2009) is one crucial role played by the oceans, which have been a net $CO_2$ sink the last 200 years (Gruber et al., 2009). Recent improvements have demonstrated that only ~ 55% of $C_{ant}$ have been transferred from the atmosphere to the ocean and land (Ballantyne et al., 2012; Le Quéré et al., 2009). Particularly, the North Atlantic Basin contains 23% of the global oceanic $C_{ant}$ (Sabine et al., 2004). A key challenge for estimating $C_{ant}$ in the ocean is that $C_{ant}$ is not a directly measurable quantity. Back-calculation techniques attempt to separate the anthropogenic component from the natural one (Khatiwala et al., 2009). Since the firsts approach of Brewer (1978) and Chen and Millero (1979), several authors have been tried to improve these back-calculation methods [$\Delta C^*$(Gruber et al., 1996), LM05 (Lo Monaco et al., 2005), TrOCA (Touratier et al., 2007) or $\varphi C_T^0$ (Vázquez-Rodríguez

et al., 2009a)]. In the present work, in order to estimate the [$C_{ant}$] of the studied area, the TrOCA (Touratier et al., 2007) and $\varphi C_T^0$ (Vázquez-Rodríguez et al., 2009a) methods were selected.

The Equatorial Atlantic Ocean is situated in a dynamically complex area characterized by currents flows mainly in the zonal direction: the North Equatorial (NEC) and South Equatorial (SEC) currents (equatorward arms of the subtropical gyres), which are separated by the eastward Equatorial Undercurrent (EUC), North Equatorial Countercurrent (NECC), and North Equatorial Undercurrent (NEUC) (Fig. 3.1). Besides, the structure and variability of them all are largely driven by the wind filed over the tropical Atlantic, in particular by the variability and/or movement of the Inter Tropical Convergence Zone (ITCZ) (Stramma and Schott, 1999; Urbano et al., 2008). Concretely, in the western basin the section is situated two to three degrees to the north of the North Equatorial Under Current (NEUC) (Arhan et al., 1998) while in the eastern basin, it is inside the cyclonic circulation of the Guinea Dome (Brandt et al., 2010) (Fig. 3.1).

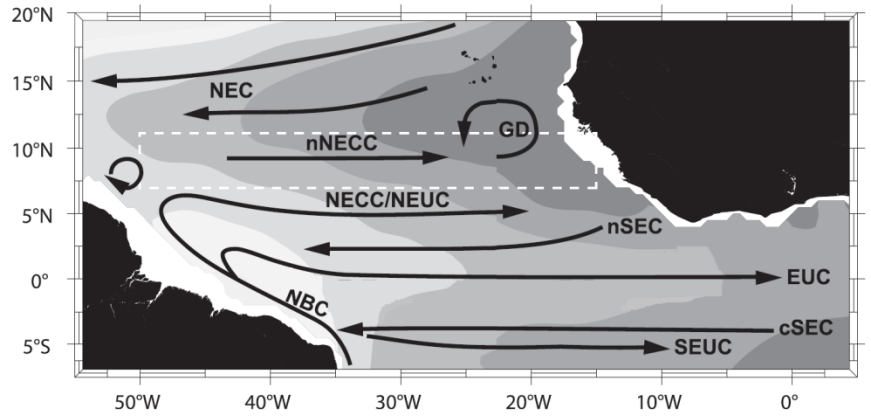


**Figure 3.1 Schematic diagram of the shallow subtropical and tropical Atlantic circulation. The studied area is indicated by the white dashed rectangle. Surface and thermocline current branches shown (black solid arrows) are NEC, nSEC, cSEC, NECC, NBC, NEUC, SEUC, EUC, and the cyclonic circulation around the Guinea Dome (GD) (Adapted from Brandt et al. (2010)).**

The vertical thermohaline structure of this region is clearly dominated by the South Atlantic Central Water (SACW) (Stramma and England, 1999; Stramma and Schott, 1999), which formation occurs in the confluence zone of Brazil and Falkland currents. Since its formation it is transported within the South Atlantic Current (SAC) until it flows in the SEC. SACW is fresher than the North Atlantic Central Water (NACW) and it has rather uniform Θ-S (potential temperature – salinity) properties southward 10ºN: from 5ºC and 34.3 of salinity to 20ºC and 36.0 of salinity (Stramma and England, 1999). The SubAntarctic Mode Water (SAMW) is formed in the South Atlantic at about 40ºS and infers anticyclonic circulation in the South Atlantic subtropical gyre (Tsuchiya et al., 1994). The SAMW is a homogeneous layer extending from near the surface to depths of more than 600m on the equatorward side of the Subantarctic Front (Herraiz-Borreguero and Rintoul, 2011). The

temperature of the SAMW is around 4 - 5ºC (Mémery et al., 2000) with salinity values around 34.2 (Brea et al., 2004; Tsuchiya et al., 1994). The Antarctic Intermediate Water (AAIW) is originated from surface waters in the northern Drake Passage and the Falkland Current loop and a southern boundary that is essentially the Subantarctic Front (Stramma and England, 1999; Stramma and Schott, 1999). The AAIW is recognized around 1000m of depth in waters with $\Theta$ = 3 - 4ºC and a salinity minimum between 34.1 and 34.3 (Murata et al., 2008). These characteristics are similar to those of the densest variety of the SAMW formed in late winter just east of the Drake Passage (4.2ºC, 34.16 psu), which points out the densest SAMW to be the direct precursor of the AAIW (Tsuchiya et al., 1994). The minimum of salinity is weakly detected northern of the equator (Tsuchiya et al., 1994) and even slightly reaches the Madeira Abyssal Plain (Ríos et al., 1992). The North Atlantic Deep Water (NADW) is formed in the Arctic Ocean and transported equatorward by the Deep Western Boundary Current (Steinfeldt et al., 2007). It is located between 1200 and 4500m of depth and it is possible to differentiate its upper (uNADW) and lower (lNADW) layers, the upper one mainly formed by Labrador Sea Water (LSW) while the densest layer is formed mainly by the Iceland Scotland Overflow and Denmark Straight Overflow waters (Johnson, 2008), showing a salinity maximum (Mémery et al., 2000). The densest water of the global ocean is the Antarctic Bottom Water (AABW), which is formed in different places around Antarctica (Johnson, 2008). The AABW is generally found underneath the NADW

(Rhein et al., 1998), with lower salinities and temperatures towards the bottom.

Considering that the Equatorial Atlantic Ocean is one of the areas outlined in the low-oxygen region with high vulnerability for deoxygenation, and taking into account that two cruises were carried out along the 7ºN with an interval of 17 years, the main objective of the present work is to evaluate the changes in $O_2$, pH, and [Cant] in the Equatorial Atlantic Ocean. These changes will be analysed in each water mass and each side of the Mid-Atlantic Ridge.

## 3.2 Data and methodology

The twice repeated 7.5ºN section within a time lag of seventeen years was analysed in terms of hydrography, paying remarkable attention in $O_2$ data. The section corresponds to the parallel 7.5ºN and was measured in 1993 during the WOCE A06 cruise (hereinafter A06), and again in 2010 during the MOC$^2$ Equatorial cruise (MOC$^2$, hereinafter). The 7.5ºN section is extended from French Guiana coast at ~ 51.3ºW to ~14.4ºW in the African Coast and crossing the Equatorial Atlantic Ocean through the 7.5ºN parallel (Fig. 3.2).

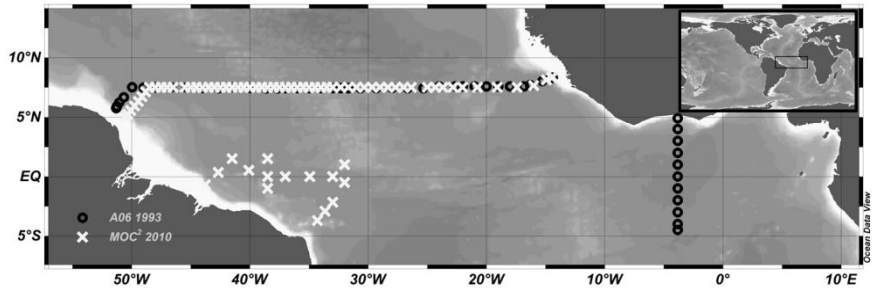


**Figure 3.2 Distribution of A06 and MOC$^2$ cruises. The empty black dots represent the A06 stations, while the white crosses are the stations of MOC$^2$. Only the common transoceanic section 7.5ºN was taken into consideration for this study.**

In the framework of the WOCE Hydrographic Program, the transatlantic A06 cruise was carried out along the parallel 7.5°N and complemented by a meridional 3.5ºW section in February– March 1993 on board the French R/V L'Atalante (Fig. 3.2). This cruise was part of the French CITHER I project (Oudot, 1993b). CTD profiles of Θ, S and nutrient [phosphate ($PO_4^{3-}$) and nitrate ($NO_3^-$)] data at thirty two depths between surface and bottom were obtained at each station (Oudot et al., 1998). CTD-$O_2$ data and $O_2$ data were also acquired and measured in the same all depths (Arhan et al., 1998). The A06 data were included in GLODAP dataset (GLODAP) (Key et al., 2004), but also in other web sites. The hydrographic and nutrient data of A06 were downloaded from W.A.V.E.S. and the corresponding bias corrections were done: + 0.45 µmol·kg$^{-1}$ for $O_2$, - 0.072 µmol·kg$^{-1}$ for $PO_4^{2-}$, and - 0.84 µmol·kg$^{-1}$ for $NO_3^{2-}$ (Gouretski and Jancke, 2001). In the present work, $O_2$ data were downloaded from the CCHDO web site (CCHDO). The secondary quality control (2$^{nd}$ QC) applied in CARINA, i.e., the crossovers analysis method (Key et al., 2010; Tanhua et al., 2010a), was used to check the confidence of these $O_2$

data. The $O_2$ crossovers analysis only produced a mean offset factor of 1.004, which was not applied due to being inside the analytical error of the measurement. Thus, the confidence of the original $O_2$ data was asserted. The same methodology was applied to $PO_4^{2-}$ and $NO_3^{2-}$ obtaining mean offsets of 1.000 and 1.003, respectively, which also stated the confidence in these nutrient data. In addition, the carbonate system variables (i.e., pH, $A_T$ and $C_T$) were download from CCHDO web site and revaluated as described in *III. Result and Discussion, Chapter 2. Carbon data of A06 and A07 WOCE cruises.*

$MOC^2$ cruise was spanned along the transoceanic 7.5ºN section during April-May in 2010 on board the Spanish R/V Hespérides (Fig. 3.2). $O_2$ and nutrient samples were taken at twenty four depths in each station, and the salinity and temperature data were provided by the conductivity sensor of the CTD. In order to auto check and give confidence to these $MOC^2$ data, the $2^{nd}$QC was applied to $O_2$, $PO_4^{3-}$ and $NO_3^-$, resulting the multiplicative offsets of 0.994, 1.032 and 1.011, respectively. pH, $A_T$ and $C_T$ data were also considered. The crossovers analysis was applied again to $A_T$ and $C_T$ data obtained a mean offset of -0.360 and 2.061 for $A_T$ and $C_T$ respectively. Due to be both offsets inside the CARINA / GLODAP permitted limits (±6 µmol·kg$^{-1}$ for $A_T$ and ±4 µmol·kg$^{-1}$ for $C_T$), the good quality of these data were considered.

The common section 7.5ºN of both A06 and $MOC^2$ cruises was selected to evaluate the hydrographic changes together with the differences in pH, $O_2$ and $C_{ant}$ from 1993 to 2010 (Fig. 3.2). In order

to estimate $C_{ant}$, the back-calculation methods $\varphi C_T^o$ and TrOCA were applied. Both methods are based on removing from $C_T$ the carbon contributions after the time of water mass formation due to oxidation-reduction processes of organic matter and processes of dissolution of $CaCO_3$ as well as the corresponding theoretical carbon content of the water mass at the time it was last in contact with the atmosphere The detailed description of these methodologies is given in *II. Data and methodology, 3. Methodology to estimate anthropogenic $CO_2$.*

The whole section was divided into four regions, two on each side of the Mid-Atlantic Ridge, and the water column was in turn divided into six vertical density layers. The selected regions westward of the Mid-Atlantic Ridge were the Region 1 (R1): from Guiana coast (~ 50ºW) to 45ºW and the Region 2 (R2): from 45ºW to 32.5ºW, while the two eastward of the Mid-Atlantic Ridge regions were the Region 3 (R3): from 32.50ºW to 21ºW and the Region 4 (R4): from 21ºW to African coast (~ 15ºW).

The selected Θ-S properties of each water mass present in the Equatorial Atlantic Ocean as well as the characteristic nutrient data are presented in table 3.1 (Brea et al., 2004).

**Table 3.1 Characteristic potential temperature (Θ), salinity and nutrient data ($SiO_2$ and $NO_3^-$) of the main water masses present in the Equatorial Atlantic Ocean (Brea et al., 2004): South Atlantic Central Water (SACW), SubAntartic Mode Water (SAMW), Antarctic Intermediate Water (AAIW), upper North Atlantic Deep Water (uNADW), lower North Atlantic Deep Water (lNADW) and Antarctic Bottom Water (AABW).**

| Water Mass | Θ (ºC) | Salinity (psu) | $NO_3^-$ (µmol·kg$^{-1}$) | $SiO_2$ (µmol·kg$^{-1}$) |
|---|---|---|---|---|
| **SACW** | 18±0.16 | 35.8±0.02 | 222±4 | 1.5±0.5 |
| **SAMW** | 4.8±0.08 | 34.2±0.01 | 490±3 | 10±0.7 |
| **AAIW** | 3.14±0.08 | 34.14±0.01 | 548±3 | 18±0.7 |
| **uNADW** | 4.3±0.1 | 35.008±0.005 | 429±2 | 16.1±0.5 |
| **lNADW** | 2.02±0.03 | 34.905±0.003 | 447±1 | 31.1±0.9 |
| **AABW** | 0.2±0.03 | 34.67±0.001 | 540±2 | 135±2 |

A Θ-S diagram was constructed in order to characterize water masses and mixing along this 7.5ºN section (Fig. 3.3).

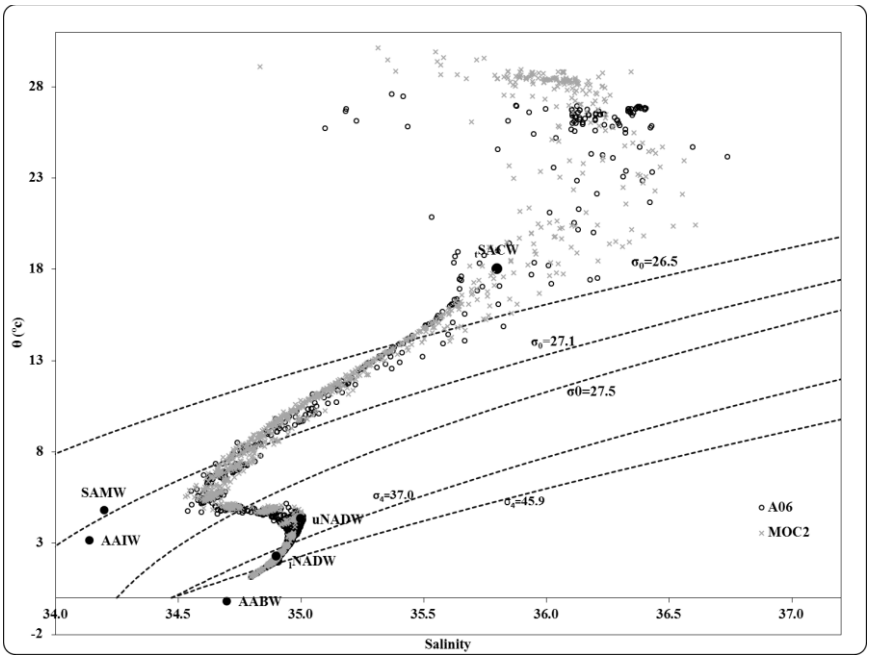


**Figure 3.3 Θ-S diagram of A06 and MOC$^2$ cruises. The empty black dots represent the Θ-S A06 data, while the grey crosses are those of MOC$^2$. The black dots are the locations of the main water masses of the Equatorial Atlantic Ocean: South Atlantic Central Water (SACW), SubAntarctic Mode Water (SAMW), Antarctic Intermediate Water (AAIW), upper and lower North Atlantic Deep Water (uNADW and lNADW) and Antarctic Bottom Water (AABW).**

The density layers were selected as function of the main water masses present in the Equatorial Atlantic Ocean, according to the Θ-S diagram from both cruises (Fig. 3.3). The uppermost layers (SACW, SAMW and AAIW) were delimited using $\sigma_0$, while 2000 dbar was the level of reference ($\sigma_2$) selected to delimit the NADW layers, uNADW and lNADW. The AABW layer was delimited using 4000 dbar as the pressure level of reference ($\sigma_4$). Then, the SACW layer (L1) involves all data from surface to isopycnal 26.5 $kg \cdot m^{-3}$ $\sigma_0$ (Stramma and Schott, 1999). The SAMW layer (L2) contains all data from 26.5 to 27.1 $kg \cdot m^{-3}$ $\sigma_0$ isolines (Mémery et al., 2000). The AAIW layer (L3) includes all data between 27.1 $kg \cdot m^{-3}$ and 27.5 $kg \cdot m^{-3}$ $\sigma_0$ isopycnals (Murata et al., 2008). In deep waters, the uNADW layer (L4) involves all data from 27.5 $kg \cdot m^{-3}$ $\sigma_0$ isopycnal to 37 $kg \cdot m^{-3}$ $\sigma_2$ isopycnal, while the lNADW layer (L5) contains all data from 37 $kg \cdot m^{-3}$ $\sigma_2$ to 45.9 $kg \cdot m^{-3}$ $\sigma_4$ isopycnals (Mémery et al., 2000). The AABW layer (L6) encloses data from 45.9 $kg \cdot m^{-3}$ $\sigma_4$ isopycnal (Rhein et al., 1998) to the bottom. These regions and layers are depicted in figure 3.4 [ODV graph (Schlitzer, R., 2011)] over the salinity distribution from the $MOC^2$ cruise.

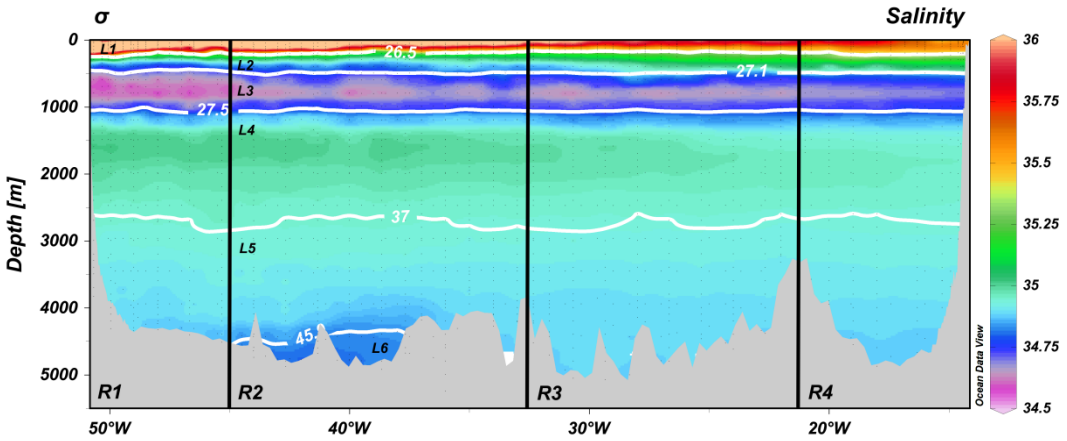


Figure 3.4 Regions and layers in which the 7.5°N section was divided. The coloured contours show salinity CTD data from MOC$^2$ cruise. The vertical black lines divide the regions: R1 and R2 are located westward of the Mid-Atlantic Ridge while the eastern regions are R3 and R4. White horizontal lines divide the layers: L1 (SACW, surface - $\sigma_0$= 26.5 kg·m$^{-3}$), L2 (SAMW, $\sigma_0$= 26.5 ≤ $\sigma_0$= 27.1 kg·m$^{-3}$), L3 (AAIW, $\sigma_0$= 27.1 ≤ $\sigma_0$= 27.5 kg·m$^{-3}$), L4 (uNADW, $\sigma_0$= 27.5 ≤ $\sigma_2$= 37 kg·m$^{-3}$) L5 (lNADW, $\sigma_2$= 37 ≤ $\sigma_4$= 45.9 kg·m$^{-3}$) and L6 (AABW, $\sigma_4$= 45.9 kg·m$^{-3}$ - bottom).

The salinity distribution from the MOC$^2$ (Fig. 3.4) shows the mean characteristic profile of the region (as it also does the one from A06 cruise). The subsurface maximum around 100m (L1) is clearly shown and also the diminution with depth (L2) and the minimum at about 800m representing the core of AAIW (L3) (Brandt et al., 2010). In deeper water (~1700m) the salinity maximum of Mediterranean origin reveals the presence of the uNADW (L4). The salinity values decrease with depth in L5 until it came to the characteristic minimum of the AABW (L6) (Arhan et al., 1998).

The mean values of each selected variable [salinity (psu), Θ (ºC), $O_2$ (µmol kg$^{-1}$), AOU (µmol kg$^{-1}$), $PO_4^{3-}$ (µmol kg$^{-1}$), $A_T$ (µmol kg$^{-1}$), $C_T$ (µmol kg$^{-1}$), pH (pH units), $\varphi C_T^0$ (µmol kg$^{-1}$) and TrOCA (µmol kg$^{-1}$)] together with the standard error of their means ($x \pm \sigma/\sqrt{N}$) were calculated for the twenty four regional layers (each one of the

layers in each one of the regions) and for A06 and MOC[2] and are shown in tables 3.2 and 3.3, respectively. The thickness (m) of each layer was computed as the average vertical distance between layers weighted by the separation between stations.

Table 3.2 Mean values of each variable ± standard error of the mean (x±σ/√n) for data of A06 cruise.

| Mean values of A06 1993 | | | | | | | | | | | | |
|---|---|---|---|---|---|---|---|---|---|---|---|---|
| | | Thickness (m) | Salinity (psu) | Θ (ºC) | $O_2$ | AOU | $PO_4^{3-}$ | $A_T$ | $C_T$ | pH | $\varphi C_T^0$ | TrOCA |
| R1 | L1 | 157±23 | 36.317±0.021 | 25.02±0.46 | 192.9±2.9 | 12.6±4.5 | 0.16±0.04 | 2377±1 | 2047±7 | 8.048±0.012 | 54±0 | 60±2 |
| | L2 | 266±26 | 35.120±0.063 | 10.78±0.44 | 122.4±3.9 | 148.0±5.1 | 1.66±0.06 | 2314±3 | 2189±3 | 7.659±0.014 | 27±2 | 29±2 |
| | L3 | 636±37 | 34.632±0.008 | 5.73±0.14 | 137.8±1.9 | 165.3±1.3 | 2.28±0.01 | 2303±0 | 2221±1 | 7.550±0.002 | 18±1 | 18±1 |
| | L4 | 1177±32 | 34.974±0.006 | 4.01±0.06 | 239.1±3.2 | 75.7±2.8 | 1.39±0.03 | 2314±0 | 2171±2 | 7.707±0.004 | 13±0 | 19±0 |
| | L5 | 1637±163 | 34.917±0.003 | 2.23±0.04 | 261.2±0.3 | 67.7±0.3 | 1.32±0.00 | 2326±0 | 2174±1 | 7.729±0.001 | 8±0 | 8±0 |
| | L6 | 167±37 | 34.880±0.003 | 1.76±0.02 | 257.0±1.2 | 76.0±1.3 | 1.43±0.02 | 2336±1 | 2189±2 | 7.717±0.002 | 9±0 | 6±1 |
| R2 | L1 | 162±19 | 36.178±0.042 | 24.68±0.70 | 184.1±5.3 | 22.9±7.7 | 0.17±0.07 | 2368±2 | 2040±10 | 8.045±0.020 | 48±3 | 48±3 |
| | L2 | 327±19 | 34.957±0.052 | 9.70±0.39 | 116.0±2.7 | 160.8±4.2 | 1.81±0.06 | 2308±2 | 2199±4 | 7.619±0.014 | 24±1 | 25±1 |
| | L3 | 544±32 | 34.679±0.010 | 5.80±0.19 | 124.9±3.3 | 177.6±2.2 | 2.30±0.02 | 2305±1 | 2230±1 | 7.533±0.004 | 16±1 | 16±1 |
| | L4 | 1315±51 | 34.963±0.006 | 3.89±0.06 | 234.8±3.2 | 81.0±2.8 | 1.42±0.03 | 2318±0 | 2177±2 | 7.704±0.004 | 12±0 | 16±0 |
| | L5 | 1696±80 | 34.914±0.003 | 2.27±0.04 | 256.5±0.3 | 72.2±0.4 | 1.37±0.01 | 2329±1 | 2179±1 | 7.724±0.001 | 8±0 | 7±0 |
| | L6 | 637±72 | 34.838±0.004 | 1.44±0.04 | 246.3±1.0 | 89.4±1.3 | 1.65±0.02 | 2345±1 | 2209±2 | 7.688±0.003 | 10±0 | 8±0 |
| R3 | L1 | 167±58 | 36.076±0.033 | 23.54±0.64 | 182.6±6.1 | 28.8±8.5 | 0.30±0.08 | 2361±2 | 2047±11 | 8.020±0.022 | 52±1 | 47±2 |
| | L2 | 380±8 | 35.111±0.032 | 11.10±0.29 | 94.1±3.4 | 174.3±4.0 | 1.81±0.04 | 2311±1 | 2202±3 | 7.619±0.011 | 24±1 | 25±1 |
| | L3 | 563±15 | 34.696±0.008 | 5.80±0.14 | 115.6±3.5 | 186.8±2.6 | 2.37±0.01 | 2304±1 | 2230±1 | 7.528±0.004 | 10±1 | 10±1 |
| | L4 | 1299±58 | 34.941±0.004 | 3.83±0.05 | 224.2±2.5 | 92.1±2.2 | 1.54±0.02 | 2319±0 | 2181±1 | 7.695±0.004 | 8±0 | 11±0 |
| | L5 | 1902±131 | 34.905±0.001 | 2.21±0.02 | 249.7±0.3 | 79.5±0.3 | 1.46±0.00 | 2337±0 | 2188±1 | 7.721±0.000 | 7±0 | 5±0 |
| R4 | L1 | 149±20 | 35.639±0.037 | 20.20±0.73 | 138.6±8.7 | 86.7±11.5 | 0.83±0.10 | 2334±2 | 2108±15 | 7.861±0.029 | 49±1 | 54±3 |
| | L2 | 349±38 | 35.179±0.034 | 11.58±0.36 | 69.1±3.3 | 196.4±5.1 | 1.91±0.06 | 2314±1 | 2220±5 | 7.575±0.016 | 28±1 | 28±1 |
| | L3 | 586±30 | 34.724±0.008 | 5.79±0.19 | 105.6±5.5 | 196.8±4.2 | 2.42±0.02 | 2306±1 | 2240±2 | 7.504±0.007 | 11±1 | 11±0 |
| | L4 | 1284±38 | 34.925±0.005 | 3.76±0.07 | 213.0±3.5 | 103.8±3.0 | 1.65±0.03 | 2319±1 | 2191±2 | 7.670±0.005 | 9±0 | 12±0 |
| | L5 | 1735±299 | 34.907±0.002 | 2.27±0.04 | 240.5±0.2 | 88.1±0.4 | 1.52±0.00 | 2341±1 | 2198±1 | 7.706±0.001 | 9±0 | 6±0 |

Table 3.3 Mean values of each variable ± standard error of the mean (x±σ/√n) for data of MOC$^2$ cruise.

| Mean values of MOC$^2$ 2010 | | | | | | | | | | | | |
|---|---|---|---|---|---|---|---|---|---|---|---|---|
| | | Thickness (m) | Salinity (psu) | Θ (ºC) | $O_2$ | AOU | $PO_4^{3-}$ | $A_T$ | $C_T$ | pH | $\varphi C_T^0$ | TrOCA |
| R1 | L1 | 174±8 | 36.089±0.032 | 25.78±0.46 | 182.9±2.7 | 20.6±4.3 | 0.21±0.04 | 2365±2 | 2054±7 | 8.024±0.012 | 71±1 | 75±1 |
| | L2 | 296±12 | 34.982±0.038 | 10.09±0.27 | 130.6±1.1 | 143.9±2.1 | 1.79±0.04 | 2308±2 | 2192±2 | 7.644±0.007 | 32±1 | 34±1 |
| | L3 | 596±18 | 34.645±0.007 | 5.96±0.12 | 130.2±1.8 | 171.3±1.2 | 2.38±0.03 | 2300±1 | 2220±1 | 7.550±0.002 | 16±1 | 16±1 |
| | L4 | 1211±62 | 34.944±0.009 | 4.23±0.11 | 222.1±5.2 | 91.1±4.5 | 1.57±0.05 | 2314±0 | 2180±2 | 7.690±0.007 | 12±0 | 17±1 |
| | L5 | 1649±83 | 34.916±0.003 | 2.30±0.05 | 261.4±0.4 | 67.0±0.4 | 1.33±0.01 | 2324±1 | 2173±1 | 7.732±0.001 | 8±0 | 9±0 |
| | L6 | 167±14 | 34.867±0.004 | 1.70±0.03 | 255.4±1.4 | 78.1±1.7 | 1.49±0.04 | 2338±1 | 2192±2 | 7.718±0.003 | 8±0 | 6±0 |
| R2 | L1 | 147±5 | 36.075±0.021 | 24.26±0.50 | 173.4±3.3 | 35.9±5.1 | 0.33±0.04 | 2364±1 | 2064±6 | 8.003±0.012 | 60±2 | 62±2 |
| | L2 | 341±12 | 35.015±0.020 | 10.38±0.16 | 120.0±1.3 | 152.7±2.0 | 1.75±0.03 | 2309±1 | 2195±2 | 7.637±0.007 | 30±1 | 31±1 |
| | L3 | 602±11 | 34.695±0.005 | 6.16±0.11 | 121.7±1.9 | 178.3±1.3 | 2.31±0.01 | 2302±0 | 2225±1 | 7.541±0.002 | 16±1 | 15±0 |
| | L4 | 1133±1 | 34.948±0.006 | 4.18±0.08 | 221.8±4.1 | 91.8±3.6 | 1.51±0.03 | 2315±0 | 2181±2 | 7.690±0.005 | 12±0 | 16±0 |
| | L5 | 1903±47 | 34.916±0.003 | 2.35±0.04 | 257.1±0.3 | 70.9±0.3 | 1.35±0.01 | 2328±1 | 2178±1 | 7.730±0.001 | 9±0 | 8±0 |
| | L6 | 499±33 | 34.827±0.003 | 1.38±0.03 | 245.3±0.7 | 90.9±1.0 | 1.68±0.02 | 2348±1 | 2211±1 | 7.692±0.002 | 10±0 | 7±0 |
| R3 | L1 | 130±4 | 35.811±0.023 | 21.32±0.56 | 151.1±4.3 | 70.1±6.4 | 0.65±0.06 | 2350±1 | 2108±8 | 7.897±0.017 | 65±1 | 65±2 |
| | L2 | 360±12 | 35.117±0.016 | 11.29±0.15 | 103.5±2.3 | 163.7±2.8 | 1.75±0.03 | 2313±1 | 2204±2 | 7.624±0.007 | 34±1 | 35±1 |
| | L3 | 599±11 | 34.721±0.008 | 6.24±0.13 | 107.9±2.7 | 191.5±1.9 | 2.39±0.01 | 2304±0 | 2235±1 | 7.517±0.003 | 15±1 | 14±0 |
| | L4 | 1171±37 | 34.927±0.007 | 4.07±0.07 | 213.9±3.9 | 100.6±3.4 | 1.61±0.03 | 2317±0 | 2187±2 | 7.679±0.006 | 10±0 | 14±0 |
| | L5 | 2000±120 | 34.907±0.002 | 2.29±0.03 | 250.0±0.4 | 78.5±0.4 | 1.43±0.01 | 2336±1 | 2188±1 | 7.722±0.000 | 9±0 | 7±0 |
| R4 | L1 | 184±12 | 35.633±0.020 | 20.26±1.09 | 122.3±10.6 | 103.5±14.7 | 0.95±0.12 | 2339±2 | 2134±18 | 7.820±0.035 | 64±2 | 64±3 |
| | L2 | 282±19 | 35.206±0.037 | 11.81±0.41 | 64.9±4.2 | 199.3±6.4 | 1.89±0.07 | 2317±2 | 2230±5 | 7.562±0.017 | 36±2 | 35±2 |
| | L3 | 625±9 | 34.736±0.012 | 6.33±0.23 | 96.3±5.6 | 202.4±4.0 | 2.42±0.03 | 2305±1 | 2243±2 | 7.497±0.007 | 16±1 | 14±1 |
| | L4 | 1000±133 | 34.905±0.013 | 4.04±0.14 | 200.2±7.8 | 114.5±6.8 | 1.70±0.06 | 2320±1 | 2198±4 | 7.660±0.012 | 9±0 | 11±0 |
| | L5 | 2105±224 | 34.906±0.005 | 2.29±0.08 | 240.8±0.4 | 87.7±0.9 | 1.45±0.01 | 2344±2 | 2199±2 | 7.715±0.001 | 9±0 | 6±0 |

The increase or decrease of each variable (Δx) from 1993 (A06) to 2010 ($MOC^2$) was calculated as the difference from $MOC^2$ data minus A06 data. The Δx for each one of the observed and estimated variables (Δvariable, with variable = the name of each one of them) are listed in table 3.4. The uncertainty of each Δvariable was calculated by propagation of the error of the standard error of the mean.

Thus each value of the table is:

Equation 24

$$\Delta x = (x_{2010}\text{-}x_{1993}) \pm \sqrt{\left(\frac{\sigma}{\sqrt{n}}\right)^2_{2010} + \left(\frac{\sigma}{\sqrt{n}}\right)^2_{1993}}$$

Table 3.4 Δvalues (Δvalue = $MOC^2_{value}$ - $A06_{value}$) of theta (ºC), salinity, $O_2$ (µmol $kg^{-1}$), AOU (µmol $kg^{-1}$), $PO_4^{-3}$ (µmol $kg^{-1}$), $A_T$ (µmol $kg^{-1}$), $C_T$ (µmol $kg^{-1}$), pH, $\phi C_T^0$ and TrOCA (µmol $kg^{-1}$) for each selected region and layer

| | | ΔSalinity | ΔΘ | $\Delta O_2$ | ΔAOU | $\Delta PO_4^{3-}$ | $\Delta A_T$ | $\Delta C_T$ | ΔpH | $\Delta\phi C_T^0$ | ΔTrOCA |
|---|---|---|---|---|---|---|---|---|---|---|---|
| R1 | L1 | -0.228±0.038 | 0.77±0.65 | -10.0±4.0 | 8.0±6.2 | 0.05±0.05 | -13±2 | 7±10 | -0.024±0.016 | 17±1 | 15±2 |
| | L2 | -0.138±0.074 | -0.69±0.51 | 8.2±4.0 | -4.1±5.5 | 0.13±0.07 | -5±3 | 3±4 | -0.015±0.015 | 5±2 | 5±2 |
| | L3 | 0.013±0.010 | 0.23±0.18 | -7.6±2.6 | 6.0±1.7 | 0.10±0.03 | -2±1 | -1±1 | -0.001±0.003 | -2±1 | -2±1 |
| | L4 | -0.031±0.011 | 0.22±0.12 | -17.0±6.1 | 15.4±5.3 | 0.19±0.05 | 0±0 | 9±3 | -0.017±0.008 | -1±1 | -2±1 |
| | L5 | -0.001±0.004 | 0.07±0.07 | 0.2±0.5 | -0.7±0.5 | 0.01±0.01 | -2±1 | -1±1 | 0.004±0.001 | 0±0 | 1±0 |
| | L6 | -0.013±0.005 | -0.06±0.04 | -1.6±1.8 | 2.1±2.1 | 0.06±0.04 | 2±2 | 4±3 | 0.001±0.003 | -1±1 | 0±1 |
| R2 | L1 | -0.103±0.047 | -0.42±0.87 | -10.7±6.3 | 13.0±9.3 | 0.15±0.08 | -4±3 | 24±12 | -0.042±0.024 | 12±4 | 14±3 |
| | L2 | 0.058±0.055 | 0.69±0.43 | 4.0±3.0 | -8.2±4.7 | -0.06±0.07 | 2±2 | -4±5 | 0.018±0.016 | 6±1 | 6±1 |
| | L3 | 0.016±0.012 | 0.35±0.22 | -3.2±3.8 | 0.7±2.6 | 0.01±0.02 | -3±1 | -5±1 | 0.009±0.004 | 0±1 | -1±1 |
| | L4 | -0.015±0.008 | 0.29±0.10 | -13.0±5.2 | 10.8±4.6 | 0.09±0.04 | -3±0 | 5±2 | -0.014±0.007 | 0±1 | 0±1 |
| | L5 | 0.002±0.004 | 0.08±0.06 | 0.6±0.5 | -1.3±0.5 | -0.02±0.01 | -1±1 | -1±1 | 0.005±0.001 | 1±0 | 1±0 |
| | L6 | -0.011±0.005 | -0.07±0.05 | -1.0±1.3 | 1.6±1.7 | 0.03±0.03 | 2±1 | 2±2 | 0.005±0.003 | -1±0 | -1±0 |
| R3 | L1 | -0.264±0.040 | -2.22±0.85 | -31.5±7.5 | 41.2±10.6 | 0.35±0.10 | -11±2 | 61±13 | -0.123±0.028 | 13±1 | 18±3 |
| | L2 | 0.006±0.035 | 0.19±0.33 | 9.4±4.1 | -10.6±4.9 | -0.06±0.05 | 2±1 | 2±4 | 0.005±0.013 | 11±1 | 10±1 |
| | L3 | 0.025±0.011 | 0.45±0.19 | -7.7±4.4 | 4.6±3.2 | 0.02±0.02 | 0±1 | 4±1 | -0.010±0.005 | 6±1 | 4±1 |
| | L4 | -0.014±0.008 | 0.24±0.09 | -10.3±4.6 | 8.5±4.1 | 0.06±0.04 | -2±1 | 6±2 | -0.015±0.007 | 2±0 | 2±0 |
| | L5 | 0.002±0.003 | 0.08±0.04 | 0.4±0.5 | -1.1±0.5 | -0.02±0.01 | -1±1 | 0±1 | 0.002±0.001 | 1±0 | 2±0 |
| R4 | L1 | -0.006±0.042 | 0.06±1.31 | -16.2±13.8 | 16.8±18.6 | 0.12±0.16 | 5±3 | 26±23 | -0.041±0.045 | 15±2 | 10±5 |
| | L2 | 0.027±0.050 | 0.24±0.55 | -4.2±5.3 | 2.8±8.2 | -0.02±0.09 | 3±2 | 9±7 | -0.014±0.023 | 8±2 | 7±3 |
| | L3 | 0.012±0.015 | 0.54±0.30 | -9.3±7.8 | 5.6±5.8 | 0.00±0.04 | -1±1 | 3±3 | -0.007±0.010 | 5±1 | 3±1 |
| | L4 | -0.020±0.014 | 0.28±0.16 | -12.8±8.6 | 10.7±7.4 | 0.05±0.07 | 1±1 | 6±4 | -0.010±0.013 | -1±0 | -1±0 |
| | L5 | -0.001±0.006 | 0.02±0.09 | 0.3±0.5 | -0.5±1.0 | -0.07±0.01 | 3±2 | 1±3 | 0.009±0.001 | 0±0 | 0±0 |

## 3.3 Results and Discussion

The general description of the Equatorial Atlantic Ocean hydrography is specified in this section, detailing, first of all, the changes in temperature and salinity. Then, the acidification of the region is evaluated by means of the changes in pH. These changes are related to $O_2$ changes, which were evaluated also in terms of the temperature and salinity after the description of the $[O_2]$ for both A06 and MOC$^2$ cruises was detailed. The changes in nutrients were also discussed in terms of AOU, and, finally, the differences in terms of $C_{ant}$ between A06 and MOC$^2$ are also given.

The common 7.5ºN section of both A06 and MOC$^2$ cruises was carried out at different seasons, being A06 a boreal winter cruise while MOC$^2$ was a boreal spring cruise. Due to the different position of the ITCZ and the associated differences in the Equatorial North Atlantic circulation, the changes of the thermohaline properties show a different behaviour in L1 respect to the other layers (Fig. 3.5).

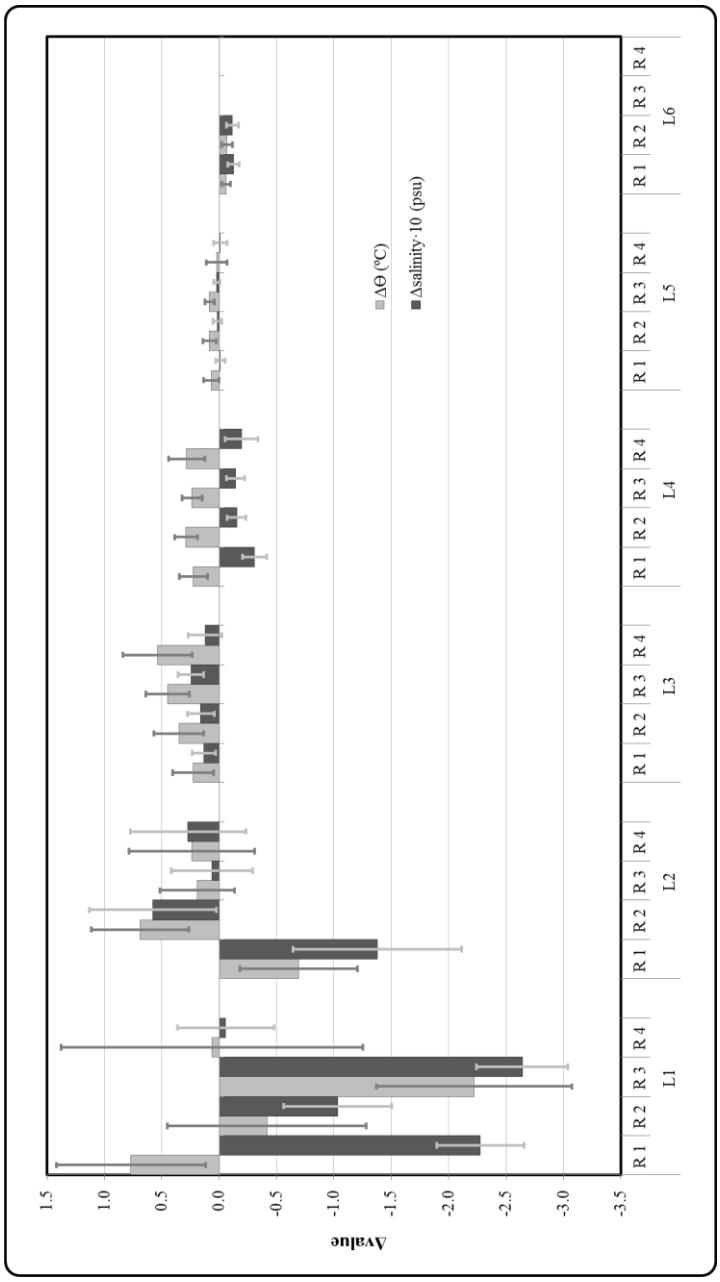


Figure 3.5 ΔΘ (ºC) and Δsalinity (psu) calculated as the difference between properties of MOC[2] (2010) minus A06 (1993). Δsalinity was multiplied by ten in order to do both scales comparable.

In general, in the L1 of all the regions (R1 – R4) the salinity decrease from 1993 to 2010 (Δsalinity < 0) associated with a decrease of temperature (ΔΘ < 0) that is explicated by the different seasons at when both cruises were carried out. But particularly, R1L1 shows higher temperatures and lower salinities in $MOC^2$ than in A06 distributions (Fig. 3.4), which are likely due to the more proximity of the Amazon River in $MOC^2$ than in A06 (Fig. 3.2). In R2L1 it is worth highlighting the strong influence of the North Brazil Current (NBC) over the seasonality, driving less haline (fresher) and relative colder water in $MOC^2$ than in A06. This influence is not so remarkable in R3 - R4 (Fig. 3.5). These differences in temperature and salinity can also be slightly seen in the Θ-S diagram (Fig. 3.3). In the case of the AAIW layer (L3), ΔΘ and Δsalinity are positive, with a slight trend to increase ΔΘ eastward (Fig. 3.5), suggesting a lees intensity of AAIW in 2010. The uNADW layer (L4), where LSW is the main component, was fresher and warmer waters in 2010 (Fig. 3.5). The signal of LWS formed during the high NAO period in 1990s, was relatively fresh (Dickson et al., 2002). Changes in Θ and salinity are low in the deepest layer (L5) in all regions (Table 3.4) but a stronger presence of AABW can be noticed in the Guiana Basin (R1 and R2) indicated by ΔΘ ≈ - 0.06 ºC and Δsalinity ≈ - 0.012 (together with an increment in $SiO_2$, from $[SiO_2]_{1993}$ = 43.2±1.5 to $[SiO_2]_{2010}$ = 47.5±2.6 µmol $kg^{-1}$ in R1 and $[SiO_2]_{1993}$ = 64.9±1.9 to $[SiO_2]_{2010}$ = 66.1±1.4 µmol $kg^{-1}$ in R2).

The pH distributions of A06 and MOC$^2$ are shown in figure 3.6. In general, the SACW layer (L1) is the most affected by high pH changes (Fig. 3.6). There is a pH decrease from 1993 to 2010, varying from ΔpH = -0.123±0.028 in R3 to ΔpH = -0.024±0.016 in R1L1 (Table 3.4). The tongue of lower pH values related to AAIW, which should appear only in L3, becomes wide and covers L2 and L3 in both A06 and MOC$^2$. Watching figure 3.6 from the eastern side (African Coast), it is easy to distinguish how the pH minimum tongue is spreading toward west. The pH isoline of 7.53 that in 1993 only reached R2, in 2010 covered the whole R1. Because of this, ΔpH is negative in R1L2 and R1L3, with values of -0.015±0.015 and -0.001±0.003, respectively (Table 3.4). Something similar happens in the eastern basin, where the lowest isoline (pH = 7.46), which in 1993 is enclosed in R4, is in 2010 more intense in R4 and reaches clearly R3. The result from this is a remarkable decrease of 0.014 units of pH in R4L2 (Table 3.4). In the L4, the lower salinity of uNADW in 2010 is linked to the decrease in pH values. The averaged acidification was of ~ 0.014 (absolute value) units of pH in L4 (varying ΔpH from -0.010±0.013 in R4 to -0.017±0.008 in R1). The pH isoline 7.72 in lNADW (L5) R1-R4 shows an eastward tongue and even the loss of the pH=7.74 isoline in R1L5 from 1993 to 2010 make us think of a weak acidification. However, the mean ΔpH is ~ 0.005 pH units in L5 for all the regions (Table 3.4). In L6, pH in AABW (only found in R1 and R2) was higher in MOC$^2$ than in A06 being ΔpH = 0.001 ± 0.003 and 0.005 ± 0.003 pH units, respectively.

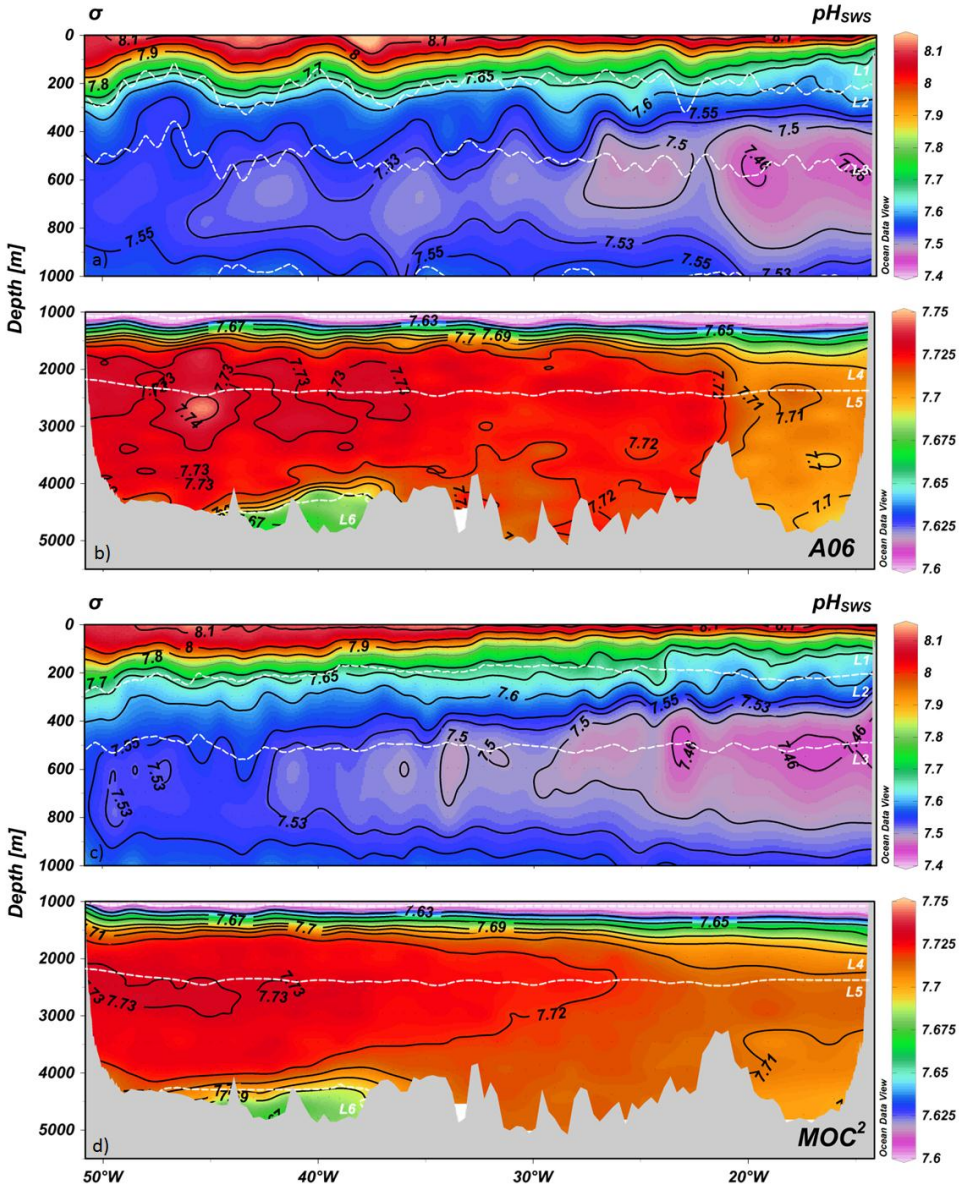


Figure 3.6 pH distribution along the 7.5°N section in A06 (a, b) and MOC$^2$ (c, d). a) and c) are a zoom from surface to 1000 m, with dashed white contours delimiting SACW, SAMW and AAIW layers (L1, L2 and L3, respectively) at the corresponding $\sigma_0$ isopycnals (26.5, 27.1 and 27.5 kg·m$^{-3}$). b) and d) show the column water from 1000m to bottom depth. The dashed white contours are the upper and lower limits of uNADW (L4), lNADW (L5) and AABW (L6) layers (i.e., $\sigma_0$ = 27.5 kg·m$^{-3}$, $\sigma_2$ = 37 kg·m$^{-3}$and $\sigma_4$ = 45.9 kg·m$^{-3}$)

The Θ and salinity changes are also translated into $O_2$ changes. Figure 3.7 shows the distributions of $O_2$ from A06 and MOC[2] datasets. The $O_2$ distribution in the ocean is usually linked to the water masses. The relative extreme values of the $O_2$ profile mark the location of specific water masses in the Equatorial Atlantic Ocean that can be seen in the $O_2$ distributions of the 7.5ºN section. In the upper waters, high oxygen values characterize the SACW layer (L1). $O_2$ maxima values of 211 µmol·kg$^{-1}$ and 217 µmol·kg$^{-1}$ are found in A06 (Fig. 3.7a) and MOC[2] (Fig. 3.7c), respectively. Both values are slightly lower than the values ($O_2$ > 220 µmol·kg$^{-1}$) found by Mémery et al. (2000). In the immediately below L2 layer, an $O_2$ minimum ($O_2$ < 100 µmol·kg$^{-1}$) (Stramma and Schott, 1999) should be found between 300 - 400m of depth (Stramma and England, 1999), just above $\sigma_0$ = 27.1 (lower limit of the SAMW layer). The $O_2$ minima that can be seen for the whole L2 in the distributions are 72 µmol kg$^{-1}$ for A06 (Fig. 3.7a) and 68 µmol·kg$^{-1}$ for MOC[2] (Fig. 3.7c). Considering the different regions, the $O_2$ minima are found in the easternmost R4 region, with values of ~47 and ~39 µmol·kg$^{-1}$ for A06 and MOC[2], respectively. In L3, the $O_2$ values rise again probably due to the relatively high oxygen content of the AAIW, which reaches the equator at a slightly lower density than its characteristic salinity minimum ($\sigma_0$ = 27.3), around 700m of depth (Stramma and England, 1999). The mean $O_2$ values in the AAIW layer (L3) are ~ 122 and ~ 117 µmol·kg$^{-1}$ for A06 and MOC[2], respectively. Close to these relative $O_2$ enriched waters lay the characteristic salinity maximum of the uNADW (L4) around 1700m (Tsuchiya et al., 1994). In fact, within the deep layers

occupied by the NADW (L4 and L5) the $O_2$ maximum can be found for the whole section in both cruises. The $O_2$ maximum in the different regions of L4 is observed in the Guiana Basin (R1), with values of ~ 264 µmol $kg^{-1}$ for A06 (Fig. 3.7a) and ~ 261 µmol·$kg^{-1}$ for MOC[2] (Fig. 3.7b). The $O_2$ maxima in the whole L5 are of 267 and 265 µmol $kg^{-1}$ for A06 and MOC[2], respectively, which are in accordance to Mémery et al. (2000) and Arhan et al. (1998), who pointed out high values of oxygen associated to the lNADW ($O_2$ > 260 µmol $kg^{-1}$). The zonal tongues of high oxygen values were also detected by Arhan et al. (1998) in the A06 section at around 3800m. Underneath the lNADW, the AABW is characterized by lower temperature and salinity and also relatively low $O_2$ values compared to those of the NADW at this latitude. In the 7.5ºN section, L6 (AABW layer) is only located at the western side of the Mid-Atlantic Ridge, in R1 and R2, with mean $O_2$ values for the whole L6 area of ~ 249 µmol $kg^{-1}$ for A06 (Fig. 5a) and ~ 247 µmol $kg^{-1}$ for MOC[2] (Fig. 3.7).

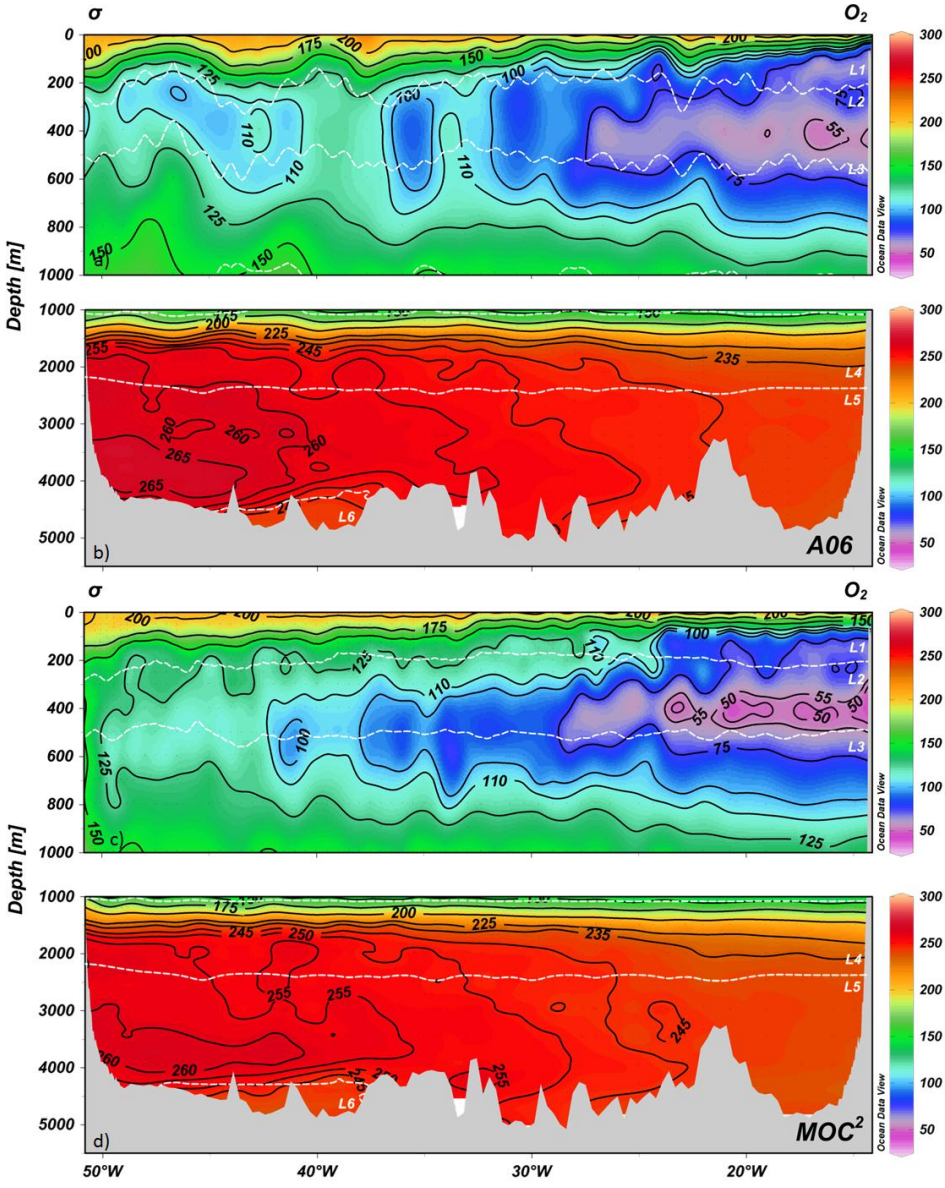


Figure 3.7 $O_2$ distributions along the 7.5°N section for A06 (a, b) and $MOC^2$ (c, d) datasets. a) and c) are a zoom from surface to 1000m, with dashed white contours delimiting SACW, SAMW and AAIW layers (L1, L2 and L3, respectively) at the corresponding $\sigma_0$ isopycnals (26.5, 27.1 and 27.5 $kg \cdot m^{-3}$). b) and d) show the column water from 1000m to bottom depth. The dashed white contours are the upper and lower limits of uNADW (L4) lNADW (L5) and AABW (L6) layers (i.e., $\sigma_0$ = 27.5 $kg \cdot m^{-3}$, $\sigma_2$ = 37 $kg \cdot m^{-3}$ and $\sigma_4$ = 45.9 $kg \cdot m^{-3}$)

Attending to the changes in [$O_2$] over time, the $O_2$ distributions show higher $O_2$ values in 1993 than in 2010 in the uppermost SACW layer (L1). A [$O_2$] increase of ~ 10 µmol $kg^{-1}$ is found in R1 and R2 and of ~16 µmol $kg^{-1}$ in R4 while $\Delta O_2$ is ~ - 30 µmol $kg^{-1}$ in R3. In L2 (SAMW layer), the isoline $O_2$ = 55 µmol $kg^{-1}$ of the $O_2$ minimum tongue only covers R4 in 1993 while it reaches R3 in 2010. Hence, $\Delta O_2$ = - 4.2 µmol $kg^{-1}$ (Table 3.4) in R4L2 because the $O_2$ minimum core is more constrained in the middle of the L2 in 2010 than in 1993. The isoline $O_2$ = 75 µmol $kg^{-1}$ moderately moves from ~ 26.5ºW in A06 to ~ 29ºW in $MOC^2$, while the isoline $O_2$ = 100 µmol $kg^{-1}$ moves a distance of around six degrees westward (from ~ 36ºW in A06 to ~ 42ºW in $MOC^2$). The $O_2$ minimum core became narrower westward in $MOC^2$, which results in mean $O_2$ values of $MOC^2$ higher than those of A06 for R1, R2 and R3 ($\Delta O_2$ > 0 in table 3.4). The lower $O_2$ values in L2 together with their downward movement through the water column are also reflected in the whole L3 area. A slightly drop in the $O_2$ values can be appreciated in figure 3.7c, in which the isoline $O_2$ = 125 µmol $kg^{-1}$ becomes deeper in $MOC^2$ than it is in A06, mainly for R4. This trend is also shown in table 3.4 by the $\Delta O_2$ values, which vary from - 3.2 µmol $kg^{-1}$ in R2 to - 9.3 µmol $kg^{-1}$ in R4. In the deep and bottom waters, the different location of the $O_2$ maximum core is notified in L4 and L5. This difference is translated into a reduction of the extension of the isoline $O_2$ = 245 µmol $kg^{-1}$ in L4, which reaches 21ºW in A06 but only 26ºW in $MOC^2$ (Fig. 3.7). The mean $\Delta O_2$ in the whole L4 area is -13 µmol $kg^{-1}$ (Table 3.4). Regarding L5, the western $O_2$ maximum core of 265 µmol $kg^{-1}$ in A06 reaches

44ºW (R2) but, at this longitude, the $O_2$ maximum core is 5 µmol $kg^{-1}$ lower (isoline $O_2$ = 260 µmol $kg^{-1}$) in $MOC^2$. However, this decrease is not shown when $\Delta O_2$ are calculated, causing positive $\Delta O_2$ values in the whole L5 area (Table 3.4). In L6, the mean $O_2$ concentration in AABW is lower in R1 and R2 of $MOC^2$ than it is in the same regions of A06, with $\Delta O_2$ = - 1.6 µmol $kg^{-1}$ and $\Delta O_2$ = - 1.0 µmol $kg^{-1}$ respectively.

To avoid salinity and temperature effects on the solubility of $O_2$, the AOU is now studied. AOU indicates how much $O_2$ has been consumed, assuming that the $O_2$ concentration was at equilibrium with the atmosphere when the water was at the surface (Stanley et al., 2012). The relationship between AOU and $O_2$ concentration obtained for the A06 and $MOC^2$ all together was $O_2 = - 0.87 \cdot AOU - 0.9$ with a relatively high determination coefficient ($R^2$) of 0.92. This $R^2$ means that ~ 92% of the $O_2$ variability is due to biological consumption, while, the remained 8% is associated to the above related changes in temperature and salinity.

In order to show the association between pH changes and AOU changes, figure 3.8 shows the good correlation between ΔpH with ΔAOU.

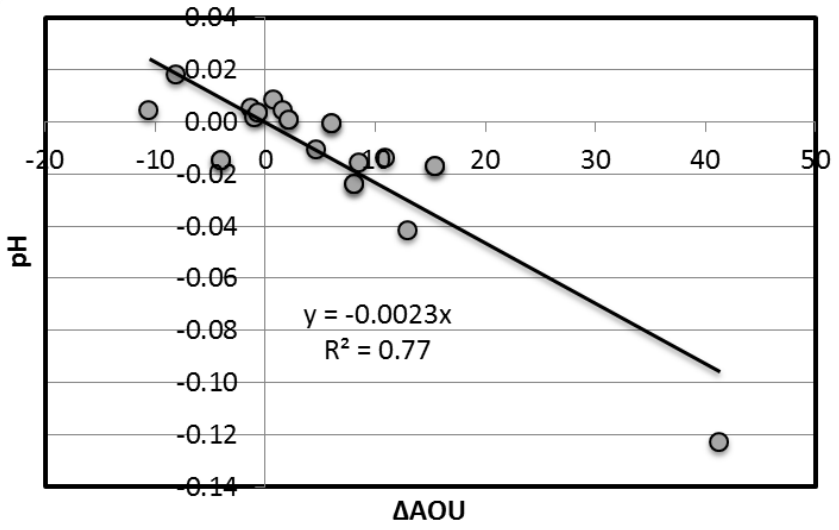


Figure 3.8 Correlation between AOU and pH changes from 1993 to 2010.

In terms of nutrients, it is worth highlighting the relationship observed between $\Delta PO_4^{-3}$ and ΔAOU. The obtained linear fit ($\Delta PO_4^{-3}$= Rp· ΔAOU) presents $R^2 = 0.73$ and a fit-coefficient value of $R_P = -\Delta AOU / \Delta PO_4^{-3} = 113$, which is in agreement with both the theoretical $R_P$ =149 ($-O_2$:C:N:P = 149:106:16:1) estimated by Fraga et al. (1998) and the theoretical $R_P$ =135 ($-O_2$:C:N:P = 135:106:16:1) from Broecker (1974). Figure 3.9 shows the bar chart for ΔAOU and $\Delta PO_4^{-3}$. As it might be expected due to the description of $O_2$ distributions, ΔAOU is positive (there is an increase of AOU in $MOC^2$) in L1, L3, L4 and L6 for the whole section, while L2 and L5 shown lower AOU values in $MOC^2$ than in A06 (Fig. 3.9).

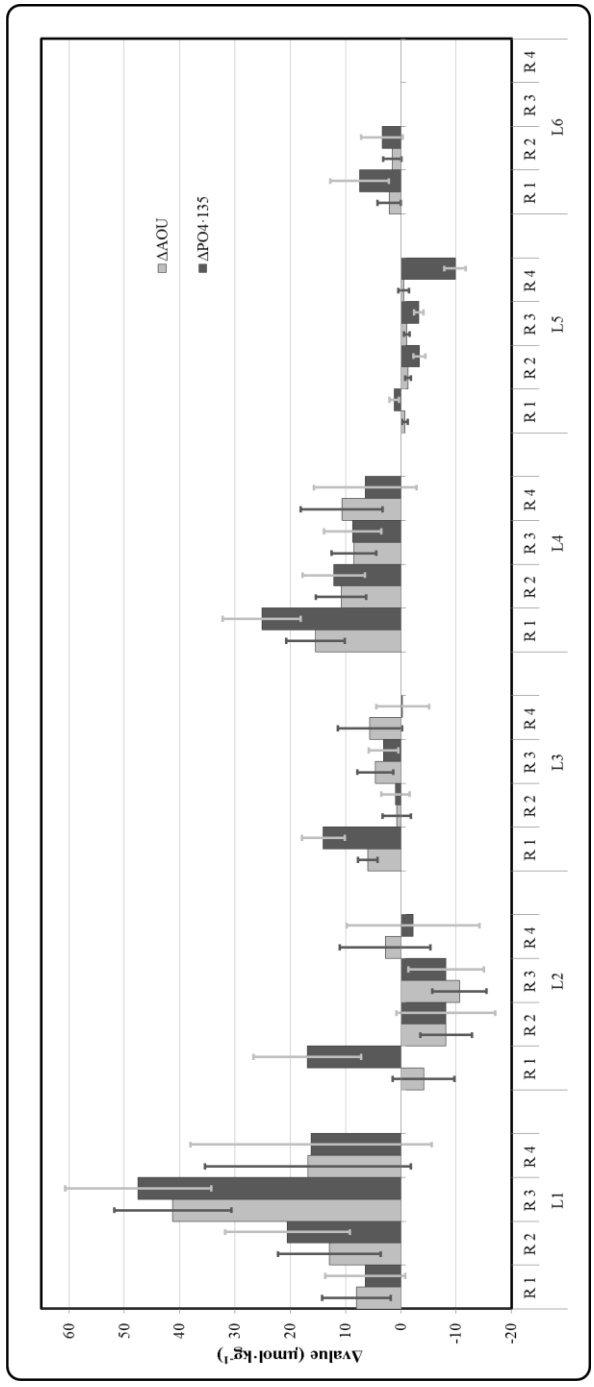


Figure 3.9 ΔAOU (μmol ·kg$^{-1}$) and $\Delta PO_4^{-3}$ (μmol ·kg$^{-1}$) calculated as the difference between properties of MOC$^2$ (2010) minus A06 (1993). $\Delta PO_4^{-3}$ is multiplied by $R_P$ (113) to adjust the different scales.

[$C_{ant}$] was estimated in the Equatorial Atlantic Ocean using TrOCA (Touratier et al., 2007) and $\Delta\varphi C_T^0$ (Vázquez-Rodríguez et al., 2009a), which, despite the fact that both methods have different assumptions, the obtained results are well correlated between them (Fig. 3.10).

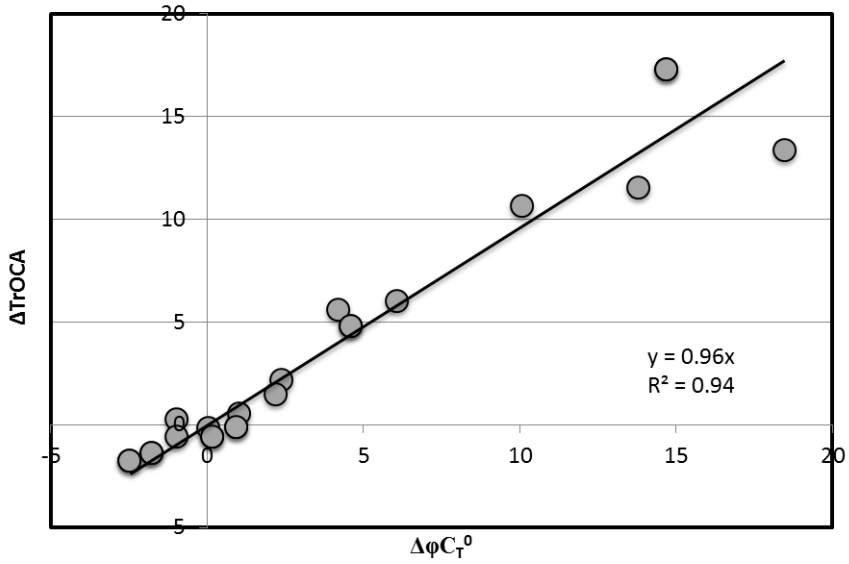


Figure 3.10 Correlation between $\Delta\phi C_T^0$ and ΔTrOCA

The $\Delta\varphi C_T^0$ and ΔTrOCA values are given in table 3.4. Due to their good agreement, the $C_{ant}$ distributions in A06 and MOC$^2$ are only depicted on the base of $\Delta\varphi C_T^0$ (Fig. 3.11). In general terms, there is a clear $C_{ant}$ increasing trend in the whole 7.5ºN section. The 1993-2010 increment in the SACW layer (L1) is ~ 14 µmol·kg$^{-1}$. The most remarkable increment in [$C_{ant}$] occurs in R1L1 where the [$C_{ant}$] was 54±0 µmol·kg$^{-1}$ in 1993 and reached a value of 71±1 µmol·kg$^{-1}$ in 2010. The same behaviour can be observed in the SAMW layer (L2). The downward movement of the $C_{ant}$ isolines shows in 1993,

that L2 gets $C_{ant}$ values varying from 20 to 25 µmol·kg$^{-1}$, while in 2010 the $C_{ant}$ values were in the main range of 25 - 40 µmol·kg$^{-1}$. The most important change occurs in R3L2, with $\Delta C_{ant}$ = 11±1 µmol·kg$^{-1}$ (Table 3.4), which is clearly seen in figure 3.11, where there is a clear difference between the eastern and western basin in L3 (Table 3.4), mostly influenced by the AAIW. While in R1L3 and R2L3, there is not an increment in [$C_{ant}$], even a decrease in R1L3 (Table 3.4), in R3L3 and R4L3 the increment is of ~5 µmol·kg$^{-1}$ in 2010 respect to the values of [$C_{ant}$] in the same areas of A06. The signal of uNADW (R1L4 and R2L4) seems reduced in 2010 because of the disappearing of the $C_{ant}$ isoline of 18 µmol·kg$^{-1}$ (western basin). However, the slight increment of $C_{ant}$ of 2±0 µmol·kg$^{-1}$ in R3L4 is in agreement with the decrease in both pH ($\Delta$pH = -0.015±0.007) and $O_2$ ($\Delta O_2$ = -10.3±4.6 µmol·kg$^{-1}$). Below 3000m, [$C_{ant}$] are inside the methodology limitations and no pattern can be found easily.

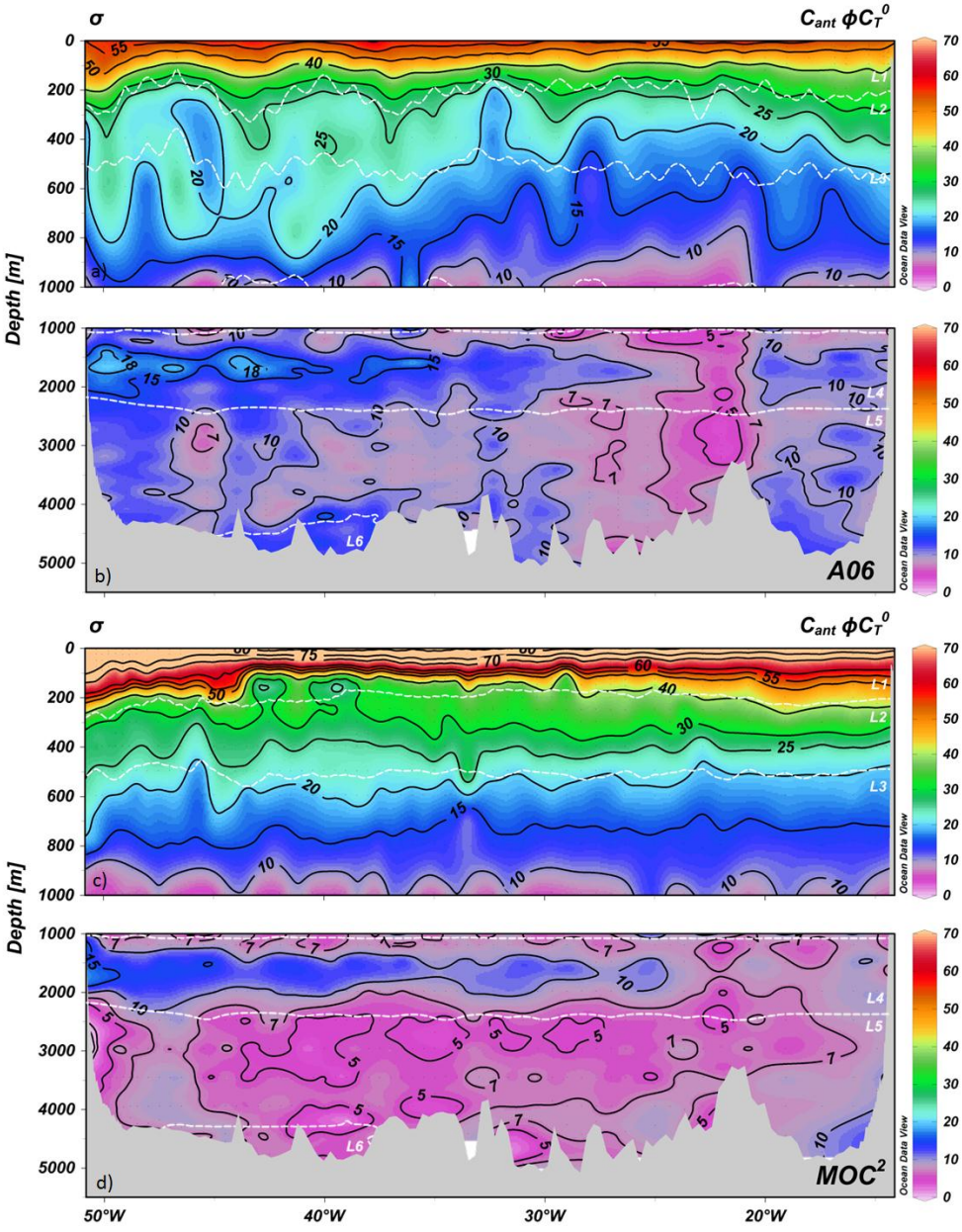


Figure 3.11 $C_{ant}$ distribution along 7.5°N section in A06 (a, b) and $MOC^2$ (c, d). a) and c) are a zoom from surface to 1000m, with dashed white contours delimiting SACW, SAMW and AAIW layers (L1, L2 and L3, respectively) at the corresponding $\sigma_0$ isopycnals (26.5, 27.1 and 27.5 kg·m$^{-3}$). b) and d) show the column water from 1000m to bottom depth. The dashed white contours are the upper and lower limits of uNADW (L4) lNADW (L5) and AABW (L6) layers (i.e., $\sigma_0$ = 27.5 kg·m$^{-3}$, $\sigma_2$ = 37 kg·m$^{-3}$ and $\sigma_4$ = 45.9 kg·m$^{-3}$)

## 3.4 Conclusions

This study pointed out the changes in pH, $O_2$ and $C_{ant}$ from 1993 to 2010 in the Equatorial Atlantic Ocean, paying attention to their relationship with the main water masses of this zone. The most relevant change in terms of pH occurred in the upper layer. In 2010, a high extension of pH minimum associated to the AAIW is shown, covering the whole 7.5ºN section. This pH minimum also became wider in its density range, covering the immediately upper layers and producing a decrease in the easternmost and westernmost regions of the section. The influence of AAIW can be also appreciated by the $O_2$ changes. However, in the immediately upper layer, there is an $O_2$ increase related to SAMW. The highest change in $[O_2]$ between cruises was the one occurred in uNADW layer, being associated with a decrease in pH. The most remarkable $\Delta C_{ant}$ values were found in the upper layers.

# Chapter 4 / *Capítulo 4*

## Trends of the anthropogenic $CO_2$ along 20ºW in the Iberian basin

## *Tendencias de $CO_2$ antropogénico a lo largo del 20ºW en la cuenca Ibérica*

# 4. Trends of the anthropogenic $CO_2$ along 20ºW in the Iberian basin.

## Resumen

El sistema del carbono en las masas de agua de la Cuenca Ibérica (Océano Atlántico Norte) se ha visto afectado en las últimas dos décadas por el aumento de $CO_2$ antropogénico ($C_{ant}$). Durante la campaña CAIBOX y con el fin de estudiar el almacenamiento de $C_{ant}$ en la Cuenca Ibérica, se midieron, entre otras variables, las del sistema del carbónico [pH, carbono inorgánico total ($C_T$) y alcalinidad total ($A_T$)]. Esta campaña, realizada entre Julio y Agosto de 2009 a bordo del "B/O Sarmiento de Gamboa", estaba incluida en el proyecto CAIBEX (Intercambios océano-plataforma en el Gran Ecosistema Marino Canario-Ibérico). Los almacenamientos de $C_{ant}$ fueron estimados usando dos técnicas diferentes de *back-calculation* (método $\varphi C_T^o$ y método TrOCA) y en seis capas de la columna de agua, correspondientes unas a la ubicación aproximada de las masas de agua típicas de la región y otras a las capas de mezcla de las masas de agua. Los almacenamientos de $C_{ant}$ en la columna de agua completa para el año 2009 fueron de 88.1±3.8 y 93.7±3.7 $molC \cdot m^{-2}$ según los métodos $\varphi C_T^o$ y TrOCA, respectivamente. Por otra parte, se estimó también la tasa de almacenamiento de $C_{ant}$ desde 1993 a 2009, teniendo en cuenta los datos de tres campañas adicionales (OACES 1993, CHAOS 1998 y OACES 2003). Las tasas de almacenamiento de $C_{ant}$ obtenidas fueron 1.41±0.25 y 1.67±0.13 $molC \cdot m^{-2} \cdot y^{-1}$ según los métodos $\varphi C_T^o$

y TrOCA, respectivamente. Al comparar estos resultados con los de Ríos et al., (2001) se observó un incremento de la captación de $CO_2$ antropogénico. Entre los períodos 1977-1997 y 1993-2009, la [$C_{ant}$] se incrementó en torno a un 28-49 % en los primeros 2000m de profundidad.

## Abstract

The carbon system in the water masses of the Iberian basin (North Atlantic Ocean) has been affected over the last two decades by the raise of the anthropogenic $CO_2$ ($C_{ant}$). In order to study the storage of $C_{ant}$ in the Iberian basin, the variables of the carbonic system were measured among others [i.e., pH, total inorganic carbon ($C_T$) and total alkalinity ($A_T$)] during the CAIBOX cruise. This cruise, conducted between July and August 2009 on board "R/V Sarmiento de Gamboa", was included on CAIBEX project (Shelf–ocean exchanges in the Canary–Iberian Large Marine Ecosystem). The storages of $C_{ant}$ were estimated using two different back-calculation techniques (i.e., $\varphi C_T^o$ method and TrOCA method) and for six layers of the water column corresponding to the approximate locations of the characteristic water masses of the region and layers of water masses mixing. For the whole water column and for the year 2009 the storages of $C_{ant}$ were of 88.1±3.8 and 93.7±3.7 $molC \cdot m^{-2}$ from $\varphi C_T^o$ and TrOCA methods, respectively. Moreover, the $C_{ant}$ storage rate from 1993 to 2009 was also estimated considering data from three additional cruises (OACES 1993, CHAOS 1998 and OACES 2003). The determined $C_{ant}$ storage rates were 1.41±0.25 and 1.67±0.13 $molC \cdot m^{-2} \cdot y^{-1}$ for $\varphi C_T^o$ and TrOCA methods, respectively. The increase of anthropogenic $CO_2$ uptake by the ocean can be seen when comparing these results with Ríos et al., (2001). Between the periods 1977-1997 and 1993-2009, the $C_{ant}$ concentration increased around 28-49 % in the first 2000m.

## 4.1 Introduction

Since the 18th century, the beginning of the industrial period, humankind has emitted large quantities of $CO_2$ into the atmosphere (Le Quéré et al., 2009) rising the global average atmospheric $CO_2$ from 280 ppm at the start of the industrial revolution to 381 ppm in 2006 (Canadell et al., 2007). Nevertheless, less than a half of these emissions remain in the atmosphere and so, the anthropogenic $CO_2$ must have been taken up by the ocean or by the land biosphere (Sabine et al., 2004). Ongoing efforts are being taken to quantify the magnitude of these two sinks with high enough accuracy. Results from state-of-the-art models constrained the mean $CO_2$ uptake rates of land and ocean to 2.6±0.7 and 2.2±0.4 Pg C $y^{-1}$, respectively for the period 1990-2000. For the 2000-2008 period, the models estimated that the $CO_2$ uptake rates were 2.7±1.0 and 2.3±0.5 Pg C $y^{-1}$, for land and ocean respectively (Le Quéré et al., 2009). These results show the variability of these $CO_2$ sinks and the decreasing trend in the ocean $CO_2$ uptake fraction. In fact, in spite of the increasing of the total amount of emitted $CO_2$, the oceanic $CO_2$ uptake fraction decreased from 27% in the period from 1990-2000 to 25% in 2000-2008 period. The main causes for this decrease could be a weak or limited transport rate of $CO_2$ from the surface to the deep ocean and also the nonlinearity in carbon chemistry that reduces the $CO_2$ capture capacity of water when its $CO_2$ concentration increases (Bindoff et al., 2007). As the World's Ocean reservoir accounts for approximately 90% of the natural carbon (Sabine and Tanhua, 2010) a better knowledge of the

variability in the rate of uptake and size of the ocean $CO_2$ sink is needed to predict global climate effects.

The attention of the marine scientific community is more concretely focussed on estimations of the anthropogenic component ($C_{ant}$) of the total inorganic carbon ($C_T$). Despite all new techniques and technological progress, discerning between natural $CO_2$ and $C_{ant}$ is quite complex. In the end of XX century, back-calculation techniques have been developed to calculate $C_{ant}$ accumulation in the oceans (Brewer, 1978). Back-calculation techniques were born with the aim of indirectly estimate $C_{ant}$ in the oceans by subtracting to $C_T$ the effects of remineralisation of organic matter (ROM), dissolution of calcium carbonate (Chen and Millero, 1979) and $CO_2$ air-sea disequilibrium (Gruber et al., 1996). From them on, several kind of these methods have been applied to the global ocean or partial regions of it: $\Delta C^*$ (Gruber et al., 1996), $C^o_{T_{IPSL}}$ (Lo Monaco et al., 2005), TrOCA (Körtzinger et al., 1998; Touratier et al., 2007) and $\varphi C^o_T$ (Pérez et al., 2008; Vázquez-Rodríguez et al., 2009a) (hereinafter VR´09). Furthermore, other methods such as pCFC-age method ["shortcut method", (Thomas and Ittekkot, 2001)] and Transient Time Distribution (TTD) method (Waugh et al., 2006) emerged based on using CFCs as tracers to estimate the age for the water masses.

In this work, the Iberian basin, a specific region of the North Atlantic basin, was studied in terms of $C_{ant}$. The importance of the North Atlantic basin in terms of $C_{ant}$ storage stems from the fact that, despite covering only 15% of the global ocean area, the North

Atlantic basin stores 23% of the total oceanic $C_{ant}$ (Sabine et al., 2004). The region of study is located in front of the Iberian peninsula and enclosed from 45ºN of latitude to the Canary Islands (25ºN) and between 20ºW and 8ºW of longitude (Fig. 4.1).

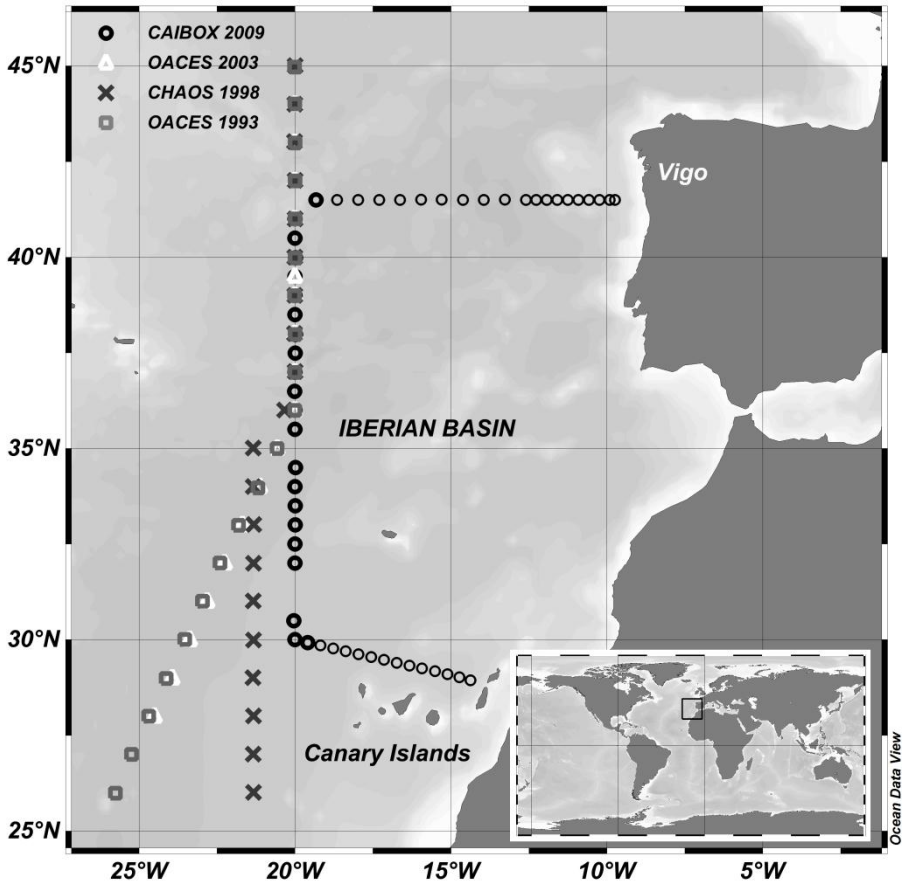


**Figure 4.1Iberian basin region and location of the cruises included in the study: OACES 1993, CHAOS 1998, OACES 2003 and CAIBOX 2009. In CAIBOX 2009 only the 20ºW section (empty circles in bold) was taken for the study**

This zone is inside the North Atlantic gyre, which is known as "the inter-gyre zone" (Pollard et al., 1996) enclosed between the North Atlantic Current (45-53ºN) and the Azores Current (34-35ºN) (Péliz

et al., 2005). The vertical thermohaline structure of this region (Carracedo et al., 2012) is clearly dominated in the upper layer by the Madeira Mode Water (MMW) (Álvarez et al., 2005), the East North Atlantic Central Water (ENACW) with differentiated branches of subpolar ($ENACW_P$) and subtropical ($ENACW_T$) origin (Álvarez et al., 2005; Castro et al., 1998; Ríos et al., 1992) and a little percentage of Antarctic Water (AA) (Álvarez et al., 2005; Ríos et al., 1992). Between intermediate and deep water masses it is important the presence of the Mediterranean Water (MW) (Fraga et al., 1982), which is the outflow from the Mediterranean Sea and the most saline water of the water column located at approximately 1000dbar. Deeper layers of the water column are dominated by the Labrador Sea Water (LSW) (Castro et al., 1998) while the North East Atlantic Deep Water (NEADW), divided in its upper ($NEADW_u$) and lower ($NEADW_l$) branches, and the Iceland Scotland Overflow Water (ISOW) are spanned in the bottom layers (Álvarez et al.,, 2005). The main properties of all these water masses are shown in Table 4.1.

**Table 4.1 Characteristic properties (Θ, salinity, nutrients, $A_T$, $C_T$ and $O_2$) of the main water masses present in the Iberian basin region: Antartic Water (AA), Subpolar East North Atlantic Central Water ($ENACW_P$), Subtropical East North Atlantic Central Water ($ENACW_T$), Iceland Scotland Overflow Water (ISOW), Labrador Sea Water (LSW), Madeira Mode Water (MMW), Mediterranean Water (MW), Lower North East Atlantic Deep Water ($NEADW_l$) and Upper North East Atlantic Deep Water ($NEADW_u$).**

| Water masses | Θ, °C | Salinity, psu | $SiO_4$, mmol | $NO_3$, mmol | $PO_4$, mmol | $A_T$, mmol | $O_2$, mmol | $C_T$, mmol |
|---|---|---|---|---|---|---|---|---|
| $ENACW_T$ | 15.3±0.4 | 36.1±0.02 | 2.24±1.7 | 2.12±1.2 | 0.15±0.05 | 2363±10 | 244±3 | 2096±6 |
| $ENACW_P$ | 8.3±0.3 | 35.23±0.01 | 10.33±0.6 | 9.58±1.3 | 0.73±0.08 | 2320±7 | 285±2 | 2112±12 |
| MW | 11.74±0.1 | 36.5±0.01 | 8.62±0.8 | 5.16±0.8 | 0.31±0.1 | 2411±1 | 262±5 | 2151±4 |
| LSW | 3.4±0.2 | 34.89±0.12 | 9.85±2.5 | 12.03±0.7 | 0.91±0.02 | 2301±7 | 320±2 | 2118±19 |
| ISOW | 1.93±0.08 | 34.96±0.02 | 11.12±5 | 9.26±2.7 | 0.85±0.13 | 2290±3 | 331±3 | 2099±4 |
| $NEADW_u$ | 2.4±0.003 | 34.93±0.003 | 35±6 | 11.95±0.2 | 0.9±0.07 | 2359±2 | 328±2 | 2139±22 |
| $NEADW_l$ | 1.92±0.003 | 34.88±0.002 | 49.85±5 | 12.94±0.4 | 1.02±0.03 | 2360±2 | 332±3 | 2147±10 |
| AA | 7.5±0.1 | 35±0.02 | 24.9±0.8 | 12.4±3.3 | 0.96±0.3 | 2320±1 | 290±2 | 2092±4 |
| MMW | 20±0.5 | 37±0.04 | 0.39±0.3 | 0.23±0.01 | 0.01±0.06 | 2418±13 | 223±9 | 2103±3 |

Taking into account the thermohaline distribution in the Iberian basin and $A_T$, $C_T$, pH and nutrients measurements, estimations of $C_{ant}$ concentrations and $C_{ant}$ storage rates have been determined in the present work. Data collected during CAIBOX cruise in 2009 were used to estimate concentrations of $C_{ant}$. The estimated $C_{ant}$ was obtained through two different back-calculation techniques, $\varphi C_T^o$ and TrOCA, for 6 layers of the water column. In order to obtain the $C_{ant}$ storage rates, data from three earlier cruises (OACES 1993, CHAOS 1998, OACES 2003) were added closing almost two decadal periods. The $C_{ant}$ storages were compared between cruises and with the results that Pérez et al., (2010a) obtained for the Azores region. The estimated $C_{ant}$ storage rates were compared to the results of Ríos et al., (2001) obtaining considerable increments of the rates for the two back-calculating techniques applied. The higher increase of the oceanic $C_{ant}$ storage rate found for the last

decade in the Iberian basin can be a reflection of the corresponding increment reported for the atmosphere.

## 4.2 Data and methodology

The CAIBOX cruise was integrated in CAIBEX project ("Shelf-ocean Exchanges in the Canary–Iberian Large Marine Ecosystem") and was spanned from 25th July to 14th August in 2009 on board of R/V Sarmiento de Gamboa. This cruise was constituted by one latitudinal section in front of Vigo coast (41.5ºN), one transversal section near the Canary Islands (from 20ºW 30ºN to 13ºW 28.6ºN), and one longitudinal section along 20ºW (Fig.4.1). The longitudinal section was chosen for this study. A General Oceanic CTD with a 24 Niskin bottles (12 L) rosette was thrown in twenty four stations along the 20ºW section. In each station 24 depth levels were selected depending on the bathymetry which varied from 3000m to more than 5000m. The distance between depth levels was approximately constant in the first 1000m of the water column. Temperature, salinity, oxygen ($O_2$) and pH were measured in each depth level, whereas nutrients and the rest of carbonic variables, i.e., total alkalinity ($A_T$), total inorganic carbon ($C_T$) were taken at specific depths according to the thermohaline distribution.

The nutrients were determined by segmented flow analysis with a Technicon II Autoanalyzer (Álvarez-Salgado et al., 1992; Mouriño and Fraga, 1985). The accuracy of nitrate and phosphate was ±0.1

and ±0.01 $\mu mol \cdot kg^{-1}$, respectively. The $O_2$ samples were analysed by the Winkler method (Winkler L. W., 1888).

Seawater pH measurements were made using the spectrophotometric method described in Clayton & Byrne (1993) adding m-cresol purple as indicator. Absorbance measurements were performed with a Shimadzu UV 2401. During all sessions the temperature was controlled by a thermostatic bath at 25ºC. The precision of the measurements with this method is estimated to be less than ±0.005 pH units (Dickson et al., 2007a) and the values of pH are given in total scale.

Measurements of $A_T$ were done by a one endpoint method using an automatic potentiometric titrator (Titrando 801 Metrohm) with a combined glass electrode (Mintrop et al., 2000) obtaining a precision of less than ± 2 $\mu mol \cdot kg^{-1}$ (Dickson et al., 2007a). Potentiometric titration was carried out in an open flask (~250 $cm^3$) with HCl (0.1 M) and using two pH endpoints very close one to another, i.e., 4.45 and 4.42 (Pérez and Fraga, 1987). In order to estimate the accuracy of the $A_T$ method, alkalinity measurements of certified reference material (CRM) of $CO_2$ from batch 84 provided by Dr. Andrew Dickson have been analysed.

The $C_T$ was determined using a SOMMA (single-operator multiparameter metabolic analyzers) system connected to a model CM101_093 coulometer (UIC.INC, Joliet, ILLINOIS, USA) (Johnson et al., 1998). The $CO_2$ is carried in this equipment by a free-$CO_2$ gas ($N_2$) into a coulometric cell, where it is quantitatively

absorbed after reacting with ethanolamine (Johnson et al., 1993). In every $C_T$-analysis session, calibrations were performed with Certified Reference Material (CRM) of $CO_2$, supplied by Andrew Dickson (Scripps Institution of Oceanography, University of California), to check for the accuracy of the measurements. The precision of this method is ±4 µmol·kg$^{-1}$ (Dickson et al., 2007a). In those levels of the water column where $C_T$ data were not measured it was calculated from $A_T$ and pH using the inorganic carbon system thermodynamic equations and the acid constants from Mehrbach et al., (1973) fitted by Dickson & Millero (1987). The goodness of this approximation can be seen in the Figure 4.2, where calculated $C_T$ fits well with measured $C_T$ ($R^2$=0.99).

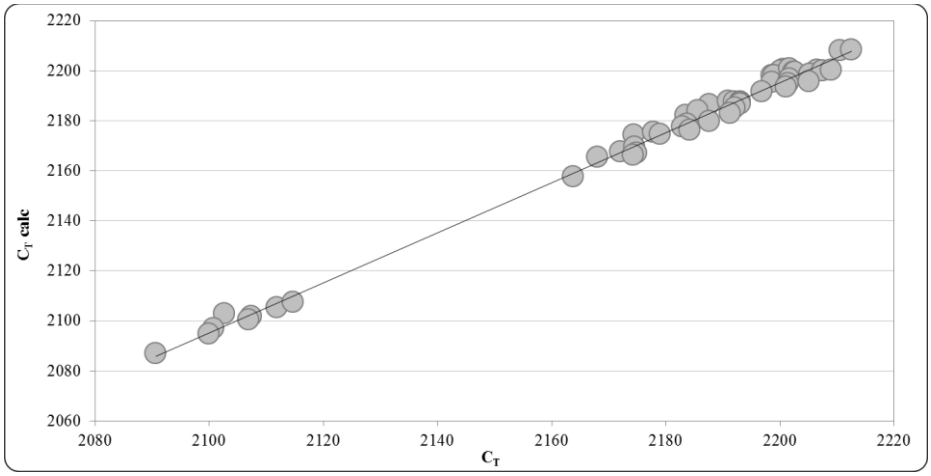


**Figure 4.2 Correlation between calculated and measured $C_T$. Units in µmol·kg$^{-1}$. The linear equation of the fit is: [$C_T$ (calc)-2000] = (0.9997 ± 0.0109)·[$C_T$ (meas)-2004.6 ± 1.9] with a $R^2$=0.994 (n=50).**

Apart from CAIBOX cruise, other three cruises have been taken into account: OACES 1993, CHAOS 1998 and OACES 2003 (Fig. 4.1, Table 4.2).

**Table 4.2 Summary of the characteristics of the cruises taken into account for the study. The year, the principal investigator (P.I.) and the number of stations are shown for each cruise .**

| *CRUISE INFORMATION* | | | | | |
|---|---|---|---|---|---|
| *Cruise* | *Section* | ***Year*** | ***P.I.*** | ***Expocode*** | ***Stations*** |
| OACES 1993 | OACES/$CO_2$-93 | 1993 | R. Wanninkhof | OACES93_A16N | 83 |
| CHAOS 1998 | WOCE A16N/AR21 | 1998 | Smythe-Wright | 74DI19980423 | 137 |
| OACES 2003 | CLIVAR A16N | 2003 | J. Bullister, N. Gruber | 3RO20030604 | 150 |
| CAIBOX 2009 | CAIBOX | 2009 | E. D. Barton | CAIBOX09 | 73 |

Stations from each one of them were selected in order to cover the area between 29ºN to 42ºN of latitude and 18ºW to 24ºW of longitude, near to the 20ºW longitudinal section of CAIBOX (Fig.4.1). The same variables as in CAIBOX cruise were taken from the three additional cruises, which can be downloaded from the Carbon in Atlantic Ocean CARINA website (CARINA). With these additional data, the combined dataset (20ºW CAIBOX cruise included) extends over 16 years (1993-2009).

Among all back-calculating techniques, two recent ones, TrOCA and $\varphi C_T^o$, have been selected in order to obtain $C_{ant}$ estimations. Both of them are based on removing from $C_T$ the carbon contributions after the time of water mass formation due to oxidation/reduction processes of organic matter and processes of dissolution of $CaCO_3$. In Section II. Data and methodology 3. *Methodology to estimate anthropogenic $CO_2$* both methods are widely described.

## 4.3 Results

$C_{ant}$ concentration (hereinafter [$C_{ant}$]) was estimated from $\varphi C_T^o$ and TrOCA methods for each of the cruises previously described, i.e., OACES 1993, CHAOS 1998, OACES 2003 and section 20ºW from CAIBOX 2009, and the distributions of the variable obtained with each method are shown in Figure 4.3.

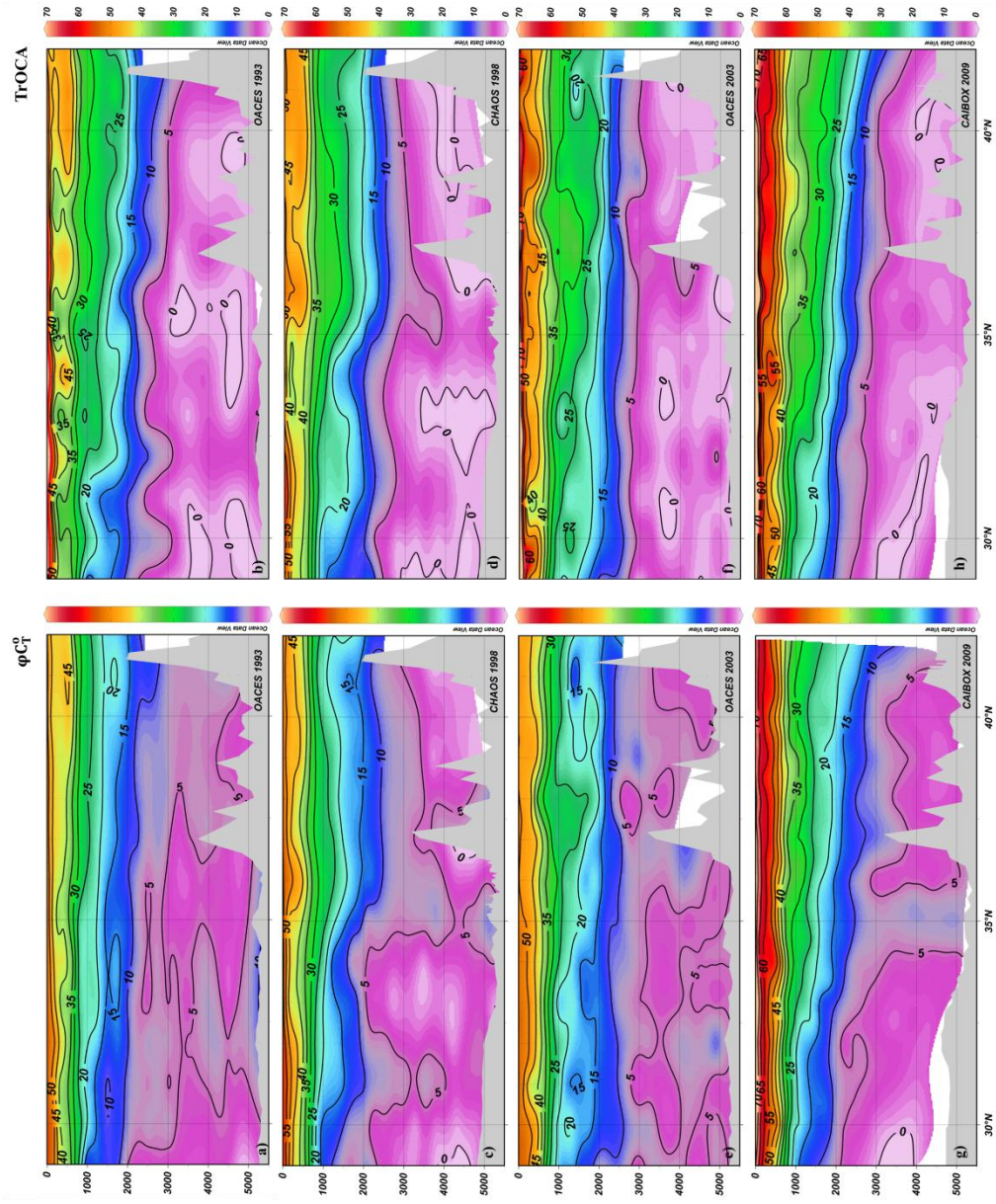


Figure 4.3 Vertical profiles of $C_{ant}$ estimated from $\varphi C_T^0$ and TrOCA methods in the Iberian basin.

Negative values of [$C_{ant}$] using the TrOCA method are showed as zeros in order to better visualize the differences. All plots show very similar vertical gradients of [$C_{ant}$] independently of the methodology used in the estimations, with the highest quantities in the warm surface waters and low values near the bottom. The range of variation depends on the cruise (year) and slightly on the method and gradually increases from 0-50 µmol·kg$^{-1}$ in OACES 1993 (Fig. 4.3a , b) to 0-70 µmol·kg$^{-1}$ in CAIBOX 2009 (Fig. 4.3g, h). In general, $\varphi C_T^o$ method estimates [$C_{ant}$] slightly higher than those from TrOCA method on deep waters (>3000dbar) for all the cruises. On the contrary, [$C_{ant}$] estimated using TrOCA method are higher near the surface (<500dbar). In intermediate layers both method estimate very similar [$C_{ant}$] values. Actually, both methods show high determination coefficients on each cruise, as it can be seen in Figure 4.4.

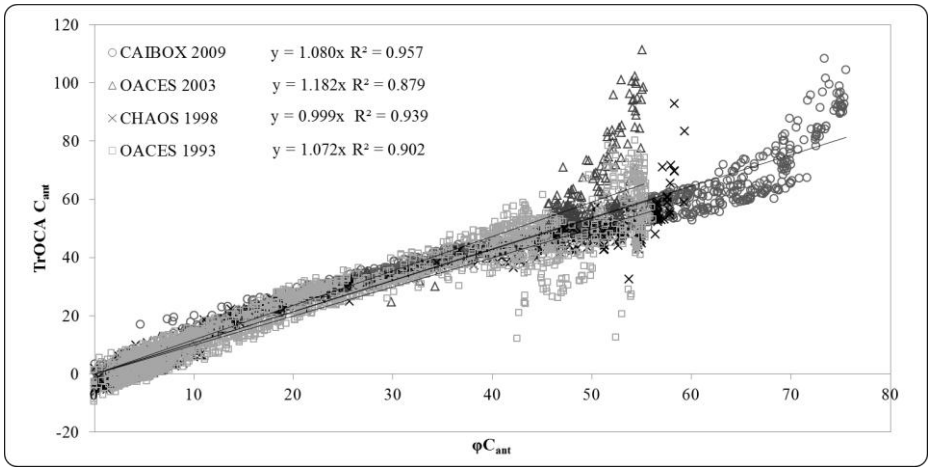


**Figure 4.4 Correlation between estimated data calculated by TrOCA and $\varphi C_T^0$ method for each cruise. Fit equations and determination coefficients for each of them are also given.**

In general, [$C_{ant}$] is importantly related to the characteristics of the water masses present in the water column. The 20ºW section from CAIBOX cruise was selected in order to study the distribution of the variables in the Iberian basin (Table 4.2, Fig. 4.5). AOU, $A_T$ and $C_T$ distributions along the selected section are shown in Figure 4.5.

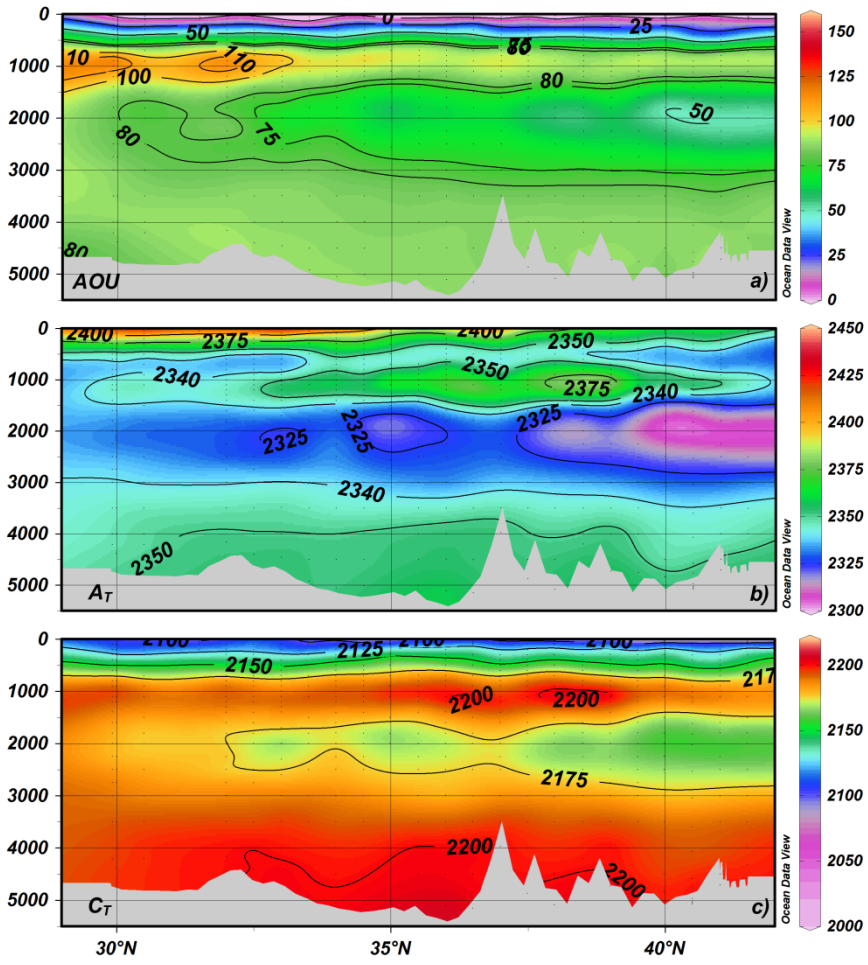


Figure 4.5 20ºW vertical distributions of: a) AOU (µmol·kg$^{-1}$, b) $A_T$ (µmol·kg$^{-1}$) and c) $C_T$ (µmol·kg$^{-1}$).

The vertical thermohaline structure is clearly dominated in the upper layers (<500dbar) by the NACW with values of AOU ranging between 20-60 µmol·kg$^{-1}$ (Fig. 4.5a). At ~1000dbar in the south part of the section, a little percentage of AA is identified by the AOU maximum (~110 µmol·kg$^{-1}$, Fig.4.5a). At the same depth but in the centre of the section, MW emphasizes its presence

performing an $A_T$ maximum (2375 µmol·kg$^{-1}$, Fig.4.5b). In the north part of the section, LSW shows its intense influence through AOU, $A_T$ and $C_T$ minima (Fig. 4.5a, b, c). The distribution of $C_T$ (Fig. 4.5c) reveals the effect of biogeochemistry over the values of this variable. In the upper layers (<500dbar) the lowest $C_T$ values (Fig. 4.5c) are due to the high quantities of $CO_2$ taken up by the photosynthesis of primary producers. In deeper layers (>3000dbar) the high values of $C_T$ (Fig. 4.5c) are due to the processes of ROM and $CaCO_3$ dissolution, which is also represented by the relatively high values of $A_T$ (Fig. 4.5b). The ROM is also detected by the steady and high values of AOU found at these depths (Fig. 4.5a).

In order to relate the values of [$C_{ant}$] to the thermohaline distribution of the region, the water column was divided into six layers distinguished in base of density ranges. These density ranges were selected according to a Θ-S diagram performed with data from all the cruises (Fig. 4.6).

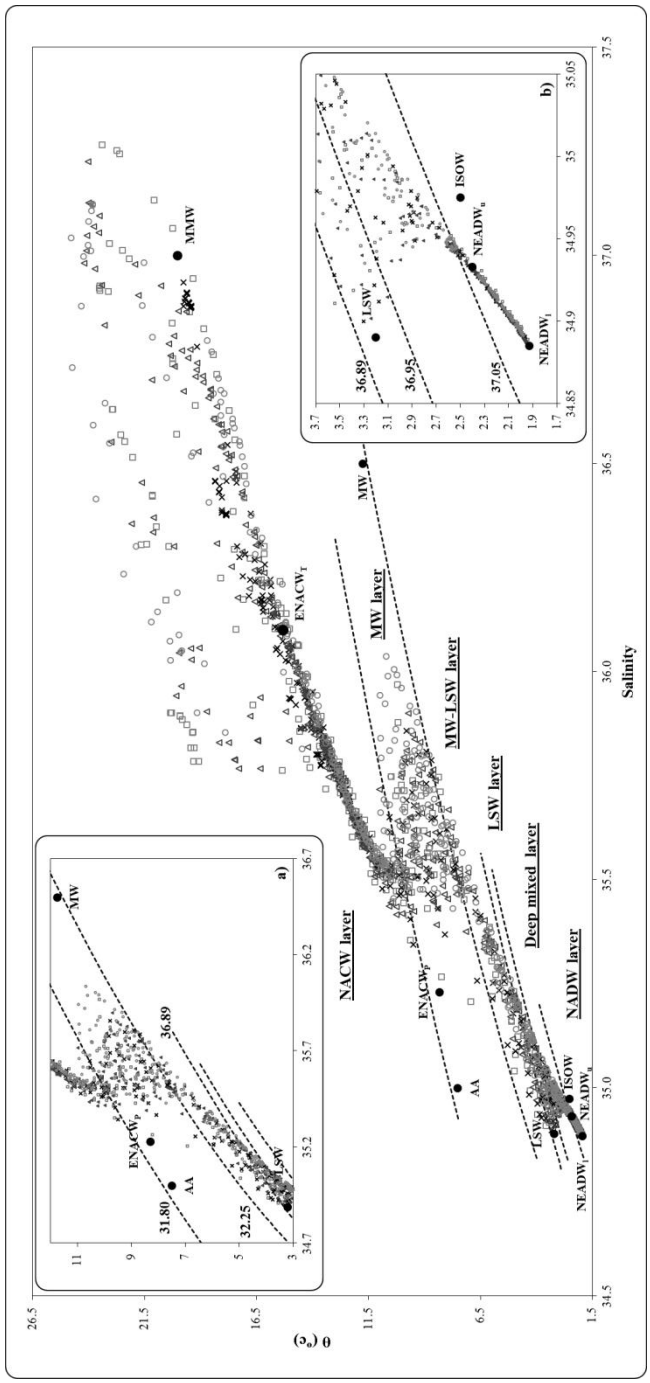


Figure 4.6 Θ-S diagram with the locations of the principal water masses of the region (black dots). Circles correspond to CAIBOX 2009 cruise data, triangles correspond to OACES 2003 data, and crosses and squares correspond to CHAOS 1998 and OACES 1993 data, respectively. The six layers in which the water column was divided are also shown: a) upper layers: NACW, MW and MW-LSW layers and b) deep layers: LSW, Deep Mixed and NADW layers. The isopycnals that limit each one of the layers are also represented (dashed lines).

The uppermost layers (NACW, MW, Fig. 4.6a) were delimited using 1000dbar as the pressure level of reference, while 2000dbar was the level of reference for deeper layers (Fig. 4.6b). NACW layer involves all data from surface to the isopycnal of 31.8 $kg \cdot m^{-3}$. MW layer contains all data from 31.8 to 32.25 $kg \cdot m^{-3}$ density isolines. Mixed MW-LSW layer includes all data between the 32.25 $kg \cdot m^{-3}$ isopycnal calculated at 1000dbar as level of reference and the 36.89 $kg \cdot m^{-3}$ isopycnal calculated at 2000dbar as level of reference. In deep waters, the LSW layer and the Deep Mixed layer can be distinguished enclosing all data between 36.89 and 36.95 $kg \cdot m^{-3}$, and 36.95 to 37.05 $kg \cdot m^{-3}$ isopycnals, respectively. At last, the upper and lower NEADW and the ISOW were included in the NADW (North Atlantic Deep Water) layer, which encloses data from the 37.05 $kg \cdot m^{-3}$ isopycnal to the bottom.

Once the layers have been defined, $[C_{ant}]$ values are obtained using $\varphi C_T^o$ and TrOCA methods and separately for each cruise (year). Mean $[C_{ant}]$ values are obtained for each layer through a vertical and horizontal integration (Pérez et al., 2010a). The thickness of each layer was computed as the average vertical distance between layers, weighted by the separation between stations. The vertical integration was done between the upper and lower limits of the layers, while the limits in the horizontal integration were consequent with each cruise (Fig. 4.1). In Table 4.3, the average values of thickness and $[C_{ant}]$ estimated from $\varphi C_T^o$ ($[C_{ant}]_\varphi$) and TrOCA ($[C_{ant}]_{TrOCA}$) methods are shown for each layer and for each cruise (denoted by the year in which each one was performed). The integrated-average values of salinity, Θ, and AOU are also shown.

**Table 4.3** Mean values (± standar error of the estimation) of thickness, salinity, potential temperature ($\Theta$), apparent oxygen utilization (AOU) and [$C_{ant}$] estimated from $\varphi C_T^o$ and TrOCA methods in each one of the six defined layers. $C_{ant}$ storages for each year are also shown.

| Year | Thickness (m) | Salinity (psu) | $\Theta$ (ºC) | AOU ($\mu mol \cdot kg^{-1}$) | $[C_{ant}]_\varphi$ ($\mu mol \cdot kg^{-1}$) | $[C_{ant}]_{TrOCA}$ ($\mu mol \cdot kg^{-1}$) |
|---|---|---|---|---|---|---|
| | | | NACW | | | |
| 1993 | 753 ± 11 | 35.947 ± 0.001 | 13.979 ± 0.002 | 45.7 ± 0.1 | 41.0 ± 0.6 | 42.0 ± 0.6 |
| 1998 | 729 ± 21 | 35.876 ± 0.001 | 13.467 ± 0.002 | 44.9 ± 0.1 | 42.9 ± 0.6 | 43.9 ± 0.6 |
| 2003 | 736 ± 25 | 35.926 ± 0.001 | 14.341 ± 0.002 | 42.1 ± 0.1 | 45.0 ± 0.5 | 50.7 ± 0.5 |
| 2009 | 722 ± 11 | 35.878 ± 0.001 | 13.652 ± 0.002 | 42.9 ± 0.1 | 55.1 ± 0.6 | 56.6 ± 0.6 |
| | | | MW | | | |
| 1993 | 481 ± 31 | 35.492 ± 0.001 | 8.443 ± 0.004 | 104.6 ± 0.2 | 18.8 ± 1.1 | 22.2 ± 0.9 |
| 1998 | 545 ± 39 | 35.556 ± 0.001 | 8.857 ± 0.004 | 100.4 ± 0.2 | 21.9 ± 1.0 | 25.8 ± 1.0 |
| 2003 | 473 ± 32 | 35.565 ± 0.001 | 8.913 ± 0.003 | 99.2 ± 0.1 | 23.9 ± 0.7 | 28.2 ± 0.7 |
| 2009 | 509 ± 15 | 35.653 ± 0.001 | 9.148 ± 0.003 | 94.2 ± 0.1 | 28.9 ± 0.6 | 33.8 ± 0.8 |
| | | | MW-LSW | | | |
| 1993 | 446 ± 48 | 35.305 ± 0.001 | 5.891 ± 0.004 | 76.0 ± 0.2 | 15.9 ± 1.0 | 21.6 ± 0.9 |
| 1998 | 420 ± 47 | 35.273 ± 0.001 | 5.689 ± 0.004 | 72.5 ± 0.2 | 16.0 ± 1.3 | 22.3 ± 1.4 |
| 2003 | 462 ± 39 | 35.336 ± 0.001 | 6.059 ± 0.004 | 76.7 ± 0.2 | 18.7 ± 1.0 | 25.1 ± 0.9 |
| 2009 | 411 ± 22 | 35.333 ± 0.001 | 5.953 ± 0.004 | 73.6 ± 0.2 | 20.7 ± 1.0 | 27.7 ± 0.9 |
| | | | LSW | | | |
| 1993 | 437 ± 54 | 35.112 ± 0.001 | 4.247 ± 0.005 | 71.2 ± 0.2 | 10.5 ± 1.2 | 13.6 ± 1.2 |
| 1998 | 339 ± 47 | 35.061 ± 0.001 | 4.004 ± 0.006 | 64.0 ± 0.3 | 12.1 ± 1.2 | 16.5 ± 1.3 |
| 2003 | 473 ± 41 | 35.100 ± 0.002 | 4.218 ± 0.007 | 67.5 ± 0.4 | 16.2 ± 1.8 | 20.4 ± 1.5 |
| 2009 | 406 ± 33 | 35.074 ± 0.001 | 4.088 ± 0.005 | 61.8 ± 0.2 | 17.5 ± 1.2 | 22.8 ± 1.2 |
| | | | deep mixed | | | |
| 1993 | 673 ± 78 | 34.990 ± 0.001 | 3.104 ± 0.004 | 69.9 ± 0.2 | 7.3 ± 1.0 | 8.2 ± 1.0 |
| 1998 | 883 ± 63 | 34.993 ± 0.001 | 3.161 ± 0.004 | 71.1 ± 0.2 | 7.3 ± 0.9 | 9.0 ± 0.8 |
| 2003 | 833 ± 78 | 34.982 ± 0.001 | 3.038 ± 0.004 | 70.2 ± 0.2 | 9.4 ± 1.0 | 10.1 ± 1.1 |
| 2009 | 880 ± 55 | 34.979 ± 0.001 | 2.990 ± 0.004 | 71.4 ± 0.2 | 9.4 ± 0.9 | 10.6 ± 0.9 |
| | | | NADW | | | |
| 1993 | 1 710 ± 151 | 34.916 ± 0.001 | 2.216 ± 0.003 | 84.7 ± 0.2 | 4.8 ± 0.8 | 1.4 ± 0.8 |
| 1998 | 1 584 ± 142 | 34.911 ± 0.001 | 2.184 ± 0.003 | 85.0 ± 0.2 | 3.6 ± 0.8 | 1.6 ± 0.8 |
| 2003 | 1 523 ± 200 | 34.908 ± 0.001 | 2.160 ± 0.003 | 84.8 ± 0.1 | 5.1 ± 0.8 | 1.4 ± 0.9 |
| 2009 | 1 572 ± 85 | 34.917 ± 0.001 | 2.219 ± 0.003 | 84.9 ± 0.1 | 4.5 ± 0.7 | 1.7 ± 0.7 |
| | | | **$C_{ant}$ storage (molC $m^{-2}$)** | | | |
| 1993 | | | | | 66.9 ± 4.1 | 67.9 ± 4.0 |
| 1998 | | | | | 68.3 ± 4.1 | 73.8 ± 4.2 |
| 2003 | | | | | 78.9 ± 4.2 | 85.0 ± 4.1 |
| 2009 | | | | | 88.1 ± 3.8 | 93.7 ± 3.7 |

In general terms, the $[C_{ant}]$ tends to increase in all the layers and decreases downward in the water column, as was previously shown in Figure 4.3. The highest $[C_{ant}]_{\varphi}$ and $[C_{ant}]_{TrOCA}$ were found in the NACW layer for 2009 with values of 55.1±0.6 and 56.8±0.6µmol·kg$^{-1}$, respectively (Table 4.3). It must be emphasized the relatively high values of $[C_{ant}]_{\varphi}$ and $[C_{ant}]_{TrOCA}$ in the MW layer whose ranges vary from 18.8±0.9 to 28.9±0.7µmol·kg$^{-1}$ and 22.2±1.0 to 33.8±0.8 µmol·kg$^{-1}$, respectively (Table 3). $[C_{ant}]_{\varphi}$ and $[C_{ant}]_{TrOCA}$ are very similar for all layers and years being $[C_{ant}]_{TrOCA}$ slightly higher than $[C_{ant}]_{\varphi}$ in almost all the cases except for the NADW layer. The differences between $[C_{ant}]_{\varphi}$ and $[C_{ant}]_{TrOCA}$ range from 6.4 µmol·kg$^{-1}$ in the MW-LSW layer to 1.2 µmol·kg$^{-1}$ in the Deep Mixed layer (Table 4.3). In the NADW layer, $[C_{ant}]_{\varphi}$ shows values of around 3.0 µmol·kg$^{-1}$ higher than $[C_{ant}]_{TrOCA}$ (Table 4.3), being the average values of $[C_{ant}]_{\varphi}$ and $[C_{ant}]_{TrOCA}$ in this layer of 4.5±0.7 µmol·kg$^{-1}$ and 1.5±0.2 µmol·kg$^{-1}$, respectively. It is also noticeable in this deep layer that the variability of $[C_{ant}]_{TrOCA}$ between years is almost null compared to that of $[C_{ant}]_{\varphi}$. Furthermore, $C_{ant}$ storages are given for each year and each method estimated by the addition of $[C_{ant}]_{\varphi}$ and $[C_{ant}]_{TrOCA}$ in each layer multiplied by the thickness of the respective layer. The storages of $C_{ant}$ range between 66.9±4.1 molC·m$^{-2}$ and 88.1±3.8 molC·m$^{-2}$ for $\varphi C_T^o$ method and between 67.9±4.0 molC·m$^{-2}$ and 93.7±3.7 molC m$^{-2}$ for TrOCA method (Table 4.3). The storages obtained with TrOCA method are between 1 molC·m$^{-2}$ and 7 molC·m$^{-2}$ higher than those obtained with $\varphi C_T^o$ method for the year 1993 and 2003,

respectively. In general, the $C_{ant}$ storages increase with the year independently of the method of estimation.

Despite the fact that a first overview of the temporal evolution of $[C_{ant}]$ between 1993 and 2009 can be perceived from previous results, temporal evolution of $[C_{ant}]_{\varphi}$ and $[C_{ant}]_{TrOCA}$ for each layer together with that of $C_{ant}$ storages and $C_{ant}^{sat}$ (in $\mu mol \cdot kg^{-1}$) are shown in Figure 4.7.

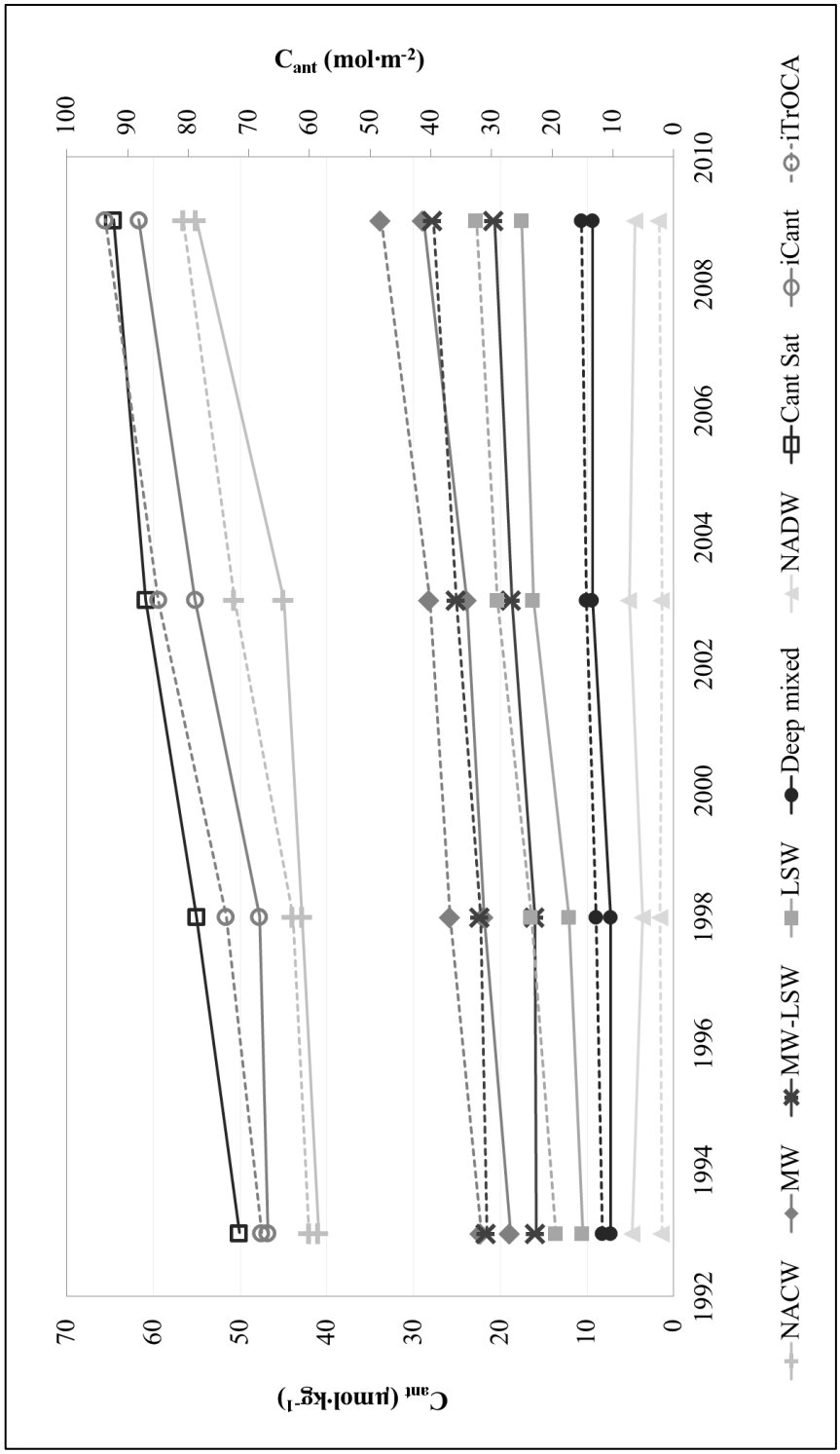


Figure 4.7 Time evolution of $C_{ant}$ (µmol·kg$^{-1}$) estimated from $\varphi C_T^0$ (continuous lines) and TrOCA (dashed lines) approaches in each layer (full symbols: sums, diamonds, crosses, squares, circles and triangles) and of $C_{ant}$ storages in molC·m$^{-2}$ (empty circles). The $C_{ant}^{sat}$ (empty squares) is also shown in µmol·kg$^{-1}$.

In this figure, the decrease in $[C_{ant}]$ with depth and the generally higher values of $[C_{ant}]_{TrOCA}$ (dashed lines in Fig. 4.7) respect to $[C_{ant}]_{\varphi}$ (solid lines in Fig. 4.7) mentioned before can be also seen. It is also noticeable that storages estimated from TrOCA method (iTrOCA, Fig. 4.7) are higher than those from $\varphi C_T^o$ method ($i\varphi C_T^o$, Fig. 4.7). There is a general increasing trend in the $[C_{ant}]_{\varphi}$ and $[C_{ant}]_{TrOCA}$ in each of the layers and of the $C_{ant}$ storages for both methods. The slopes of the different lines (Fig. 4.7) give the values of $[C_{ant}]$ rates (in $\mu mol \cdot kg^{-1} \cdot y^{-1}$) and $C_{ant}$ storage rates (in $molC \cdot m^{-2} \cdot y^{-1}$) shown in Table 4.4.

**Table 4.4** $[C_{ant}]$ **rates estimated from** $\varphi C_T^o$ **and TrOCA methods in each one of the six defined layers and** $C_{ant}$ **storage rates for the whole water column.**

| LAYER | $[C_{ant}]_{\varphi}$ rate ($\mu mol \cdot kg^{-1} y^{-1}$) | $[C_{ant}]_{TrOCA}$ rate ($\mu mol \cdot kg^{-1} y^{-1}$) |
|---|---|---|
| NACW | 0.85 ± 0.24 | 0.95 ± 0.13 |
| MW | 0.61 ± 0.06 | 0.70 ± 0.06 |
| MW-LSW | 0.32 ± 0.07 | 0.40 ± 0.06 |
| LSW | 0.47 ± 0.08 | 0.59 ± 0.05 |
| Deep Mixed Layer | 0.16 ± 0.06 | 0.16 ± 0.02 |
| NADW | 0.01 ± 0.07 | 0.02 ± 0.01 |
| $C_{ant}$ **storage rate (molC** $m^{-2}$ $y^{-1}$) | 1.41 ± 0.25 | 1.67 ± 0.13 |

The same pattern found for $[C_{ant}]$ is also seen in $[C_{ant}]$ rates with high values of the trend in the upper layers and very low values in the NADW layer (Table 4.4). For instance, the $[C_{ant}]$ rate in the NACW layer varies from 0.85±0.24 to 0.95±0.13 $\mu mol \cdot kg^{-1}$ $y^{-1}$ estimated by $\varphi C_T^o$ and TrOCA, respectively while in the NADW layer the $[C_{ant}]$ rates from $\varphi C_T^o$ and TrOCA methods are of 0.01±0.07 and 0.02±0.01 $\mu mol \cdot kg^{-1} \cdot y^{-1}$, respectively (Table 4.4). It is worth highlighting the high $[C_{ant}]$ rates that appear in the MW

layer, i.e, 0.61±0.06 and 0.70±0.06 µmol·kg$^{-1}$·y$^{-1}$ for $\varphi C_T^o$ and TrOCA methods, respectively (Table 4.4). The [$C_{ant}$] rates do not depend on neither of the two methods of estimation. Although [$C_{ant}$] rates from TrOCA method seem generally higher than those from $\varphi C_T^o$ method the differences between them are not statistically significant. The trend for the $C_{ant}$ storage rates in the studied region is also positive, with $C_{ant}$ storage rates of 1.41±0.25 and 1.67±0.13 molC·m$^{-2}$·y$^{-1}$ for $\varphi C_T^o$ and TrOCA, respectively.

## 4.4 Discussion

Two methods were used to estimate the distribution and temporal variability of [$C_{ant}$] along the Iberian Basin region, $\varphi C_T^o$ method and TrOCA method. Six vertical layers were defined in agreement with the thermohaline distribution of the region in order to relate the estimations of [$C_{ant}$] to the water masses present in the region. In general terms, the results obtained from both methods are quite similar, given the same pattern in the vertical distribution of [$C_{ant}$] (Fig. 4.3, Table 4.3). The values of [$C_{ant}$] are higher in the upper NACW layer (between 41.0±0.6 and 55.1±0.6 µmol·kg$^{-1}$ for $\varphi C_T^o$ method and between 42.0±0.6 and 56.6±0.6 µmol·kg$^{-1}$ for TrOCA method) but close to the expected values when seawater is in equilibrium with the increasing atmospheric $pCO_2$. These values progressively descend (Table 4.3, Fig. 4.7) from the upper layer to the NADW layer, where the [$C_{ant}$] are between 3.6±0.8 and 5.1±0.8 µmol·kg$^{-1}$ and between 1.4±0.8 and 1.7±0.7 µmol·kg$^{-1}$ for $\varphi C_T^o$ and TrOCA methods, respectively. Specifically, TrOCA method

estimates higher values of $[C_{ant}]$ than $\varphi C_T^o$ method for all layers except the NADW layer. This likely overestimation of $[C_{ant}]$ by TrOCA method has been also concluded in the work of Yool et al., (2010), who analysed the method from a theoretical standpoint. The same results have been reported for the Atlantic basin after comparison with others back-calculation methods (Vázquez-Rodríguez et al., 2009b). Moreover, Huertas et al., (2009) found an increase of $[C_{ant}]$ estimated by TrOCA method with depth in the Gibraltar Strait, contrary to the results present here, which points out the not-universal appliance of TrOCA method. Even in a completely different oceanic area, the eastern South American coast (Ríos et al., 2010) high values of $[C_{ant}]_{TrOCA}$ (some of them over the theoretical limit of $C_{ant}^{sat}$) have been found in the upper layers. The reason for this bias in TrOCA method probably relays on the assumption that air-sea flux of $CO_2$ scales with temperature and alkalinity (Yool et al., 2010). In the NADW layer the estimations of $[C_{ant}]_{TrOCA}$ are lower than $[C_{ant}]_{\varphi}$. Actually, the low values of $[C_{ant}]_{TrOCA}$ for this layer are obtained after assuming zero all negative $[C_{ant}]_{TrOCA}$ estimations (approximately 70% of TrOCA estimations in the NADW layer are negative), which help in terms of comparison between methods but corroborates the existence of important bias in TrOCA method at least in some areas. Negative results around bottom layers using TrOCA method were also observed for the whole Atlantic Ocean by Vázquez-Rodríguez et al., (2009b). On the other hand, $[C_{ant}]_{\varphi}$ never exceed the $C_{ant}^{sat}$ values in the upper layers because the $\varphi C_T^o$ method is limited in surface to saturation values and it is constrained to keep negative disequilibria

($\Delta\Delta C_{dis}$<0) in relation to the pre-industrial era (VR'09). These slight differences between both methods estimations can also be a consequence of the $\Delta\Delta C_{dis}$ term. This term is assumed zero in the TrOCA method whereas in the $\varphi C_T^o$ method it stems from the main assumption that $\Delta C_{dis}$ vary with time, contrary to the classical assumption of invariability of $\Delta C_{dis}$ in the classical back-calculating methods (Gruber et al., 1996; Lo Monaco et al., 2005; Sabine and Tanhua, 2010). This same pattern, i.e., higher values of $[C_{ant}]_{TrOCA}$ in all water column except near the bottom where $[C_{ant}]_{\varphi}$ are higher than $[C_{ant}]_{TrOCA}$ estimations, is also found in the Azores region (Pérez et al., 2010a), which is a very close region to the Iberian basin.

The $C_{ant}$ storages obtained separately for each cruise were also very similar for both methods varying from 66.9±4.1 to 88.1±3.8 molC·m$^{-2}$ for $\varphi C_T^o$ method and from 67.9±4.0 to 93.7±3.7 molC·m$^{-2}$ for TrOCA method and clearly indicating an increase of the $C_{ant}$ storage of the Iberian basin with time. In order to have a quantitative comparison of these data, results from the work of Pérez et al., (2010a) in the Azores region were considered. In this work, data from the AZORES I (1998), OACES 1993 and METEOR 2004 cruises were studied among others. OACES 1993 is also included in this work and the other two cruises are inside the period of time studied here. Pérez et al., (2010a) obtained higher values of the $C_{ant}$ storages in the OACES 1993, with differences respect to the results obtained here of ~3 molC·m$^{-2}$ and ~6 molC·m$^{-2}$ for $\varphi C_T^o$ and TrOCA method, respectively. Interestingly, these

differences are attributed to the different methodology in the vertical integration of [$C_{ant}$] which in Pérez et al., (2010a) was made in base of an average profile of [$C_{ant}$] and not in base of a more-realistic mean-layered [$C_{ant}$] as it was done here. Moreover, for the Iberian basin more stations than in Pérez et al., (2010a) were taken into account. The $C_{ant}$ storage estimated for AZORES I (Pérez et al., 2010a) was ~10 molC·m$^{-2}$ (approximated for the two back-calculating methods) higher than the value found here for CHAOS 1998. In spite of the different vertical integration method, this difference could also be due to the different location of AZORES I cruise (Fig. 4.1 in Pérez et al., 2010a) respect to CHAOS 1998 (Fig. 4.1). AZORES I spans close to the Mid-Atlantic Ridge, so higher proportions of LSW with high [$C_{ant}$] are sampled. Nonetheless, the METEOR 2004 cruise gives $C_{ant}$ storages of 87±1 and 92±1 molC·m$^{-2}$ for $\varphi C_T^o$ and TrOCA, respectively (Pérez et al., 2010a), very close to those values for OACES 2003 (78.9±4.2 and 85.0±4.1 molC·m$^{-2}$ for $\varphi C_T^o$ and TrOCA, respectively) but higher, thus corroborating the temporal increase in the $C_{ant}$ storage of the Iberian basin. In this sense, there is also good consistence with the $C_{ant}$ storages of 87±5 and 95±5 molC·m$^{-2}$ for $\varphi C_T^o$ and TrOCA methods, respectively, obtained for the Biscay Bay during VACLAN-2005 (Castaño-Carrera et al., 2012).

The [$C_{ant}$] rates estimated in the Iberian basin for each one of the layers show high values in the NACW layer and in the MW layer (~0.90 and ~0.65 µmol·kg$^{-1}$·y$^{-1}$, respectively) and a progressive descend of the rates toward the bottom. For the whole water

column, the $C_{ant}$ storage rates were 1.41±0.25 molC·m$^{-2}$·y$^{-1}$ for $\varphi C_T^o$ method and 1.67±0.13 molC·m$^{-2}$·y$^{-1}$ for TrOCA method. Importantly, all rates show no-statistically significant differences between the two estimating methods. No methodology dependent results were also obtained by Pérez et al., (2010a) for the period 1981-2004 in the Azores region, where the $C_{ant}$ storage rates were 1.32±0.11 molC·m$^{-2}$·y$^{-1}$ for $\varphi C_T^o$ method and 1.18±0.16 molC·m$^{-2}$·y$^{-1}$ for TrOCA method. The $C_{ant}$ storage rates found here for the period 1993-2009 are higher than those found by Pérez et al., (2010a) which can be a signal of an acceleration of the $C_{ant}$ uptake by the ocean, at least in the Iberian basin region.

In order to look for a more reliable sign of this acceleration $C_{ant}$ storage rate estimations from older periods of time can be of great help. From 1977 to 1997, Ríos et al., (2001) estimated [$C_{ant}$] in the Iberian Peninsula coast by a back-calculation technique obtaining a $C_{ant}$ storage rate of 0.95 molC·m$^{-2}$·y$^{-1}$ for the upper 2000m. In order to compare two periods of time, all data (1993-2009) were recalculated for the first 2000m in the Iberian basin, finding that the average percentage of $C_{ant}$ storage between 0-2000m represents 80.6±1.4 and 86.7±1.1 % of the total $C_{ant}$ storage for $\varphi C_T^o$ and TrOCA, respectively. Thus, the $C_{ant}$ storage rates in the upper 2000m estimated by $\varphi C_T^o$ and TrOCA method are 1.21±0.18 and 1.42±0.19 molC·m$^{-2}$·y$^{-1}$, respectively. These rates, respect to the value found by Ríos et al., (2001), mean an increase of $C_{ant}$ storage rate of around 28% considering $\varphi C_T^o$ method and of ~49% according to TrOCA method.

The cause of this increase in the $C_{ant}$ storage rate found in the Iberian basin could be linked to a similar increase in the atmospheric $CO_2$. According to the Mauna Loa annual mean $CO_2$ data (Dr Pieter Tans, NOAA/ESRL http:/www.esrl.noaa.gov/gmd/ccgg/trends) the atmospheric $CO_2$ increased from ~334 ppm in 1977 to ~387 ppm in 2009. Splitting these increasing trends into the two periods previously mentioned, 1977-1997 and 1993-2009, the average $CO_2$ rates were 1.49±0.02 and 1.92±0.02 $ppm \cdot y^{-1}$, for each period respectively. The increase of $CO_2$ rate in the atmosphere is of ~29%, which is a value very close to the increase in the ocean $C_{ant}$ storage rate found here (~28-49%). Nevertheless, Pérez et al., (2010b), for the region of the North Atlantic Subpolar Gyre (where the Iberian basin region is partially included) found a decrease of ~48% in the $C_{ant}$ storage rates from the first half of the 1990s to the period 1997-2006. According to Pérez et al., (2010b) this decrease is linked to the high and low NAO phases which act over the volumetric census of the water masses present in the region. As can be deduced from these results, the storage rates can vary between close areas depending on the dynamics of the region and also on the time period studied. Owing to all these different quantities found, more insight into $C_{ant}$ storages and $C_{ant}$ storages rates is needed in order to get a better understanding of the carbon cycle in the atmosphere-ocean system.

## 4.5 Conclusions

Taking into account the 20ºW CAIBOX section, together with OACES 1993, CHAOS 1998 and OACES 2003, two back-calculation techniques, $\varphi C_T^o$ and TrOCA were used to estimate the distribution and temporal variability of [$C_{ant}$] along the Iberian Basin. The values of [$C_{ant}$] are higher in the upper NACW layer (between 41.0±0.6 and 55.1±0.6 µmol·kg$^{-1}$ for $\varphi C_T^o$ method and between 42.0±0.6 and 56.6±0.6 µmol·kg$^{-1}$ for TrOCA method). These values progressively descend from the upper layer to the NADW layer, where the [$C_{ant}$] are between 3.6±0.8 and 5.1±0.8 µmol·kg$^{-1}$ and between 1.4±0.8 and 1.7±0.7 µmol·kg$^{-1}$ for $\varphi C_T^o$ and TrOCA methods, respectively. In addition, the $C_{ant}$ storages obtained separately for each cruise were also very similar for both methods varying from 66.9±4.1 to 88.1±3.8 molC·m$^{-2}$ for $\varphi C_T^o$ method and from 67.9±4.0 to 93.7±3.7 molC·m$^{-2}$ for TrOCA method, and clearly indicating an increase of the $C_{ant}$ storage of the Iberian basin with time. For the whole water column, the $C_{ant}$ storage rates were 1.41±0.25 molC·m$^{-2}$·y$^{-1}$ for $\varphi C_T^o$ method and 1.67±0.13 molC·m$^{-2}$·y$^{-1}$ for TrOCA method. Importantly, all rates show no-statistically significant differences between the two estimating methods. From 1977 to 1997, Ríos *et al.* (2001) estimated [$C_{ant}$] in the Iberian Peninsula coast by a back-calculation technique obtaining a $C_{ant}$ storage rate of 0.95 molC·m$^{-2}$·y$^{-1}$ for the upper 2000m. In order to compare two periods of time, all data (1993-2009) were recalculated for the first 2000m in the Iberian basin, where the $C_{ant}$ storage rates were 1.21±0.18 and 1.42±0.19 molC·m$^{-2}$·y$^{-1}$ estimated by $\varphi C_T^o$ and TrOCA method respectively.

Respect to the value found by Ríos *et al.* (2001), these values mean an increase of $C_{ant}$ storage rate of around 28% considering $\varphi C_T^o$ method and of ~49% according to TrOCA method.

# IV. Conclusiones / *Conclusions*

## Conclusiones

El presente trabajo se diferenció en cuatro secciones principales: la evaluación de las medidas del sistema del $CO_2$ y los procesos de control de calidad de los datos obtenidos se tratan en los capítulos 1 y 2, respectivamente, mientras que la evaluación de cambios en las variables medidas estimadas se realizó en los capítulos 3 y 4 para el Océano Atlántico Ecuatorial y la Cuenca Ibérica, respectivamente

### *Capítulo 1. Medidas del sistema del carbonato y consistencia interna en el Atlántico Norte*

Considerando las medidas de laboratorio de $CO_3^{2-}$, $C_T$, $A_T$ y pH realizadas durante las campañas CAIBOX, MOC$^2$, OVIDE y A24N del Atlántico Norte, este estudio ha señalado que las constantes de disociación del ácido carbónico estimados en aguas naturales [Mehrbach et al., (1973) reajustadas por Dickson y Millero (1987), Lueker et al., (2000) y Millero et al., (2006)] son más fiables tanto para su uso en agua de mar como en medidas de laboratorio, que las estimadas en aguas sintéticas Goyet y Poisson (1989). Entre ellas, el conjunto de constantes de Millero et al., (2006) han sido identificadas como las más internamente consistentes, a la hora de obtener las mínimas diferencias entre $C_T$ y $CO_3^{2-}$ calculados y medidos. Cabe destacar que estas desviaciones mínimas se obtienen cuando se combinan estas constantes con la nueva relación B / Cl de Lee et al, (2010). En cuanto al nuevo método de medida

espectrofotométrica de $CO_3^{2-}$, se ha demostrado la influencia de la temperatura y de la adición de $PbCl_2$. Además, se propone una nueva ecuación par el cálculo de la $[CO_3^{2-}]$ permitiendo la reducción de los errores relativos en 1.2 %. Teniendo en cuenta la buena correlación alcanzada entre las $[CO_3^{2-}]$ medidas y las $[CO_3^{2-}]$ calculadas, se han podido representar las distribuciones de $[CO_3^{2-}]_{in.situ.}$ para todas las campañas estudias, destacando el mínimo de $[CO_3^{2-}]$ relacionado con la AAIW.

## *Capítulo 2. Datos de carbono de las campañas WOCE A06 y A07*

Se han revaluado los datos de $C_T$ y $A_T$ de las campañas A06 y A07, que no se incluyeron en GLODAP, y por consiguiente, los datos de pH existentes para ambas campañas tampoco de incluyeron, años después, en CARINA. Sin embargo, la aplicación del nuevo método 3DwMLR a las bases de datos GLODAP y CARINA ha permitido estimar la $A_{T\ 3DwMLR}$ para las campañas A06 y A07 con un error medio inferior a 5 $\mu mol \cdot kg^{-1}$. Además, los datos de $pH_{NBS}$ de A06 y A07, se han re-escalado a $pH_{SWS25}$, y se le han aplicado las correcciones de 0.028 y 0.024 para A06 y A07, respectivamente, obteniendo el $pH_{SWS25new}$ para cada campaña. Teniendo en cuenta el $pH_{SWS25new}$ y la $A_{T\ 3DwMLR}$, se han podido calcular también nuevos datos $C_T$ para cada campaña, de modo que se han recuperado exitosamente los datos de carbono para las campañas A06 y A07.

## *Capítulo 3. Cambios de $O_2$ y variables del sistema del carbonato en el Océano Atlántico Ecuatorial*

Con este estudio se indicaron los cambios en el pH, $O_2$ y $C_{ant}$ en la zona ecuatorial del océano Atlántico desde 1993 hasta 2010. Además se ha prestado especial atención a la relación entre estos cambios y las masas de agua principales de esta zona. En términos de pH, el cambio más importante se produce en las capas superiores de la columna de agua. En 2010, en la capa AAIW, se observó una gran extensión del mínimo de pH que cubrió toda la sección 7.5ºN. Este mínimo pH también amplió su gama de densidad, cubriendo la capa inmediatamente superior y produciendo un descenso de pH en las regiones orientales y occidental de la sección. La influencia de AAIW se aprecia también en los cambios de $O_2$. Sin embargo, en la capa inmediatamente superior, hay un aumento de $O_2$ relacionado con la SAMW. El mayor cambio en [$O_2$] entre las dos campañas ocurrió en la capa uNADW, que se asocia también con una disminución en el pH. Los valores ΔCant más notables se encuentran en las capas superiores.

## *Capítulo 4. Tendencias de $CO_2$ antropogénico a lo largo del 20ºW en la cuenca Ibérica*

Considerando la sección 20ºW de CAIBOX, junto con las campañas OACES 1993, CHAOS1998 y OACES 2003, se han utilizado los

métodos $\varphi C_T^o$ y TrOCA para estimar la distribución y variabilidad temporal de [$C_{ant}$] a lo largo de la Cuenca Ibérica. Las [$C_{ant}$] son más altas en la capa superior NACW (entre 41.0±0.6 y 55.1±0.6 µmol·kg$^{-1}$ con el método $\varphi C_T^o$ y entre 42.0±0.6 y 56.6±0.6 µmol·kg$^{-1}$ con el método TrOCA). Estos valores descienden progresivamente hasta la capa NADW, donde las [$C_{ant}$] están entre 3.6±0.8 y 5.1±0.8 µmol·kg$^{-1}$ y entre 1.4±0.8 y 1.7±0.7 µmol·kg$^{-1}$ para los métodos $\varphi C_T^o$ y TrOCA respectivamente. Además se han calculado los almacenamientos de $C_{ant}$, para cada campaña, variando desde 66.9±4.1 a 88.1±3.8 molC·m$^{-2}$ con el método $\varphi C_T^o$ y desde 67.9±4.0 a 93.7±3.7 molC·m$^{-2}$ con el método TrOCA, y que, claramente indican un aumento con el tiempo. Las tasas de almacenamiento de $C_{ant}$ estimadas en la Cuenca Ibérica en toda la columna de agua fueron de 1.41±0.25 molC·m$^{-2}$·y$^{-1}$ según el método $\varphi C_T^o$ y 1.67±0.13 molC·m$^{-2}$·y$^{-1}$ según el método TrOCA. Es importante destacar que todas las tasas muestran diferencias no estadísticamente significativas entre los dos métodos de estimación. Desde 1977 a 1997, Ríos *et al.* (2001) obtuvieron una tasa de almacenamiento de $C_{ant}$ de 0.95 molC·m$^{-2}$·y$^{-1}$ para los 2000m superiores. Con el fin de comparar dos periodos de tiempo, todos los datos (1993-2009) se recalcularon para los primeros 2000m en la Cuenca Ibérica, encontrando unas tasas de almacenamiento de $C_{ant}$ son de 1.21±0.18 y 1.42±0.19 molC·m$^{-2}$·y$^{-1}$ según $\varphi C_T^o$ y TrOCA respectivamente. Estas tasas, respecto al valor encontrado por Ríos *et al.* (2001), significan un incremento de la tasa de almacenamiento de $C_{ant}$ en torno al 28% considerando el método $\varphi C_T^o$ y al ~49% según el método TrOCA.

# Referencias
## *References*

## Referencias / *References*

Álvarez, M., Pérez, F. F., Bryden, H. L. and Ríos, A. F.: Physical and biogeochemical transports structure in the North Atlantic subpolar gyre, Journal of Geophysical Research, 109, doi:10.1029/2003JC002015 [online] Available from: http://www.agu.org/pubs/crossref/2004/2003JC002015.shtml (Accessed 6 October 2011), 2004.

Álvarez, M., Pérez, F. F., Shoosmith, D. R. and Bryden, H. L.: Unaccounted role of Mediterranean Water in the drawdown of anthropogenic carbon, Journal of Geophysical Research, 110(C9), C09S03, 2005.

Álvarez, M., Ríos, A. F., Pérez, F. F., Bryden, H. L. and Rosón, G.: Transports and budgets of total inorganic carbon in the subpolar and temperate North Atlantic, Global Biogeochem. Cycles, 17(1), 1002, 2003.

Álvarez-Salgado, X., Fraga, F. and Pérez, F. .: Determination of nutrient salts by automatic methods both in seawater and brackish water: the phosphate blank, Marine Chemistry, 39, 311–319, doi:10.1016/0304-4203(92)90016-4, 1992.

Anderson, L. A. and Sarmiento, J. L.: Redfield Ratios of Remineralization Determined by Nutrient Data Analysis, Global Biogeochemical Cycles, 8, 65–80, 1994.

Anon: IOCCP Report Number 24, Sixth Session of the Scientific Steering Group, IOC-SCOR International Ocean Carbon Coordination Project, París, France., 2011.

Arhan, M., Mercier, H., Bourles, B. and Gouriou, Y.: Hydrographic sections across the Atlantic at 7 30N and 4 30S, Deep Sea Research Part I: Oceanographic Research Papers, 45(6), 829–872, 1998.

Ballantyne, A. P., Alden, C. B., Miller, J. B., Tans, P. P. and White, J. W. C.: Increase in observed net carbon dioxide uptake by land and oceans during the past 50 years, Nature, 488(7409), 70–72, 2012.

Barker, S. and Ridgwell, A.: Ocean Acidification, Nature Education Knowledge, 3(3), 3, 2012.

Bindoff, N. L., Willebrand, J., Artale, V., Cazenave, A., Gregory, J. M., Gulev, S., Hanawa, K., Le Quere, C., Levitus, S., Nojiri, Y., Shum, C. K., et

al.: Observations: oceanic climate change and sea level. In: Climate Change 2007: The Physical Science Basis, Cambridge University Press, Cambridge, United Kingdom and New York, NY, USA. [online] Available from: http://nora.nerc.ac.uk/id/eprint/15400 (Accessed 13 November 2012), 2007.

Bradshaw, A. L. and Brewer, P. G.: High precision measurements of alkalinity and total carbon dioxide in seawater by potentiometric titration. 1. Presence of unknown protolyte (s)?, Marine Chemistry, 23(1), 69–86, 1988a.

Bradshaw, A. L. and Brewer, P. G.: High precision measurements of alkalinity and total carbon dioxide in seawater by potentiometric titration. 2. Measurements on standard solutions, Marine Chemistry, 24(2), 155–162, 1988b.

Brandt, P., Hormann, V., Körtzinger, A., Visbeck, M., Krahmann, G., Stramma, L., Lumpkin, R. and Schmid, C.: Changes in the ventilation of the oxygen minimum zone of the tropical North Atlantic, Journal of Physical Oceanography, 40(8), 1784–1801, 2010.

Brea, S., Álvarez-Salgado, X. A., Álvarez, M., Pérez, F. F., Mémery, L., Mercier, H. and Messias, M. J.: Nutrient mineralization rates and ratios in the eastern South Atlantic, Journal of Geophysical Research, 109, doi:10.1029/2003JC002051 [online] Available from: http://www.agu.org/pubs/crossref/2004/2003JC002051.shtml (Accessed 6 October 2011), 2004.

Brewer, P. G.: Direct observation of the oceanic CO2 increase, Geophysical Research Letters, 5(12), 997–1000, 1978.

Broecker, W.: The oceanic $CaCO_3$ cycle, Treatise on geochemistry, 6, 529–549, doi:10.1016/B0-08-043751-6/06119-3, 2003.

Broecker, W. S.: “NO”, a conservative water-mass tracer, Earth and Planetary Science Letters, 23, 1974.

Brown, P. J., Bakker, D. C. E., Schuster, U. and Watson, A. J.: Anthropogenic carbon accumulation in the subtropical North Atlantic, Journal of Geophysical Research, 115(C4), C04016, doi:10.1029/2008JC005043, 2010.

Bryden, H. L., Griffiths, M. J. and Lavin, A. M.: Decadal changes in water mass characteristics at 24 ${$degrees$}$ N in the subtropical North Atlantic Ocean, Journal of Climate, 9(12) [online] Available from: http://www.osti.gov/energycitations/product.biblio.jsp?osti_id=447204 (Accessed 11 October 2012), 1996.

Bryden, H. L., Longworth, H. R. and Cunningham, S. A.: Slowing of the Atlantic meridional overturning circulation at 25°N, Nature, 438(1), 655–57, 2005.

Buch, K., Harvey, H. W., Wattenberg, H. and Gripenberg, S.: Über das Kohlensäuresystem im Meerwasser, Rapp. P.-v. Réun. Cons. perm. int. Explor. Mer, 79, 1–70, 1932.

Byrne, R. H. and Breland, J. A.: High precision multiwavelength pH determinations in seawater using cresol red, Deep Sea Research Part A. Oceanographic Research Papers, 36(5), 803–810, 1989.

Byrne, R. H. and Yao, W.: Procedures for measurement of carbonate ion concentrations in seawater by direct spectrophotometric observations of Pb(II) complexation, Marine Chemistry, 112(1-2), 128–135, doi:10.1016/j.marchem.2008.07.009, 2008.

Byrne, R., McElligott, S., Feely, R. and Millero, F.: The role of pHT measurements in marine CO2-system characterizations, Deep Sea Research Part I: Oceanographic Research Papers, 46(11), 1985–1997, 1999.

Byrne, R., Robert-Baldo, G., Thompson, S. and Chen, C.: Seawater pH measurements: an at-sea comparison of spectrophotometric and potentiometric methods, Deep Sea Research Part A. Oceanographic Research Papers, 35(8), 1405–1410, 1988.

Canadell, J. G., Le Quéré, C., Raupach, M. R., Field, C. B., Buitenhuis, E. T., Ciais, P., Conway, T. J., Gillett, N. P., Houghton, R. A. and Marland, G.: Contributions to accelerating atmospheric $CO_2$ growth from economic activity, carbon intensity, and efficiency of natural sinks, Proceedings of the National Academy of Sciences, 104, 18866, 2007.

Canadell, P. and Shobhakar, D.: The Global Carbon Project, Global Carbon Project [online] Available from: http://www.globalcarbonproject.org/index.htm, 2001.

Carracedo, L. I., Pardo, P. C., Villacieros-Robineau, N., De la Granda, F., Gilcoto, M. and Pérez, F. F.: Temporal changes in the water mass distribution and transports along the 20°W CAIBOX section (NE Atlantic), Ciencias Marinas, 38(1B), 263–286, 2012.

Castaño-Carrera, M., Pardo, P. C., Alvarez, M., Lavín, A., Rodríguez, C., Carballo, R., Ríos, A. F. and Pérez, F. F.: Anthropogenic carbon and water masses in the Bay of Biscay, Ciencias Marinas, 38(1B), 191–207, 2012.

Castro, C. G., Pérez, F. F., Holley, S. E. and Ríos, A. F.: Chemical characterisation and modelling of water masses in the Northeast Atlantic, Progress In Oceanography, 41, 249–279, doi:10.1016/S0079-6611(98)00021-4, 1998.

Chanson, M. and Millero, F. J.: Effect of filtration on the total alkalinity of open-ocean seawater, Limnology and Oceanography: Methods, 5, 293–295, 2007.

Chen, G.-T. and Millero, F. J.: Gradual increase of oceanic CO2, , Published online: 18 January 1979; | doi:10.1038/277205a0, 277(5693), 205–206, doi:10.1038/277205a0, 1979.

Clayton, T. D. and Byrne, R. H.: Spectrophotometric seawater pH measurements: total hydrogen ion concentration scale calibration of m-cresol purple and at-sea results, Deep-Sea Research, 40, 2115–2129, 1993.

DelValls, T. and Dickson, A.: The pH of buffers based on 2-amino-2-hydroxymethyl-1, 3-propanediol (“tris”) in synthetic sea water, Deep-Sea Research Part I, 45(9), 1541–1554, 1998.

Dickson, A. G.: Standard potential of the reaction:, and and the standard acidity constant of the ion HSO4-in synthetic sea water from 273.15 to 318.15 K, The Journal of Chemical Thermodynamics, 22(2), 113–127, 1990a.

Dickson, A. G.: Thermodynamics of the dissociation of boric acid in synthetic seawater from 273.15 to 318.15 K, Deep Sea Research Part A. Oceanographic Research Papers, 37(5), 755–766, 1990b.

Dickson, A. G.: The measurement of sea water pH, Marine chemistry, 44, 131–142, 1993.

Dickson, A. G., Sabine, C. L. and Christian, J. R.: Guide to best practices for ocean $CO_2$ measurements, PICES Special Publication, 3, 191 pp, 2007a.

Dickson, A. G., Sabine, C. L. and Christian, J. R., Eds.: Guide to best practices for ocean CO2 measurements. North Pacific Marine Science Organization (PICES)., PICES Special Publication, 3, 191 pp, 2007b.

Dickson, A. and Millero, F.: A comparison of the equilibrium constants for the dissociation of carbonic acid in seawater media, Deep-Sea Research, 34, 1733–1743, 1987.

Dickson, A. and Riley, J.: The estimation of acid dissociation constants in seawater media from potentiometric titrations with strong base. I. The ionic product of water (Kw), Marine Chemistry, 7, 89–99, 1979.

Dickson, B., Yashayaev, I., Meincke, J., Turrell, B., Dye, S. and Holfort, J.: Rapid freshening of the deep North Atlantic Ocean over the past four decades, Nature, 416(6883), 832–837, 2002.

Doney, S. C.: The growing human footprint on coastal and open-ocean biogeochemistry, Science, 328(5985), 1512–1516, 2010.

Doney, S. C., Fabry, V. J., Feely, R. A. and Kleypas, J. A.: Ocean acidification: the other CO2 problem, Marine Science, 1, 2009.

Fajar, N. M., Pardo, P. C., Carracedo, L., Vazquez-Rodriguez, M., Rios, A. F. and Pérez, F. F.: Trends of anthropogenic CO2 along 20$^{o}$ W in the Iberian Basin, Ciencias Marinas, 38 (1B), 287–306, 2012.

Feely, R. A., Doney, S. C. and Cooley, S. R.: Ocean acidification: present conditions and future changes in a high-CO2 world, [online] Available from: https://darchive.mblwhoilibrary.org/handle/1912/3180 (Accessed 21 November 2012), 2009.

Flecha, S., Pérez, F. F., Navarro, G., Ruíz, J., Olivé, I., Rodríguez-Gálvez, S., Costas, E. and Huertas, I. E.: Anthropogenic carbon inventory in the Gulf of Cádiz, Journal of Marine Systems, 92, 67–75, 2012.

Fraga, F., Mouriño, C. and Manríquez, M.: Las masas de agua en la costa de Galicia: junio-octubre, Res. Exp. Cient, 10, 51–77, 1982.

Fraga, F., Ríos, A. F., Pérez, F. F. and Figueiras, F. G.: Theoretical limits of oxygen:carbon and oxygen:nitrogen ratios during photosynthesis and

mineralisation of organic matter in the sea, Scientia Marina, 62 (1-2), 161–168, 1998.

Friis, K., Körtzinger, A., Pätsch, J. and Wallace, D. W. R.: On the temporal increase of anthropogenic CO2 in the subpolar North Atlantic, Deep Sea Research Part I: Oceanographic Research Papers, 52(5), 681–698, 2005.

Gattuso, J. P. and Hansson, L.: Ocean acidification, Oxford University Press. [online] Available from: http://www.lavoisier.fr/livre/notice.asp?id=OR6W6AA6ROSOWQ (Accessed 28 November 2012), 2011.

Gouretski, V. V. and Jancke, K.: Systematic errors as the cause for an apparent deep water property variability: global analysis of the WOCE and historical hydrographic data, Progress in Oceanography, 48, 337–402, 2001.

Goyet, C. and Poisson, A.: New determination of carbonic acid dissociation constants in seawater as a function of temperature and salinity, Deep-Sea Research, 36, 1635–1654, 1989.

Gruber, N.: Warming up, turning sour, losing breath: ocean biogeochemistry under global change, Philosophical Transactions of the Royal Society A: Mathematical, Physical and Engineering Sciences, 369(1943), 1980–1996, 2011.

Gruber, N., Gloor, M., Mikaloff Fletcher, S. E., Doney, S. C., Dutkiewicz, S., Follows, M. J., Gerber, M., Jacobson, A. R., Joos, F., Lindsay, K., Menemenlis, D., et al.: Oceanic sources, sinks, and transport of atmospheric $CO_2$, Global Biogeochemical Cycles, 23, doi:10.1029/2008GB003349 [online] Available from: http://www.agu.org/pubs/crossref/2009/2008GB003349.shtml (Accessed 13 November 2011), 2009.

Gruber, N., Sarmiento, J. L. and Stocker, T. F.: An improved method for detecting anthropogenic $CO_2$ in the oceans, Global Biogeochemical Cycles, 10, 809–837, 1996.

Hall, T. M., Waugh, D. W., Haine, T. W. N., Robbins, P. E. and Khatiwala, S.: Estimates of anthropogenic carbon in the Indian Ocean with allowance for mixing and time-varying air-sea CO2 disequilibrium, Global biogeochemical cycles, 18(1), GB1031, 2004.

Hansson, I.: A new set of pH scales and standard buffers for sea water, Deep-Sea Research, 20, 471–491, 1973.

Herraiz-Borreguero, L. and Rintoul, S. R.: Subantarctic mode water: distribution and circulation, Ocean Dynamics, 61(1), 103–126, 2011.

Huertas, I. E., Ríos, A. F., García-Lafuente, J., Makaoui, A., Rodríguez-Gálvez, S., Sánchez-Román, A., Orbi, A., Ruíz, J. and Pérez, F. F.: Anthropogenic and natural $CO_2$ exchange through the Strait of Gibraltar, Biogeosciences, 6, 647–662, 2009.

Johnson, G. C.: Quantifying Antarctic bottom water and North Atlantic deep water volumes, J. Geophys. Res, 113, C05027, 2008.

Johnson, K. M., Dickson, A. G., Eischeid, G., Goyet, C., Guenther, P., Key, R. M., Millero, F. J., Purkerson, D., Sabine, C. L., Schottle, R. G. and others: Coulometric total carbon dioxide analysis for marine studies: Assessment of the quality of total inorganic carbon measurements made during the US Indian Ocean CO2 Survey 1994-1996, Marine Chemistry, 63(1-2), 21–37, 1998.

Johnson, K. M., Wills, K. D., Butler, D. B., Johnson, W. K. and Wong, C. S.: Coulometric total carbon dioxide analysis for marine studies: maximizing the performance of an automated gas extraction system and coulometric detector, Marine Chemistry, 44(2-4), 167–187, 1993.

Keeling, C. D.: The concentration and isotopic abundances of carbon dioxide in the atmosphere, Tellus, 12(2), 200–203, 1960.

Keeling, R. F. and Garcia, H. E.: The change in oceanic O2 inventory associated with recent global warming, Proceedings of the National Academy of Sciences, 99(12), 7848, 2002.

Keeling, R. F., Körtzinger, A. and Gruber, N.: Ocean deoxygenation in a warming world, Annual Review of Marine Science, 2, 199–229, 2010.

Key, R. M., Kozyr, A., Sabine, C. L., Lee, K., Wanninkhof, R., Bullister, J. L., Feely, R. A., Millero, F. J., Mordy, C. and Peng, T. H.: A global ocean carbon climatology: Results from Global Data Analysis Project (GLODAP), Global Biogeochemical Cycles, 18, GB4031, 2004.

Key, R. M., Tanhua, T., Olsen, A., Hoppema, M., Jutterström, S., Schirnick, C., Van Heuven, S., Kozyr, A., Lin, X., Velo, A., Wallace, D. W. R., et al.: The

CARINA data synthesis project: Introduction and overview, Earth Syst. Sci. Data, 2, 105–121, 2010.

Khatiwala, S., Primeau, F. and Hall, T.: Reconstruction of the history of anthropogenic CO2 concentrations in the ocean, Nature, 462(7271), 346–349, 2009.

Körtzinger, A., Mintrop, L. and Duinker, J. C.: On the penetration of anthropogenic CO2 into the North Atlantic Ocean, Journal of geophysical research, 103(C9), 18681–18, 1998.

Laffoley, D. d'a and Baxter, J. M.: Ocean Acidification Reference User Group, European Project on Ocean Acidification (EPOCA)., 2010.

Lamb, M., Sabine, C., Feely, R., Wanninkhof, R., Key, R., Johnson, G., Millero, F., Lee, K., Peng, T. H., Kozyr, A. and others: Consistency and synthesis of Pacific Ocean CO2 survey data, Deep Sea Research Part II: Topical Studies in Oceanography, 49(1-3), 21–58, 2001.

Lee, K., Kim, T. W., Byrne, R. H., Millero, F. J., Feely, R. A. and Liu, Y. M.: The universal ratio of boron to chlorinity for the North Pacific and North Atlantic oceans, Geochimica et Cosmochimica Acta, 74(6), 1801–1811, 2010.

Lee, K. and Millero, F. J.: Thermodynamic studies of the carbonate system in seawater, Deep Sea Research Part I: Oceanographic Research Papers, 42(11-12), 2035–2061, 1995.

Lee, K., Millero, F. J., Byrne, R. H., Feely, R. A. and Wanninkhof, R.: The recommended dissociation constants for carbonic acid in seawater, Geophysical Research Letters, 27(2), 229–232, 2000.

Lee, K., Millero, F. J. and Campbell, D. M.: The reliability of the thermodynamic constants for the dissociation of carbonic acid in seawater, Marine chemistry, 55(3-4), 233–245, 1996.

Lee, K., Millero, F. J. and Wanninkhof, R.: The carbon dioxide system in the Atlantic Ocean, Journal of geophysical research, 102(C7), 15693–15, 1997.

Lee, K., Tong, L. T., Millero, F. J., Sabine, C. L., Dickson, A. G., Goyet, C., Park, G.-H., Wanninkhof, R., Feely, R. A. and Key, R. M.: Global relationships of total alkalinity with salinity and temperature in surface

waters of the world's oceans, Geophys. Res. Lett., 33(19), L19605, doi:10.1029/2006GL027207, 2006.

Liu, X., Patsavas, M. C. and Byrne, R. H.: Purification and Characterization of meta-Cresol Purple for Spectrophotometric Seawater pH Measurements, Environmental science & technology, 2011.

Lueker, T. J., Dickson, A. G. and Keeling, C. D.: Ocean pCO2 calculated from dissolved inorganic carbon, alkalinity, and equations for K1 and K2: validation based on laboratory measurements of CO2 in gas and seawater at equilibrium, Marine Chemistry, 70(1-3), 105–119, 2000.

Lyman, J.: Buffer mechanism of seawater, University of California, Los Ángeles., 1956.

Macdonald, A. M., Baringer, M. O., Wanninkhof, R., Lee, K. and Wallace, D. W. R.: A 1998–1992 comparison of inorganic carbon and its transport across 24.5°N in the Atlantic, Deep Sea Research Part II: Topical Studies in Oceanography, 50(22–26), 3041–3064, doi:10.1016/j.dsr2.2003.07.009, 2003.

Martz, T. R., Jannasch, H. W. and Johnson, K. S.: Determination of carbonate ion concentration and inner sphere carbonate ion pairs in seawater by ultraviolet spectrophotometric titration, Marine Chemistry, 115(3-4), 145–154, 2009.

Matsumoto, K. and Gruber, N.: How accurate is the estimation of anthropogenic carbon in the ocean? An evaluation of the DeltaC* method, Global biogeochemical cycles, 19(3), GB3014, 2005.

Mehrbach, C., Culberson, C., Hawley, J. and Pytkowicz, R.: Measurement of the apparent dissociation constants of carbonic acid in seawater at atmospheric pressure, Limnology and Oceanography, 897–907, 1973.

Mémery, L., Arhan, M., Álvarez-Salgado, X. A., Messias, M. J., Mercier, H., Castro, C. G. and Ríos, A. F.: The water masses along the western boundary of the south and equatorial Atlantic, Progress in Oceanography, 47, 69–98, 2000.

Millero, F.: The marine inorganic carbon cycle, Chemical Reviews-Columbus, 107, 308–341, 2007.

Millero, F. J.: Thermodynamics of the carbon dioxide system in the oceans, Geochimica et Cosmochimica Acta, 59(4), 661–677, doi:10.1016/0016-7037(94)00354-O, 1995.

Millero, F. J.: Chemical oceanography, Third., CRC press, Boca Ratón., 2006.

Millero, F. J.: Carbonate constants for estuarine waters, Marine and Freshwater Research, 61(2), 139–142, 2010.

Millero, F. J., Byrne, R. H., Wanninkhof, R., Feely, R., Clayton, T., Murphy, P. and Lamb, M. F.: The internal consistency of CO2 measurements in the equatorial Pacific, Marine Chemistry, 44(2-4), 269–280, 1993.

Millero, F. J., Graham, T. B., Huang, F., Bustos-Serrano, H. and Pierrot, D.: Dissociation constants of carbonic acid in seawater as a function of salinity and temperature, Marine Chemistry, 100(1-2), 80–94, 2006.

Millero, F. J., Lee, K. and Roche, M.: Distribution of alkalinity in the surface waters of the major oceans, Marine Chemistry, 60(1-2), 111–130, doi:10.1016/S0304-4203(97)00084-4, 1998.

Millero, F. J., Pierrot, D., Lee, K., Wanninkhof, R., Feely, R., Sabine, C. L., Key, R. M. and Takahashi, T.: Dissociation constants for carbonic acid determined from field measurements, Deep Sea Research Part I: Oceanographic Research Papers, 49(10), 1705–1723, 2002.

Mintrop, L., Pérez, F., González-Dávila, M., Santana-Casiano, J. and Körtzinger, A.: Alkalinity determination by potentiometry: Intercalibration using three different methods, Ciencias Marinas, 26, 23–37, 2000.

Mojica Prieto, F. J. and Millero, F. J.: The values of $pK_1$+ $pK_2$ for the dissociation of carbonic acid in seawater, Geochimica et Cosmochimica Acta, 66(14), 2529–2540, 2002.

Lo Monaco, C., Goyet, C., Metzl, N., Poisson, A. and Touratier, F.: Distribution and inventory of anthropogenic CO2 in the Southern Ocean: Comparison of three data-based methods, J. Geophys. Res, 110, 9, 2005.

Mouriño, C. and Fraga, F.: Determinacion de nitratos en agua de mar, Investigacion Pesquera, 49, 81–96, 1985.

Murata, A., Kumamoto, Y., Sasaki, K., Watanabe, S. and Fukasawa, M.: Decadal increases of anthropogenic $CO_2$ in the subtropical South Atlantic Ocean along 30 S, J. Geophys. Res, 113, C06007, 2008.

Orr, J. C., Fabry, V. J., Aumont, O., Bopp, L., Doney, S. C., Feely, R. A., Gnanadesikan, A., Gruber, N., Ishida, A. and Joos, F.: Anthropogenic ocean acidification over the twenty-first century and its impact on calcifying organisms, Nature, 437(7059), 681–686, 2005.

Oudot, C.: Carbon data obtained during the R/V L'Atalante cruise in the Atlantic Ocean (WOCE Section A07, 13 Feb.- 19 Mar., 1993). [online] Available from: http://cdiac.ornl.gov/ftp/oceans/a07woce/, 1993a.

Oudot, C.: Total $CO_2$ and Total Alkalinity Data Obtained during the R/V L'Atalante cruise in the Atlantic Ocean (WOCE Section A06, 02 Jan. - 10 Feb., 1993). [online] Available from: http://cdiac.ornl.gov/ftp/oceans/a06woce/, 1993b.

Oudot, C., Morin, P., Baurand, F., Wafar, M. and Corre, P. L.: Northern and southern water masses in the equatorial Atlantic distribution of nutrients on the WOCE A6 and A7 lines, Deep-Sea Research Part I, 45(6), 873–902, 1998.

Oudot, C., Ternon, J. F. and Lecomte, J.: Measurements of atmospheric and oceanic CO2 in the tropical Atlantic: 10 years after the 1982-1984 FOCAL cruises, Tellus B, 47(1-2), 70–85, 1995.

Pelejero, C., Calvo, E. and Hoegh-Guldberg, O.: Paleo-perspectives on ocean acidification, Trends in Ecology & Evolution, 25(6), 332–344, 2010.

Péliz, Á., Dubert, J., Santos, A. M. P., Oliveira, P. B. and Le Cann, B.: Winter upper ocean circulation in the Western Iberian Basin—Fronts, Eddies and Poleward Flows: an overview, Deep Sea Research Part I: Oceanographic Research Papers, 52(4), 621–646, 2005.

Pérez, F. F., Arístegui, J., Vázquez-Rodríguez, M. and Ríos, A. F.: Anthropogenic $CO_2$ in the Azores region, Scientia Marina, 74, 11–19, doi:10.3989/scimar.2010.74s1011, 2010a.

Perez, F. F. and Fraga, F.: A precise and rapid analytical procedure for alkalinity determination, Marine Chemistry, 21(2), 169–182, 1987.

Pérez, F. F. and Fraga, F.: A precise and rapid analytical procedure for alkalinity determination, Marine Chemistry, 21(2), 169–182, 1987.

Pérez, F. F., Vázquez-Rodríguez, M., Louarn, E., Padín, X. A., Mercier, H. and Ríos, A. F.: Temporal variability of the anthropogenic CO2 storage in the Irminger Sea, Biogeosciences, 5, 1669–1679, 2008.

Pérez, F. F., Vázquez-Rodríguez, M., Mercier, H., Velo, A., Lherminier, P. and Ríos, A. F.: Trends of anthropogenic $CO_2$ storage in North Atlantic water masses, Biogeosciences, 7(5), 1789–1807, doi:10.5194/bg-7-1789-2010, 2010b.

Pierrot, D., Lewis, E. and Wallace, D.: MS Excel Program Developed for $CO_2$ System Calculations, ORNL/CDIAC-105a. Carbon Dioxide Information Analysis Center, Oak Ridge National Laboratory, US Department of Energy, Oak Ridge, TN, doi:10.3334/CDIAC/otg.CO2SYS_XLS_CDIAC105a, 2006.

Pollard, R. T., Griffttths, M. J., Cunningham, S. A., Read, J. F., Pérez, F. F. and Ríos, A. F.: Vivaldi 1991 - A study of the formation, circulation and ventilation of Eastern North Atlantic Central Water, Progress In Oceanography, 37, 167–192, doi:10.1016/S0079-6611(96)00008-0, 1996.

Le Quéré, C., Raupach, M. R., Canadell, J. G., Marland, G., Bopp, L., Conway, T. J., Doney, S. C., Feely, R. A., Foster, P., Friedlingstein, P., Gurney, K., et al.: Trends in the sources and sinks of carbon dioxide, Nature Geoscience, 2(12), 831–836, 2009.

Rhein, M., Stramma, L. and Krahmann, G.: The spreading of Antarctic Bottom Water in the tropical Atlantic, Deep Sea Research-Part I-Oceanographic Research Papers, 45(4), 507–528, 1998.

Riebesell, U., Fabry, V. J., Hansson, L. and Gattuso, J. P.: Guide to best practices for ocean acidification research and data reporting, Publications Office of the European Union, Luxembourg., 2010.

Ríos, A. F., Perez, F. F. and Fraga, F.: Water masses in the upper and middle North Atlantic Ocean east of the Azores, Deep Sea Research Part A. Oceanographic Research Papers, 39, 645–658, doi:10.1016/0198-0149(92)90093-9, 1992.

Ríos, A. F., Pérez, F. F. and Fraga, F.: Long-term (1977-1997) measurements of carbon dioxide in the eastern North Atlantic:

evaluation of anthropogenic input, Deep Sea Research Part II: Topical Studies in Oceanography, 48(10), 2227–2239, 2001.

Ríos, A. F., Vázquez-Rodríguez, M., Padin, X. A. and Pérez, F. F.: Anthropogenic carbon dioxide in the South Atlantic western basin, Journal of Marine Systems, 83, 38–44, doi:10.1016/j.jmarsys.2010.06.010, 2010.

Rios, A. F., Velo, A., Pardo, P. C., Hoppema, M. and Pérez, F. F.: An update of anthropogenic CO2 storage rates in the western South Atlantic basin and the role of Antarctic Bottom Water, Journal of Marine Systems, 94, 197–203, 2012.

Rosón, G., Rios, A. F., Pérez, F. F., Lavin, A. and Bryden, H. L.: Carbon distribution, fluxes, and budgets in the subtropical North Atlantic Ocean (24.5 N), Journal of geophysical research, 108(C5), 3144, doi:10.1029/1999JC000047, 2003.

Roy, R. N., Roy, L. N., Vogel, K. M., Porter-Moore, C., Pearson, T., Good, C. E., Millero, F. J. and Campbell, D. M.: The dissociation constants of carbonic acid in seawater at salinities 5 to 45 and temperatures 0 to 45 C, Marine Chemistry, 44(2), 249–267, 1993.

Sabine, C., Key, R., Kozyr, A., Feely, R., Wanninkhof, R., Millero, F., Peng, T., Bullister, J. and Lee, K.: Global Ocean data Analysis Project (GLODAP): Results and data, NDP-083, 110 pp, Carbon Dioxide Inf. Anal. Cent., Oak Ridge Natl. Lab., Oak Ridge, Tenn, 2005.

Sabine, C. L., Feely, R. A., Gruber, N., Key, R. M., Lee, K., Bullister, J. L., Wanninkhof, R., Wong, C. S., Wallace, D. W. R. and Tilbrook, B.: The oceanic sink for anthropogenic $CO_2$, Science, 305, 367–371, doi:10.1126/science.1097403, 2004.

Sabine, C. L. and Tanhua, T.: Estimation of anthropogenic CO2 inventories in the ocean, Annual review of marine science, 2, 175–198, 2010.

Schlitzer, R.: Ocean Data View. [online] Available from: http://odv.awi.de, 2011.

Schmitz Jr, W.: On the World Ocean Circulation: Volume I: some global features/North Atlantic Circulation. Woods Hole Oceanogr, Inst. Tech. Rep. WHOI-96-03, 150 pp.[Available from Woods Hole Oceanographic Institution, Woods Hole, MA 02543.]., 1996.

Soli, A. L., Stewart, Z. I. and Byrne, R. H.: The influence of temperature on PbCO30 formation in seawater, Marine Chemistry, 110(1-2), 1–6, 2008.

Stanley, R. H. R., Doney, S. C., Jenkins, W. J. and Lott III, D. E.: Apparent oxygen utilization rates calculated from tritium and helium-3 profiles at the Bermuda Atlantic Time-series Study site, Biogeosciences, 9, 1969–1983, doi:10.5194/bg-9-1969-2012, 2012.

Steinfeldt, R., Rhein, M. and Walter, M.: NADW transformation at the western boundary between 66W/20N and 60W/10N, Deep Sea Research Part I: Oceanographic Research Papers, 54(6), 835–855, 2007.

Stendardo, I. and Gruber, N.: Oxygen trends over five decades in the North Atlantic, JOURNAL OF GEOPHYSICAL RESEARCH, 117(C11004), 18pp, doi:10.1029/2012JC007909, 2012.

Stramma, L. and England, M.: On the water masses and mean circulation of the South Atlantic Ocean, Journal of Geophysical Research, 104(C9), 20863–20, 1999.

Stramma, L., Johnson, G. C., Sprintall, J. and Mohrholz, V.: Expanding oxygen-minimum zones in the tropical oceans, Science, 320(5876), 655–658, 2008.

Stramma, L., Oschlies, A. and Schmidtko, S.: Ocean oxygen minima expansions and their biological impacts, Biogeosciences, 9, Mismatch between observed and modeled trends in dissolved upper–ocean oxygen over the last 50 yr, 2012.

Stramma, L. and Schott, F.: The mean flow field of the tropical Atlantic Ocean, Deep Sea Research-Part II-Topical Studies in Oceanography, 46(1), 279–304, 1999.

Tanhua, T.: Matlab Toolbox to Perform Secondary Quality Control (2nd QC) on Hydrographic Data., ORNL/CDIAC-158. Carbon Dioxide Information Analysis Center, Oak Ridge National Laboratory, U.S. Department of Energy, Oak Ridge, Tennessee. [online] Available from: http://cdiac.ornl.gov/oceans/2nd_QC_Tool/, 2010.

Tanhua, T., Van Heuven, S., Key, R. M., Velo, A., Olsen, A. and Schirnick, C.: Quality control procedures and methods of the CARINA database, Earth Syst. Sci. Data, 2, 35–49, 2010a.

Tanhua, T., Steinfeldt, R., Key, R. M., Brown, P., Gruber, N., Wanninkhof, R., Perez, F., Körtzinger, A., Velo, A., Schuster, U., Van Heuven, S., et al.: Atlantic Ocean CARINA data: overview and salinity adjustments, Earth System Science Data, 2, 17–34, 2010b.

Tanhua, T., Waugh, D. W. and Wallace, D. W. R.: Use of SF 6 to estimate anthropogenic CO 2 in the upper ocean, Journal of Geophysical Research-Oceans, 113, C04037, 2008.

Thomas, H. and Ittekkot, V.: Determination of anthropogenic CO2 in the North Atlantic Ocean using water mass ages and CO2 equilibrium chemistry, Journal of Marine Systems, 27, 325–336, 2001.

Touratier, F., Azouzi, L. and Goyet, C.: CFC-11, D14C and 3H tracers as a means to assess anthropogenic $CO_2$ concentrations in the ocean, Tellus B, 59, 318–325, 2007.

Touratier, F. and Goyet, C.: Applying the new TrOCA approach to assess the distribution of anthropogenic CO< sub> 2</sub> in the Atlantic Ocean, Journal of marine systems, 46(1), 181–197, 2004.

Trans, P. and Keeling, R. F.: Trends in Atmospheric Carbon Dioxide: Recent Mauna Loa CO2, [online] Available from: http://www.esrl.noaa.gov/gmd/ccgg/trends/, 2012.

Tsuchiya, M., Talley, L. D. and McCartney, M. S.: Water-mass distributions in the western South Atlantic; A section from South Georgia Island (54S) northward across the equator, Journal of Marine Research, 52(1), 55–81, 1994.

Uppstrom, L. R.: The boron/chlorinity ratio of deep-sea water from the Pacific Ocean, Deep Sea Research and Oceanographic Abstracts, 21, 161–162, 1974.

Urbano, D. F., De Almeida, R. A. F., Nobre, P., Hay, A. E., Williams, G. D., Bindoff, N. L., Marsland, S. J., Rintoul, S. R., Anderson, C. R. and Siegel, D. A.: Equatorial Undercurrent and North Equatorial Countercurrent at 38 W: A new perspective from direct velocity data, J. Geophys. Res, 113(C04041), C04041, 2008.

Vázquez-Rodríguez, M., Padín, X. A., Pardo, P. C., Ríos, A. F. and Pérez, F. F.: The subsurface layer reference to calculate preformed alkalinity and

air–sea CO2 disequilibrium in the Atlantic Ocean, Journal of Marine Systems, 94, 52–63, 2012.

Vázquez-Rodríguez, M., Padín, X. A., Ríos, A. F., Bellerby, R. G. J. and Pérez, F. F.: An upgraded carbon-based method to estimate the anthropogenic fraction of dissolved $CO_2$ in the Atlantic Ocean, Biogeosciences Discuss., 6, 4527–4571, 2009a.

Vázquez-Rodríguez, M., Touratier, F., Lo Monaco, C., Waugh, D. W., Padin, X. A., Bellerby, R. G. J., Goyet, C., Metzl, N., Ríos, A. F. and Pérez, F. F.: Anthropogenic carbon distributions in the Atlantic Ocean: data-based estimates from the Arctic to the Antarctic, Biogeosciences, 6, 439–451, 2009b.

Velo, A., Pérez, F. F., Lin, X., Key, R. M., Tanhua, T., Paz, M., Olsen, A., Van Heuven, S., Jutterström, S., Ríos, A. F. and others: CARINA data synthesis project: pH data scale unification and cruise adjustments,, 2010a.

Velo, A., Pérez, F. F., Tanhua, T., Gilcoto, M., Ríos, A. F. and Key, R. M.: Total alkalinity estimation using MLR and neural network techniques, Journal of Marine Systems [online] Available from: http://www.sciencedirect.com/science/article/pii/S0924796312001728 (Accessed 7 November 2012), 2012.

Velo, A., Vázquez-Rodríguez, M., Padín, X. A., Gilcoto, M., Ríos, A. F. and Pérez, F. F.: A multiparametric method of interpolation using WOA05 applied to anthropogenic $CO_2$ in the Atlantic, Scientia Marina, 74, 21–32, doi:10.3989/scimar.2010.74s1021, 2010b.

Wanninkhof, R., Tsung-Hung, P., Huss, B., Sabine, C. L. and Lee, K.: Comparison of inorganic carbon system parameters measured in the Atlantic Ocean from 1990 to 1998 and recommended adjustments, Carbon Dioxide Information Analysis Center, Oak Ridge National Laboratory, ORNL/CDIAC-140., 2003.

Waugh, D. W., Hall, T. M., McNeil, B. I., Key, R. and Matear, R. J.: Anthropogenic $CO_2$ in the oceans estimated using transit time distributions, Tellus B, 58, 376–389, 2006.

Winkler L. W.: Die Bestimmung des im Wasser gelösten Sauerstoffes, Berichte der deutschen chemischen Gesellschaft, 21, 2843–2854, doi:doi:10.1002/cber.188802102122, 1888.

Yao, W., Liu, X. and Byrne, R. H.: Impurities in indicators used for spectrophotometric seawater pH measurements: Assessment and remedies, Marine Chemistry, 107(2), 167–172, 2007.

Yashayaev, I., Holliday, N. P., Bersch, M. and Aken, H. M.: The History of the Labrador Sea Water: Production, Spreading, Transformation and Loss, in Arctic–Subarctic Ocean Fluxes, edited by R. R. Dickson, J. Meincke, and P. Rhines, pp. 569–612, Springer Netherlands. [online] Available from: http://dx.doi.org/10.1007/978-1-4020-6774-7_25, 2008.

Yool, A., Oschlies, A., Nurser, A. J. G. and Gruber, N.: A model-based assessment of the TrOCA approach for estimating anthropogenic carbon in the ocean, Biogeosciences, 7, 723–751, 2010.

Zeebe, R. and Wolf-Gladrow, D.: CO2 in seawater: equilibrium, kinetics, isotopes, Elsevier Science., 2001.

# Anexos/*Appendix*

## i. Acrónimos / *Acronym*

| | |
|---|---|
| [$C_{ant}$]TrOCA | $C_{ant}$ estimated by TrOCA back-calculation method |
| [$C_{ant}$]φ | $C_{ant}$ estimated by φCT0 back-calculation method |
| 3DwMLR | 3D moving window Multiple Linear Regression |
| A24N | Cruise 2011 |
| AA | Antarctic Water |
| AABW | Antartic Bottom Water |
| AAIW | Antartic Intermediate Water |
| AOU | Apparent Oxygen Utilization |
| $A_T$ | Total alkalinity |
| B/Cl | Boron to chlorinity ratio |
| B/O | Buque Oceanográfico |
| CAIBEX | Shelf-ocean Exchanges in the Canary – Iberian Large Marine Ecosystem |
| CAIBOX | Cruise 2009 |
| $C_{ant}$ | Anthropogenic carbon |
| CARINA | Carbon in the Atlantic Ocean |
| CCHDO | Carbon Hydrographic Data Office |
| CDIAC | Carbon Dioxide Information Analysis Center |
| CFC | Chlorofluorocarbon |
| CHAOS | Cruise 1998 |

| | |
|---|---|
| CITHER I | Cruise 1993 |
| CLIVAR | Climate variability and predictability |
| $CO_2$sys | Program developed for $CO_2$ system calculations |
| $[CO_3^{2-}]$ | Carbonate ion concentration |
| CRM | Certified Reference Material |
| CSIC | Consejo Superior de Investigaciones Científicas |
| $C_T$ | Total inorganic carbon |
| $C_{Tcalc}$ | Calculated $C_T$ |
| CTD | Conductivity temperature depth |
| $C_{Tmeas}$ | Measured $C_T$ |
| DIC | Dissolved inorganic carbon |
| DSOW | Denmark Straight Overflow Water |
| ENACW | East North Atlantic Central Water |
| ENACWP | Subpolar East North Atlantic Central Water |
| ENACWT | Subtropical East North Atlantic Central Water |
| eOMP | extended Optimum MultiParameter |
| $fCO_2$ | Fugacity of $CO_2$ |
| FSE | Fondo Social Europeo |
| GLODAP | Ocean Data Analysis Project |
| GOSHIP | Global ocean ship-based Hydrographic Investigations |
| GP89 | Pair of dissociation constants for carbonic acid calculated in synthetic waters by Goyet and Poisson (1989) |

| | |
|---|---|
| IIM | Instituto de Investigaciones Marinas |
| IOCCP | International Ocean Carbon Coordination Project |
| ISOW | Iceland Scotland Overflow Water |
| ITCZ | Inter Tropical Convergence Zone |
| JAE | Junta para la Ampliación de Estudios |
| JGOFS | Joint Global Ocean Flux Study |
| $K_1$* | First dissociation constants of carbonic acid |
| $K_2$* | Second dissociation constants of carbonic acid |
| LDK00 | Pair of constants for carbonic acid calculated in natural seawater by Lueker et al. (2000) |
| LM05 | Back-calculation method to estimate [Cant] |
| lNADW | lower North Atlantic Deep Water |
| LSW | Labrador Sea Water |
| M06 | Pair of constants for carbonic acid calculated in natural seawater by Millero et al. -2006 |
| mCP | Indicator m-cresol purple |
| MDM87 | Pair of constants for carbonic acid calculated in natural seawater by Mehrbach et al. (1973) refitted by Dickson and Millero (1987) |
| MLR | Multiple Linear regression |
| MMW | Madeira Mode Water |
| MOC[2] | Equatorial Meridional Overturning Circulation - Memoria Oceánica del Clima: mecanismos y rutas de formación de aguas superficiales en el Atlántico ecuatorial |

| | |
|---|---|
| MW | Mediterranean Water |
| NACW | North Atlantic Central Water |
| NADW | North Atlantic Deep Water |
| NAO | North Atlantic Oscillation |
| NBC | North Brazil Current |
| $_{N}C_{T}$ | Normalized total inorganic carbon |
| NEADW | North East Atlantic Deep Water |
| NEADWl | Lower North East Atlantic Deep Water |
| NEADWu | Upper North East Atlantic Deep Water |
| NEC | North Equatorial Current |
| NEUC | North Equatorial Under Current |
| NOAA/ESRL | National Oceanic And Atmospheric Administration / Earth System Research Laboratory |
| OACES | Ocean-Atmosphere Carbon Exchange Study and 1993 and 2003 cruises. |
| OMZ | Oxygen Minimun Zones |
| OUR | Oxygen Utilization Rate |
| OVIDE | Observatoire de la variabilité interannuelle et décennale en Atlantique Nord |
| $pCO_2$ | Partial pressure of $CO_2$ |
| pH | Potential of hydrogen |
| $pH_{SWS}$ | SW scale pH |

| | |
|---|---|
| $pH_T$ | Total scale pH |
| QC | Quality control |
| R/V | Research vessel |
| ROM | Remineralisation of organic matter |
| $R_p$ | Redfield Ratio of $PO_4^{3-}$ |
| SAC | South Atlantic Current |
| SACW | South Atlantic Central Water |
| SAMW | SubAntarctic Mode Water |
| SEC | South Equatorial Current |
| SOMMA | Single-Operator Multiparameter Metabolic Analyzer |
| TDN | Dissolved organic nitrogen |
| TOC | Total organic carbon |
| TrOCA | Tracer combinig Oxygen, inorganic Carbon and total Alkalinity, back-calculation methods to estimate [$C_{ant}$] |
| $TrOCA^0$ | Conservative TrOCA tracer |
| TTD | Transient Time Distribution |
| uNADW | upper North Atlantic Deep Water |
| UNESCO | United Nations Educational, Scientific and Cultural Organization |
| UV-VIS | Ultraviolet-visible |
| VACLAN | Climate Variability in the North Atlantic |
| WOCE | World Ocean Circulation Experiment |

| | |
|---|---|
| WOCE | A06 WOCE cruise |
| WOCE | A07 WOCE cruise |
| $\Delta C^*$ | back-calculation method to estimate [$C_{ant}$] |
| $\Delta C_{dis}$ | Air-sea $CO_2$ disequilibrium of a water parcel |
| $\delta CO_3^{2-}$ | Difference between $[CO_3^{2-}]_{calc}$ and $[CO_3^{2-}]_{meas}$ |
| $\delta C_T$ | Difference between $C_{Tcalc}$ and $C_{Tmeas}$ |
| $\Delta R$ | pH correction |
| $\Delta\Delta C_{dis}$ | Spatial and temporal variability of $\Delta$Cdis |
| $\Theta$ | Potential temperature |
| $\Theta$-S | Potential temperature versus salinity diagram |
| $\varphi$CT0 | Back-calculation method to estimate [$C_{ant}$] |
| $\Omega_{arag}$ | Saturation estate of aragonite |

## ii. Índice de tablas / *Table index*

## iii. Índice de figuras / *Figures index*

I. Introducción / *Introduction*

II. Datos y métodos / *Data and methodology*